

Bioinorganic Hydrocarbon Oxidation: Mechanistic and Kinetic
Studies of the Soluble Methane Monooxygenase from
Methylococcus capsulatus (Bath)

by
Ann M. Valentine
B.S., University of Virginia (1993)

SUBMITTED TO THE DEPARTMENT OF CHEMISTRY IN PARTIAL
FULFILLMENT OF THE REQUIREMENTS FOR THE DEGREE OF

DOCTOR OF PHILOSOPHY IN CHEMISTRY
AT THE
MASSACHUSETTS INSTITUTE OF TECHNOLOGY

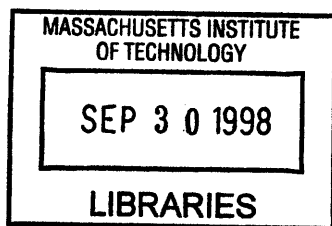
September 1998

© Massachusetts Institute of Technology, 1998
All rights reserved

Signature of Author: _____
Department of Chemistry
August 20, 1998

Certified by: _____
Stephen J. Lippard
Thesis Supervisor

Accepted by: _____
Dietmar Seyferth
Chairman, Departmental Committee on Graduate Studies



Science

This doctoral thesis has been examined by a Committee of the Department of Chemistry as follows:

Daniel G. Nocera
Professor of Chemistry
Committee Chairman

Stephen J. Lippard
Arthur Amos Noyes Professor of Chemistry
Thesis Supervisor

JoAnne Stubbe
Novartis Professor of Chemistry and Professor of Biology

Bioinorganic Hydrocarbon Oxidation: Mechanistic and Kinetic Studies of the Soluble Methane Monooxygenase from *Methylococcus capsulatus* (Bath)

by

Ann M. Valentine

Submitted to the Department of Chemistry on August 20, 1998, in partial fulfillment of the requirements for the Degree of Doctor of Philosophy

Abstract

Chapter 1. Principles of Small Molecule Activation by Metalloproteins as Exemplified by the Soluble Methane Monooxygenase

Many metalloenzymes activate small molecules in a manner that is unique to natural systems. In this perspective we discuss the soluble protein system from *Methylococcus capsulatus* (Bath), which uses a mixed-function hydroxylase to convert methane selectively to methanol. Through a series of biophysical studies, theoretical calculations, synthetic model studies, and mechanistic biochemical experiments, the respective roles of the carboxylate-bridged non-heme diiron center and the protein environment in controlling the enzyme mechanism have been delineated. These results are used to identify themes common among metalloenzymes that activate small molecules and to identify future directions for the study of this protein system.

Chapter 2. Small Molecule Binding to the Mixed-Valent Diiron Center of Methane Monooxygenase Hydroxylase from *Methylococcus capsulatus* (Bath) as Revealed by ENDOR Spectroscopy

The binding of several exogenous molecules at the active site of the soluble methane monooxygenase hydroxylase (MMOH) from *Methylococcus capsulatus* (Bath) is described. The interaction of methanol, the product of methane hydroxylation, with the mixed-valent $\text{Fe}^{\text{II}}\text{Fe}^{\text{III}}$ form of the enzyme induces a change in the EPR spectrum of the unmodified protein from $g = 1.940, 1.865, \text{ and } 1.740$ to one with $g_1 = 1.963$ and $g_2 = 1.862$. This spectral change arises from coordination of methanol to the diiron center, as demonstrated by ENDOR spectroscopic studies of mixed-valent MMOH prepared with CD_3OD added to a DMSO-treated sample, which displayed a ^2H interaction with an isotropic hyperfine splitting of ~ 0.5 MHz. A detailed analysis indicates that methanol binds to the ferrous iron without displacing a terminally bound water molecule identified previously. Acetate labeled with ^{13}C at the carboxylate carbon atom also gives rise to ENDOR signals, whereas no such signals are seen when the label is at the methyl carbon atom or when the methyl group is deuterated. These results suggest that acetate is oriented in the active site with its carboxylate group pointing towards the iron center, confirming a previous interpretation of X-ray crystallographic

experiments. Four coordination positions at the MMOH diiron core not usually occupied by endogenous protein ligands are identified which can simultaneously accommodate DMSO, methanol, and water. The implications of these results for the catalytic mechanism of the enzyme are discussed.

Chapter 3. An EPR Study of the Dinuclear Iron Site in the Soluble Methane Monooxygenase Reduced by One Electron at 77 K: the Effect of Component Interactions and the Binding of Small Molecules to the Dinuclear Ferric Center

EPR spectra of cryogenically reduced diferric sites from the soluble methane monooxygenase hydroxylase (MMOH) were examined as probes of active site structure. In the absence of exogenous ligands and coupling protein (MMOB), two populations of active sites were observed, one species (H1) having g values of 1.94, 1.86, and 1.79 and the other more anisotropic signal (H2) having g values of 1.82, 1.77, and 1.68. These forms can be distinguished by the temperature- and power-dependence of their EPR signal. H1 and H2 are postulated to be related by proton movements, and they interact differently with small exogenous molecules. Some interactions, such as that of DMSO with the oxidized MMOH, are mediated by MMOB. Additional species afforded by small molecule and protein binding are interpreted according to this model, with additional modifications afforded by carboxylate shifts of a flexible glutamate ligand.

Chapter 4. An Investigation of the Reaction of Diferrous Methane Monooxygenase Hydroxylase with Dioxygen and Substrates by Rapid Freeze-Quench and Stopped-Flow Spectroscopy

Single turnover reactions of MMOH are studied in the presence and absence of substrate and by continuous and discontinuous techniques. The electronic absorption spectrum ($\lambda_{\max} = 725$ nm, $\epsilon = 1500 \text{ M}^{-1} \text{ cm}^{-1}$) of the H_{peroxo} intermediate is presented for the first time and activation parameters for its formation are reported. The rate constant for formation of H_{peroxo} is not dioxygen concentration dependent. Activation parameters for the decay of H_{peroxo} and the formation of Q are in good agreement with each other. Photoreactivity of intermediate Q is described, and the mechanism of its decay in the absence of substrate studied. Irradiation of a frozen solution of Q by γ rays produces a new paramagnetic species, Q_χ , which is spectroscopically similar to intermediate X in ribonucleotide reductase R2 cofactor assembly. The Mössbauer characterization of Q_χ is reported. A new oxo-bridged diferric species is detected by rapid freeze-quench (RFQ) Mössbauer. Finally, the reactions of substrates with intermediate species are studied by using RFQ Mössbauer and single and double mixing stopped flow spectroscopy. The data suggest that H_{peroxo} or a related species other than Q is competent to oxidize olefins. The reactions of substrates with Q are studied. The data support a more complicated mechanism than a simple bimolecular collision, with the reaction order in substrate decreasing with increasing substrate size.

Chapter 5. Oxidation of Radical Clock Substrate Probes by the Soluble Methane Monooxygenase System Radical clock substrate probes have been employed to assess the viability of a discrete substrate radical species in the mechanism of oxidation by sMMO. New probes were designed with very fast ring opening rate constants and other desirable attributes, such as the ability to discriminate between radical and cationic intermediates. Oxidation of these new probes by a reconstituted sMMO system results in no rearranged product, allowing an upper limit to be placed on the lifetime of a putative radical species, and suggesting that there is no such substrate radical intermediate. Each diastereomer of *trans*-1-methyl-2-phenyl-cyclopropane has been prepared and the regioselectivity of oxidation is examined.

Chapter 6. Tritiated Chiral Alkanes as Probes for the Mechanism of Hydroxylation by the Soluble Methane Monooxygenase

The tritiated chiral alkanes (S)-[1-²H₁,1-³H]ethane, (R)-[1-²H₁,1-³H]ethane, (S)-[1-²H₁,1-³H]butane, (R)-[1-²H₁,1-³H]butane, (S)-[2-³H]butane, (R)-[2-³H]butane, and racemic [2-³H]butane were oxidized by soluble methane monooxygenase (sMMO) from *Methylococcus capsulatus* (Bath) and the absolute stereochemistry of the resulting product alcohols determined in order to probe the mechanism of substrate hydroxylation. When purified hydroxylase, coupling protein, and reductase components were used, the product alcohol displayed 72% retention of stereochemistry at the labeled carbon for the ethane substrates and 77% retention for the butanes labeled at the primary carbon. A putative alkyl radical which would yield these product distributions would have a lifetime of 100 fs, a value too short to correspond to a discrete intermediate. Intramolecular k_H/k_D ratios of 3.4 and 2.2 were determined for ethane and butane, respectively. When the hydroxylations were performed with purified hydroxylase but only a partially purified cellular extract for the coupling and reductase proteins, different product distributions were observed. These apparently anomalous results could be explained by invoking exchange of hydrogen atoms at the α carbon of the product alcohols. The characteristics of this exchange reaction are discussed. Hydroxylation of [2-³H]butanes by the latter system yielded ~90% retention of stereochemistry at the labeled carbon. The implication of these results for the catalytic mechanism of sMMO is discussed. Together with the mechanistic information available from a range of substrate probes, the results are best accounted for by a nonsynchronous concerted process involving attack of the C-H bond to form a pentavalent carbon transition state.

Thesis Supervisor: Stephen J. Lippard

Title: Arthur Amos Noyes Professor of Chemistry

This thesis is dedicated to my family, and especially to my grandparents, John N. and Margaret McCagh Nolan, in gratitude for their many gifts.

Acknowledgments

So many people to thank...starting with my advisor, Steve Lippard. Steve entrusted a great project to me five years ago and supported me in the time since. His enthusiasm, suggestions, and interest have been unflagging. He arranged great collaborations inside and outside of MIT, and filled our laboratory with incredibly bright and wonderful scientists with whom to interact. Over the course of my graduate career, Steve has also done his best to see that I can write and communicate, think and execute experiments, and organize. Hopefully some of that training took hold. I must say, though, that because of Steve, there will forever be a few phrases which disturb me, including "Thing B." Steve, here's to the breezes!

Before I came to graduate school, there were teachers and professors who inspired and encouraged me to go into science. Ada Margaret Hutchison urged me to envision a science career back when I just wanted a driver's licence, and Hugh Carr made chemistry look pretty good. At UVA, Lester Andrews and Dean Harman reinforced that interest in chemistry and extended it to include independent research. Tim Macdonald let this very inexperienced undergraduate loose in his lab, for which I am eternally grateful. Jim Demas has been a mentor and a friend, and taught me invaluable Chemdraw skills which continue to serve.

Other groups at MIT provided advice and experimental assistance, and made their equipment available to me. In particular, I thank JoAnne Stubbe and her group, especially Pam Riggs-Gelasco and Doug Burdi, for their extensive help with freeze-quench experiments. Outside of MIT, I've had many wonderful collaborators, notably Vincent Huynh and his postdocs Danli Wang, Alice Pereira, Pedro Tavares, and Carsten Krebs, and also Dale Edmondson at Emory University for rapid freeze-quench experiments and Mössbauer spectroscopy (and margaritas). Brian Hoffman, Roman Davydov, Jean-Paul Willems, and Stoyan Smoukov at Northwestern collaborated on EPR, ENDOR, and radiolytic reduction experiments. Heinz Floss and Barrie Wilkinson at Washington University and Phil Williams and Hiromi Morimoto at the National Tritium Labeling Facility worked on the chiral tritiated alkane experiments. Finally Martin Newcomb and his coworkers Marie-Helene LeTadic-Biadatti and Patrick Toy collaborated with us on the radical clock substrate probe experiments.

When I got to MIT, I was incredibly fortunate to have Kathy Liu as a teacher and mentor. She patiently taught many techniques and answered ten times that many questions. Andrew Feig was another great influence... although sometimes in subgroup meetings I felt as though I had two advisors! My coworkers in the MMO subgroup have been a constant source of help, encouragement, and entertainment. They have included Thanos Salifoglou, Amy Rosenzweig, Sonja Komar-Panicucci, George Gassner, Jessica Blazyk, Shannon Stahl, and Dan Kopp. I want to make special mention of Dave Coufal and Doug Whittington, the other "senior" members of the subgroup, and thank them for their years of friendship, antics, and (naturally) scientific discourse, and in particular for their very frequent computer help.

The rest of the Lippard lab has also provided scientific and personal support. My classmates Deborah Zamble and Dan LeCloux did plenty of BOTH of those things. Deb's and my foray into DNA repair (with superglue and rubber bands) was just *one* of our escapades. Thank you and Brian for years of friendship, good times, and pad thai. Dan was always up for a debate about chemistry, sports, or human nature, and could be counted on for his honest opinion. The lab hasn't been the same since he left. Linda Doerrer was a great friend and example from the day I joined the lab. Maria Bautista's arrival shot the amusement level right through the roof - and she turned into a valued friend as well. Susanna Herold introduced us all to "jumping" and the true meaning of "caos!" The new generation of "jumpers" - Uta-Maria Ohndorf, Kathy Franz, and Qing He - helped continue that great tradition. Thanks to Jed Goldstone and Chris Morse (not Lippard lab members, but who's counting?) for early support through TA-ing and cumes followed by years of camaraderie and excellent parties. To Rob Niger I say "RAH!" A special thank you goes out to Dietrich Steinhuebel, Justin Du Bois, Jack Mizoguchi, Kathy Franz, Shannon Stahl, and Shawn Burdette, who collaborated to provide much entertainment, especially these past few months. Scientifically, they were all generous with their time and insightful in their discussions. Dietrich, I will miss my coach and fellow caffeine addict. Justin, I concede that occasionally you have been right (you got me!). Jack, I will miss you but I look forward to a new place where nobody has memorized my weird eating habits. Kathy, you're such a together person that I don't worry about you - but try to keep "the guys" out of trouble. Shannon, whatever it is that you're thinking, I disagree. And Shawn, take comfort in the fact that before you know it you'll be the senior grad student dishing out the abuse. To all of the above people I wish the best always.

This thesis is dedicated to my family, and without their encouragement it wouldn't exist. Mom and Dad, you have been my role models in every sense. I love you both. To my sisters and brothers - Amy, James, Elizabeth, and John - if I could choose siblings, I couldn't hope to find four like you. I want to be just like you guys when I grow up. Thank you so much for all your support from afar and for making home such a terrific place to come home to. I look forward to returning the favor you've done me and cheering you all on as you set out in the world. Thank you also to Uncle John, to my cousins, and Bill and Ruth and the rest of the family for all they've done.

In my first year of graduate school, I went out one evening in February and met a nice Penguin fan from Pittsburgh. Little did I know that Michael Lawlor would become my best friend and the one person I'd want to spend my life with. Mike, thank you for all the support you've given me over the years, for all the free organic chemistry consults, and for the outings that have left me with so many happy memories of our time in New England. Thank you to your marvelous family for welcoming me from the very beginning. And now, well, you promised it would happen and it has - the time of waiting impatiently is over.

Table of Contents

Abstract.....	3
Dedication.....	6
Acknowledgments.....	7
Table of Contents	9
List of Tables.....	13
List of Schemes.....	14
List of Figures.....	15
Chapter One: Principles of Small Molecule Activation by Metalloproteins as Exemplified by the Soluble Methane Monooxygenase	19
Introduction.....	20
Common Themes in Small Molecule Activation	23
Achievement of Kinetically Difficult Transformations.....	23
Multi-Protein Enzyme Systems.....	25
Electron Transfer Over a Distance.....	26
Access to the MMOH Active Sites.....	28
Substrate Selectivity and Diagnostic Probes.....	29
Detailed Steps in the Catalytic Mechanism.....	32
Conclusions.....	36
References.....	38
Chapter Two: Small Molecule Binding to the Mixed-Valent Diiron Center of Methane Monooxygenase Hydroxylase from <i>Methylococcus capsulatus</i> (Bath) as Revealed by ENDOR Spectroscopy	50
Introduction.....	51
Materials and Methods.....	52
Protein Purification.....	52
Sample Preparation.....	52
ENDOR Spectroscopy.....	53
Results.....	54
EPR Spectroscopy	54
ENDOR Spectroscopy.....	55
Addition of Methanol and Acetate to MMOH _{mv}	55
Addition of DMSO and Acetate to MMOH _{mv}	56
DMSO and Methanol Binding to MMOH _{mv}	56

Discussion.....	60
Conclusion	62
References.....	63
Chapter Three: An EPR Study of the Dinuclear Iron Site in the Soluble Methane Monooxygenase Reduced by One Electron at 77 K: the Effect of Component Interactions and the Binding of Small Molecules to the Dinuclear Ferric Center	74
Introduction.....	75
Materials and Methods.....	77
Results.....	79
One-Electron Cryogenic Reduction of Hydroxylase	79
Effect of Small Molecules on Hox _{mv}	80
Cryogenic Reduction of the Hox+MMOB Complex in the Presence and Absence of Small Molecules and MMOR.....	82
Discussion.....	85
Conclusions.....	91
References.....	93
Chapter Four: An Investigation of the Reaction of Reduced Methane Monooxygenase Hydroxylase with Dioxygen and Substrates by Rapid Freeze-Quench and Stopped-Flow Spectroscopy	108
Introduction.....	109
Experimental.....	113
Protein Isolation and Characterization.....	113
Single Turnover Reactions. Preparation of H _{red}	113
Rapid Freeze-Quench.....	113
Mössbauer Spectroscopy	114
Radiolytic Reduction.....	114
Stopped-Flow Spectroscopy	114
Quantitation of Hydrogen Peroxide.....	115
Detection of Products in the Propylene Reaction	116
Results.....	116
Optical Spectra of Intermediate Species	116
Dioxygen Dependence of Hperoxo Formation.....	116
Activation Parameters for the Formation and Decay of Intermediates.....	117
Photoreactivity of Intermediate Q.....	118

Decay of Q in the Absence of Substrate	118
Generation of Q _X	119
Identification of a New Species.....	120
Reactions of Intermediate Species with Substrates	120
Rapid Freeze-Quench Mössbauer Spectroscopy.....	120
Stopped-Flow Optical Spectroscopy	121
Discussion.....	123
Characterization of Intermediates. Optical Spectrum of H _{peroxo}	123
Reaction of H _{red} with O ₂	124
Activation Parameters.....	127
Model for the Evolution of Intermediate Species in a Single Turnover Reaction Without Substrate.....	127
Generation of Q _X and Comparison to RNR-R2-X.....	129
Species V.....	130
Reactions of Intermediates With Substrates. H _{peroxo}	131
Reactions of Substrates with Q.....	133
Conclusion	134
References.....	136
Chapter Five: Oxidation of Radical Clock Substrate Probes by the Soluble Methane Monooxygenase	167
Introduction.....	168
Experimental.....	171
Protein Preparation and Characterization.....	171
Radical Clock Substrate Probes and Products.....	171
Enzymatic Oxidations and Product Characterization	171
Results and Discussion.....	173
Characterization of Oxidation Products.....	173
Calculation of a Lower Limit for the Rebound Rate Constant of a Putative Radical Intermediate	175
Mechanistic Implications and Comparisons to Literature Results.....	175
Conclusions.....	179
References.....	180
Chapter Six: Tritiated Chiral Alkanes as Substrates for Soluble Methane Monooxygenase from <i>Methylococcus capsulatus</i> (Bath): Probes for the Mechanism of Hydroxylation	195
Introduction.....	196

Experimental.....	200
Bacterial Growth and Protein Purification.....	200
Isolation of sMMO Reductase from Soluble Cell Extract	200
Determination of Conditions for Oxidizing Labeled Alkanes.....	202
Reagent Synthesis.....	203
Enzymatic Reactions	203
Oxidation of C ₂ D ₆	204
Exchange Reactions	204
Results.....	204
Synthesis of Chiral Tritiated Alkanes	204
Analysis of Lyophilizates.....	205
Analysis of Derivatives	207
Oxidation by Purified Components	208
Oxidation by Hydroxylase and B/R Mix.....	209
Oxidations of C ₂ D ₆ and Exchange Reactions.....	210
Discussion.....	210
Differences Between H + B/R Mix and Purified Protein Components.....	210
Alkanes are Not Highly Constricted in the Active Site Prior to Hydroxylation.....	212
Kinetic Isotope Effects	213
Calculation of an Apparent Rebound Rate Constant	213
Comparisons with Literature.....	214
Mechanistic Implications.....	216
References.....	219
Appendix One: Attempts to Inhibit sMMO Activity by using Small Molecules.....	236
Appendix Two: Binding of Fluorinated Small Molecules to the Mixed- Valent Diiron Center of Methane Monooxygenase Hydroxylase from <i>Methylococcus capsulatus</i> (Bath) as Revealed by ENDOR Spectroscopy	243
Appendix Three: Isolation of Two Components of the Alkene Monooxygenase System from Xanthobacter Py2 and Preliminary Stopped-Flow Studies	249
Biographical Note.....	254

List of Tables

Table 4.1. Rate Constants for Formation and Decay of H _{peroxo} under Conditions of Varying Dioxygen Concentration at 4 °C.....	143
Table 4.2. Rate Constants for Formation and Decay of H _{peroxo} under Conditions of Varying Temperature in the Presence of 8.75 mM acetylene.....	144
Table 4.3. Rate Constants for Formation and Decay of Q at 420 nm under Conditions of Varying Temperature in the Absence of Substrate and with Detection by a Photomultiplier Tube.....	145
Table 4.4. Rate Constants for Formation and Decay of Q with Varying Temperature in the Absence of Substrate with Detection by Diode Array.....	146
Table 4.5. Activation Parameters for the Formation and Decay of Intermediate Species.....	147
Table 4.6. Mössbauer Parameters for Q _X and Related Species.....	148
Table 4.7. Reaction Order in Substrate and Second Order Rate Constants for the Reactions of Substrates with Intermediate Q at 20 °C.....	149
Table 5.1. Radical Clock Substrate Probes used in the Current Study and the Ring Opening Rate of the Cyclopropylcarbinyl Radical Derived from the Probes.....	184
Table 5.2. Products from Oxidation of Radical Clock Substrate Probes by sMMO.....	186
Table 5.3. Products from Oxidation of Racemic <i>trans</i> -1-Phenyl-2-methylcyclopropane and of each Diastereomer.....	187
Table 6.1. Results of Oxidizing (R)- and (S)-[1- ² H ₁ ,1- ³ H]Ethane with Purified H, B, and R.....	224
Table 6.2. Results of Oxidizing (R)- and (S)-[1- ² H ₁ ,1- ³ H]Butane with Purified H, B, and R.....	225
Table 6.3. Results of Oxidizing (R)- and (S)-[1- ² H ₁ ,1- ³ H]Ethane with a Mixture Containing sMMO and other Cellular Proteins.....	226
Table 6.4. Results of Oxidizing (R)- and (S)-[1- ² H ₁ ,1- ³ H]Butane with a Mixture Containing sMMO and other Cellular Proteins.....	227
Table 6.5. Results of Oxidizing (R)-, (S)-, and Racemic [2- ³ H]Butane with a Mixture of H, B, and R Containing other Cellular Proteins.....	228
Table A1.1. Attempts to Reactivate MeHgNO ₃ -inhibited MMOH by Dialysis against β-Mercaptoethanol.....	240

List of Schemes

Scheme 3.1.....96
Scheme 3.2.....97

List of Figures

Figure 1.1. Small molecules activated by metalloenzymes	43
Figure 1.2. Schematic representation of a metalloprotein active site.....	44
Figure 1.3. View of the non-heme diiron active site housed in the α subunit of the sMMO hydroxylase enzyme	45
Figure 1.4. The α subunit of sMMO hydroxylase showing the hydrophobic cavities leading from the active site to the protein surface.....	46
Figure 1.5. (A) Ring opening of a radical clock substrate probe. (B) Oxidation of chiral tritiated ethane.....	47
Figure 1.6. Candidates for the structures of intermediates in the sMMO catalytic cycle	48
Figure 1.7. Catalytic cycle for sMMO from <i>M. capsulatus</i> (Bath) including all observed intermediates.....	49
Figure 2.1. A model of the hydroxylase active site with anchor positions occupied by amino acids and potential catalytic positions numbered 1-4.....	67
Figure 2.2. 35 GHz CW EPR spectra of MMOH_{mv}	68
Figure 2.3. A series of 35 GHz pulsed Mims ENDOR spectra of MMOH_{mv} at a field position corresponding to g_3	69
Figure 2.4. 35 GHz Mims ENDOR spectra across the EPR envelope of $\text{MMOH}_{\text{mv}}[\text{DMSO}]$ with deuterated methanol.....	70
Figure 2.5. 35 GHz CW proton ENDOR spectra of MMOH_{mv} at g_1	71
Figure 2.6. 35 GHz CW ENDOR spectra of MMOH_{mv} at g_1	72
Figure 2.7. The catalytic cycle of sMMO, depicting the likely binding sites for small molecule substrates.....	73
Figure 3.1. The diiron active site of MMOH in the oxidized diferric and reduced diferrous states.....	98
Figure 3.2. X-band EPR spectra of mixed-valent forms of MMOH (pH 7.0) generated chemically at room temperature and in 4:1 buffer-glycerol generated radiolytically at 77 K.....	99
Figure 3.3. X-band EPR spectra of $\text{MMOHox}_{\text{mv}}$ in buffer-glycerol (4:1).....	100
Figure 3.4. X-band EPR spectra of chemically reduced MMOH_{mv} in the presence of DMSO or methanol	101
Figure 3.5. 35 GHz EPR spectra of MMOH_{mv} in the presence of 50 mM phenols.....	102

Figure 3.6. X-band EPR spectra of oxidized hydroxylase in the presence of 0.25 M DMSO and 50 mM <i>p</i> -nitrophenol radiolytically reduced at 77 K.....	103
Figure 3.7. X-band EPR spectra of mixed-valent form of MMOH in the presence of 2% methanol produced by reduction at 77 K.....	104
Figure 3.8. X-band EPR spectra of mixed-valent forms of the hydroxylase + component B complex produced by chemical reduction at room temperature and by radiolytic reduction at 77 K.....	105
Figure 3.9. X-band EPR spectra of the (Hox+MMOB) _{mv} complex in 1:1 buffer-glycerol.....	106
Figure 3.10. X-band EPR spectra of the (Hox+ MMOB) _{mv} complex in the presence of 2% DMSO and 2% methanol.....	107
Figure 4.1. Single turnover reaction of H _{red} in the presence of two equivalents of MMOB with dioxygen.....	150
Figure 4.2. Diode array data collected after the rapid mixing of H _{red} /2B with dioxygen at 20 °C.....	151
Figure 4.3. Fits of the data from Figure 4.2 with the global analysis package Specfit.....	152
Figure 4.4. Oxygen concentration dependence of formation and decay of the H _{peroxo} signal at 4 °C as determined by global analysis.....	153
Figure 4.5. Eyring plots describing the formation and decay of H _{peroxo} and Q.....	154
Figure 4.6. Formation and decay of Q at 4 °C when irradiated with 420 nm light from a 30 W quartz-halogen lamp and a 75 W xenon lamp.....	155
Figure 4.7. Mössbauer spectra of a rapid freeze quench sample from the reaction of H _{red} /2B with dioxygen at 4 °C.....	156
Figure 4.8. Mössbauer spectral comparison of Q _X and R2-X.....	157
Figure 4.9. Mössbauer spectrum of intermediate V prepared by subtracting the known spectra of other components.....	158
Figure 4.10. Mössbauer analysis of freeze-quench samples from the reaction of reduced hydroxylase with buffer containing dioxygen and methane.....	159
Figure 4.11. Diode array spectra after mixing H _{red} /2B with dioxygen and 1 mM methane or 3 mM propylene and dioxygen at 20 °C.....	160

Figure 4.12. (A) A plot of k_{obs} for H_{peroxo} decay vs. [methane]. (B) A plot of k_{obs} for H_{peroxo} decay vs. [propylene].....	161
Figure 4.13. (A) Raw data resulting from mixing acetylene (438 μM after mixing) with the evolving intermediates after a 0.4 s delay after mixing $\text{H}_{\text{red}}/2\text{B}$ with dioxygen. (B) Traces at 415 nm after similar experiments employing a range of concentrations of acetylene.....	162
Figure 4.14. (A) The fit of a single exponential decay to the kinetic data at 415 nm describing the reaction of acetylene with intermediate Q pictured in Figure 4.13A. (B) A plot of $\ln(k_{\text{obs}})$ vs. $\ln([\text{acetylene}])$. (C) A plot of k_{obs} for Q decay vs. [acetylene]	163
Figure 4.15. (A) Plot of k_{obs} vs. [substrate]. (B) Plot of $\ln(k_{\text{obs}})$ vs. $\ln[\text{substrate}]$ for the same substrates.	164
Figure 4.16. Proposal for the species observed in the single turnover reaction of $\text{H}_{\text{red}}/2\text{B}$ with O_2 in the absence of substrate.....	165
Figure 4.17. Possible mechanisms for the oxidation of substrates by sMMO.....	166
Figure 5.1. Ring opening of cyclopropylcarbinyl radicals resulting from hydrogen atom abstraction from a radical clock substrate probe.	188
Figure 5.2. Ring opening of probe 5	189
Figure 5.3. GC analysis of products from the hydroxylation of racemic 1 by a reconstituted sMMO system.....	190
Figure 5.4. Calibration curve for <i>trans</i> -1-phenyl-2-methyl-cyclopropane with reference to 1 mM ethylbenzoate as an internal standard.....	191
Figure 5.5. Binding of the diastereomers of probe 1 in the MMOH active site	192
Figure 5.6. Binding of probe 5 in the MMOH active site.....	193
Figure 5.7. Possible mechanisms for the oxidation of substrates by sMMO.....	194
Figure 6.1. Oxidation of (S)-[1- $^2\text{H}_1$,1- ^3H]ethane at the C- ^1H bond via a proposed substrate radical intermediate.....	229
Figure 6.2. Possible reaction products from the oxidation of (S)-[1- $^2\text{H}_1$,1- ^3H]ethane.....	230
Figure 6.3. ^3H NMR analyses of the oxidation products of (S)-[1- $^2\text{H}_1$,1-	

^3H]ethane.....	231
Figure 6.4. ^3H NMR analyses of the oxidation products of (S)-[1- ^3H ,1- $^2\text{H}_1$]butane	232
Figure 6.5. ^3H NMR analyses of the oxidation products of (S)-[2- ^3H]butane.....	233
Figure 6.6. A scenario in which an alcohol dehydrogenase exchange reaction would cause inverted kinetic isotope effects and apparent inversion of stereochemistry in the products of oxidation of chiral (R)-ethane.....	234
Figure 6.7. A nonsynchronous concerted mechanism for oxidation of an alkane by sMMO.....	235
Figure A1.1. (A) Concentration-dependent inhibition of sMMO activity by EMTS. (B) Time-dependent inhibition by 0.5 mM EMTS.....	241
Figure A1.2. Concentration- and time- dependent inhibition of sMMO activity by MeHgNO_3	242
Figure A2.1. Interval-dependent ENDOR spectra of $(\text{MMOH}+\text{CF}_3\text{CH}_2\text{OH})_{\text{mv}}$	246
Figure A2.2. Field-dependent ENDOR spectra of $(\text{MMOH}+\text{CF}_3\text{CH}_2\text{OH})_{\text{mv}}$	247
Figure A2.3. Field-dependent ENDOR spectra of a $(\text{MMOH}+\text{CF}_3\text{CH}_2\text{OH})_{\text{mv}}$ sample prepared in D_2O and d^8 -glycerol	248
Figure A3.1. SDS-PAGE of AMO Proteins.....	252
Figure A3.2. (A) Data from a stopped-flow experiment in which reduced AMO oxygenase in the presence of two equivalents of the small protein was mixed with dioxygen-saturated buffer at 4 °C. (B) Spectral changes at 450 nm and 725 nm over the first 5 s of reaction. (C) Results of global fitting to the rate constants determined by single wavelength fits.....	253

Chapter One:

Introduction: Principles of Small Molecule Activation by Metalloproteins as Exemplified by the Soluble Methane Monooxygenase

Introduction^{1,2}

Although the field of bioinorganic chemistry is young compared to other areas of chemistry, such as organic synthesis, its history may be traced perhaps even to the origin of life itself. In particular, nickel and iron sulfide surfaces have been implicated as catalysts responsible for the chemoautotrophic events which occurred during primordial metabolism.³ In this scenario, chemical sources rather than sunlight provided energy for emerging organisms, and bioinorganic units were vital in harnessing this energy. During the subsequent evolution of higher life forms, the special properties of transition metals as catalysts were preserved in the form of metalloenzymes which could achieve difficult feats of activation such those occurring in CO dehydrogenase and acetyl CoA synthase.⁴ As modern biochemistry evolved in the current century, metalloproteins attracted attention because of their bright colors and magnetic properties, the heme proteins providing especially good examples of these phenomena. Other, equally important, proteins which lacked these distinguishing features were sometimes overlooked, however. Urease, the first enzyme to be crystallized,⁵ contains nickel, but this fact was revealed only decades following its isolation.⁶ Today, catalysis by metal-containing enzymes is a topic of great interest, not only to provide an understanding of a specific biological function, but also because knowledge of these processes provides clues to fundamental principles of chemical reactivity, which are of potential utility in chemical industry.⁷

With the maturing of bioinorganic chemistry,⁸ it became possible to formulate general principles which together created a body of knowledge by which new phenomena could be understood. Metalloenzymes have been a prominent focus of this work and will be the topic of most of the discussion in this perspective. Apart from accelerating the rates of chemical reactions,

however, metal ions can play key structural roles in biology by effecting the long distance transfer of electrons and controlling fundamental signaling mechanisms in the cell. Moreover, several active pharmaceuticals depend on metal chemistry, examples being bleomycin and cisplatin.⁷

Metal ions are often key components of enzymes which manipulate or activate chemical units having only two to five atoms.⁹ What might be the role of the metal in such a metalloenzyme? A classical view of enzyme mechanisms holds that binding energy provides a significant amount of the rate enhancement observed in biocatalysis.¹⁰ By using binding energy, an enzyme increases the effective concentrations of reactants and holds them in the optimal position to react with one another or with a protein component. When the substrate is a large molecule, such as a carbohydrate or another protein, binding energy is afforded by multiple weak, noncovalent forces such as hydrogen bonds or hydrophobic interactions. When the substrate is dioxygen or another small molecule (Figure 1.1),^{4,11-16} this form of rate enhancement is unavailable because molecules having so few atoms cannot provide a sufficient number of such weak interactions. Instead, advantage may be taken of coordination chemistry, the binding of small substrates as ligands to metal centers, thereby effecting kinetically difficult transformations. In addition, many of the metals employed in biological systems have redox potentials within the physiological range of ± 800 mV. This characteristic, and the ability of these potentials to be tuned by the ligand environment, are exploited in the activation of several of the molecules in Figure 1.1.⁷

Redox-active metalloenzymes facilitate reactions of dioxygen because the metal can overcome the kinetic barrier imposed by the triplet ground state of O₂. Reactions of triplet oxygen with organic compounds are slow because they are spin-forbidden.¹⁷ The barrier to reactions with photochemically gen-

erated singlet oxygen is 15 kcal/mol lower in energy than that with triplet oxygen. To react with a hydrocarbon by a non-photochemical route, triplet oxygen must be converted to singlet oxygen by a radical process or must be activated by coordination to a transition metal having an incompletely filled shell of d-electrons. Because radical processes often leak toxic by-products capable of damaging organisms, many of the systems which require dioxygen employ metalloenzymes.

The discussion thus far has stressed the role of the metal in a metalloenzyme, but the amino acid side chains at the active site cannot be ignored. Proteins can use such cavities, as illustrated by the gray area in Figure 1.2, to guide substrates to the active site, orient them with respect to metal-activated species, and increase the local concentration of substrates at the reactive center. An advantage of metalloproteins over simpler coordination compounds as catalysts is that a kinetically labile and reactive moiety can be stabilized by the protein environment. These stabilizing forces are represented in Figure 1.2 by solid lines which tether metal ions to the active site cavity. Reactive intermediates, which convert to non-productive products in free solution, are sequestered within the protein environment, as symbolized in Figure 1.2 by the striped enclosure. The presence of the protein scaffolding adds an element of control to the system by facilitating interactions with other protein molecules that modulate the activity of the catalyst. It can be disadvantageous for an enzyme to produce active species indiscriminately, and protein-protein interactions can regulate the formation and quantity of such species during catalysis.

Common Themes in Small Molecule Activation

Some of the reasons nature employs metalloenzymes to activate small molecules have been discussed. Beyond these rather basic concepts, however, additional common themes are emerging as more systems are examined. In the following sections we discuss these points and illustrate them with results of studies on the soluble methane monooxygenase (sMMO) from *M. capsulatus* (Bath), carried out mainly in our laboratory. Certain of the conclusions have a generality which provide a common ground for comparing and contrasting the outcome of experiments performed on related systems.

Achievement of Kinetically Difficult Transformations. Metalloenzymes can catalyze reactions which are difficult to duplicate outside of a natural system. Even when the active site structure can be modeled, its function is frequently not achieved. There are exceptions, of course, and some of the reactions catalyzed by metalloenzymes can be carried out by non-biomimetic systems, but mimicking bioinorganic reactions remains a significant challenge.

The (sMMO) system oxidizes methane to methanol with dioxygen, as indicated in eq. 1.¹⁸⁻²⁰ In this mixed-function oxidation chemistry, one atom



of dioxygen is incorporated into substrate and the other into water. The remarkable chemical reaction occurs at a carboxylate-bridged non-heme diiron active site housed in the hydroxylase enzyme, as illustrated in Figure 1.3. The enzyme releases methanol before further oxidation can occur. For methane-

requiring bacteria which employ sMMO, the reaction supplies both carbon and energy.^{18,21} These methanotrophs and others like them play an important role in the global carbon cycle, preventing most of the methane produced by anaerobic microflora from reaching the atmosphere, where it contributes to the greenhouse effect, and recycling it back into the biosphere.²² Methanotrophic bacteria have been used to remove oil spills from contaminated beaches and to degrade haloalkane contaminants in drinking water.²³

The carboxylate-bridged diiron centers in sMMO activate two small molecules, dioxygen and methane, to achieve a reaction which cannot be duplicated industrially except at high temperatures and pressures.²⁴ The conversion of methane to methanol is desirable because most of the abundant sources of natural gas are located in remote areas, and transport of a combustible gas poses significant problems. Conversion to methanol is economically competitive with shipping liquefied natural gas, even with the present inefficient conversion processes. The transformation of methane to methanol involves first its conversion to syngas by desulfurization followed by steam reforming (eq 2), a process requiring temperatures in excess of 800 °C.



Syngas is then converted into methanol at 200-300 °C and 50-100 atm. Methods being developed for the direct oxidation of methane to methanol currently produce only very low yields of the desired product. If such methods could be improved, the liquefaction of methane would accrue significant economic benefits.

Apart from its industrial potential, the selective activation of unactivated carbon-hydrogen bonds in homogeneous solution was recently identi-

fied as one of the “Holy Grails” of modern chemistry.²⁵ Attempts to achieve this transformation have typically failed by virtue of their inability to mimic one or more of the steps in the biological oxidation of methane by sMMO. Some reactions are not catalytic, others require *tert*-butylhydroperoxide or another active oxygen source other than O₂, and still others demand high temperatures (>100 °C) and pressures (>50 atm). Many simply cannot oxidize methane or they oxidize it beyond the level of methanol. Recently, methane was oxidized to methanol by using dioxygen at 40 °C.^{26,27} The best catalytic system, a EuCl₃-Zn-CF₃CO₂H-TiO₂ system, converted methane to methanol with a turnover number of about 0.003 s⁻¹.²⁷ The sMMO enzyme from *M. capsulatus* (Bath) performs the reaction with a turnover number of ≥ 0.19 s⁻¹.²⁸

Multi-Protein Enzyme Systems. Like many bioinorganic systems, sMMO is a multi-protein construct. Our group focuses on sMMO from *Methylococcus capsulatus* (Bath), a strain native to the thermal springs at Bath, England, whereas other laboratories investigate material isolated from another bacterial strain, *Methylosinus trichosporium* OB3b.^{19,20} The sMMO from *M. capsulatus* (Bath) has been resolved into three constituent proteins.²⁹ The hydroxylase is a dimeric 251 kDa enzyme (MMOH) having α₂β₂γ₂ stoichiometry with one non-heme diiron active site in each α subunit.³⁰ Its x-ray crystal structure^{14,31,32} revealed the active site and overall protein structure shown schematically in Figure 1.3. A second component protein is a 38.5 kDa reductase (MMOR) which contains an Fe₂S₂ cluster and an FAD moiety which accepts electrons in the form of hydride ion from NADH.^{29,33,34} A 16 kDa coupling protein, designated protein B (MMOB),³⁵ couples consumption of electrons by the reductase with reduction of the diiron centers in the hydroxylase, preparing them for reaction with dioxygen

and, ultimately, productive hydroxylation of the substrate. Binding of protein B to the hydroxylase affects the active site geometry, the regioselectivity of oxidation, and the lifetime of intermediates observed spectroscopically in single turnover reactions (*vide infra*).³⁶

The compartmentalization of functions among the three proteins regulates the system at several levels. If the hydroxylase active sites were to react directly with NADH, this reducing agent might be consumed in the absence of substrate, undergoing non-productive futile reaction cycles with dioxygen to make water or perhaps hydrogen peroxide. Early evidence that component protein interactions regulate the system was the discovery that the resting state Fe(III)Fe(III) hydroxylase could be titrated with electrons to yield the mixed valent Fe(II)Fe(III) and fully reduced Fe(II)Fe(II) forms,³⁷ but that, in a reconstituted system containing MMOH, MMOR, MMOB, and substrate, the potential for transfer of the second electron became more positive than for the first.³⁴ As a consequence, the diiron site was reduced by two electrons from the diferric directly to the diferrous state, forming little or none of the non-physiologically active mixed valent Fe(II)Fe(III) form. Recently, the reductase was identified as the component responsible for this behavior, and remarkably, it could exert the effect when present at only 10% of the concentration of active sites.³⁸ These and other experiments indicate that the MMOB and MMOR components help maintain exquisite control of the catalytic activity of the dinuclear iron active sites in MMOH.

Electron Transfer Over a Distance. A significant property of metal ions is their ability to undergo reversible electron transfer reactions at physiologically relevant potentials. In bioinorganic systems in which redox catalysis is employed, electrons are often transported over long distances (>10 - 20 Å)

such that sites of reduction and oxidation can be widely separated. The donor and acceptor sites can even be in different proteins in a multi-component system, as discussed in the previous section, requiring long range electron transfer between protein molecules. The pathway of electron transfer from donor to acceptor through and between protein molecules has also been the subject of intense experimental and theoretical scrutiny, with attention focused on the question of whether through-bond or through-space movements are more likely to be involved.³⁹

As mentioned earlier, the initial electron acceptor from the NADH molecule in sMMO is MMOR. This protein in turn reduces the hydroxylase, poisoning it to react with dioxygen. Exactly how MMOH and MMOR interact and how electrons access the diiron active sites remain unresolved. As of this writing, no crystal structures of complexes between sMMO components are available, although chemical cross-linking studies have indicated that MMOR binds to the β subunit of MMOH.⁴⁰ To address this question further, the MMOH crystal structures were systematically examined to identify putative sites of protein-protein interaction.⁴¹ In this analysis, it was hypothesized that extended helix-helix contacts between two individual hydroxylase molecules in a crystal lattice might mimic contacts between MMOH and either of its partner proteins, MMOB and MMOR. Interacting regions having more than three helical turns were analyzed to determine whether they shared homology with sequences in MMOB and MMOR. One eleven-amino-acid sequence in domain 2 of the α subunit of MMOH³¹ displayed homology to a region of MMOR. This peptide was synthesized and added to a kinetic assay of MMO activity which it inhibited with an IC_{50} corresponding to a K_d value of $< 100 \mu\text{M}$. By using the structure of a homologous reductase, a binding model was developed for the interaction between MMOH and MMOR, which if

correct would help to identify the point of initiation of electron transfer into the hydroxylase.

Access to the MMOH Active Sites. The three-dimensional structure of a metalloenzyme, determined by x-ray crystallographic or NMR spectroscopic methods, reveals the position and geometry of the active site. When the metal core is buried within the protein matrix, it is interesting to inquire how the substrates reach the active site and by what pathway products depart.

The sMMO hydroxylase can oxidize a broad range of substrates, including alkanes, alkenes, ethers, amines, and halocarbons.⁴²⁻⁴⁷ The binding of these different substrates in the vicinity of the diiron centers in the α subunits was considered following the determination of the MMOH x-ray crystal structure.^{31,41} Hydrophobic pockets were identified in a chain leading from the very hydrophobic cavity right at the active site, cavity 1, and extending outward through domain 1 of the α subunit toward the protein surface (Figure 1.4).³¹ The cavities were not connected into a channel, however. For example, in the first structure analyzed the cavity adjacent to the active site, cavity 2 in Figure 1.4, was partitioned from cavity 1 by side chains of a leucine, a phenylalanine and a threonine residue. Similar side chain contacts separated other pairs of adjacent cavities from one another. In more recent experiments, xenon gas was used as a probe for putative methane binding pockets in MMOH. Xenon has same size as methane but, owing to its high electron density, is much more readily identified by x-ray crystallography. When MMOH crystals were pressurized with Xe gas, a well-ordered xenon atom was found in cavity 2.⁴¹ In other forms of the crystal, including one grown from solutions containing MMOB, the leucine residue blocking access to cavity 1 from cavity 2 had an altered side chain conformation such as to

open a connection between the two cavities.^{41,48} This so-called "leucine gate" was also in the open position in crystals where the diiron center had been chemically reduced to the Fe(II)Fe(II) state. The leucine gate thus appears to regulate substrate access to the active site, and may represent one way in which protein-protein interactions might control the chemistry at the catalytic iron center. For example, dioxygen or methane might be excluded from the active site until the gate opens, a process which could be triggered by binding of one of the other protein components and/or reduction of the hydroxylase diiron centers.

Theoretical calculations have also been used to identify possible sites of substrate binding to MMOH. One study⁴⁹ used a docking methodology and energy minimization which combined Monte Carlo and molecular dynamics techniques. Several putative binding sites were identified, with the favored ones depending mostly on the size of the substrate. A site corresponding to cavity 1 (Figure 1.4) was favored by small substrates such as methane. Two other sites displayed favorable interactions with larger substrates and were located in pockets at or near the protein surface, somewhat removed from the active site. None of the sites was the one occupied by Xe in the crystal structure experiment.⁴¹ Studies of this kind do not address the dynamics of substrate binding to the active site, and it is not obvious how substrates would make their way to the catalytic center without movement of protein side chains.

Substrate Selectivity and Diagnostic Probes. Bioinorganic catalysts act upon a selected set of substrates, accelerating the rate of the desired chemical transformation. The attendant selectivity and rate enhancement may reflect the steric requirements of a substrate binding pocket and the power of the ac-

tive species generated in the catalytic reaction cycle. The wide range of substrates oxidized by the soluble MMO systems,⁴³ for example, contrasts with the relatively narrow set of molecules which can be hydroxylated by the copper-containing particulate MMO (pMMO) hydroxylase.⁵⁰ Both will oxidize methane, which has a C–H bond energy of 104 kcal/mol, and release the product without further oxidation, despite the fact that the C–H bond strength of methanol is only 94 kcal/mol.⁵¹ Mechanistic proposals must account for these properties. Since hydroxylating species in both sMMO and pMMO must be sufficiently powerful to be able to oxidize methane, one might therefore surmise that the active site of the latter is smaller to account for its more stringent substrate specificity. Both must be sufficiently hydrophobic such that methanol is extruded before further oxidation can occur. The hydrophobic character of the active site of sMMOH has already been established from the x-ray crystal structure determination.³¹

The ability of sMMO to oxidize a wide range of substrates has enabled the use of diagnostic substrate probes to delineate aspects of the enzyme mechanism. Such probes were used extensively in mechanistic studies of cytochrome P-450, the heme iron analog of sMMO.⁵² Radical clock substrate probes are molecules that contain strained rings which open if radical intermediates are formed during the course of an oxidation reaction (Figure 1.5A). When the rate constant for the ring opening step is known, the lifetime of the putative radical intermediates can be estimated from the ratio of acyclic to cyclic products obtained in the reaction. The oxidation of such probes by the cytochrome P-450 enzyme system has been used as evidence to support the widely accepted radical rebound mechanism,⁵² although recent work has questioned this interpretation.⁵³ Radical clock substrate probes applied in the sMMO system revealed no or only very small amounts of ring opened prod-

ucts with *M. trichosporium* sMMO^{45,46} and none for the *M. capsulatus* sMMO enzyme.^{46,47} These results suggested either formation of a radical species with an exceedingly short lifetime ($\tau < 10^{13}$ s) or no substrate radical at all during the course of the hydroxylation reaction.⁴⁶

Both sMMO systems have been probed mechanistically by using alkanes made chiral through the use of the three isotopes of hydrogen.^{54,55} If a substrate radical were to form upon activation of $^1\text{H}^2\text{H}^3\text{HC}-\text{CH}_3$, for example, rotation about the C-C bond in the resulting ethyl radical before recombination would give rise to inverted products (Figure 1.5B). The rate of this rotation can be calculated at a given temperature from transition state theory and the free energy for the process. As in the case of the radical clock substrate probes, the product distribution can be used to compute a rate constant for a putative radical rebound step. If a very long-lived radical develops, racemization will occur, whereas fully concerted processes will give rise either to complete retention or complete inversion. The sMMO systems from both *M. capsulatus* (Bath) and *M. trichosporium* OB3b yielded ~30% inverted products when chiral ethane was employed as the substrate, and even less when the butane analog was used. In the case of *M. trichosporium* OB3b, the presence of inverted products was interpreted as evidence for a very short lived alkyl radical intermediate.⁵⁴ For the *M. capsulatus* (Bath) enzyme, the calculated radical lifetime of less than 100 femtoseconds was deemed too short to support a radical intermediate, and a nonsynchronous concerted mechanism was invoked instead.⁵⁵ The question of whether or not discrete substrate radicals are formed during the course of sMMO oxidations remains a topic of debate.

Detailed Steps in the Catalytic Mechanism. When a catalytic reaction can be synchronized so that all of the active sites undergo the same transformations simultaneously, transient kinetics can be employed to identify possible intermediate species. In this manner, the discrete steps between the initiation of a reaction and return to the enzyme resting state can be defined. Metalloenzymes are often amenable to such studies because spectroscopy often can be applied to probe the existence of intermediates as well as stable states.⁹ Charge transfer or d-d electronic transitions enable the use of UV/visible spectroscopy, and when excitation of one of these electronic bands enhances a vibrational mode, resonance Raman spectra can be obtained. Unpaired electrons at the metal center allow the use of electron paramagnetic (EPR) and other more advanced magnetic resonance techniques. Mössbauer spectroscopy provides valuable insight into the oxidation state and electronic environment of iron proteins, in particular. X-ray absorption spectroscopy can provide information about oxidation state and geometry of the metal. Information about meta-stable intermediates is helpful in constructing the detailed reaction cycle of a metalloenzyme and guides the synthesis of spectroscopic and functional models.

For sMMO, the hydroxylase can be chemically reduced in an anaerobic environment. When MMOB is added and the resulting solution mixed rapidly with dioxygen in the absence of substrate, several intermediate species are observed.³⁶ The single turnover reaction can be monitored continuously, by using stopped-flow spectroscopy, or discontinuously, with freeze-quench methodology. Experiments of this kind led to the postulated existence of an early intermediate in the reaction cycle of MMOH from *M. trichosporium* OB3b,⁵⁶ and this species was directly observed in subsequent studies of the *M. capsulatus* (Bath) proteins. In a series of freeze-quench Mössbauer experi-

ments, the intermediate was determined to attain its maximum concentration 156 ms after mixing.⁵⁷ The isomer shift ($\delta = 0.66$ mm/s) suggested a diferric site and later stopped-flow UV/visible spectroscopic experiments accumulated additional evidence that the species was a (μ -1,2-peroxo) diiron(III) complex, designated H_{peroxo} or P.^{58,59} In particular, it had an optical absorption band with $\lambda_{\text{max}} \sim 725$ nm. Several possible symmetric diferric peroxo structures for H_{peroxo} are depicted in Figure 1.6A-C. Shortly after the peroxo intermediate was identified in MMOH, three model compounds featuring (μ -1,2-peroxo)diiron(III) cores were crystallographically characterized,⁶⁰⁻⁶² all having spectral features similar to those of the protein intermediate. In two of the three complexes,^{61,62} the Fe-O-O-Fe dihedral angles were approximately 0° , resembling the structure in Figure 1.6B. In the third, however, the conformation of the peroxo unit more closely resembled bridging mode C in Figure 1.6, with a dihedral angle of 53° .⁶⁰ The single quadrupole doublet in its Mössbauer spectrum and isomer shift were nearly identical to the corresponding values in H_{peroxo} . Because of the close match in Mössbauer parameters, this bridging mode is the one currently favored as that most likely to occur in H_{peroxo} .

The nature of intermediates in the MMOH reaction cycle has been probed by various theoretical methods. An approximate extended Hückel calculation interrogated structures for the peroxo intermediate,^{63,64} the one of lowest energy being the μ -1,2-peroxo binding mode of Figure 1.6C. Methane did not interact favorably with the peroxo intermediate in any of the binding modes investigated. Density functional theory (DFT) has also been employed to investigate the sMMO oxidation mechanism.⁶⁵ The lowest energy structure for the peroxo intermediate was similar to that favored by the extended

Hückel calculations, but with one iron atom experiencing η^2 character with respect to peroxide ligand (Figure 1.6D).

Despite the availability of several structural and spectroscopic models for the diiron(III) peroxo intermediate of sMMO, none exhibits properties that mimic its functional chemistry. Such a species should, like the enzyme active site, spontaneously convert to intermediates observed later in the catalytic cycle and/or selectively hydroxylate alkanes. Instead, without the protective scaffolding afforded by the protein, the peroxo complexes are metastable and decay mainly by nonproductive bimolecular pathways.^{66,67} Complexes with more steric protection show more promise.⁶⁸ The formation of an active hydroxylating species from a diferric peroxo intermediate remains a major goal of this field.

In the protein system, H_{peroxo} spontaneously converts to a bright yellow intermediate known as Q, which has been extensively studied by Mössbauer ($\delta = 0.21$ mm/s, $\Delta E_Q = 0.68$ mm/s and $\delta = 0.14$ mm/s, $\Delta E_Q = 0.55$ mm/s) and optical spectroscopy ($\lambda_{\text{max}} = 350$ and 420 nm).^{36,56,69} These spectral properties suggest a diamagnetic, high valent iron(IV) oxo species but offer no unique interpretation. A recent extended X-ray absorption fine structure (EXAFS) experiment provided evidence for a 2.45 Å Fe··Fe distance in Q from *M. trichosporium* OB3b, together with two 1.77 Å Fe–O bonds.⁶⁹ The former distance is short and suggests multiple single atom bridges linking the iron atoms. The Fe–O bond lengths are consistent with either Fe(III) or Fe(IV) oxidation levels. The EXAFS results were interpreted as evidence for a di(μ -oxo)diiron(IV) rhombus like the one illustrated in Figure 1.6F, but other structures are equally likely.

The nature of intermediate Q has also been investigated by extended Hückel theory.^{63,64} A di(μ -oxo) structure like the one just discussed⁶⁹

interacted repulsively with methane and therefore was excluded as the active hydroxylating species. Instead, a five-coordinate ferryl intermediate was preferred that interacted with methane, distorting it into a geometry having C_{3v} symmetry and an Fe–C bond. In the DFT calculations,⁶⁵ the di(μ -oxo)diiron(IV) structure was invoked as being on the pathway, but was not considered to be the likely activator of substrate. Instead, this configuration was proposed to rearrange into an Fe(III)-O-Fe(IV)-O \cdot species (Figure 1.6I), which would react with methane by hydrogen atom abstraction and Fe–C bond formation. These issues must be resolved because, if there is to be any hope of producing functional models of enzymatic systems, we must understand the transient intermediates, what causes them to form, and what chemistry they can achieve.

Intermediate Q is widely held to be the one which reacts with substrate to form product. Its decay is accelerated by addition of substrate,^{36,59} and several intermediates following Q in the reaction cycle have been postulated.²⁰ A product-bound intermediate has been observed by optical spectroscopy for the reaction of nitrobenzene with *M. trichosporium* OB3b hydroxylase.⁵⁶ Once Q delivers its oxidizing equivalents to substrate, the diiron center returns to the Fe(III)Fe(III) resting state. In the absence of additional reducing equivalents in the form of NADH/MMOR or another reductant, the single turnover experiment is concluded. The *M. capsulatus* (Bath) catalytic cycle showing the intermediates thus far identified is depicted schematically in Figure 1.7.

The identification of intermediates on the catalytic pathway is key to understanding all metalloenzymes. Because many small molecule substrates have strong or multiple bonds, very reactive species may be required for their activation. In order for a spectroscopically identified species to qualify as an

intermediate on the catalytic pathway, it must be both catalytically and chemically competent. Catalytic competence requires that the observed transient appear and convert on a time scale fast enough for it to account for product accumulation. This criterion requires study of the system under steady-state conditions. In the present example, the turnover number for methane has been reported to be 0.19 s^{-1} ,²⁸ and a more recent determination suggests a value of 0.6 s^{-1} .⁷⁰ No step can occur more slowly than this limiting value, and postulated mechanisms which include slower steps can be discounted. The second criterion, that of chemical competence, means that the observed intermediate can effect the transformation attributed to it. Comparisons with known model chemistry can help to assure chemical competence, as can well-executed theoretical calculations.

Conclusions

Significant progress has been made in understanding how the soluble methane monooxygenase system achieves the hydroxylation of methane under physiological conditions. Through application of a wide range of methodologies from both biochemistry and inorganic chemistry, we now know the three-dimensional structure of the hydroxylase enzyme, the nature of key intermediates in the reaction cycle, and aspects of how the three protein components interact and regulate the system. Several issues remain unresolved, however. We should like to understand more fully the mechanisms which control the selectivity of hydrocarbon oxidation, determine the structures of the MMOB and MMOR components and complexes between all three proteins, uncover how substrates and products traverse the protein matrix into and out of the active site, and probe the mechanism by which different substrates react. The nature of the existing intermediates is not fully

understood and, especially, the key C–H bond cleavage and C–O bond-forming steps are unknown. Finally, we should also like to be able to mimic the alkane hydroxylation chemistry with small molecule synthetic analogs.

What features of the sMMO system are likely to be shared by other metalloproteins that activate small molecules? Coordinative unsaturation and unusual oxidation states observed in the reduced hydroxylase and intermediate Q are two properties that are likely to be of more general consequence. The control of the system by multi-protein interactions, and the separation of electron transfer from substrate activation units on different proteins, should also find common ground among the systems that achieve some of the other functions illustrated in Figure 1.1. Formation of reactive intermediates, and protection of those intermediates by the protein environment, may also be recurring features of these systems. Specific mechanisms that recruit small substrates to the active sites will be better defined with additional macromolecular structure determinations.

Enough work has now been done in the area of bioinorganic enzymology to define it as a distinct field, to fill textbooks and special issues of journals, and to begin to identify common themes. Still, many key problems in the field are far from being solved. The perspective in five years time should look quite different.

References

- (1) This work was already published in a slightly different form. See reference 2.
- (2) Valentine, A. M.; Lippard, S. J. *J. Chem. Soc., Dalton Trans.* **1997**, *21*, 3925-3931.
- (3) Huber, C.; Wächtershäuser, G. *Science* **1997**, *276*, 245-247.
- (4) Ragsdale, S. W.; Kumar, M. *Chem. Rev.* **1996**, *96*, 2515-2540.
- (5) Sumner, J. B. *J. Biol. Chem.* **1926**, *69*, 435-441.
- (6) Dixon, N. E.; Gazzola, C.; Blakeley, R. L.; Zerner, B. *J. Am. Chem. Soc.* **1975**, *97*, 4131-4133.
- (7) Lippard, S. J.; Berg, J. M. *Principles of Bioinorganic Chemistry*; University Science Books: Mill Valley, CA, 1994.
- (8) Lippard, S. J. *Science* **1993**, *261*, 699-700.
- (9) Holm, R. H.; Kennepohl, P.; Solomon, E. I. *Chem. Rev.* **1996**, *96*, 2239-2314.
- (10) Jencks, W. A. *Adv. Enzymol.* **1975**, *43*, 219-410.
- (11) Thauer, R. K.; Klein, A. R.; Hartmann, G. C. *Chem. Rev.* **1996**, *96*, 3031-3042.
- (12) Ferguson-Miller, S.; Babcock, G. T. *Chem. Rev.* **1996**, *96*, 2889-2907.
- (13) Averill, B. A. *Chem. Rev.* **1996**, *96*, 2951-2964.
- (14) Rosenzweig, A. C.; Nordlund, P.; Takahara, P. M.; Frederick, C. A.; Lippard, S. J. *Chem. Biol.* **1995**, *2*, 409-418.
- (15) Yachandra, V. K.; Sauer, K.; Klein, M. P. *Chem. Rev.* **1996**, *96*, 2927-2950.
- (16) Howard, J. B.; Rees, D. C. *Chem. Rev.* **1996**, *96*, 2965-2982.
- (17) Kappock, T. J.; Caradonna, J. P. *Chem. Rev.* **1996**, *96*, 2659-2756.
- (18) Liu, K. E.; Lippard, S. J. In *Advances in Inorganic Chemistry*; Sykes, A. G., Eds.; Academic Press: San Diego, 1995; Vol. 42; pp 263-289.

- (19) Lipscomb, J. D. *Annu. Rev. Microbiol.* **1994**, *48*, 371-399.
- (20) Wallar, B. J.; Lipscomb, J. D. *Chem. Rev.* **1996**, *96*, 2625-2657.
- (21) Anthony, C. *The Biochemistry of Methylophs*; Academic Press: New York, 1982, p 296-379.
- (22) Higgins, I. J.; Best, D. J.; Hammond, R. C. *Nature* **1980**, *286*, 561-564.
- (23) Bragg, J. R.; Prince, R. C.; Harner, E. J.; Atlas, R. M. *Nature* **1994**, *368*, 413-418.
- (24) *Methanol Production and Use*; Cheng, W.-H.; Kung, H. H., Ed.; Marcel Dekker: New York, 1994.
- (25) Arndsten, B. A.; Bergman, R. G.; Mobley, T. A.; Peterson, T. H. *Acc. Chem. Res.* **1995**, *28*, 154-162.
- (26) Yamanaka, I.; Soma, M.; Otsuka, K. *J. Chem. Soc., Chem. Commun.* **1995**, *95*, 2235-2236.
- (27) Yamanaka, I.; Soma, M.; Otsuka, K. *Chem. Lett.* **1996**, 565-566.
- (28) Green, J.; Dalton, H. *Biochem. J.* **1986**, *236*, 155-162.
- (29) Colby, J.; Dalton, H. *Biochem. J.* **1978**, *171*, 461-468.
- (30) Woodland, M. P.; Dalton, H. *J. Biol. Chem.* **1984**, *259*, 53-59.
- (31) Rosenzweig, A. C.; Frederick, C. A.; Lippard, S. J.; Nordlund, P. *Nature* **1993**, *366*, 537-543.
- (32) Rosenzweig, A. C.; Lippard, S. J. *Acc. Chem. Res.* **1994**, *27*, 229-236.
- (33) Colby, J.; Dalton, H. *Biochem. J.* **1979**, *177*, 903-908.
- (34) Liu, K. E.; Lippard, S. J. *J. Biol. Chem.* **1991**, *266*, 12836-12839.
- (35) Green, J.; Dalton, H. *J. Biol. Chem.* **1985**, *260*, 15795-15801.
- (36) Liu, K. E.; Valentine, A. M.; Wang, D.; Huynh, B. H.; Edmondson, D. E.; Salifoglou, A.; Lippard, S. J. *J. Am. Chem. Soc.* **1995**, *117*, 10174-10185.
- (37) Woodland, M. P.; Patil, D. S.; Cammack, R.; Dalton, H. *Biochim. Biophys. Acta* **1986**, *873*, 237-242.

- (38) Liu, Y.; Nesheim, J. C.; Paulsen, K. E.; Stankovich, M. T.; Lipscomb, J. D. *Biochemistry* **1997**, *36*, 5223-5233.
- (39) Gray, H. B.; Winkler, J. R. *Ann. Rev. Biochem.* **1996**, *65*, 537-561.
- (40) Fox, B. G.; Liu, Y.; Dege, J. E.; Lipscomb, J. D. *J. Biol. Chem.* **1991**, *266*, 540-550.
- (41) Rosenzweig, A. C.; Brandstetter, H.; Whittington, D. A.; Nordlund, P.; Lippard, S. J.; Frederick, C. A. *Proteins* **1997**, *29*, 141-152.
- (42) Colby, J.; Stirling, D. I.; Dalton, H. *Biochem. J.* **1977**, *165*, 395-402.
- (43) Green, J.; Dalton, H. *J. Biol. Chem.* **1989**, *264*, 17698-17703.
- (44) Fox, B. G.; Borneman, J. G.; Wackett, L. P.; Lipscomb, J. D. *Biochemistry* **1990**, *29*, 6419-6427.
- (45) Ruzicka, F.; Huang, D.-S.; Donnelly, M. I.; Frey, P. A. *Biochemistry* **1990**, *29*, 1696-1700.
- (46) Liu, K. E.; Johnson, C. C.; Newcomb, M.; Lippard, S. J. *J. Am. Chem. Soc.* **1993**, *115*, 939-947.
- (47) Choi, S.-Y.; Eaton, P. E.; Hollenberg, P. F.; Liu, K. E.; Lippard, S. J.; Newcomb, M.; Putt, D. A.; Upadhyaya, S. P.; Xiong, Y. *J. Am. Chem Soc.* **1996**, *118*, 6547-6555.
- (48) Whittington, D. A.; Lippard, S. J. unpublished results.
- (49) George, A. R.; Wilkins, P. C.; Dalton, H. *J. Mol. Cat. B* **1996**, *2*, 103-113.
- (50) Smith, D. D. S.; Dalton, H. *Eur. J. Biochem.* **1989**, *182*, 667.
- (51) *CRC Handbook of Chemistry and Physics*; 64 ed.; Weast, R. C., Ed.; CRC Press, Inc.: Boca Raton, Florida, 1983.
- (52) Ortiz de Montellano, P. R. In *Cytochrome P450: Structure, Mechanism, and Biochemistry*; 2nd ed.; Ortiz de Montellano, P. R., Eds.; Plenum Press: New York, 1995; pp 245-303.

- (53) Newcomb, M.; Le Tadic-Biadatti, M.-H.; Chestney, D. L.; Roberts, E. S.; Hollenberg, P. F. *J. Am. Chem. Soc.* **1995**, *117*, 12085-12091.
- (54) Priestley, N. D.; Floss, H. G.; Froland, W. A.; Lipscomb, J. D.; Williams, P. G.; Morimoto, H. *J. Am. Chem. Soc.* **1992**, *114*, 7561-7562.
- (55) Valentine, A. M.; Wilkinson, B.; Liu, K. E.; Komar-Panicucci, S.; Priestley, N. D.; Williams, P. G.; Morimoto, H.; Floss, H. G.; Lippard, S. J. *J. Am. Chem. Soc.* **1997**, *119*, 1818-1827.
- (56) Lee, S.-K.; Nesheim, J. C.; Lipscomb, J. D. *J. Biol. Chem.* **1993**, *268*, 21569-21577.
- (57) Liu, K. E.; Wang, D.; Huynh, B. H.; Edmondson, D. E.; Salifoglou, A.; Lippard, S. J. *J. Am. Chem. Soc.* **1994**, *116*, 7465-7466.
- (58) Liu, K. E.; Valentine, A. M.; Qiu, D.; Edmondson, D. E.; Appelman, E. H.; Spiro, T. G.; Lippard, S. J. *J. Am. Chem. Soc.* **1995**, *117*, 4997-4998; Correction **1997**, *119*, 11134.
- (59) Valentine, A. M.; Lippard, S. J. unpublished results.
- (60) Kim, K.; Lippard, S. J. *J. Am. Chem. Soc.* **1996**, *118*, 4914-4915.
- (61) Ookubu, T.; Sugimoto, H.; Nagayama, T.; Masuda, H.; Sato, T.; Tanaka, K.; Madea, Y.; Okawa, H.; Hayashi, Y.; Uehara, A.; Suzuki, M. *J. Am. Chem. Soc.* **1996**, *118*, 701-702.
- (62) Dong, Y.; S., Y.; Young, V. G. J.; Que, L. J. *Angew. Chem. Int. Ed. Engl.* **1996**, *35*, 618-620.
- (63) Yoshizawa, K.; Hoffmann, R. *Inorg. Chem.* **1996**, *35*, 2409-2410.
- (64) Yoshizawa, K.; Yamabe, T.; Hoffmann, R. *New J. Chem.* **1997**, *21*, 151-161.
- (65) Siegbahn, P. E. M.; Crabtree, R. H. *J. Am. Chem. Soc.* **1997**, *119*, 3103-3113.

- (66) Feig, A. L.; Becker, M.; Schindler, S.; Eldik, R. v.; Lippard, S. J. *Inorg. Chem.* **1996**, *35*, 2590-2601.
- (67) Feig, A. L.; Masschelein, A.; Bakac, A.; Lippard, S. J. *J. Am. Chem. Soc.* **1997**, *119*, 334-342.
- (68) LeCloux, D. D.; Barrios, A. M.; Mizoguchi, T. J.; Lippard, S. J. *J. Am. Chem. Soc.* **1998**, in press.
- (69) Shu, L.; Nesheim, J. C.; Kauffmann, K.; Münck, E.; Lipscomb, J. D.; Que, L., Jr. *Science* **1997**, *275*, 515-518.
- (70) Gassner, G. T.; Lippard, S. J. submitted for publication.

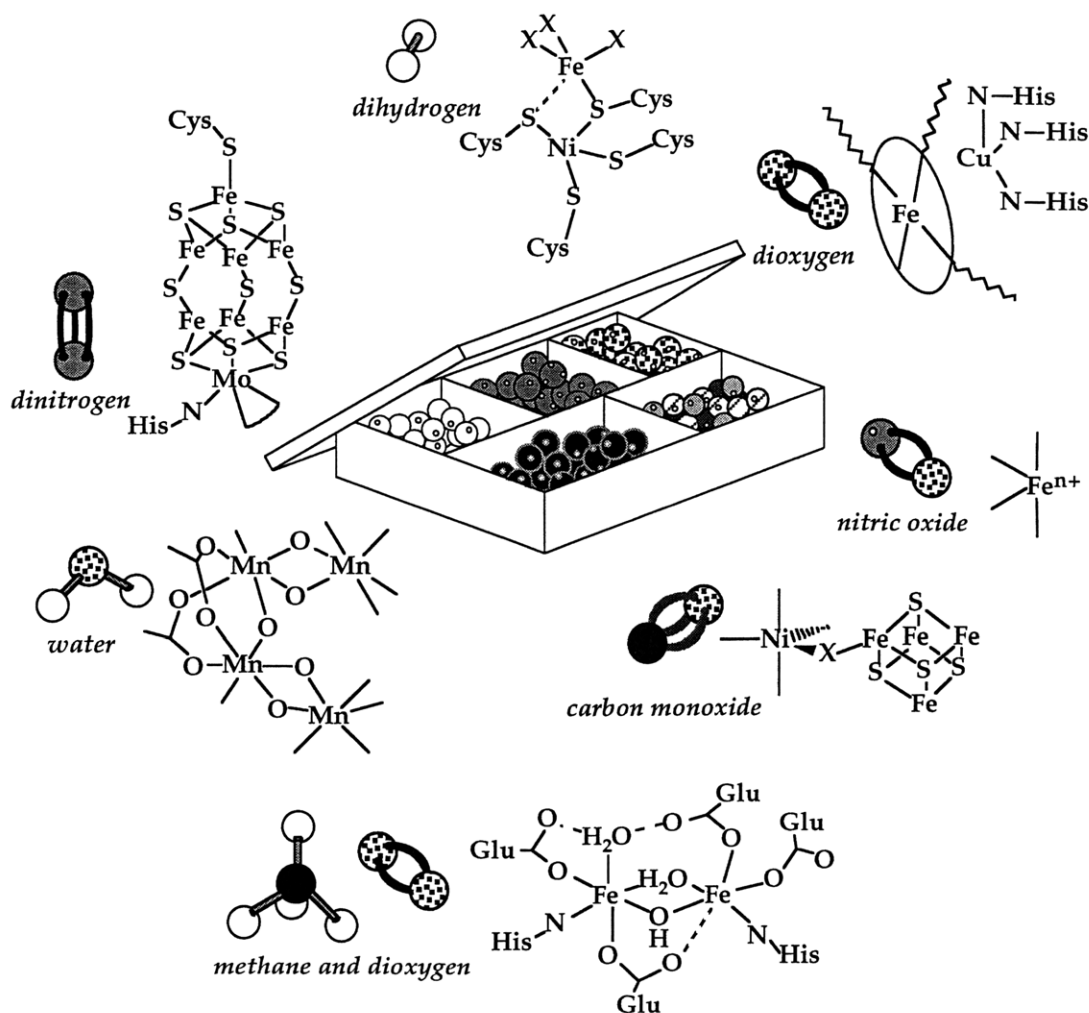


Figure 1.1. Small molecules activated by metalloenzymes. Clockwise from top: H_2 and the active site of hydrogenase;¹¹ O_2 and the heme $a_3\text{-Cu}_B$ site of cytochrome c oxidase;¹² NO and a model for the mononuclear iron active site of nitric oxide reductase;¹³ CO and the nickel-iron-sulfur center of carbon monoxide dehydrogenase/acetyl CoA synthase;⁴ CH_4 , O_2 , and the non-heme diiron active site of methane monooxygenase;¹⁴ H_2O and a proposed model for the oxygen-evolving complex of photosystem II;¹⁵ and N_2 and the iron-molybdenum cofactor of nitrogenase.¹⁶

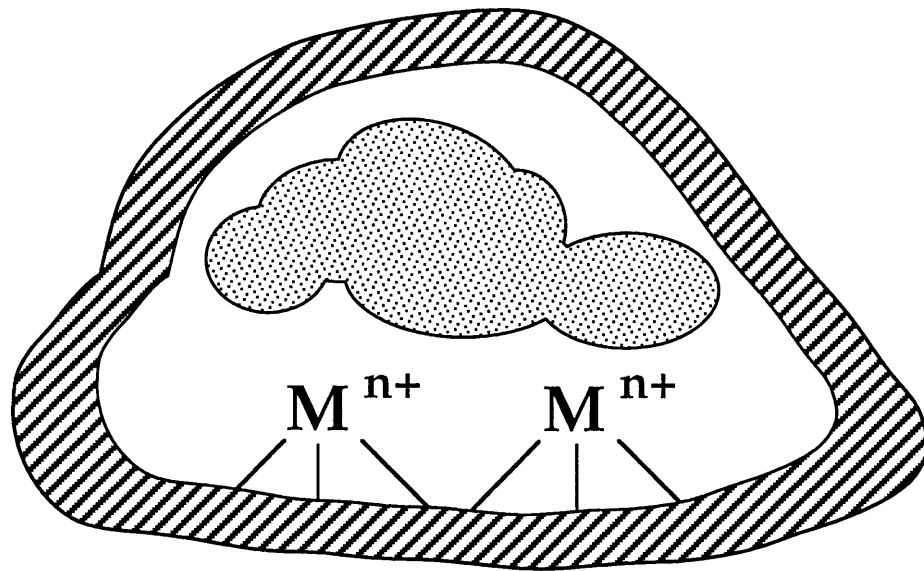


Figure 1.2. Schematic representation of a metalloprotein active site. The protein construct stabilizes kinetically labile metals (forces represented by lines), sequesters active intermediates (barrier shown by striped bar), and provides a substrate binding site (depicted in gray).

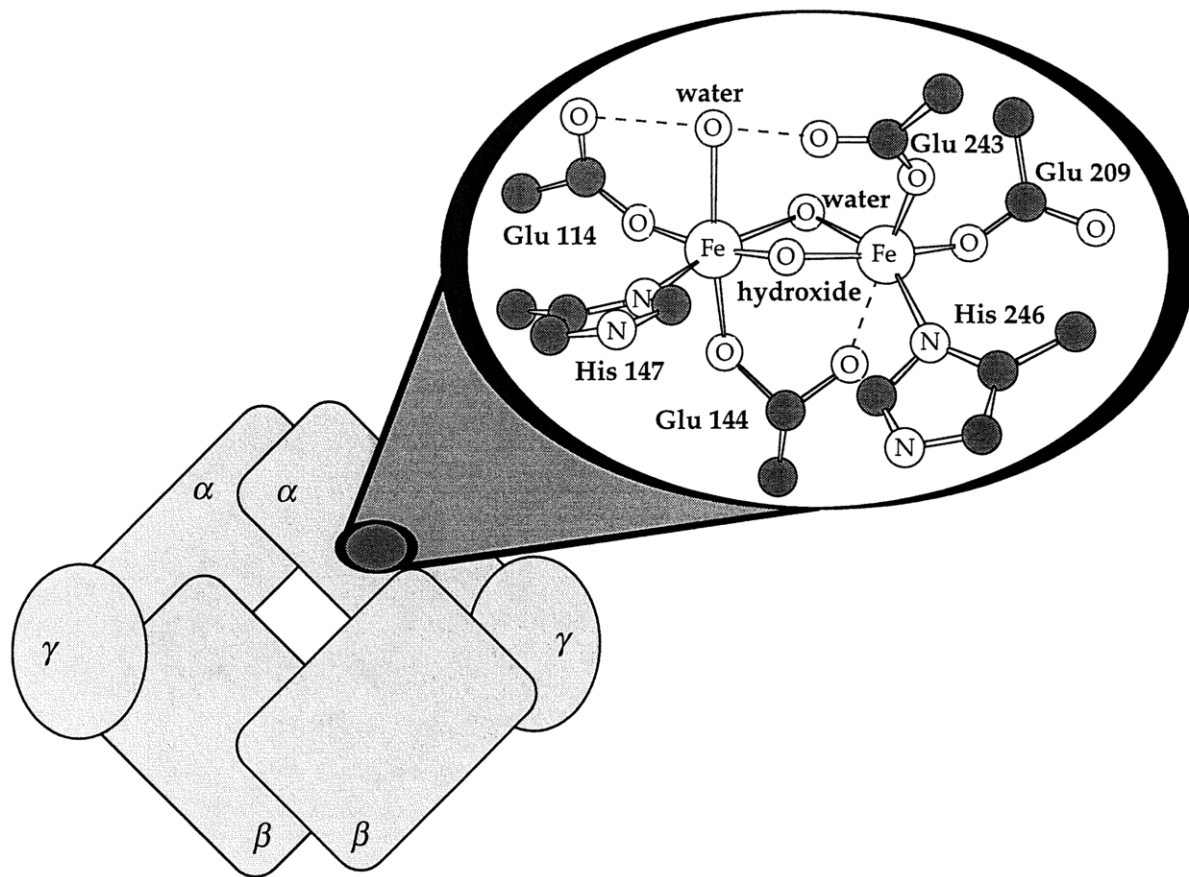


Figure 1.3. View of the non-heme diiron active site housed in the α subunit of the sMMO hydroxylase enzyme. This diferric active site structure was determined at $-160\text{ }^{\circ}\text{C}$.¹⁴



Figure 1.4. The α subunit of sMMO hydroxylase showing the hydrophobic cavities leading from the active site (cavity 1) to the protein surface (cavity 3). Iron atoms are depicted as striped spheres.

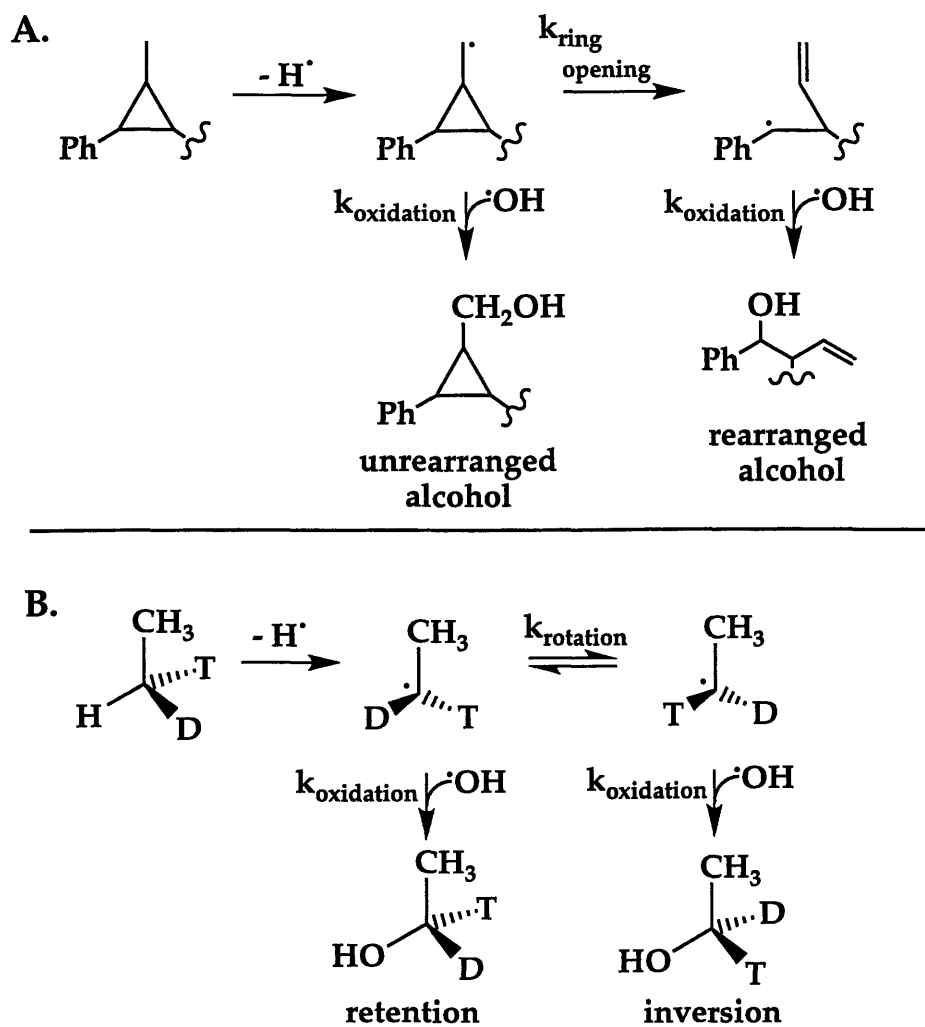


Figure 1.5. (A) Ring opening of a radical clock substrate probe. If hydrogen atom abstraction occurs, hydroxylation competes with ring opening, giving rise to cyclic and acyclic products. (B) Oxidation of chiral tritiated ethane. If a radical is formed, rotation about the C-C bond results in products displaying retention or inversion of configuration.

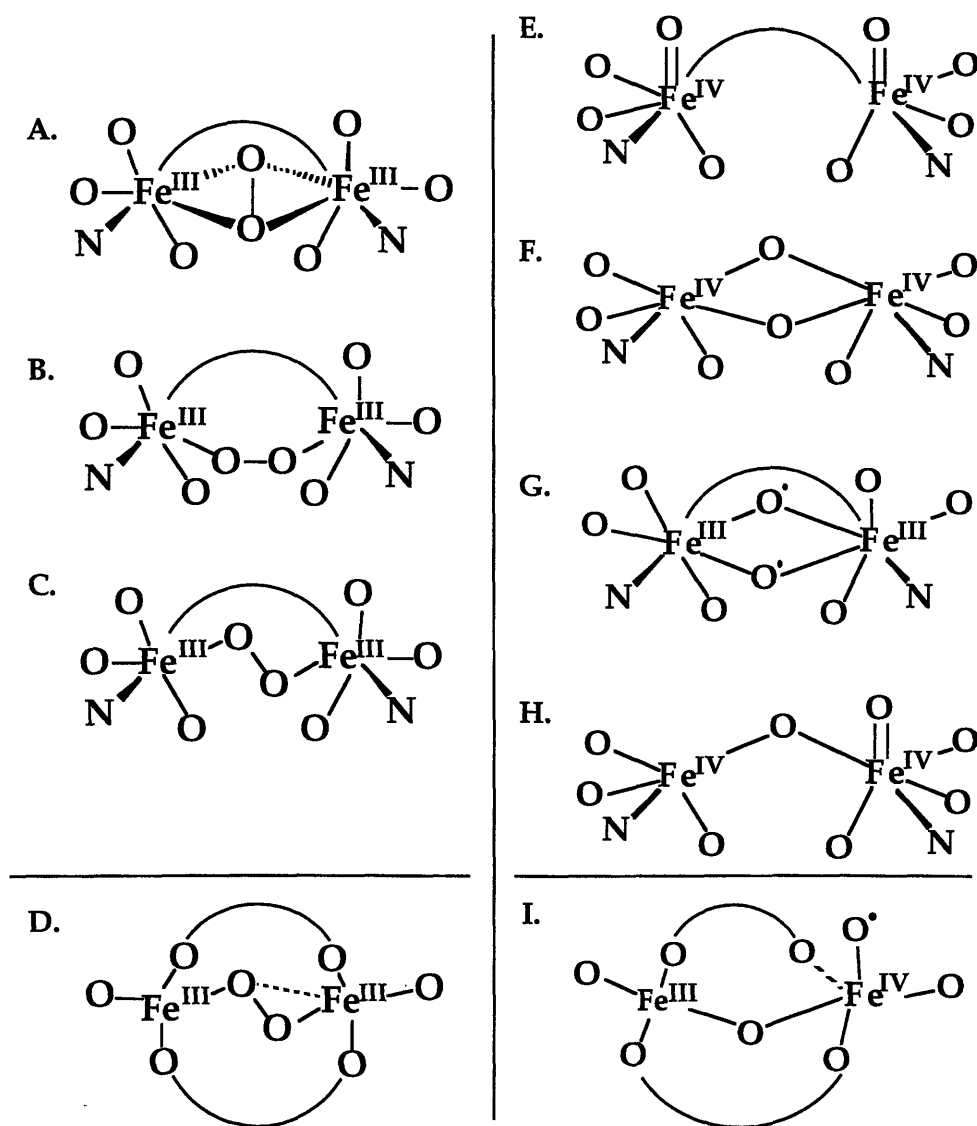


Figure 1.6. Candidates for the structures of intermediates in the sMMO catalytic cycle. (A-D) Possible structures of the diiron(III) peroxo intermediate. (A) An η^2, η^2 -peroxo species. The Fe_2O_2 unit could be either planar or folded about the O–O bond. (B) An η^1, η^1 species with a dihedral Fe–O–O–Fe angle of 0° . (C) Another version of the η^1, η^1 -peroxo conformation with a significant dihedral angle. (D) The lowest energy configuration of a diiron(III) peroxo species as determined by density functional theory.⁶⁵ (E-I) Possible structures of intermediate Q. (E) A diiron(IV) dioxo, or diferryl, configuration. (F) A di(μ -oxo)diiron(IV) species. (G) A di(μ -oxyl)radical diiron(III) species. (H) A species with one bridging and one terminal oxo group. (I) A configuration determined by density functional calculations, featuring an oxo-bridged structure with a terminal oxygen radical.⁶⁵

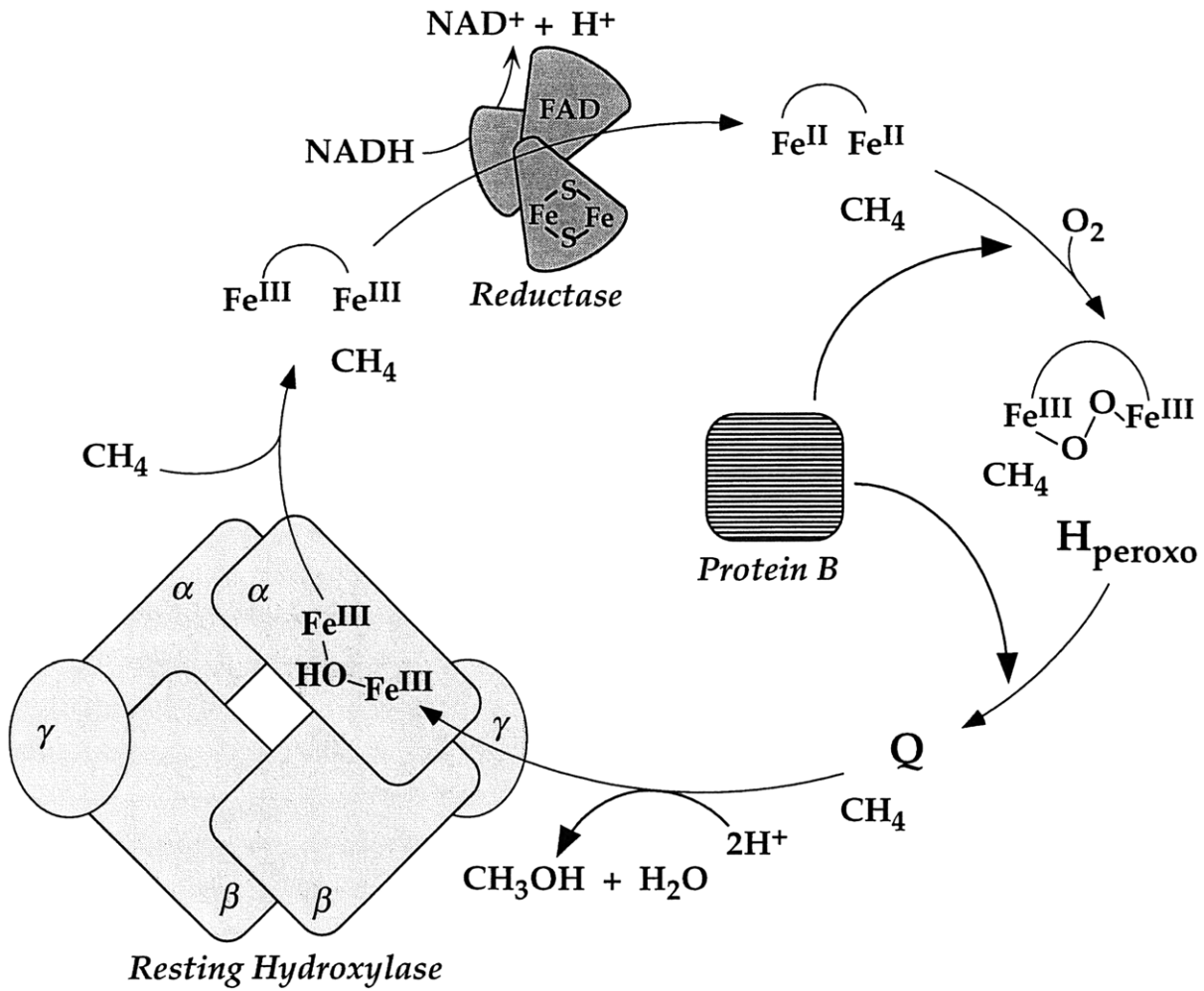


Figure 1.7. Catalytic cycle for sMMO from *M. capsulatus* (Bath) including all observed intermediates.

Chapter Two:

**Small Molecule Binding to the Mixed-Valent Diiron Center of Methane
Monooxygenase Hydroxylase from *Methylococcus capsulatus* (Bath) as
Revealed by ENDOR Spectroscopy**

Introduction^{1,2}

An understanding of the intimate mechanism of alkane oxidation by the soluble methane monooxygenase (sMMO) system of proteins³⁻⁵ requires knowledge of coordination sites at the carboxylate-bridged diiron catalytic center in the hydroxylase enzyme (MMOH) that can be occupied by substrate or product molecules during turnover. X-ray crystal structure studies of MMOH from *Methylococcus capsulatus* (Bath)^{6,7} have revealed four such positions (Figure 2.1), identified by the fact that they are not usually occupied by protein residues but accommodate ligands contributed by solvent or buffer components.⁸⁻¹⁰ Electron nuclear double resonance (ENDOR) spectroscopy offers a powerful, selective, and sensitive ally to X-ray crystallography for addressing the question of exogenous ligand binding sites and interrogating metastable intermediates in the reaction cycle. This technique requires a paramagnetic center which, in the case of MMOH, can be obtained by preparing the active site in the mixed-valent, Fe^{II}Fe^{III} or Fe^{III}Fe^{IV} states,^{9,11,12} or by analyzing the even-spin diiron(II)^{13,14} form of the protein.

Previously we applied ENDOR spectroscopy to identify a bridging hydroxide at site 2, a terminal DMSO bound to the ferric iron, and protein-derived ligands in mixed-valent sMMO from *M. capsulatus* (Bath).^{9,11,13,14} In the present work we have extended these studies to provide evidence that acetate ion binds with its carboxylate group directed toward the diiron center, supporting a previous assignment as acetate ion of electron density of uncertain origin in X-ray crystal structure maps.^{6,7} We also offer the first direct proof that methanol, the product of methane oxidation by the enzyme, coordinates directly to the diiron center, in contrast to the conclusion of a previous ENDOR study of MMOH from *Methylosinus trichosporium* OB3b.¹⁵ Finally, we demonstrate that the coordination positions for exogenous

ligands denoted in Figure 2.1 can simultaneously accommodate DMSO, methanol, and water. This information should facilitate both theoretical and experimental investigations of details of the catalytic mechanism of MMOH.

Materials and Methods

Protein Purification. Growth of native *M. capsulatus* (Bath) was carried out as described elsewhere.¹⁶ Purification of MMOH was performed by using a modification of a published procedure.¹⁷ The crude protein obtained from a DEAE Sepharose anion exchange column¹⁸ was pooled and concentrated to approximately 0.2 mM. A 5 mL portion of this crude preparation was loaded onto a Superdex 200 column (2.6 x 80 cm) and eluted with 25 mM MOPS (pH 7.0) containing 120 mM NaCl, 5% glycerol, and 1 mM dithiothreitol. Specific activities and iron content were in the ranges previously described.^{19,20}

Sample Preparation. Solutions of MMOH (1 mM) were prepared by concentrating purified protein with centrifugal concentrators (Centriprep and Centricon, Amicon) having a molecular weight cutoff of 30,000. An electron transfer mediator solution containing 10 mM phenazine methosulfate, 10 mM methylene blue, and 10 mM potassium indigotetrasulfonate was added to a final concentration of 0.5 mM. The samples were reduced to the Fe^{II}Fe^{III} mixed-valent state, MMOH_{mv}, as reported elsewhere.¹¹ In studies with exogenous ligands, the reagents were added prior to reduction; in all cases their final concentration was 0.1 M. Samples in 23% ¹⁷O water were prepared by exchanging the purified hydroxylase into 50 mM MOPS, pH 7.0, then twice diluting the sample with an equal volume of H₂¹⁷O and concentrating it to 1 mM MMOH by using a Microcon centrifugal concentrator (Amicon) with a molecular weight cutoff of 50,000. Isotopically enriched methanol (CD₃OH, 99.5% or ¹³CH₃OH, 99%), sodium acetate (¹³CH₃CO₂Na, 99% or CH₃¹³CO₂Na,

99%), and DMSO [(CD₃)₂SO, 99.9%] were obtained from Cambridge Isotope Labs, CD₃CO₂Na (99%) was purchased from Aldrich, and H₂¹⁷O (30.4%) was supplied by Isotec.

ENDOR Spectroscopy. EPR and ENDOR spectra were collected by Jean-Paul Willems and Ryzard Gurbiel of Brian Hoffman's laboratory at Northwestern University. The continuous wave (CW) ENDOR spectrometer and procedures employed in this study have been briefly reported.²¹ A description of the 35 GHz pulse ENDOR spectrometer employed in this study has been published recently.²² The proton CW ENDOR spectra were recorded by using 'Packet-Shifting' ENDOR.²³ This type of ENDOR spectroscopy has many advantages when studying metalloproteins, including excellent signal-to-noise ratios at low sample temperature where relaxation rates are slow. A ¹³C ENDOR signal consists of a doublet centered at the ¹³C Larmor frequency (ν_C) and split by the nuclear hyperfine coupling (A_C); a ²H signal consists of a doublet centered at ν_D and split by A_D , with an additional splitting caused by the nuclear quadrupole interaction.

²H and ¹³C ENDOR spectra were collected by using the Mims stimulated-echo ENDOR pulse sequence.^{24,25} In this protocol the ENDOR response R depends jointly on the nuclear hyperfine coupling A and the interval between the first and second microwave pulses according to eq. 1.

$$R \propto [1 - \cos(2\pi A\tau)] \quad (1)$$

This equation shows that the ENDOR response will fall to zero for integer values of $A\tau$ and will reach a maximum for half-integer $A\tau$ values. Such 'hyperfine selectivity' normally is considered to be one of the key benefits of pulsed ENDOR techniques. Orientation-selective ENDOR analysis of frozen

solutions relies on accurate line shapes and intensities, however. Our experience with Mims ENDOR of powder or frozen-solution samples shows that one obtains ENDOR patterns essentially undistorted by the blind spots only for couplings in the range $A < 1/(2\tau)$.²⁶ Thus, in practice, in the study of frozen solutions the maximum hyperfine value, A^{\max} , that should be studied by a Mims ENDOR sequence is restricted by the minimum usable value of τ , denoted as the deadtime, t_d , with the result that $A^{\max} \approx 1/(2t_d)$. The deadtime is defined as the minimum time after the last pulse that the ENDOR effect can be detected against the resonator ringdown, and it depends not only on the spectrometer performance but also on the strength of the ENDOR signal. The value, $\tau = 480$ ns, used in all reported spectra maximizes the sensitivity for a hyperfine value of 1.05 MHz.

Results

EPR Spectroscopy. Both native and dimethyl sulfoxide (DMSO) treated MMOH_{mv} display an anisotropic g tensor which normally would produce excellent orientation selection at 35 GHz (Figure 2.2). Native MMOH_{mv} , $g = 1.94(0), 1.86(5), 1.74(0)$, shows a distribution in the values of g_2 and g_3 ,²⁷⁻²⁹ however, which hinders the analysis of the ENDOR data. The EPR spectrum of the DMSO-treated mixed-valent hydroxylase,¹⁵ $\text{MMOH}_{\text{mv}}[\text{DMSO}]$, $g = 1.95(0), 1.87(0), 1.80(5)$, does not show this distribution in g values, and as a result gives better orientation-selective ENDOR spectra.¹¹ As first reported by others,¹⁵ addition of methanol to native MMOH_{mv} (Figure 2.2a) induces clear changes in the EPR spectrum, shifting g_1 to higher (1.963) and g_2 to lower (1.862) values. The addition of methanol to the DMSO treated sample does not further alter the EPR spectrum of $\text{MMOH}_{\text{mv}}[\text{DMSO}]$ (Figure 2.2b).

ENDOR Spectroscopy. Figure 2.3 shows 35 GHz Mims pulsed ENDOR spectra of MMOH_{mv} samples treated with various reagents. Each spectrum is taken at the magnetic field which gives the best signal-to-noise ratio for the specific sample. These spectra are composites of subspectra taken in the vicinity of the ^2H Larmor frequency as well as the ^{13}C Larmor frequency, which are denoted by arrows.

Addition of Methanol and Acetate to MMOH_{mv} . Figure 2.3a presents a ^2H Mims ENDOR spectrum of native MMOH_{mv} to which deuterated methanol and [$^{13}\text{C}_1$]-acetate, hereafter 1- ^{13}C -acetate, have been added. The ENDOR spectrum clearly shows a resolved ^2H signal comprising a pair of featureless peaks split by the hyperfine coupling, $A(^2\text{H}) \sim 0.5$ MHz; the quadrupole splitting is smaller than the linewidth of the peaks and is therefore indistinguishable. This ^2H signal is the same in the absence of acetate. The small change in the EPR spectrum seen upon methanol addition is therefore not a consequence of nonspecific, solvent-induced protein perturbations; the observation of this ENDOR signal establishes that methanol is incorporated into the active site of the enzyme. The existence of substantial hyperfine splitting, which corresponds to $A(^1\text{H}) \sim 3.3$ MHz, strongly suggests that methanol binds directly to iron. The small change in the EPR spectra further indicates that this binding is not accompanied by a major structural perturbation, although a carboxylate shift or displacement of the water/hydroxide ligand coordinated to Fe^{II} as identified by ENDOR spectroscopy may have occurred.⁹

The sample includes 1- ^{13}C acetate in the solution, and its ENDOR spectra show a low-intensity ^{13}C peak centered at the ^{13}C Larmor frequency (Figure 2.3a). This peak is present in mixed-valent enzyme prepared with 1- ^{13}C acetate both without (data not shown) and with methanol present,

indicating that acetate can be accommodated at the diiron center in a site where it is not displaced by methanol. A ^{13}C signal could not be detected when 2- ^{13}C acetate was employed (Figure 2.3b) nor could a ^2H signal be seen when deuterated acetate was used (data not shown). These observations indicate that the acetate is positioned with its carboxyl group pointing *toward* the diiron center.

Addition of DMSO and Acetate to MMOH_{mv}. Figure 2.3b presents an ENDOR spectrum of MMOH_{mv} with ^2H -DMSO prepared in the presence of ^{13}C -labeled acetate. This spectrum shows a ^2H signal from the ^2H -DMSO and a ^{13}C ENDOR signal from acetate. Thus, binding of DMSO to the Fe^{III} ion⁹ does not preclude incorporation of acetate into the active site. An attempt was made to obtain a full 2-D data set of ENDOR spectra in order to determine the 1- ^{13}C hyperfine tensor of labeled acetate incorporated into MMOH_{mv}[DMSO]. The presence or absence of an isotropic ^{13}C hyperfine component would show whether or not acetate actually is coordinated to the diiron center. Unfortunately, at g values higher than g_2 the intensity of the ^{13}C ENDOR signals dropped below a detectable level, and the ENDOR pattern of ^{13}C labeled acetate could be recorded only for g values between g_2 and g_3 . Although the shape of the ^{13}C ENDOR signal in Figure 2.3b is slightly different from that in Figure 2.3a, the differences are too small and the signal-to-noise ratio of the ^{13}C spectra is too low to allow any meaningful interpretation.

DMSO and Methanol Binding to MMOH_{mv}. DMSO binds to the Fe^{III} site of the valence-localized mixed-valent diiron center, changing its EPR signal (Figure 2.2) and giving rise to ^2H ENDOR and ESEEM spectra when deuterated DMSO is utilized.⁹ A spectrum of MMOH_{mv}[^2H -DMSO] prepared with ^{13}C -methanol shows both a ^2H signal from ^2H -DMSO, as well as a ^{13}C

ENDOR signal from the labeled methanol (Figure 2.3c). Thus, the diiron site can *simultaneously* accommodate DMSO and methanol, which do not compete for the same coordination position. The changes in EPR signal upon treatment of native MMOH_{mv} with DMSO and methanol separately show that each by itself binds to the iron cluster with complete site occupancy. The fact that the ²H spectra from ²H-DMSO (Figures 3b and 3c) and ²H-MeOH (Figure 2.3a) have a better signal-to-noise ratio than the ¹³C spectrum of ¹³C-MeOH (Figure 2.3b) shows that the intensities of the ¹³C signals in different protein states cannot be used reliably to deduce site occupancies.

Although addition of methanol to MMOH_{mv}[DMSO] causes no appreciable changes in its EPR spectrum, when deuterated methanol is used one obtains ²H ENDOR spectra (Figure 2.4). With the aim of determining the details of methanol binding, we collected a full 2-D field-dependent ²H ENDOR pattern from MMOH_{mv}[DMSO] prepared in the presence of ²H-methanol (Figure 2.4). The observed ENDOR signals are a statistical average over the contributions of three ²H atoms having different orientations with respect to the diiron site, and hence different dipolar hyperfine tensors. As a result, it was not possible to determine precisely the individual ²H hyperfine tensors. Numerous simulations of the 2-D data, in which we assumed hyperfine tensors that ranged from purely dipolar to nearly isotropic, indicated that the experimental pattern does not exhibit the strong dependence on field expected for a purely dipole-coupled nucleus, and that the ²H couplings have a substantial isotropic component, $A_{iso}({}^2\text{H}) \sim 0.5$ MHz. This result implies that the methanol molecule is coordinated to the diiron cluster, rather than merely being held nearby. The simulations further suggest that the largest component of the dipolar contribution can be no greater than $T({}^2\text{H})^{\max} \approx 0.4$ MHz ($T({}^1\text{H})^{\max} \approx 2.6$ MHz). Calculations of the

dipolar interaction for a proton on a ligand bound to a diiron center^{30,31} indicate that this value is small for methanol to be bound to Fe^{III} or as an alkoxo bridge. We therefore conclude that the methanol molecule is bound to the Fe^{II}. The intensity of the ¹³C ENDOR signals is too low to allow a reliable analysis of the ¹³C hyperfine tensor as corroboration.

Our earlier work⁹ revealed that there is an aqua ligand attached to the Fe^{II} ion of MMOH_{mv}[DMSO]. This study further indicated that each iron atom has six ligands bound to it. If methanol binds to the diiron site of MMOH_{mv}[DMSO], either a carboxylate group must shift to accommodate the incoming ligand, or the water molecule bound to Fe^{II} must be displaced by methanol. As a first attempt to evaluate these possibilities, CW proton ENDOR spectra were recorded to see whether the exchangeable proton signals assigned to the aqua ligand disappear when methanol binds. In accord with previous observations,⁹ MMOH_{mv} shows ¹H ENDOR signals with A ~ 7 MHz (Figure 2.5a) that arise from an exchangeable aqua ligand. The signals disappear when MMOH_{mv} is exchanged in D₂O buffer (Figure 2.5b). ²H-MeOH was added to MMOH_{mv}, with the deuteration acting to suppress any possible proton signals from bound methanol. The resulting ¹H ENDOR spectrum (Figure 2.5c) also shows a signal from exchangeable proton(s) with A ~ 7 MHz, but with slightly different line shapes. Similar results are found for MMOH_{mv}[DMSO]. These CW ¹H ENDOR data indicate either that water/hydroxide and methanol are simultaneously bound to Fe^{II} or that a methanol replaces the aqua ligand and the OH-proton of methanol gives comparable ¹H CW ENDOR spectra.

To distinguish between these two possibilities, we performed ¹⁷O ENDOR studies on MMOH_{mv}[DMSO] in H₂¹⁷O buffer, both in the presence and absence of methanol. Figure 2.6 shows three CW ENDOR spectra taken at

a field position corresponding to g_1 . The dotted spectrum represents the ENDOR signal of a sample which had not been labeled with ^{17}O and can therefore be used as a reference. This reference spectrum displays sharp intense peaks at 8.7 and 12.2 MHz as well as some less intense, broader signals at 10 and 14 MHz. The signal at 8.7 MHz is located at the Larmor frequency of ^2H and can be attributed to the ^2H nuclei of labeled methanol. All other signals can be assigned to the ν_+ transitions of ^{14}N . The spectrum displayed using a dashed line shows the ENDOR signal of $\text{MMOH}_{\text{mv}}[^2\text{H-DMSO}]$ in H_2^{17}O buffer. The presence of an additional, rather broad, featureless ^{17}O signal with a maximum intensity at 18.2 MHz is obvious. The ENDOR spectrum of $\text{MMOH}_{\text{mv}}[\text{DMSO}]$ in H_2^{17}O buffer in the presence of deuterated methanol (solid line) is almost identical to that of $\text{MMOH}_{\text{mv}}[\text{DMSO}]$ in H_2^{17}O buffer without methanol. It shows the ^2H signal of methanol as well as the oxygen signal of water. The simplest interpretation of this result is that the observed ^{17}O ENDOR signal from $\text{MMOH}_{\text{mv}}[\text{DMSO}]$ in H_2^{17}O buffer arises from the labeled aqua ligand and that it is not displaced by methanol. An alternative interpretation might be that ^{17}O exchanges into the bridge as well as into the terminal aqua site, and that methanol displaces only the ^{17}O aqua ligand. In such a model, the ^{17}O signal from $\text{MMOH}_{\text{mv}}[\text{DMSO}]$ in H_2^{17}O buffer would display both signals, whereas added methanol, by replacing the aqua ligand, would leave an ^{17}O signal from the bridge. We do not favor this alternative because we would expect some change in the ^{17}O contribution to the spectrum upon addition of methanol. If a full ^{17}O ENDOR pattern across the EPR envelope could be acquired and analyzed, we might be able to confirm the assignment of the oxygen ENDOR signal. Such a determination is not possible because the ^{17}O signal broadens and decreases in intensity at

higher magnetic field values, until it is no longer visible at a field value corresponding to g_2 .

The ENDOR pattern arising from a diiron center containing both a bridging oxygen atom and an oxygen atom terminally attached to Fe^{III} has been well characterized for an $\text{Fe}^{\text{III}}\text{Fe}^{\text{IV}}$ cluster.³² For both oxygen atoms the hyperfine tensor is almost axial, although the A_1 component of the bridging oxygen atom is much smaller than the other two tensor components, whereas the A_1 component of the terminally bound oxygen atom is significantly larger than A_2 and A_3 . In case of MMOH_{mv} we are not able to determine the full hyperfine tensor for ^{17}O , but the ^{17}O ENDOR pattern shows that A_1 is larger than both A_2 and A_3 . This observation supports our conclusion that the oxygen atom from water binds terminally to the Fe^{II} ion in MMOH_{mv} .

Discussion

The observation of ENDOR signals from acetate shows this ion to be located in the vicinity of the diiron cluster of MMOH_{mv} , confirming the assignment of electron density in the X-ray structure as acetate and its orientation with respect to the iron atoms.^{6,7} Given the impossibility of collecting a full field dependence of the ^{13}C ENDOR data from labeled acetate, it is not possible to prove the presence of isotropic coupling, and hence that acetate acts as an iron ligand. Combined with the electron density in the crystal structure determination, however, we can be fairly confident in such an assignment.

Figure 2.1 shows four positions at the active site of MMOH which can be occupied by exogenous ligands and thus are available for methanol binding. Our previous ENDOR study⁹ revealed that position 2 contains a

solvent exchangeable hydroxo ion, and DMSO was modeled at position 4. The study also revealed that a water molecule resides either at site 1 or 3. In the current work, and within the context of the previous model, the remaining site, either 3 or 1, can be occupied by coordinated methanol. Simulations of the ENDOR data suggest that methanol is bound to Fe^{II} . These conclusions further support the idea that acetate does not bind to the diiron center when a sufficient number of exogenous molecules is present to occupy all the available sites. The relative inability of acetate to compete for binding sites is supported by its inability to inhibit catalytic activity. That acetate can be contained in the active site but not ligated to iron is in agreement with previous X-ray crystallographic studies. This work indicated that the bidentate bridging ligand assigned as acetate in the structure of MMOH_{ox} at 4°C is replaced by a monoatomic water bridge in the structure determined at -160°C .⁷

Combining the results of the current investigation with those of previous X-ray⁷ and ENDOR⁹ studies, we can speculate on aspects of the MMOH mechanism of methane oxidation (Figure 2.7), while recognizing as important caveats that the diiron center has an oxidation level in the ENDOR experiment not yet observed in the catalytic cycle and that the coupling protein MMOB is not present. The structure of the reduced, diferrous MMOH (H_{red}) in the absence of MMOB is known from X-ray crystallography. It has a bridging carboxylate ligand, Glu243, which is carboxylate shifted relative to the resting oxidized configuration. The first isolable intermediate in the reaction of dioxygen with diferrous MMOH is a putative peroxodiiron(III) species designated H_{peroxo} . Previously we suggested that O_2 coordinates at the site where DMSO binds to the cluster, site 4 in Figure 2.1.⁹ In Figure 2.7, we depict the peroxo moiety bound in sites (3,4) and 2. This formulation agrees with the previous suggestion, as well as spectroscopic data,³³⁻³⁵ theoretical

calculations,^{36,37} and results from model compounds,³⁸⁻⁴⁰ but it is not a unique interpretation. The H_{peroxo} intermediate converts to a high-valent species designated Q which has been characterized by a variety of techniques.^{12,33,35,41-43} The reaction of Q with methane, whether or not direct interaction of carbon with an iron atom occurs, could in principle involve any of the sites 1 - 4 depicted in Figure 2.7, at least one of which will contain an oxo ligand derived from the peroxo intermediate. The current ENDOR experiments suggest that the product methanol binds preferentially to the iron atom which houses the potential binding sites 1 and 3. It is not known whether methanol binds as the neutral molecule⁴⁴ or as methoxide, but it is presumably replaced by a water ligand, following protonation if necessary, to regenerate the resting state of MMOH and complete the catalytic cycle.

Conclusion

The current study supplies the first direct proof that methanol binds to the active site of MMOH, inducing a change in the EPR spectrum of the mixed-valent enzyme and giving rise to an ENDOR interaction when labeled methanol is used. Methanol most likely binds to the ferrous iron in MMOH_{mv} , modeled as Fe1, and it apparently does so without displacing a bound water molecule. This investigation also confirms the assignment and disposition of the acetate molecule modeled in X-ray crystallographic studies. ENDOR experiments indicate that the active site can accommodate several small molecules bound simultaneously. Comparing the binding of methanol and acetate in the presence and absence of DMSO, the binding site of which in MMOH_{mv} has been previously identified, with the available sites on the iron atoms affords insights into elements of the mechanism of methane oxidation by MMOH.

References

- (1) This work has been submitted for publication in a slightly different form. See reference 2.
- (2) Willems, J. P.; Valentine, A. M.; Gurbiel, R.; Lippard, S. J.; Hoffman, B. M. *J. Am. Chem. Soc.* **1998**, *120*, in press.
- (3) Liu, K. E.; Lippard, S. J. *Advances in Inorganic Chemistry*; Academic Press: San Diego, 1995; Vol. 42, p 263-289.
- (4) Wallar, B. J.; Lipscomb, J. D. *Chem. Rev* **1996**, *96*, 2625-2657.
- (5) Valentine, A. M.; Lippard, S. J. *J. Chem. Soc., Dalton Trans.* **1997**, *21*, 3925-3931.
- (6) Rosenzweig, A. C.; Frederick, C. A.; Lippard, S. J.; Nordlund, P. *Nature* **1993**, *366*, 537-543.
- (7) Rosenzweig, A. C.; Nordlund, P.; Takahara, P. M.; Frederick, C. A.; Lippard, S. J. *Chem. Biol.* **1995**, *2*, 409-418.
- (8) Whittington, D. A.; Lippard, S. J. In *ACS Symposium Series*; Hodgson, K. O. and Solomon, E. I., Eds.; American Chemical Society: Washington, D.C., 1998.
- (9) DeRose, V. J.; Liu, K. E.; Lippard, S. J.; Hoffman, B. M. *J. Am. Chem. Soc* **1996**, *118*, 121-134.
- (10) The opposite assignment was incorrectly given in the ^{57}Fe ENDOR results section of reference 8. The remainder of the paper, however, is consistent, and describes Fe1 as the ferrous iron and Fe2 as the ferric iron. This assignment is only a working model, and the reverse may be true.
- (11) DeRose, V. J.; Liu, K. E.; Kurtz, D. M., Jr.; Hoffman, B. M.; Lippard, S. J. *J. Am. Chem. Soc.* **1993**, *115*, 6440-6441.

- (12) Valentine, A. M.; Tavares, P.; Pereira, A. S.; Davydov, R.; Krebs, C.; Hoffman, B. M.; Edmondson, D. E.; Huynh, B. H.; Lippard, S. J. *J. Am. Chem. Soc.* **1998**, *120*, 2190-2191.
- (13) Hoffman, B. M.; Sturgeon, B. E.; Doan, P. E.; DeRose, V. J.; Liu, K. E.; Lippard, S. J. *J. Am. Chem. Soc.* **1994**, *116*, 6023-6024.
- (14) Sturgeon, B. E.; Doan, P. E.; Liu, K. E.; Burdi, D.; Tong, W. H.; Nocek, J. M.; Gupta, N.; Stubbe, J.; Kurtz, D. M., Jr.; Lippard, S. J.; Hoffman, B. M. *J. Am. Chem. Soc.* **1997**, *119*, 375-386.
- (15) Hendrich, M. P.; Fox, B. G.; Andersson, K. K.; Debrunner, P. G.; Lipscomb, J. D. *J. Biol. Chem.* **1992**, *267*, 261-269.
- (16) Pilkington, S. J.; Dalton, H. In *Methods In Enzymology* Academic Press: New York, 1990; Vol. 188; pp 181-190.
- (17) Fox, B. G.; Froland, W. A.; Jollie, D. R.; Lipscomb, J. D. In *Methods In Enzymology* Academic Press: New York, 1990; Vol. 188; pp 191-202.
- (18) Valentine, A. M.; Wilkinson, B.; Liu, K. E.; Komar-Panicucci, S.; Priestley, N. D.; Williams, P. G.; Morimoto, H.; Floss, H. G.; Lippard, S. J. *J. Am. Chem. Soc.* **1997**, *119*, 1818-1827.
- (19) DeWitt, J. G.; Bentsen, J. G.; Rosenzweig, A. C.; Hedman, B.; Green, J.; Pilkington, S.; Papaefthymiou, G. C.; Dalton, H.; Hodgson, K. O.; Lippard, S. J. *J. Am. Chem. Soc.* **1991**, *113*, 9219-9235.
- (20) Liu, K. E.; Johnson, C. C.; Newcomb, M.; Lippard, S. J. *J. Am. Chem. Soc.* **1993**, *115*, 939-947.
- (21) Werst, M. M.; Davoust, C. E.; Hoffman, B. M. *J. Am. Chem. Soc.* **1991**, *113*, 1533-1538.
- (22) Davoust, C. E.; Doan, P. E.; Hoffman, B. M. *J. Mag. Res., A* **1996**, *119*, 38-44.

- (23) DeRose, V. J.; Hoffman, B. M. ; Academic Press: New York, 1995; Vol. 246, p 554-589.
- (24) Mims, W. B. *Proc. Roy. Soc. Lond* **1965**, 283, 452-457.
- (25) Gemperle, C.; Schweiger, A. *Chem. Rev.* **1991**, 91, 1481-1505.
- (26) Doan, P. E.; Fan, C.; Hoffman, B. M. *J. Am. Chem. Soc* **1994**, 116, 1033-1041.
- (27) Froncisz, W.; Hyde, J. S. *J. Chem. Phys.* **1980**, 73, 3123.
- (28) Hagen, W. R. *J. Magn. Res.* **1981**, 44, 447.
- (29) Hagen, W. R. In *Advanced EPR; Applications in Biology and Biochemistry*; Hoff, A. J., Eds.; Elsevier: Amsterdam, 1989.
- (30) Willems, J.-P.; Lee, H.-I.; Burdi, D.; Doan, P. E.; Stubbe, J.; Hoffman, B. M. *J. Am. Chem. Soc.* **1997**, 9816-9824.
- (31) Randall, D. W.; Gelasco, A.; Caudle, M. T.; Pecoraro, V. L.; Britt, R. D. *J. Am. Chem. Soc.* **1997**, 119, 4481-4491.
- (32) Burdi, D.; Sturgeon, B. E.; Tong, W. H.; Stubbe, J.; Hoffman, B. M. *J. Am. Chem. Soc* **1996**, 118, 281-282.
- (33) Liu, K. E.; Wang, D.; Huynh, B. H.; Edmondson, D. E.; Salifoglou, A.; Lippard, S. J. *J. Am. Chem. Soc.* **1994**, 116, 7465- 7466.
- (34) Liu, K. E.; Valentine, A. M.; Qiu, D.; Edmondson, D. E.; Appelman, E. H.; Spiro, T. G.; Lippard, S. J. *J. Am. Chem. Soc.* **1995**, 117, 4997; **1997**, 119, 11134.
- (35) Liu, K. E.; Valentine, A. M.; Wang, D.; Huynh, B. H.; Edmondson, D. E.; Salifoglou, A.; Lippard, S. J. *J. Am. Chem. Soc.* **1995**, 117, 10174-10185.
- (36) Siegbahn, P. E. M.; Crabtree, R. H. *J. Am. Chem. Soc.* **1997**, 119, 3103-3113.
- (37) Yoshizawa, K.; Yamabe, T.; Hoffmann, R. *New J. Chem.* **1997**, 21, 151-161.

- (38) Kim, K.; Lippard, S. J. *J. Am. Chem. Soc.* **1996**, *118*, 4914-4915.
- (39) Dong, Y.; S., Y.; Young, V. G., Jr.; Que, L., Jr. *Angew. Chem. Int. Ed. Engl.* **1996**, *35*, 618-620.
- (40) Ookubu, T.; Sugimoto, H.; Nagayama, T.; Masuda, H.; Sato, T.; Tanaka, K.; Madea, Y.; Okawa, H.; Hayashi, Y.; Uehara, A.; Suzuki, M. *J. Am. Chem. Soc.* **1996**, *118*, 701-702.
- (41) Lee, S.-K.; Fox, B. G.; Froland, W. A.; Lipscomb, J. D.; Munck, E. *J. Am. Chem. Soc.* **1993**, *115*, 6450-6451.
- (42) Lee, S.-K.; Nesheim, J. C.; Lipscomb, J. D. *J. Biol. Chem.* **1993**, *268*, 21569-21577.
- (43) Shu, L. J.; Nesheim, J. C.; Kauffmann, K.; Munck, E.; Lipscomb, J. D.; Que, L. *Science* **1997**, *275*, 515-518.
- (44) Watton, S. P.; Masschelein, A.; Rebek, J., Jr.; Lippard, S. J. *J. Am. Chem. Soc.* **1994**, *116*, 5196-5205.

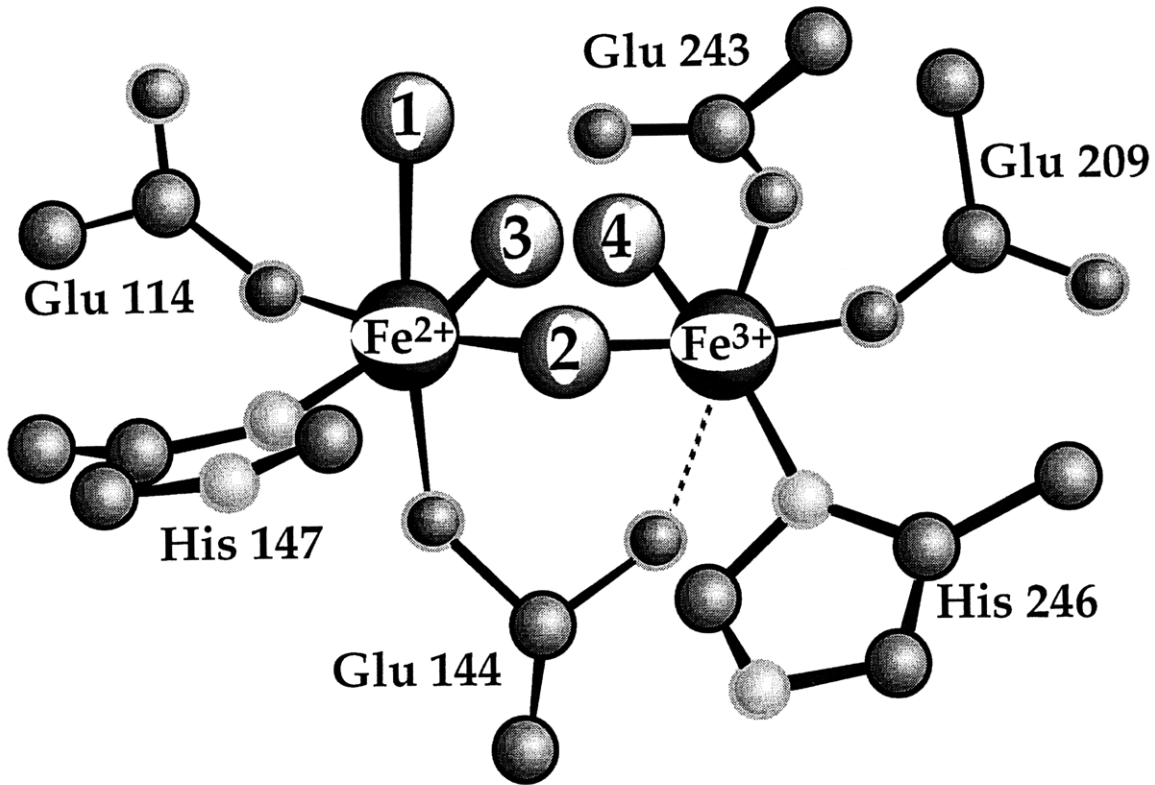


Figure 2.1. A model of the hydroxylase active site with anchor positions occupied by amino acids and potential catalytic positions numbered 1-4. Fe1 has been modeled as the ferrous iron and Fe2 as the ferric iron.^{9,10} Adapted from reference 8.

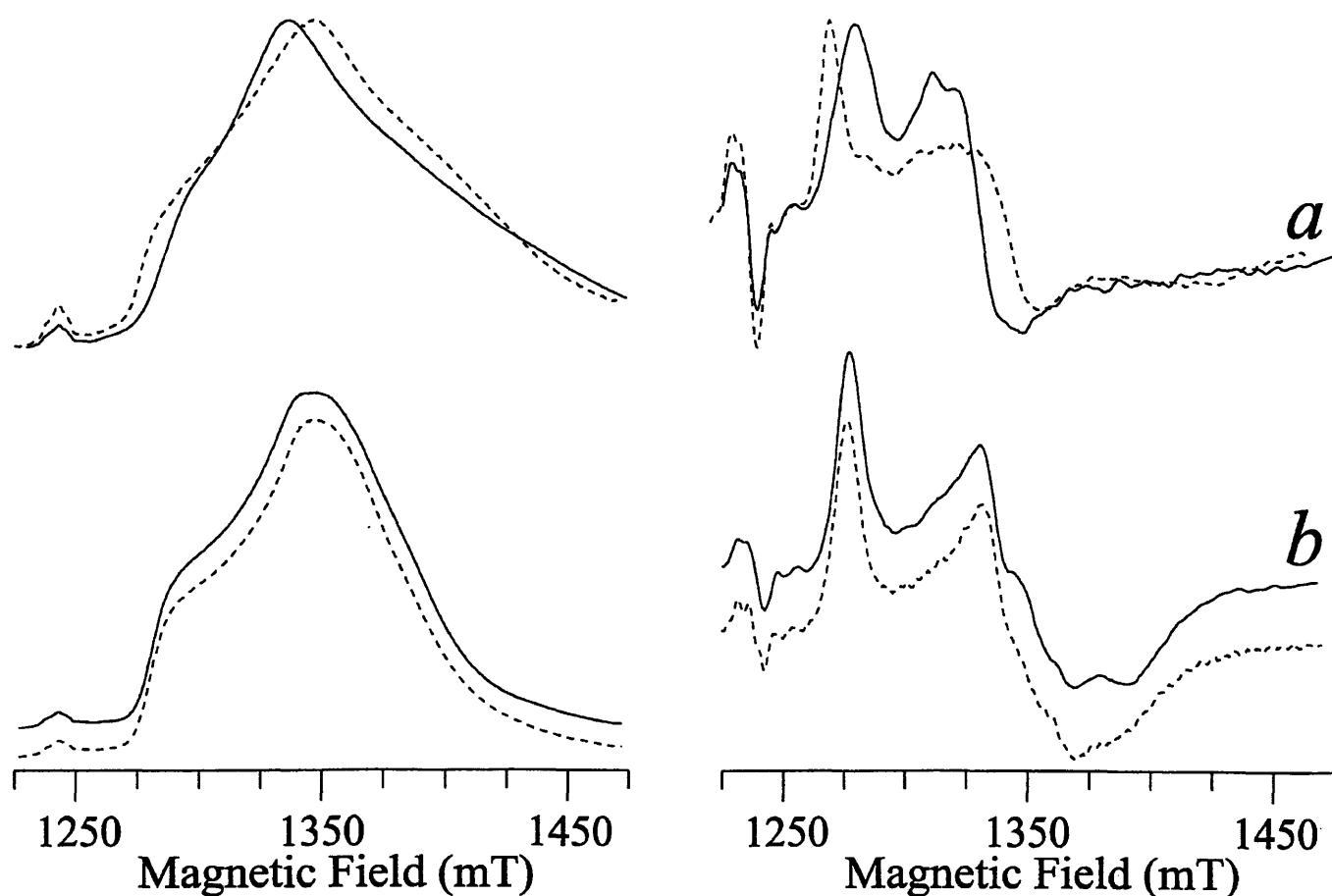


Figure 2.2. 35 GHz CW EPR spectra of MMOH_{mv} ; left: EPR absorption envelopes obtained from 100 kHz detection under conditions of rapid passage, right: numerical derivatives of these spectra. a) Solid line: native MMOH_{mv} , microwave frequency 34.955 GHz, modulation amplitude 2.5 G. Dashed line: methanol added to the native protein, microwave frequency 34.988 GHz, modulation amplitude 2 G. (b) Solid line: MMOH_{mv} treated with DMSO, microwave frequency 35.008 GHz, modulation amplitude 2 G. Dashed line: methanol added to the previous sample, microwave frequency 35.013 GHz, modulation amplitude 2 G.

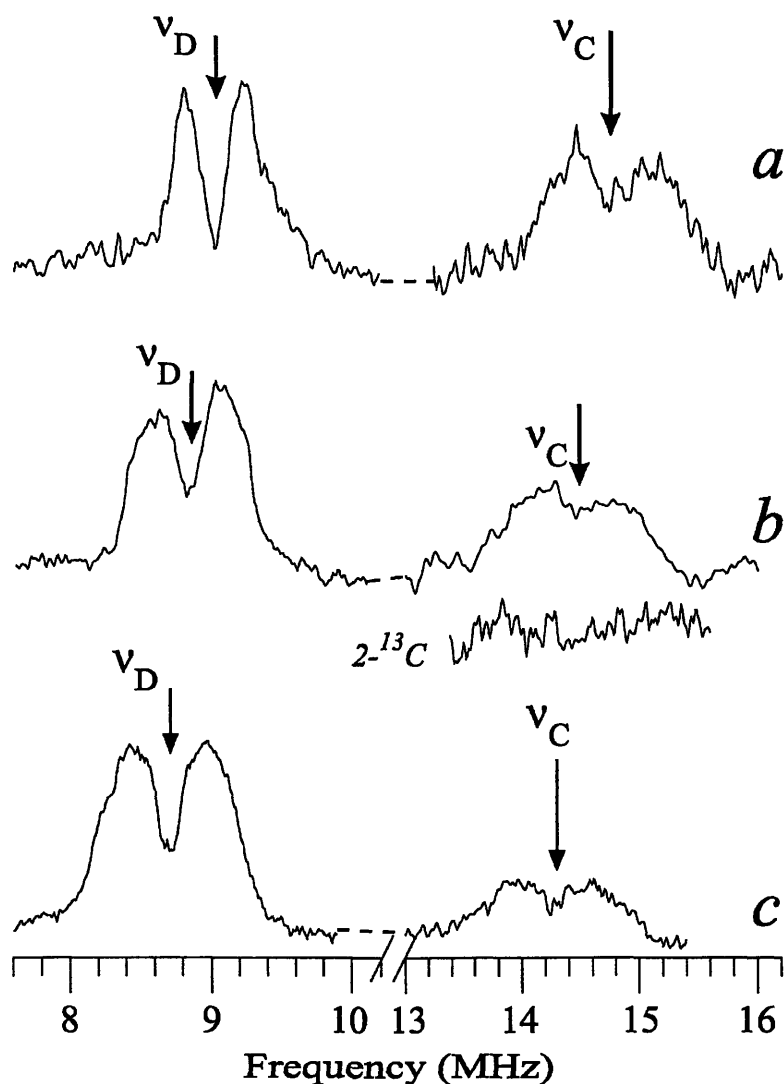


Figure 2.3. A series of 35 GHz pulsed Mims ENDOR spectra of MMOH_{mv} at a field position corresponding to g_3 . The ^2H and ^{13}C Larmor frequencies are indicated by black arrows. (a) MMOH_{mv} with deuterated methanol in the presence of $1\text{-}^{13}\text{C}$ acetate, microwave frequency 34.741 GHz, $\tau = 480$ ns. The field position corresponds to g_3 . (b) $\text{MMOH}_{\text{mv}}[\text{DMSO}(d_6)]$ with $1\text{-}^{13}\text{C}$ acetate, microwave frequency 34.657 GHz, $\tau = 480$ ns. The field corresponds to a value in between g_2 and g_3 . A spectrum of a sample prepared with $2\text{-}^{13}\text{C}$ acetate was recorded in the ^{13}C frequency range (13-15.5 MHz) and is depicted under that of the labeled sample. (c) ^{13}C labeled methanol added to $\text{MMOH}_{\text{mv}}[\text{DMSO}(d_6)]$, microwave frequency 34.734 GHz, $\tau = 480$ ns. This spectrum is recorded at a g_2 . In all spectra the RF pulse width was 60 ms, the microwave pulse width was 48 ns and $T = 2\text{K}$.

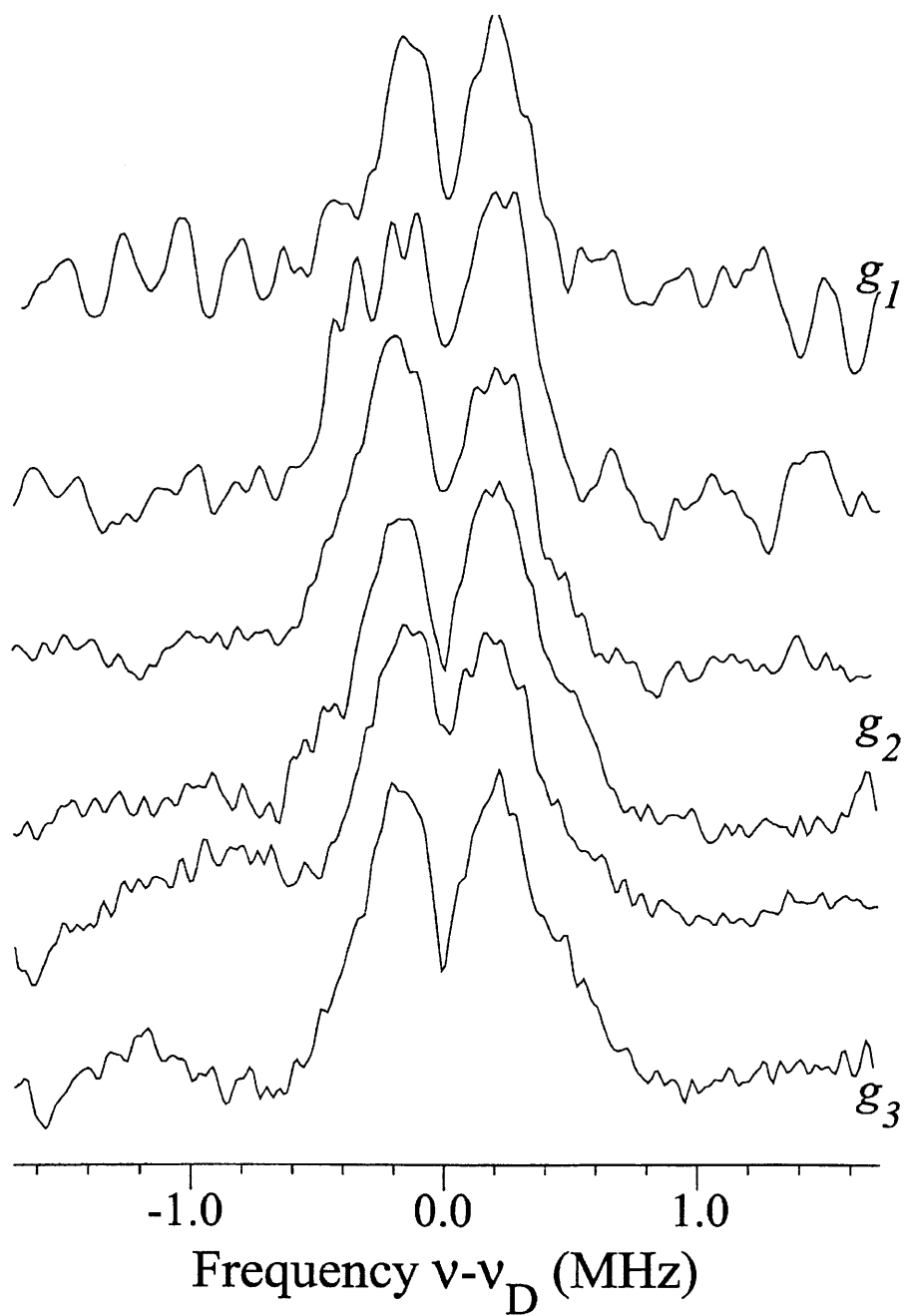


Figure 2.4. 35 GHz Mims ENDOR spectra across the EPR envelope of $\text{MMOH}_{\text{mv}}[\text{DMSO}]$ with deuterated methanol, RF pulse width 60 ms; microwave pulse width 40 ns, $\tau = 480$ ns, microwave frequency 34.68 GHz. temperature: 2K. The spectra are centered around the ^2H Larmor frequency.

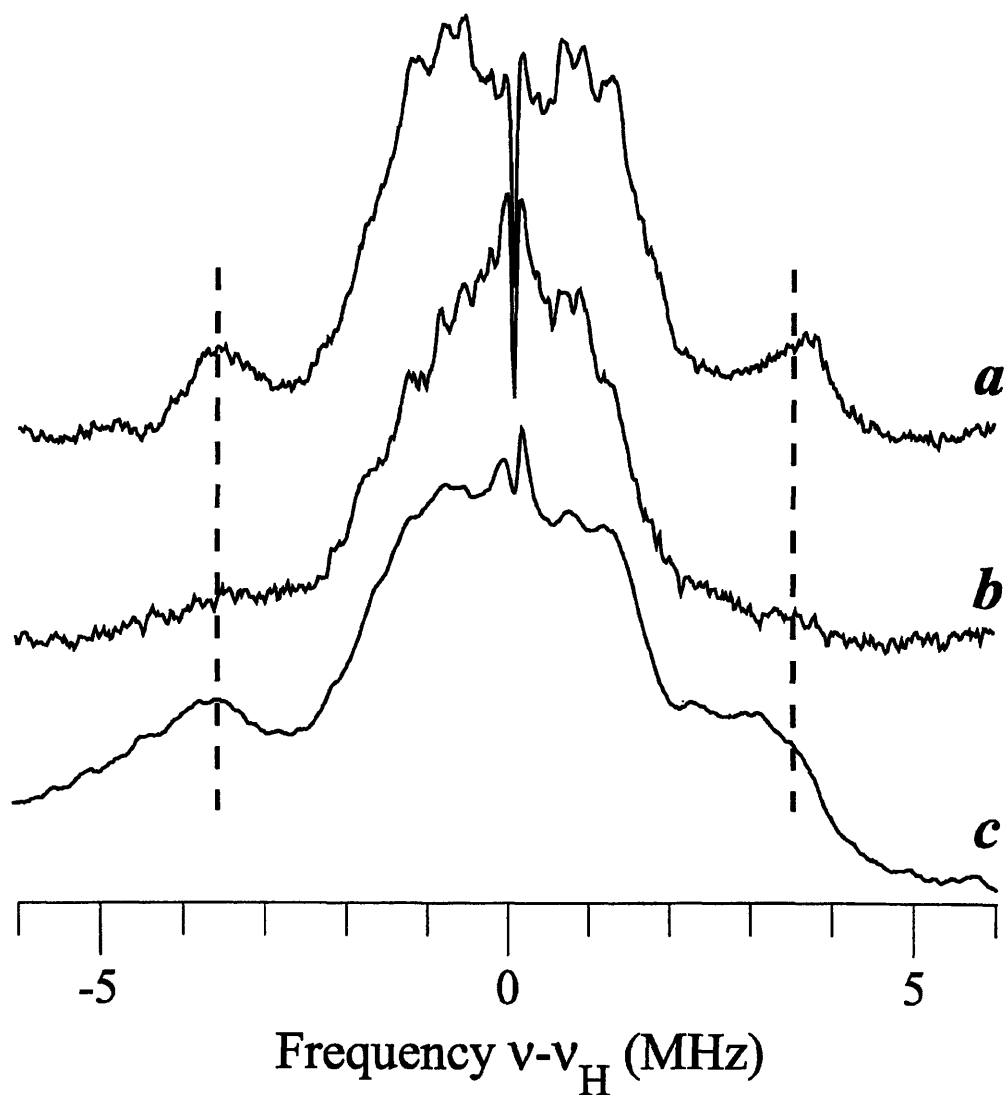


Figure 2.5. 35 GHz CW proton ENDOR spectra of MMOH_{mv} at g_1 . All spectra have been centered around the proton Larmor frequency. (a) MMOH_{mv} in H_2O , microwave frequency 35.1 GHz, modulation amplitude 0.17 G, modulation frequency 100 kHz, RF scan speed 0.5 MHz/s. RF frequency sweep: from low frequency to high. (b) MMOH_{mv} in D_2O as in (a). (c) MMOH_{mv} treated with deuterated methanol in H_2O , microwave frequency 34.9 GHz, modulation amplitude 4 G, modulation frequency 100 kHz, RF scan speed 1 MHz/s. RF frequency sweep: from low frequency to high.

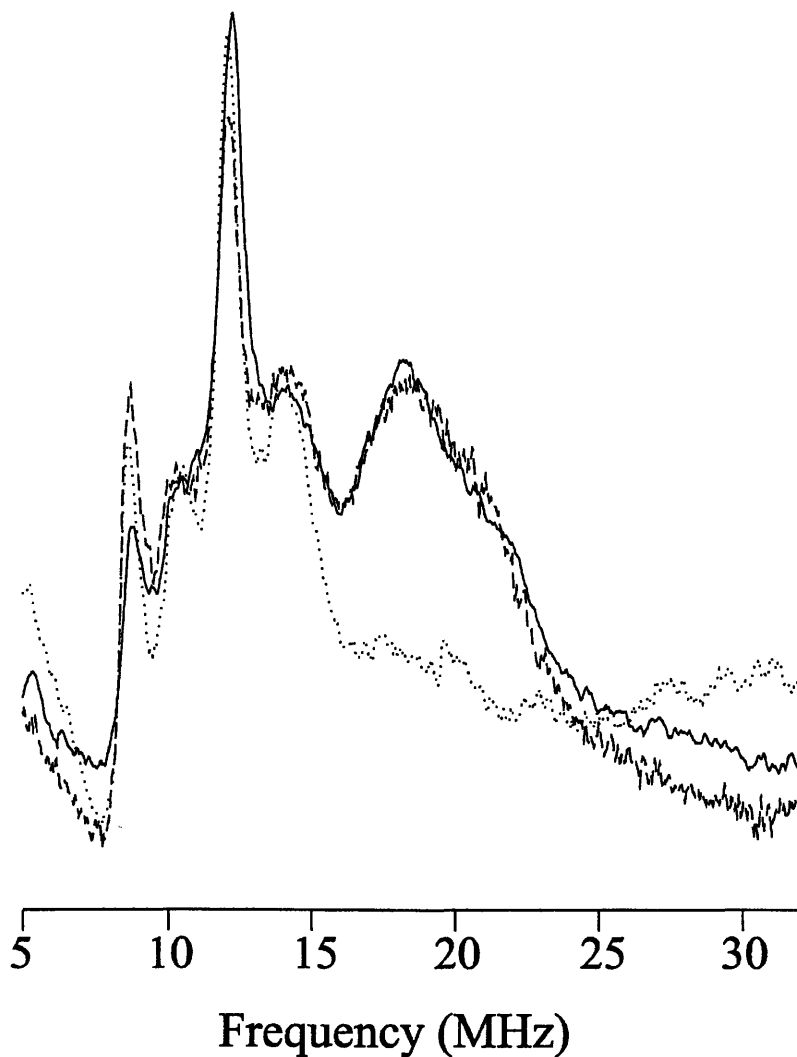


Figure 2.6. 35 GHz CW ENDOR spectra of MMOH_{mv} at g_1 . Dotted line: $\text{MMOH}_{\text{mv}}[\text{DMSO}]$ with deuterated methanol, microwave frequency 34.991 GHz. Dashed line: $\text{MMOH}_{\text{mv}}[{}^2\text{H-DMSO}]$ exchanged in H_2^{17}O , microwave frequency 35.054 GHz. Solid line: $\text{MMOH}_{\text{mv}}[\text{DMSO}]$ with deuterated methanol and exchanged in H_2^{17}O , microwave frequency 35.119 GHz. In all spectra the modulation amplitude was 8 G, modulation frequency 100 kHz, RF scan speed 1 MHz/s, RF frequency sweep from low frequency to high, and temperature 2 K.

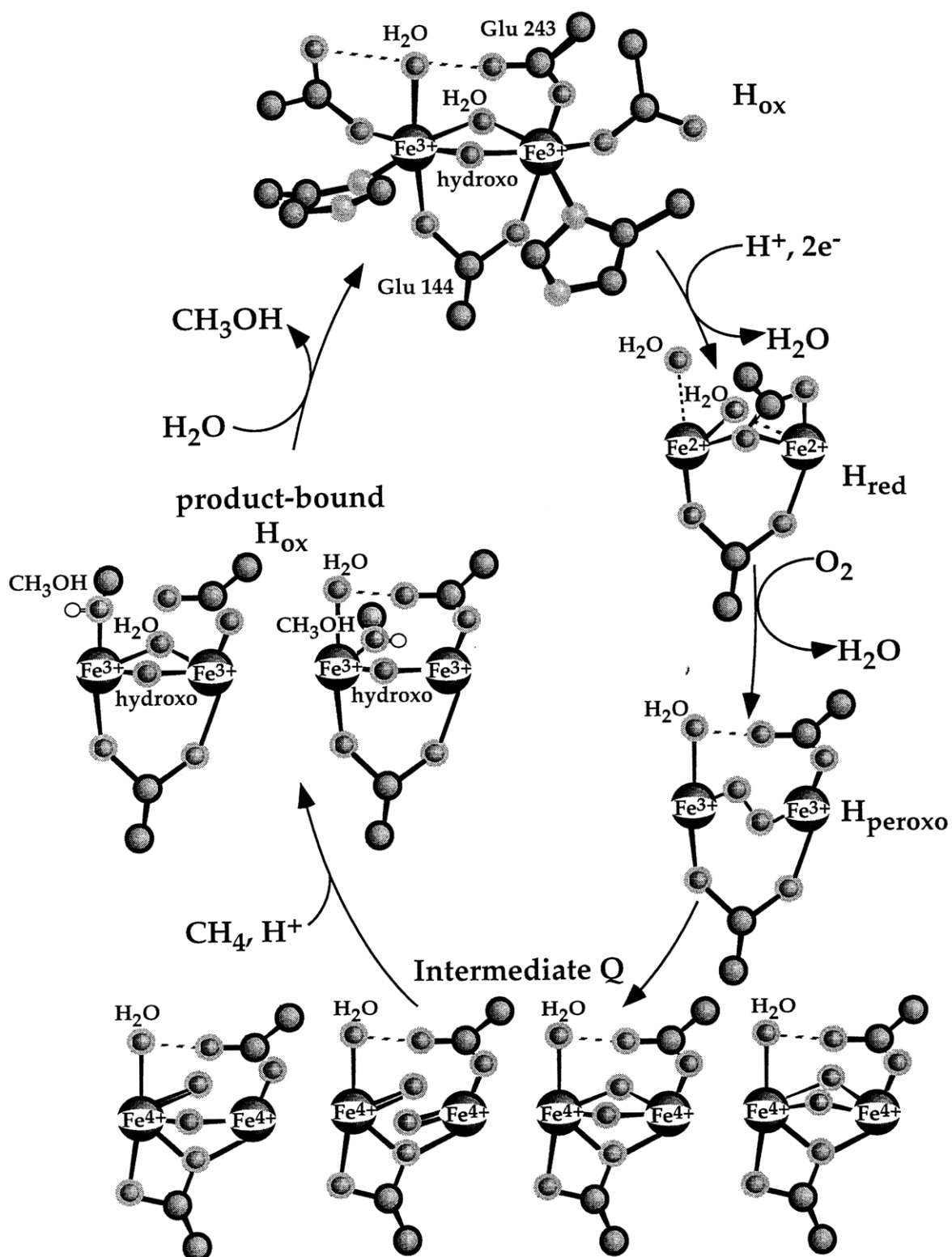


Figure 2.7. The catalytic cycle of sMMO, depicting the likely binding sites for small molecule substrates. Amino acid ligands in anchor positions are omitted in all but the oxidized structure. Glu 144 is drawn in a carboxylate-shifted conformation in the structures of intermediate Q to furnish a third single-atom bridge and promote a short Fe...Fe distance. Such a bridge might alternatively be made by a similarly shifted Glu 243 or by a solvent-derived oxo moiety.

Chapter Three:

**An EPR Study of the Dinuclear Iron Site in the Soluble Methane Monooxygenase
Reduced by One Electron at 77 K: the Effect of Component Interactions and the
Binding of Small Molecules to the Dinuclear Ferric Center**

Introduction^{1,2}

The methanotrophic bacterium *Methylococcus capsulatus* (Bath) can express a soluble, multi-component enzyme system, methane monooxygenase or sMMO, responsible for the NADH- and dioxygen-dependent hydroxylation of methane to methanol.³⁻⁵ Substrate binding and O₂ activation occur at non-heme diiron catalytic sites located in the α subunits of the 251 kDa hydroxylase component, MMOH, an $\alpha_2\beta_2\gamma_2$ homodimer. A 15.8 kDa monomeric protein termed component B, MMOB, couples hydrocarbon oxidation in MMOH with the transfer of electrons from the NADH-reduced form of MMOR, the 38.5 kDa reductase component.^{6,7} Kinetic and potentiometric studies indicate that interactions with MMOR and MMOB affect the electron transfer, oxygenase activity, redox properties and electronic structure of the dinuclear iron sites in MMOH.^{6,8} Spectroscopic experiments further reveal that binding of MMOB as well as small exogenous molecules can alter the properties of the active site diiron clusters in their mixed-valent and fully reduced states. In particular, the electron paramagnetic resonance (EPR) spectrum of the mixed-valent form of MMOH in the presence of MMOB is significantly different following treatment with exogenous ligands such as dimethylsulfoxide (DMSO) or methanol,^{9,10} exhibiting a large shift in g_{av} from 1.82 and displaying altered power saturation behavior.^{9,11} Also, CD and MCD studies reveal the binding of MMOB and some substrates and inhibitors to perturb the diiron(II) clusters in the reduced hydroxylase component from *Methylosinus trichosporium* OB3b.¹²

The three-dimensional structures of the resting, oxidized state of MMOH from *M. capsulatus* (Bath)^{13,14} and from *M. trichosporium* OB3b¹⁵ have been determined. The iron atoms in the *M. capsulatus* (Bath) enzyme are bridged by a hydroxide ion and an additional bidentate, semibridging glutamate ligand. Each metal atom is also coordinated to a histidine ligand. Two additional glutamate residues ligate one iron atom in a monodentate fashion, whereas the other iron

atom has a monodentate glutamate and a water molecule in its coordination sphere. Finally, octahedral coordination at each of the iron atoms is completed by an exogenous bridging ligand, assigned either as water in flash frozen (-160 °C) crystals¹⁴ or acetate from the crystallization buffer in crystals prepared at 4 °C.¹³ The structure of the diiron core in the hydroxylase from *M. trichosporium* OB3b crystallized at 18 °C is very similar to that in flash frozen crystals of MMOH from *M. capsulatus* (Bath).¹⁵ In the reduced diiron(II) form of the latter enzyme, the metal atoms are no longer bridged by exogenous OH⁻ and H₂O ligands but by the oxygen atom of glutamate coordinated in a μ - η^2 fashion.^{14,16} Structural diagrams of the diiron cores of oxidized and reduced MMOH from *M. capsulatus* (Bath) are presented in Figure 3.1.

Although the effects of MMOB and small molecule binding to the mixed-valent and diferrous states of MMOH have been studied, very little information is available concerning the structural consequences of MMOB and substrate/inhibitor interactions with the resting, diferric MMOH. Studies using Mössbauer^{11,17} and EXAFS spectroscopy^{18,19} have failed to detect any significant alterations in the diiron cluster that could account for the dramatic effects of MMOB, reductase, and substrate on catalysis.

Previously the EPR spectra of dinuclear clusters in the R2 protein of ribonucleotide reductase (R2 of RNR), hemerythrin (Hr) and MMOH from *M. trichosporium* OB3b, reduced by one electron in frozen solutions, proved to be structurally sensitive probes for the EPR-silent diferric states of these proteins.²⁰⁻²³ In these studies, the bridged diiron(III) sites of the proteins at 77 K were reduced by mobile electrons generated by γ -irradiation. The mixed-valent diiron cluster trapped in this fashion retains a conformation close to that of the original diferric state because of its inability to relax to an equilibrium state in the solid matrix. The conformation of the mixed-valent species so constrained will be in a non-

equilibrium state if the coordination environment of the diiron cluster depends on the redox state of the iron atom(s). The mixed-valent species in such a non-equilibrium state can relax to the corresponding equilibrium state at higher temperatures, 160 K - 270 K for the R2 protein of RNR, Hr, and MMOH.²⁰⁻²³ The EPR spectra of species obtained by such an annealing process are identical to those obtained following chemical reduction in fluid solution.

Application of this approach to MMOH from *M. trichosporium* OB3b revealed the presence of two different conformers in the resting, diferric state, the structures of which differed from that of the mixed-valent state.²² Moreover, MMOB had an effect on the diiron site of oxidized MMOH which was different than that previously observed for the mixed-valent state. In the present work we have used this methodology to probe the oxidized form of the hydroxylase component from *M. capsulatus* (Bath), examining the effects not only of component B but also of MMOR and several small molecules which bind at the active site. The results are interpreted in terms of a model that involves carboxylate shifts at the diiron center upon addition of one electron to the diiron(III) resting state of MMOH as well as participation of residues in the mainly hydrophobic substrate binding cavity adjacent to that center (see Figure 3.1).

Materials and Methods

MMOH and MMOR from *Methylococcus capsulatus* (Bath) and recombinant protein B were isolated, purified and characterized as previously described.^{11,24,25} All reagents including D₂O (99.9% D; Cambridge Isotope Labs) were obtained from commercial sources and used as received. Unless otherwise specified, protein samples were prepared in buffer, 25 mM MOPS (pH 7.0)/glycerol, 4:1 by volume. In order to reduce the intensity of free radical signals induced in the matrix by γ -radiolysis which partly overlap with the mixed-valent diiron signal, H₂O was

exchanged into D₂O by overnight dialysis. The final concentration of hydroxylase in the samples was 0.65 - 0.90 mM. For hydroxylase samples prepared with MMOB present, the MMOB:MMOH ratio was 2:1. A ternary mixture MMOH-MMOB-MMOR was prepared by adding a stoichiometric amount (1xMMOH) of reductase to the preformed 1:2 complex of Hox with MMOB. Typically 2% by volume of dimethyl sulfoxide (DMSO), methanol (MeOH), or phenol was added to sMMO in studies with these reagents present.

Protein samples were chemically reduced to the mixed-valent state according to a previously reported method.¹⁰ Reoxidized protein was prepared from diferrous MMOH in the presence of two equivalents of MMOB by reduction according to a published procedure⁸ followed by rapid reoxidation in air with gentle agitation and freezing to 77 K within two minutes. Oxidized protein samples were frozen in liquid nitrogen in 3 mm I.D. EPR quartz tubes and exposed to γ -irradiation from a ⁶⁰Co at a dose rate of 0.46 Mrad h⁻¹ for a time sufficient to achieve a total dose of 2.7 - 3.2 Mrad.

X-band EPR spectra were recorded on Bruker ESP300 or EMX spectrometers equipped with an Oxford Instrument ESR900 liquid helium cryostat. The field modulation was set at 100 kHz. The spin concentration of the mixed-valent signal was quantitated under non-saturating conditions by using a standard 1 mM Cu(II)-EDTA solution.²⁰ The half-saturation power, $P_{1/2}$, was determined graphically. EPR spectra at 35 GHz were recorded at 2 K in the rapid-passage dispersion mode on a locally constructed instrument described elsewhere.²⁶

Annealing of cryogenically reduced samples was performed in cooled isopentane for the given time at the stated temperature. Samples were then rapidly cooled to 77 K prior to recording spectra.

Results

One-Electron Cryogenic Reduction of Hydroxylase. Figure 3.2 presents the low-temperature X-band EPR spectra of MMOH in the mixed-valent state generated either by chemical reduction at room temperature (H_{mv}) (Figure 3.2A) or by radiolytic reduction at 77 K (Hox_{mv}) (Figure 3.2B-C). H_{mv} gives rise to a rhombic signal with g values of 1.94, 1.87 and 1.72, similar to that reported previously.¹⁰ Cryogenically reduced Hox exhibits a more complex $g < 2$ EPR spectrum (Figure 3.2B), the shape of which is nearly independent of irradiation dose in the 0.8 - 3.8 Mrad range. Quantitation of the mixed-valent spectrum in Figure 3.2B under nonsaturating conditions indicates that the total yield of a paramagnetic, $S = 1/2$ species upon cryogenic reduction of Hox is $25 \pm 5\%$ of the diiron centers at a dose of 2.7 Mrad. This spectrum varies only slightly with the glycerol content of the sample in the 15-50% range (data not shown).

The spectrum of Hox_{mv} is broadened above 15 K and its shape depends both upon temperature and applied microwave power below 6 K (Figure 3.2C). In the temperature range between 7 K and 15 K, a rhombic mixed-valent pattern with g values of 1.94, 1.86 and 1.79 (g_{av} 1.85, designated H1) dominates, but additional high-field resonances belonging to a signal designated H2 are also observed (Figure 3.2B). Q-band EPR spectra (not shown) indicate that a set of very similar species contribute to the H1 signal. The intensities of the H2 features increase markedly at 3.9 K (Figure 3.2C) as applied microwave power is increased up to 70 mW, and the H2 signal may be obtained by subtraction of the scaled H1 signal. The difference spectrum presented in Figure 3.2D reveals the resulting signal of H2, which has characteristic effective g values of 1.82, 1.77 and 1.68 (g_{av} 1.74). Since cryogenic reduction retains a "footprint" of the diferric geometry, the occurrence of two different signals indicates that Hox exists in two chemically or conformationally distinct forms. We estimate that the H2

population is less than 20% of the total mixed-valent species generated, but accurate quantitation is not possible.

Spectra of Hox_{mv} depend slightly on pH in the 6.1-8.2 range (Figure 3.3). Reducing the pH to 6.1 results in a slight modification of the shape of signal H2 (Figure 3.3A). At pH 8.2, the $g_2 = 1.86$ component of H1 becomes slightly broadened and the relative intensity of the H2 component decreases so that the ratio of the populations H1 and H2 becomes roughly 9:1 (Figure 3.3B).

Effect of Small Molecules on Hox_{mv} . The EPR spectrum of H_{mv} is sensitive to exogenous ligands such as dimethyl sulfoxide^{10,25} and methanol^{17,25} (see also Figure 3.4). Addition of phenol, *p*-nitrophenol, or *p*-fluorophenol also significantly perturbs the EPR spectrum of H_{mv} (Figure 3.5). In the presence of 50 mM phenols, the g_{eff} values shift to 1.94, 1.88 and 1.82 (phenol), 1.95, 1.86 and 1.75 (*p*-nitrophenol) and 1.94, 1.86 and 1.78 (*p*-fluorophenol), respectively.

Unlike the spectral changes that occur when DMSO is added to H_{mv} produced at room temperature, EPR spectra of Hox_{mv} generated at 77 K in the presence (Figure 3.6A) or absence (Figure 3.2B) of 0.25 M DMSO are indistinguishable. This result indicates that DMSO does not bind to the diferric cluster. Some spectroscopic distinctions between Hox_{mv} and $(\text{Hox}+\text{DMSO})_{\text{mv}}$ appear, however, after annealing the samples at 115 K for 15 min. Annealing the samples reduces the H1 signal intensity and perturbs the shape and increases the intensity of the H2 signal (data not shown). The spectroscopic distinctions between the annealed samples are mainly due to species H2. These changes may be indicative of some nonspecific interaction between DMSO and the protein.

By contrast, *p*-nitrophenol and methanol cause dramatic changes in the EPR spectrum of Hox_{mv} , as shown in Figures 6B, 6C, 7A, and 7B. This result suggests that these exogenous agents bind to the diferric cluster. There is prior spectroscopic evidence, formation of a purple color assigned as a ligand-to-metal charge transfer

band, for direct binding of phenol to the diiron cluster of Hox from *M. trichosporium* OB3b,²⁷ although no such feature has yet been detected for the *M. capsulatus* (Bath) enzyme. In the EPR spectra of (Hox+*p*-nitrophenol)_{mv} (Figures 6B, C), signal H2 remains practically unchanged whereas signal H1 disappears and at least two new EPR signals, designated H1Pa and H1Pb, can be identified from their different temperature-dependent relaxation behavior. At 5 K and below (Figure 3.6C), an axial signal H1Pa having $g_{||}=1.95$ and $g_{\perp}=1.80$ is clearly seen, whereas at higher temperatures (data not shown) an additional signal(s) H1Pb, slightly different from signal H1 and having g values of 1.94, 1.87 and 1.81, is observed. We conclude that *p*-nitrophenol binds to the diferric cluster of H1Pa and binds at or near the diferric cluster of H1Pb. Conformer H2 either does not interact with the exogenous ligand under the conditions employed or, less likely, its binding in the active site cavity does not noticeably perturb the EPR properties of the mixed-valent state. The EPR properties of phenol complexes of Hox reduced at 77 K also depend on the nature of substituent in para position. Hox cryogenically reduced in the presence of 50 mM phenol affords a rhombic EPR signal with g values of 1.92, 1.87 and 1.82 (data not shown); this complex was not studied in detail because of its low solubility.

The EPR spectra of (Hox+MeOH)_{mv} (Figures 3.7A, B) comprise at least three distinct EPR signals. The sharp H1 signal from Hox_{mv} is easily distinguished at $T > 9$ K. The main intensities come from two new species (H1M and H2M). The H1M signal can be resolved in a 35 GHz spectrum and is characterized by $g_{\text{eff}} = 1.95, 1.87$ and 1.75 ($g_{\text{av}} = 1.86$); signal H2M is observable below 6 K and was detected by subtracting mixed-valent spectra recorded at 4.3 K and 7 K (Figure 3.7C). The dramatic perturbations in the EPR spectra of cryogenically reduced MMOH induced by methanol strongly indicate that MeOH binds to the diferric active site. Furthermore in (Hox+MeOH)_{mv}, the relative content of H2M species is remarkably increased relative to that of species H2 in the Hox_{mv} sample.

Cryogenic Reduction of the Hox+MMOB Complex in the Presence and Absence of Small Molecules and MMOR. Addition of MMOB to H_{mv} generated at room temperature perturbs the EPR properties of the latter.^{9,11,17} The $(H_{mv}+MMOB)$ complex affords a broad EPR signal (HB1) with effective g values of 1.88, 1.77 and 1.63 (Figure 3.8A) that is difficult to detect at 7K and above. It differs significantly from the EPR spectrum of the $(Hox+MMOB)_{mv}$ generated at 77 K (Figure 3.8B). Mixed-valent species trapped upon cryogenic reduction of MMOHox+B sometimes include a very small percentage (2-5%) of an unusual, very narrow $S=1/2$ signal with g values of 1.96, 1.94 and 1.89 observable even at 77 K. Such a narrow spread in g values is characteristic of oxo-bridged Fe(II)Fe(III) cores.²⁸ MMOB binding does not alter the shape of the Hox_{mv} H2 signal and only slightly perturbs the shape of the $g_2 = 1.86$ component of the Hox_{mv} H1 signal. MMOB does diminish the relative contribution of the H2 signal, however, by factor of 1.6 (cf. Figures 3.8B and 3.2B). These results reveal that binding of MMOB to the resting hydroxylase changes the relative populations of the two diferric forms, while not perturbing the diferric cluster sufficiently to change the spectroscopic properties of Hox_{mv} . When the $(Hox+MMOB)$ complex is prepared by reoxidation of the fully reduced complex $(H_{red}+MMOB)$ with O_2 , the amount of species H2 increases by a factor of 3.

The perturbing effect of MMOB complex formation on the EPR properties of the diiron cluster in Hox_{mv} is significantly enhanced in the presence of higher glycerol concentrations, although glycerol itself does not perturb the EPR spectrum of Hox_{mv} . In 50% glycerol, a new signal for $(Hox+MMOB)_{mv}$ appears at the expense of H1 and H2 (Figure 3.9A). This signal, designated HB2 and shown in Figure 3.9B, is detected by subtracting the EPR spectrum of uncomplexed Hox_{mv} from that of Figure 3.6A. It is characterized by effective g values of 1.9, 1.87 and 1.83 ($g_{av} = 1.87$). The signal is relatively easily saturated at 7 K, with $P_{1/2} < 2$ mW. The observed effect of

MMOB binding on the EPR properties of Hox_{mv} at high concentrations of glycerol may be due to binding of this small molecule at the active site.

Although DMSO has no influence on the EPR spectrum of Hox_{mv} , addition of this reagent has a profound effect on the EPR spectrum of $(\text{Hox}+\text{MMOB})_{\text{mv}}$ (Figure 3.10A vs Figure 3.8B). Spectra recorded below 5 K reveal the loss of the anisotropic EPR signal from species H2 (data not shown), leaving only signals that are of the H1 type. In addition, the 7K spectrum (Figure 3.10A) of these H1-type signals differs from that of $(\text{MMOB}+\text{Hox})_{\text{mv}}$ in the absence of DMSO (Figure 3.9B). The similarity in relaxation properties of mixed-valent species in $(\text{MMOB}+\text{Hox}+\text{DMSO})_{\text{mv}}$ makes it difficult to deconvolute unambiguously the spectra into separate EPR signals. Nonetheless, these observations provide evidence that DMSO changes the relative population of H1 and H2 diiron clusters and in some manner affects the active site H1 diferric centers in Hox when complexed with MMOB, a result not observed in the absence of this protein.

MMOB binding also perturbs the mixed-valent spectra of methanol- and phenol-treated Hox reduced at 77 K. In the EPR spectrum of $(\text{MMOB}+\text{Hox}+\text{MeOH})_{\text{mv}}$, the anisotropic H2M signal completely disappears (Figure 3.10B), signal H1M becomes better resolved (Figure 3.7C) and a new signal appears (Figure 3.10B, C). The cryogenically-reduced MMOB+Hox complex in the presence of phenol exhibits a more anisotropic mixed-valent EPR signal ($g_1=1.91$, $g_2=1.88$ and $g_3=1.79$) compared to phenol-treated Hox alone ($g_1 = 1.92$, $g_2 = 1.87$, $g_3 = 1.82$). In contrast, component B exerts a minor effect on the mixed-valent spectrum of low-temperature reduced, Hox + *p*-nitrophenol complex (data not shown).

Taken together, these results indicate that the EPR spectroscopic properties of the cryogenically reduced diiron cluster, which reflect the diferric active site structure, are sensitive to MMOB binding only when the exogenous agents DMSO, glycerol, methanol, or phenol are present.

Neither methane nor MMOR affects the mixed-valent spectra of the $(\text{MMOB}+\text{Hox})_{\text{mv}}$ complex (data not shown). Weak but reproducible distinctions between the EPR spectra of cryogenically reduced $\text{MMOB}+\text{Hox}$ and $\text{MMOB}+\text{Hox}+\text{MMOR}$ ternary mixtures appear only after annealing the samples at 115 K for 15 min. Annealing the samples reduces the H1 signal intensity and perturbs the shape and increases the intensity of the H2 signal (data not shown). The spectroscopic distinctions between the annealed samples are manifest mainly as differences in the line shapes of the anisotropic H2 signal (data not shown). Annealing experiments at 115 K in frozen water-glycerol solutions carried out with other carboxylate-bridged diiron proteins and model compounds reduced at 77 K similarly revealed only minor alterations in the EPR spectra attributed to outer sphere perturbations of ligation geometry.^{20-23,28} More significant structural rearrangements or diffusion-controlled intermolecular processes do not occur at this low annealing temperature. This result implies that reductase forms a complex with $\text{Hox}+\text{MMOB}$ and thereby affects in some way the relaxation mechanism of the diiron core by perturbing the protein structure.

The mixed-valent species of Hox alone as well as DMSO-, methanol- or phenol-treated Hox, and the $\text{Hox}+\text{MMOB}$ complex all relax to their corresponding equilibrium states after annealing the samples at 293 K for 3-7 min (data not shown). The EPR properties of these relaxed forms are nearly indistinguishable from those of the respective mixed-valent forms of MMOH generated at room temperature. It is of particular interest that $(\text{MMOB}+\text{Hox}+\text{L})_{\text{mv}}$, where $\text{L} = \text{MeOH}$ or phenol, annealed at 293 K exhibit mixed-valent spectra comprising only two EPR signals identical to those of $\text{H}_{\text{mv}}+\text{ligand}$ and $\text{H}_{\text{mv}}+\text{MMOB}$. The spectrum of annealed $(\text{MMOB}+\text{Hox}+\text{DMSO})_{\text{mv}}$ was the same as that of annealed $(\text{Hox}+\text{DMSO})_{\text{mv}}$. As discussed below this observation may be interpreted in terms of competing equilibria between complexation of H_{mv} with MMOB or exogenous ligand. The

transition of the matrix-constrained mixed-valent hydroxylase to the equilibrium state proceeds through several EPR-distinguishable transient intermediates which are differentially stabilized at intermediate temperatures. In particular, upon annealing at 240 K for 3 min, all cryoreduced MMOB+Hox samples displayed a new transient mixed-valent intermediate having a rhombic EPR signal with g values centered at 1.836, 1.67 and 1.47 (data not shown). In most cases, however, the samples annealed at temperatures below 240 K revealed several mixed-valent intermediates present simultaneously, making it difficult to identify and analyze unambiguously the EPR component signals.

Discussion

Radiolytic reduction of the diiron(III) core at the active site of the MMO hydroxylase enzyme in frozen 4:1 buffer/glycerol solutions at 77 K affords transient Fe(II)Fe(III) mixed-valent species in $25 \pm 5\%$ yield based on iron sites at a dose of 3 Mrad. In the absence of MMOB or other additives, the spectrum of MMOH reduced by one electron at 77 K revealed at least two populations of distinct Fe(II)Fe(III) clusters giving rise to the $g < 2$ EPR signals H1 and H2 (Figures 3.2B and 3.2D). The relative contributions of these species were almost independent of irradiation dose in the studied range. Similar transient mixed-valent intermediates with cognate EPR properties were recently reported for MMOH from *M. trichosporium* OB3b radiolytically reduced at 77 K in a frozen 1:1 buffer/glycerol glass.²² The latter H1 EPR signal was more homogeneous and more intense than signal H2. The signals H1 and H2 differ from that of H_{mv} generated at room temperature both in g values and relaxation characteristics. These observations suggest that the mixed-valent species produced at 77 K and room temperature have distinct diiron cluster structures.

Assuming that cryogenic reduction preserves the active site diferric cluster geometry we may draw the following conclusions. The resting oxidized hydroxylase in solution has at least two populations of distinct diiron sites and their structures are different from that of the Fe(II)Fe(III) center in the equilibrium form of the protein generated at room temperature. The observation of two distinguishable diiron(III) structures for the resting form of enzyme is not surprising given the variety of oxidized structures exhibiting carboxylate-shifted glutamate residues revealed by X-ray crystallography¹³⁻¹⁵ and the heterogeneity uncovered by rapid freeze-quench Mössbauer spectroscopy of protein from *M. capsulatus* (Bath)⁸ and EXAFS studies of Hox from *M. trichosporium* (OB3b) hydroxylase.¹⁹ Scheme 3.1 depicts four possible structures that might be considered. Structure 1 contains a bis(μ -hydroxo)diiron(III) core and a terminal water molecule on Fe1. In structure 2, the proton has shifted from the terminal water to one of the bridging positions, affording a (μ -aqua)(μ -hydroxo)diiron(III) unit. Both types of solvent-bridging units have been observed in the X-ray structures of Hox.^{14,15} The third possibility (structure 3) is that only one solvent-derived ligand, a hydroxo group, links the two iron atoms in addition to Glu 144, as suggested to explain the EXAFS results.¹⁹ Structure 4 is a close relative to 2. These structures would be expected to have different exchange coupling constants, J , and zero-field parameters, D . The bis(μ -hydroxo)diiron(III) core (1) would be expected to have the largest magnitude J and probably the lowest $P_{1/2}$ value. Because a bridging water molecule will be easier to deprotonate than a terminal one, 1 would form preferentially at higher pH. We therefore tentatively assign H1 to this structure. Both 2/4 and 3 should afford a more anisotropic signal upon cryoreduction, and we suggest that H2 may correspond to one of these two alternative geometries. The intensity of the H2 signal depends on pH, the presence of component B, reoxidation of the MMOH/MMOB complex, and

annealing of the sample at 115 K for 20 min. These observations provide indirect evidence that H1 and H2 are in dynamic equilibrium.

Although we do not yet have direct X-ray diffraction evidence for the equilibrium structure of H_{mv} , it is possible that a carboxylate shift takes place, similar to that observed for the fully reduced, diiron(II) form of the enzyme (Figure 3.1B).^{14,16} Such a structure would exhibit an EPR spectrum distinct from that of both H1 and H2. It would, moreover, open one or more sites for binding of exogenous ligands such as DMSO and phenols, which alter the spectrum. Scheme 3.2 depicts three such possible structures, which differ in a manner similar to that observed for the fully reduced enzyme.^{14,16} ENDOR studies of DMSO-treated H_{mv} from *M. capsulatus* (Bath) indicate that this exogenous ligand binds through its oxygen atom to Fe(III) and perturbs the geometry of both histidines coordinated to the center.¹⁰

Relaxation of the spectra of cryoreduced Hox to the equilibrium state proceeds via a few EPR distinguishable transient forms differentially stabilized at higher annealing temperatures and is complete, given sufficient time, only at 273-293 K. By contrast, mixed-valent species generated by cryoreduction at 77 K from R2 of RNR,^{20,21,23} hemerythrin,²⁰ and dinuclear iron model compounds²⁸ trapped at 77 K relaxed to their equilibrium states below 230 K. The relatively high temperature of relaxation of the cryogenically produced mixed-valent forms of MMOH is consistent with carboxylate shifting as depicted in Scheme 3.2.

DMSO does not measurably perturb the EPR properties of Hox reduced at 77 K, indicating that it most likely does not bind directly to the diiron(III) center. This result is consistent with other observations. The crystal structure of Hox from *M. capsulatus* (Bath) soaked in DMSO failed to reveal this molecule in the active site.²⁹ Moreover, addition of 0.3 M DMSO to the resting Hox from *M. trichosporium* OB3b had no effect on the Mössbauer spectrum of the diiron center.¹⁷ The spectral distinctions between cryogenically reduced Hox and DMSO which appear after

annealing at 115 K might reflect the carboxylate shift postulated for H_{mv} , opening a site for DMSO coordination. Alternatively, this solvent could affect ordered water structure in the active site cavity (Figure 3.1), switching interligand hydrogen bonding interactions at the diiron center and altering the EPR spectrum. Species 2 and 4 in Scheme 3.1 illustrate how such an effect might be manifest.

Unlike DMSO, phenols can apparently coordinate directly to iron at the active site of Hox.²⁷ Accordingly, this interaction is evident in the EPR spectrum of mixed-valent species trapped at 77 K. Two signals, HP1a and HP1b, are observed which we assign to *p*-nitrophenol complexes with the H1 form (1) of the diiron cluster. That signal H2 remains unchanged in the mixed-valent EPR spectrum suggests that the phenol displaces the terminally coordinated water in 1, which is not available in 2, and provides evidence that H1 and H2 diiron(III) centers react differently toward exogenous ligands.

The significant changes in the EPR spectra of cryoreduced Hox in the presence of methanol reflect perturbations of the active site local structure suggesting that this exogenous ligand, the product of methane oxidation, binds directly to the diiron(III) center. Two new EPR signals, H1M and H2M, were identified, which might arise in several ways. One likely possibility is that the terminal water molecule in 1 (Scheme 1) is displaced by methanol, the less demanding steric properties of which might make it better suited for such a displacement reaction than DMSO, which apparently does not undergo such a reaction. Moreover, like the phenols, methanol can serve as both a hydrogen bond donor and acceptor and thus perturb the water structure at the active site. Such an interaction could alter the intracomplex H-bonding interactions, and possibly even the positioning of the hydroxo and aqua ligands, e. g., 1 vs 2 (or 4), perturbing the EPR spectra. Another possible explanation is that two methanol molecules might be bound to the diiron(III) center. Quantitation reveals that cryogenically reduced Hox forms mixed-

valent species H1 accounting for 80% of the signal, whereas in the methanol-treated affords species less than 40 ± 15 % of H1M. We have no evidence that mixed-valent species H1M and H2M originate from H1 and H2, respectively, but the ability of methanol to affect the relative amounts of cryogenerated mixed-valent hydroxylase centers supports the previous conclusion that the resting oxidized hydroxylase isomers are in dynamic equilibrium with one another in solution.

As already mentioned, the results of EPR and CD/MCD investigations have been taken as evidence that MMOB perturbs the structure of the diiron site in mixed-valent³⁰ and fully reduced MMOH.¹² Our results reveal, however, that the complexation formation between Hox and MMOB does not measurably affect the H1 and H2 EPR signal lineshapes and only slightly reduces the relative intensity of signal H2. We therefore conclude that only minor alterations in ligand binding occur at the dinuclear iron center of resting MMOH induced by MMOB complex formation. For example, changes in intraligand H-bonding might occur, but carboxylate shifts are less likely. Possibly MMOB binding affects the orientation of the side chain of Leu 110, which adopts two conformations in crystalline MMOH and may gate the access of substrates to the active site cavity.³¹ Such a conclusion would be qualitatively consistent with the published X-ray absorption studies on MMOH from both *M. capsulatus* (Bath) and *M. trichosporium* OB3b.^{18,19} For MMOH from the latter organism, a difference occurred in the distribution of long (3.4 Å) versus short (3.0 Å) Fe...Fe distance contributions to the first shell in the presence of component B present.¹⁹

An alteration in ligand environment induced by MMOB binding would also explain its ability to facilitate binding of DMSO and high concentrations of glycerol to the diiron center. Complexation with MMOB dramatically perturbs the EPR spectra of cryogenically reduced MMOH in the presence of both DMSO and glycerol at high concentrations. Several distinct EPR signals may be identified in the

spectrum of the irradiated Hox+MMOB+DMSO system, each of which differs from the H1 and H2 signals observed in the mixed-valent spectrum of hydroxylase with DMSO present. This result in turn implies that more than one population of diiron cluster is present in the Hox+MMOB complex treated with DMSO. In the presence of 50% glycerol, a new EPR signal (HB2), as well as signals H1 and H2, appear for cryogenically reduced Hox complexed with MMOB. A similar EPR signal was previously reported in the EPR spectrum of the Hox+MMOB complex from *M. trichosporium* OB3b in 50% glycerol solution, γ -irradiated at 77 K.²² Like DMSO, glycerol can bind to the diferric cluster of Hox with MMOB present. The binding is much weaker, however, because much higher concentrations of glycerol are required to detect the EPR signal.

Since MMOB can affect the binding of exogenous ligands to the diiron center in Hox, we were especially interested to examine cryogenically reduced Hox+MMOB in the presence of methane or reductase. Addition of methane under saturating concentrations had no effect on the mixed-valent spectrum of Hox complexed with MMOB. This result implies either that the substrate has a low affinity for the Hox+MMOB complex or that its binding in cavity 1 is such that the spectrum remains unchanged. The influence of MMOR on the EPR properties of the Hox+MMOB complex reduced at 77 K is manifest only after annealing the sample at 115 K. This observation suggests that reductase binding perturbs in some manner the active site pocket structure and influences the relaxation mechanism of the constrained mixed-valent cluster. Possibly, like MMOB, reductase binding perturbs slightly the coordination environment of the diiron(III) cluster and these structural changes can noticeably modify reactivity of the active site as reported elsewhere.^{8,24,32}

The results on cryogenically reduced Hox+MMOB+exogenous ligands annealed at room temperature are of particular interest because they may shed light on the ability of MMOB to affect the binding of substrates and products to H_{mv} . If, as

suggested in Scheme 3.2, H_{mv} is structurally analogous to H_{red} , this information might help to delineate how component B prepares the reduced hydroxylase for dioxygen binding and activation. The low-temperature reduced Hox+MMOB complex, after annealing at room temperature, displays an EPR spectrum characteristic of H_{mv} complexed with component B (Figure 3.5A). We conclude that a carboxylate-shift has occurred, as indicated in Scheme 3.2. The spectrum of annealed H_{mv} +MMOB+DMSO, however, contains only the EPR signal typical of DMSO-treated H_{mv} . Previous work has determined that DMSO binds to the ferric iron in H_{mv} , modeled as Fe_2 .¹⁰ and we suggest that the presence of MMOB does not impede formation of carboxylate-shifted Glu 243 and loss of water to open a site on Fe2 (Scheme 2). The EPR spectra of cryogenically reduced Hox+MMOB+L (L = methanol, phenol, or *p*-nitrophenol) after annealing at room temperature comprises two signals which appear to be identical to those of H_{mv} +MMOB and H_{mv} +exogenous ligand, respectively. In light of the data revealing that MMOB can affect the EPR properties of cryogenically reduced Hox in the presence of small molecules, it seems unlikely that binding exogenous ligands to the diiron cluster of the H_{mv} +MMOB complex or of component B to H_{mv} complexed with exogenous ligands would not perturb the mixed-valent signals. It therefore seems likely that alcohol or phenol binding occurs at Fe1 and that MMOB opens a site on Fe2, as depicted by the structures in Scheme 3.2. These findings further underscore the conclusion that component B and the redox state of the diiron clusters in MMOH both substantially affect the binding of exogenous ligands.

Conclusions

The results of the present work, taken together with other physicochemical results reported for the MMO system, provide insights into the structural basis for the regulatory effect of component B. Spectroscopic data show that the interaction of

MMOB with MMOH depends on the oxidation state of the diiron center, accounting thereby for observed changes in redox potentials of MMOH induced by binding MMOB. The ability of component B to alter the structure of the MMOH diiron(III) cluster containing bound methanol or phenol suggests that this component may also exert a similar effect on substrate or product binding in the active site. Opening the leucine gate and facilitating carboxylate shifts of the coordinated glutamates are suggested as specific chemical steps which could account for such behavior.

The EPR spectra of the cryoreduced samples also reveal that the resting state, oxidized hydroxylase has at least two populations of diiron cluster, the structures of which are different from that of the equilibrium Fe(II)Fe(III) site. Their relative contributions depend on pH, component B and enzyme turnover. Specific proposals involving proton and carboxylate shifts at the diiron center have been put forward as a working hypothesis to explain these observations. Complex formation among MMOB, MMOR, and MMOHox does not measurably affect the diferric site structure. Cryogenic reduction in combination with EPR spectroscopy has provided information about the interaction of Hox with small molecules. The diiron(III) site of the hydroxylase binds methanol and phenols, whereas DMSO and methane have no measurable effect on the EPR properties of subsequently cryoreduced samples. Addition of component B favors binding of some exogenous ligands such as DMSO and glycerol to the active site diferric state and perturbs remarkably the structure of the diiron(III) cluster complexed with exogenous ligand (methanol, phenol). This study also reveals different reactivity of the Fe(III,III) and Fe(II,III) sites of MMOH toward small molecule substrates.

References

- (1) This work will be submitted for publication in a slightly different form. See reference 2.
- (2) Davydov, R.; Valentine, A. M.; Hoffman, B. M.; Lippard, S. J. 1998, to be submitted for publication.
- (3) Dalton, H. In *Adv. Appl. Microbiol.* Academic Press: 1980; Vol. 26; pp 71-87.
- (4) Liu, K. E.; Lippard, S. J. In *Advances in Inorganic Chemistry*; Sykes, A. G., Eds.; Academic Press: San Diego, 1995; Vol. 42; pp 263-289.
- (5) Wallar, B. J.; Lipscomb, J. D. *Chem. Rev.* 1996, 96, 2625-2657.
- (6) Lund, J.; Dalton, H. *Eur. J. Biochem.* 1985, 147, 291-296.
- (7) Gassner, G. T.; Lippard, S. J. to be submitted for publication.
- (8) Liu, K. E.; Valentine, A. M.; Wang, D.; Huynh, B. H.; Edmondson, D. E.; Salifoglou, A.; Lippard, S. J. *J. Am. Chem. Soc.* 1995, 117, 10174-10185.
- (9) Fox, B. G.; Liu, Y.; Dege, J. E.; Lipscomb, J. D. *J. Biol. Chem.* 1991, 266, 540-550.
- (10) DeRose, V. J.; Liu, K. E.; Lippard, S. J.; Hoffman, B. M. *J. Am. Chem. Soc.* 1996, 118, 121-134.
- (11) DeWitt, J. G.; Bentsen, J. G.; Rosenzweig, A. C.; Hedman, B.; Green, J.; Pilkington, S.; Papaefthymiou, G. C.; Dalton, H.; Hodgson, K. O.; Lippard, S. J. *J. Am. Chem. Soc.* 1991, 113, 9219-9235.
- (12) Pulver, S. C.; Froland, W. A.; Lipscomb, J. D.; Solomon, E. I. *J. Am. Chem. Soc.* 1997, 119, 387-395.
- (13) Rosenzweig, A. C.; Frederick, C. A.; Lippard, S. J.; Nordlund, P. *Nature* 1993, 366, 537-543.
- (14) Rosenzweig, A. C.; Nordlund, P.; Takahara, P. M.; Frederick, C. A.; Lippard, S. *J. Chem. Biol.* 1995, 2, 409-418.
- (15) Elango, N.; Radhakrishnan, R.; Froland, W. A.; J., W. B.; Earhart, C. A.; Lipscomb, J. D.; Ohlendorf, D. H. *Protein Sci.* 1997, 6, 556-558.

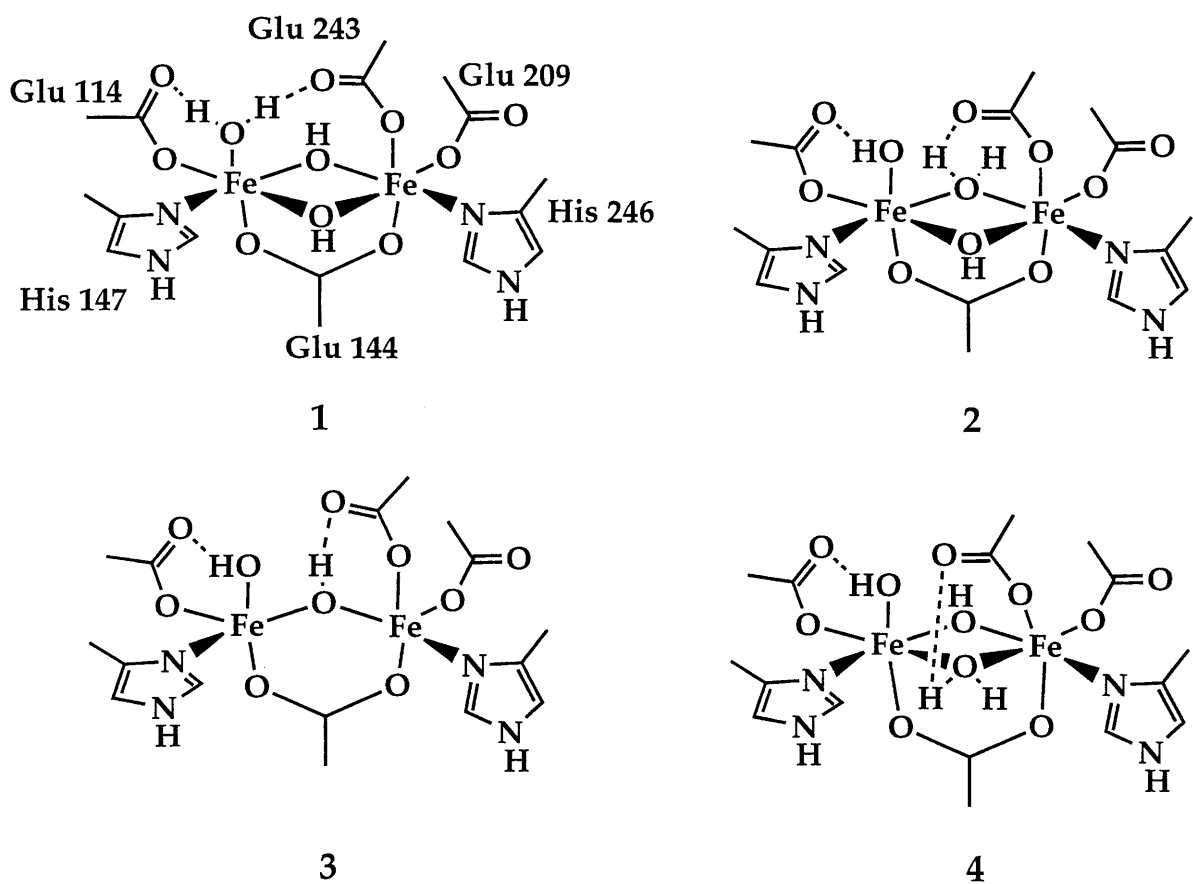
- (16) Whittington, D. A.; Lippard, S. J. to be submitted for publication.
- (17) Fox, B. G.; Hendrich, M. P.; Surerus, K. K.; Andersson, K. K.; Froland, W. A.; Lipscomb, J. D.; Münck, E. J. *Am. Chem. Soc.* **1993**, *115*, 3688-3701.
- (18) DeWitt, J. G.; Rosenzweig, A. C.; Salifoglou, A.; Hedman, B.; Lippard, S. J.; Hodgson, K. O. *Inorg. Chem.* **1995**, *35*, 2505-2515.
- (19) Shu, L.; Liu, Y.; Lipscomb, J. D.; Que, L., Jr. *J. Bioinorg. Chem.* **1996**, *1*, 297-304.
- (20) Davydov, R.; Kuprin, S.; Gräslund, A.; Ehrenberg, A. *J. Am. Chem. Soc.* **1994**, *116*, 11120-11128.
- (21) Davydov, R.; Shalin, M.; Kuprin, S.; Gräslund, A.; Ehrenberg, A. *Biochemistry* **1996**, *35*, 5571-5576.
- (22) Davydov, A.; Davydov, R.; Gräslund, A.; Lipscomb, J. D.; Andersson, K. K. *J. Biol. Chem.* **1997**, *272*, 7022-7026.
- (23) Davydov, R.; Davydov, A.; Ingemarsson; Thelander, L.; Ehrenberg, A.; Gräslund, A. *Biochemistry* **1997**, *36*, 9093-9100.
- (24) Valentine, A. M.; Wilkinson, B.; Liu, K. E.; Komar-Panicucci, S.; Priestley, N. D.; Williams, P. G.; Morimoto, H.; Floss, H. G.; Lippard, S. J. *J. Am. Chem. Soc.* **1997**, *119*, 1818-1827.
- (25) Willems, J.-P.; Valentine, A. M.; Gurbiel, R.; Lippard, S. J.; Hoffman, B. M. *J. Am. Chem. Soc.* **1998**, *120*, in press.
- (26) Werst, M. M.; Davoust, C. E.; Hoffmann, B. M. *J. Am. Chem. Soc.* **1991**, *113*, 1533-1538.
- (27) Andersson, K. K.; Elgren, T. E.; Que, L., Jr.; Lipscomb, J. D. *J. Am. Chem. Soc.* **1992**, *114*, 8711-8713.
- (28) Davydov, R.; Menage, S.; Fontecave, M.; Gräslund, A.; Ehrenberg, A. *J. Biol. Inorg. Chem.* **1997**, *2*, 242-255.
- (29) Rosenzweig, A. C.; Frederick, C. A.; Lippard, S. J. *Carboxylate Shifts in the Active Site of the Hydroxylase Component of Soluble Methane Monooxygenase*

from *Methylococcus capsulatus* (Bath); Kluwer Academic Publishers: Dordrecht, 1996, p 141-149.

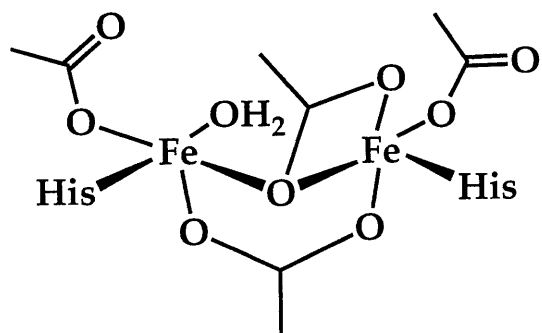
(30) Froland, W. A.; Andersson, K. K.; Lee, S.-K.; Liu, Y.; Lipscomb, J. D. *J. Biol. Chem.* **1992**, *267*, 17588-17597.

(31) Rosenzweig, A. C.; Brandstetter, H.; Whittington, D. A.; Nordlund, P.; Lippard, S. J.; Frederick, C. A. *Proteins* **1997**, *29*, 141-152.

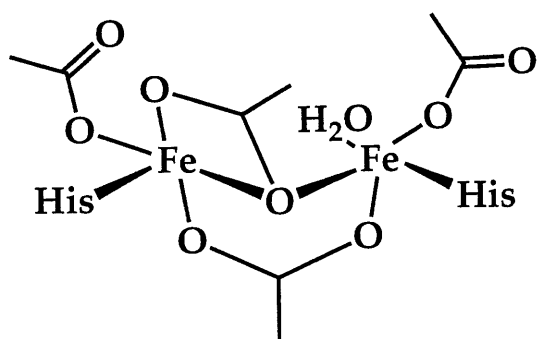
(32) Liu, Y.; Nesheim, J. C.; Paulsen, K. E.; Stankovich, M. T.; Lipscomb, J. D. *Biochemistry* **1997**, *36*, 5223-5233.



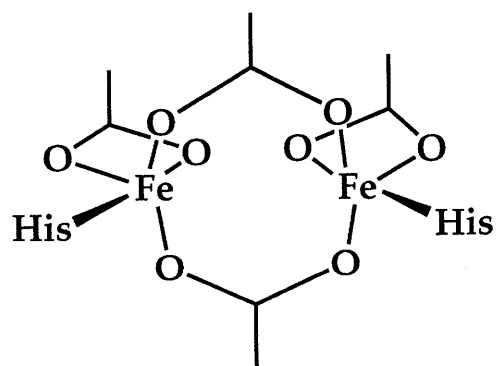
Scheme 3.1.



5



6



7

Scheme 3.2.

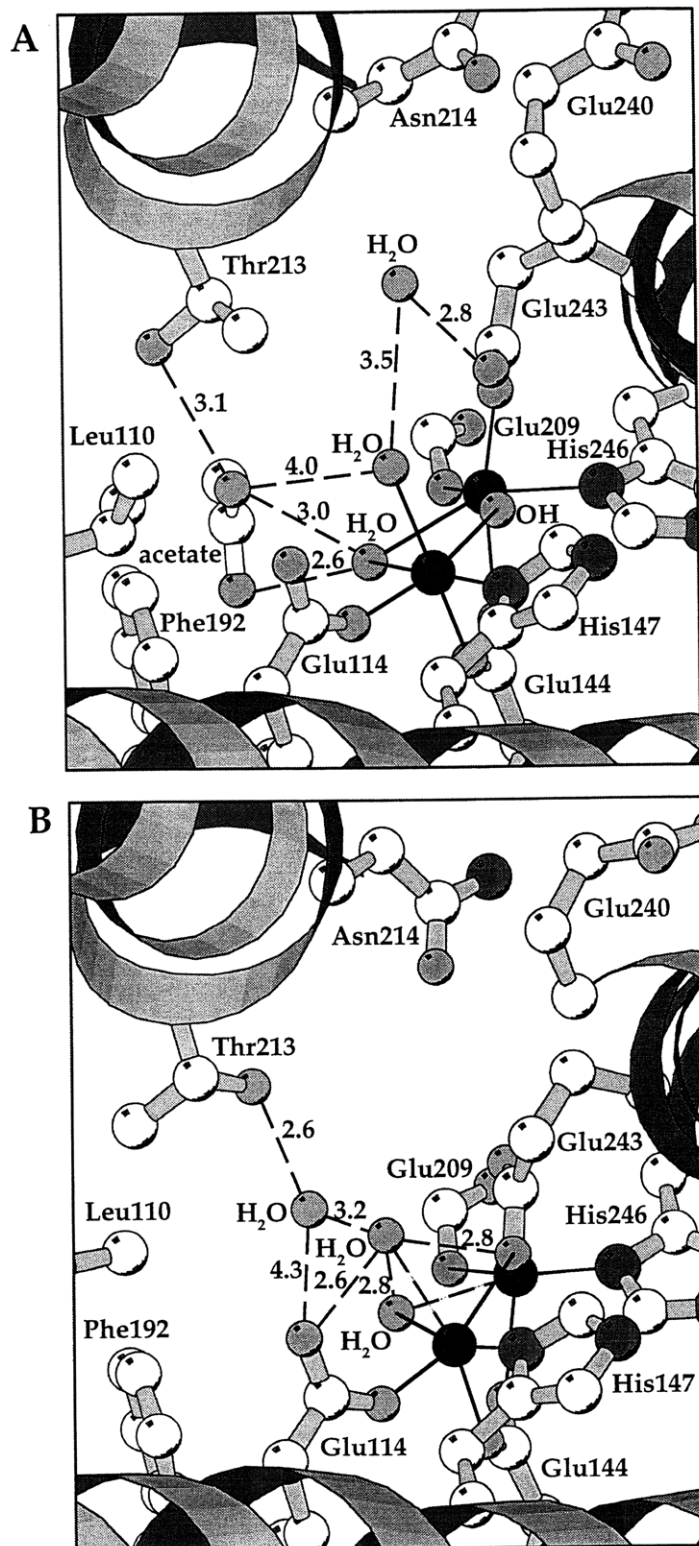


Figure 3.1. The diiron active site of MMOH in the oxidized diferric (A) and reduced diferrous (B) states.¹⁴ Hydrogen bonding interactions are depicted along dotted lines, with the distances indicated.

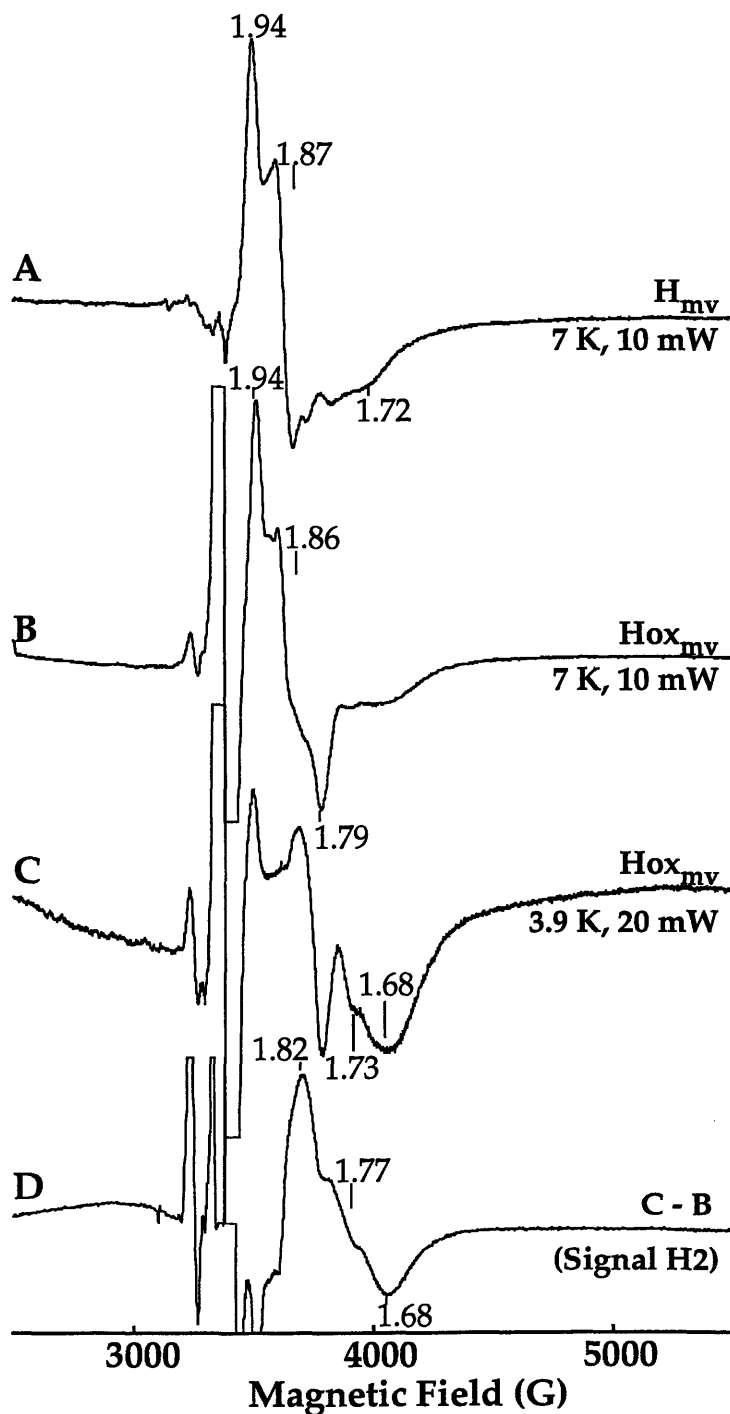


Figure 3.2. X-band EPR spectra of mixed-valent forms of MMOH (pH 7.0) generated chemically at room temperature (A) and in 4:1 buffer-glycerol generated radiolytically at 77 K (B, C); (D) difference spectrum of the signal H2 obtained by subtraction of scaled spectrum (B) from spectrum (C) as described in text. Instrument parameters: modulation frequency, 100 kHz; modulation amplitude, 10 G; gain, 5000; frequency 9.235.

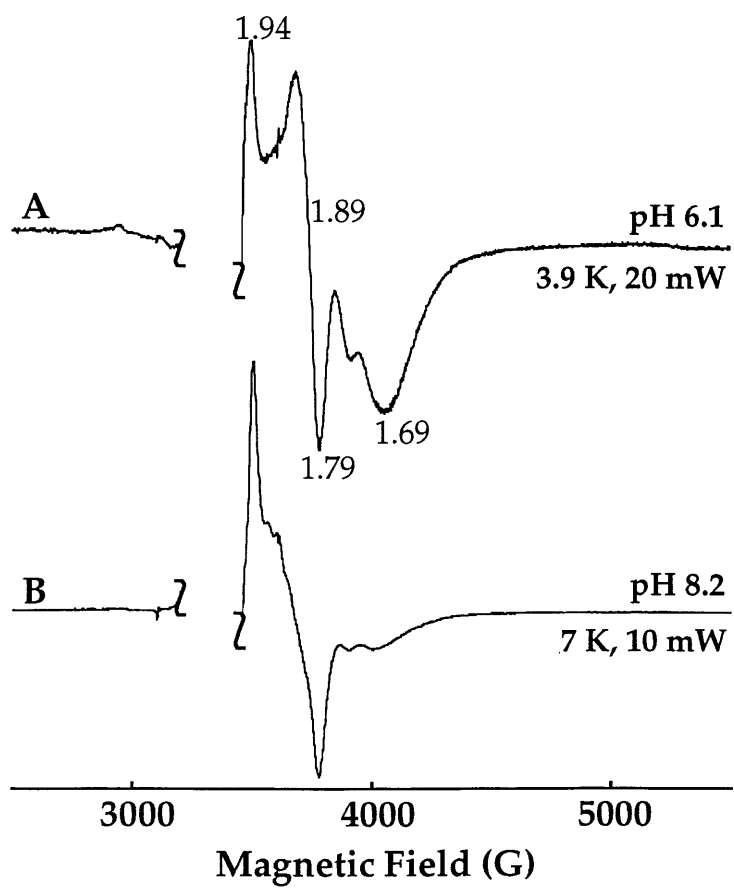


Figure 3.3. X-band EPR spectra of $\text{MMOHox}_{\text{mv}}$ in buffer-glycerol (4:1).

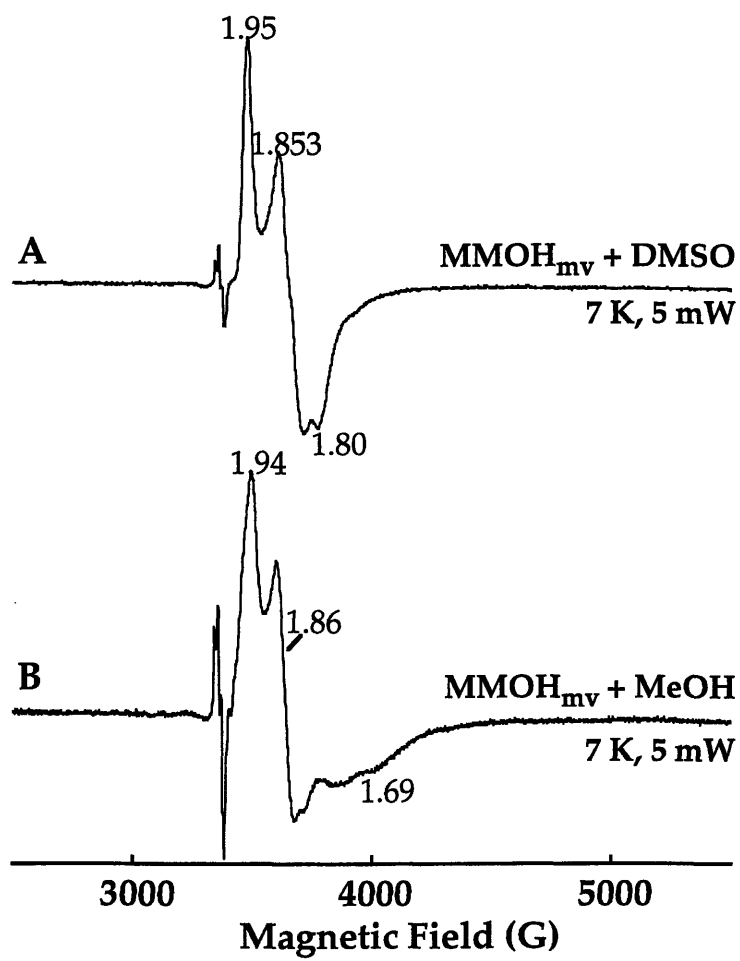


Figure 3.4. X-band EPR spectra of chemically reduced MMOH_{mv} in the presence of DMSO (A) or methanol (B).

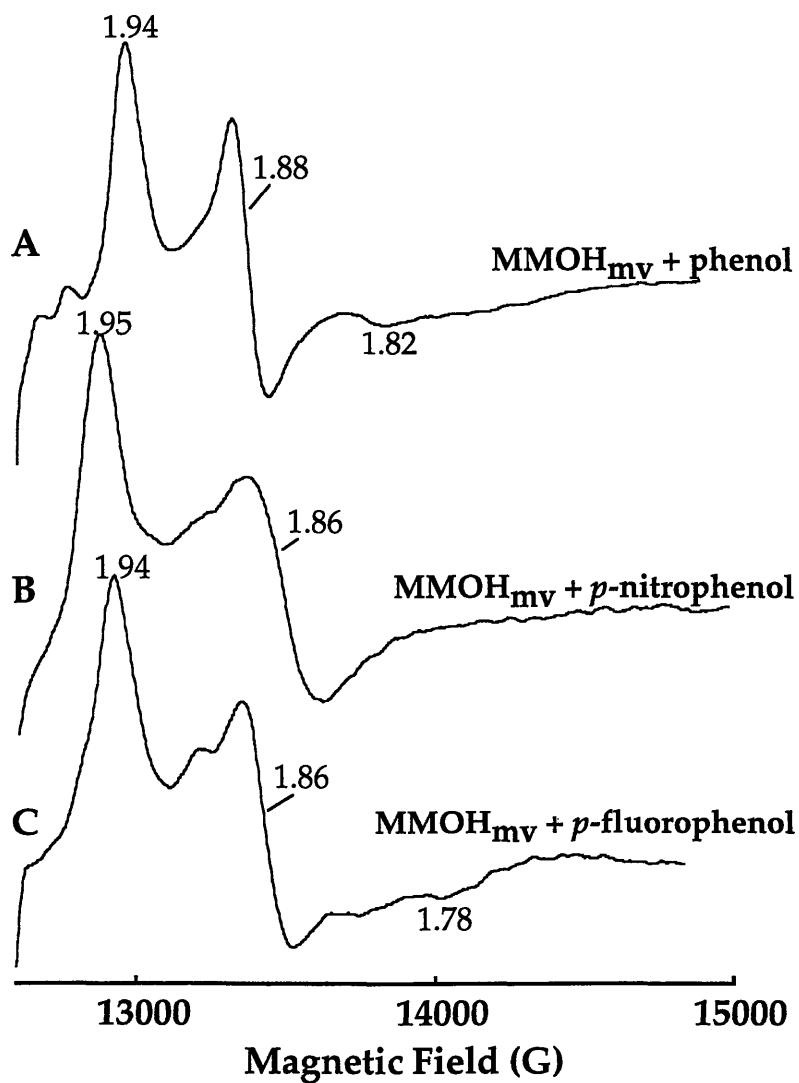


Figure 3.5. 35 GHz EPR spectra of MMOH_{mv} in the presence of 50 mM phenols. Samples were prepared by radiolytic reduction followed by annealing to give the equilibrium H_{mv} + phenol form. The EPR spectrum of a sample prepared by addition of *p*-nitrophenol to chemically reduced H_{mv} was identical to (B). All spectra were acquired at 2K, 2G, 30 db with (A) 35.13 GHz, (B) 35.043 GHz, and (C) 35.045 GHz.

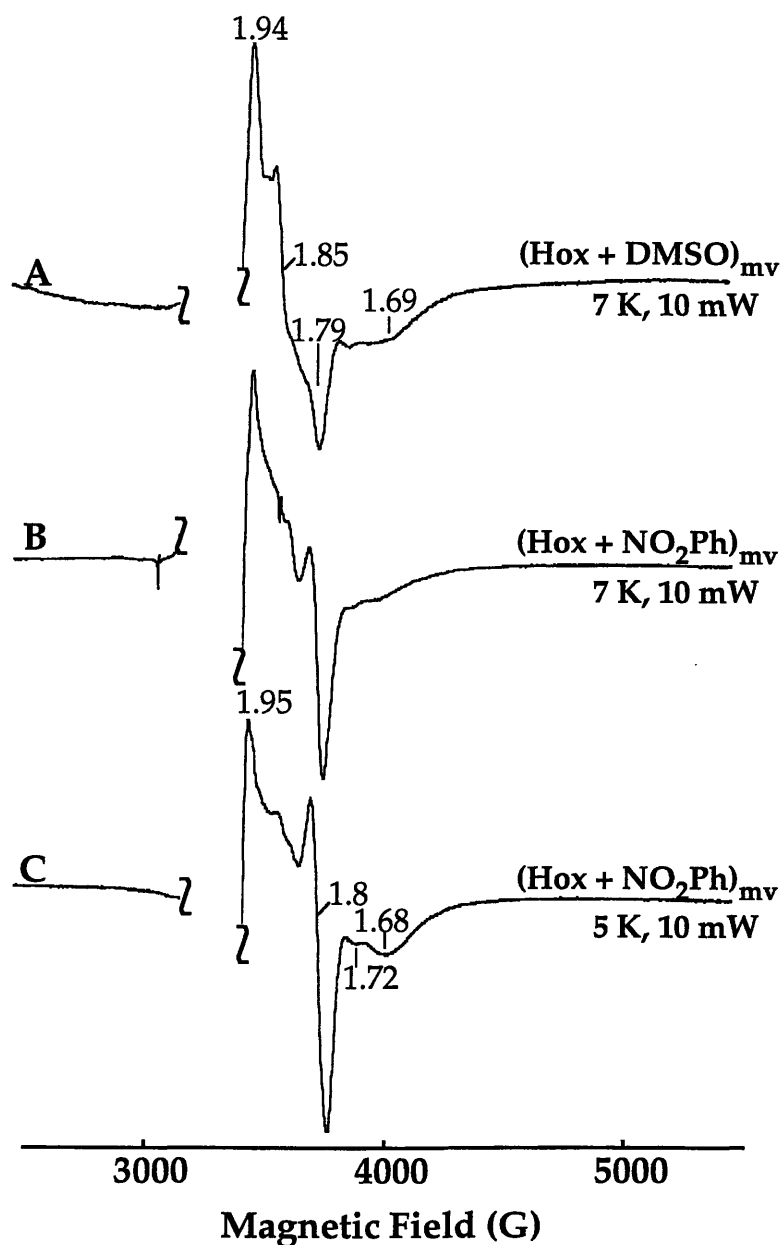


Figure 3.6. X-band EPR spectra of oxidized hydroxylase in the presence of 0.25 M DMSO (A) and 50 mM *p*-nitrophenol (B, C) radiolytically reduced at 77 K. In this and the remaining figures, the offscale $g = 2$ signal due to radical species generated by radiolytic reduction (see Figures 3.2A, B, C) is truncated for clarity. Instrument conditions were as in Figure 3.2 except for temperature and power as noted.

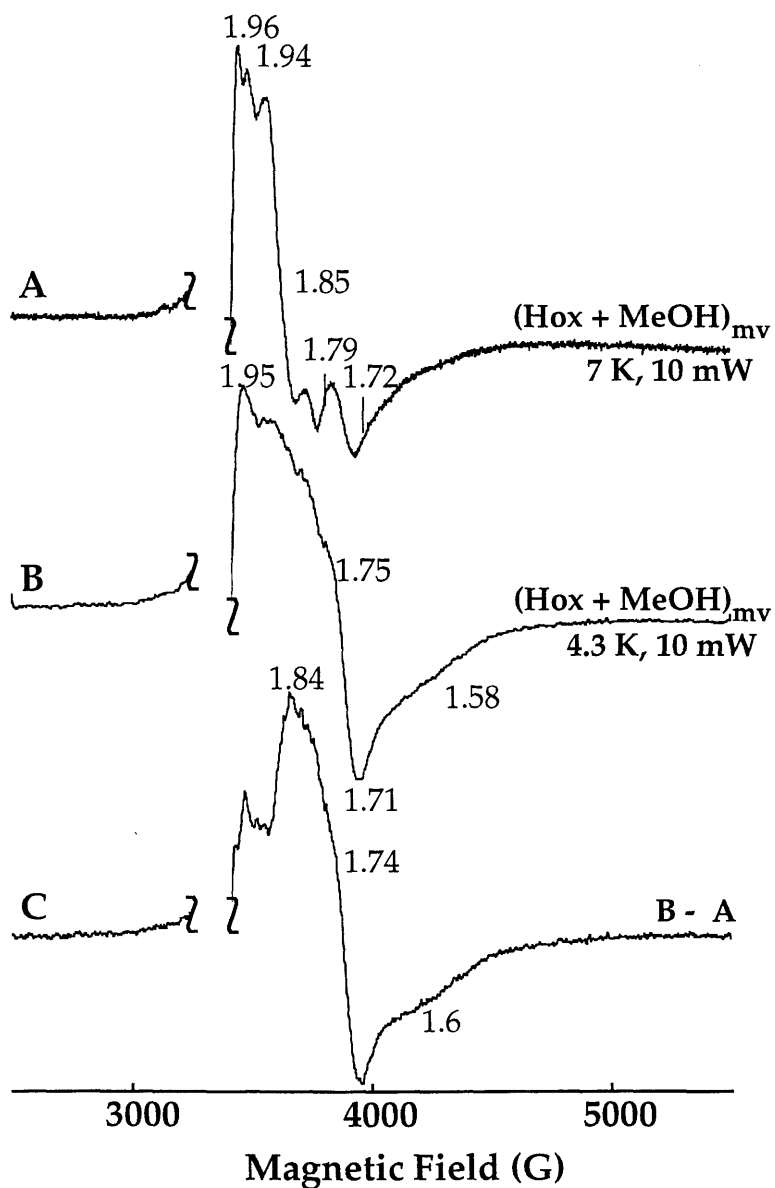


Figure 3.7. X-band EPR spectra of mixed-valent form of MMOH in the presence of 2% methanol produced by reduction at 77 K (A, B); (C) difference spectrum (B)-(A). Instrument parameters were as in Figure 3.2 except temperature and power as noted.

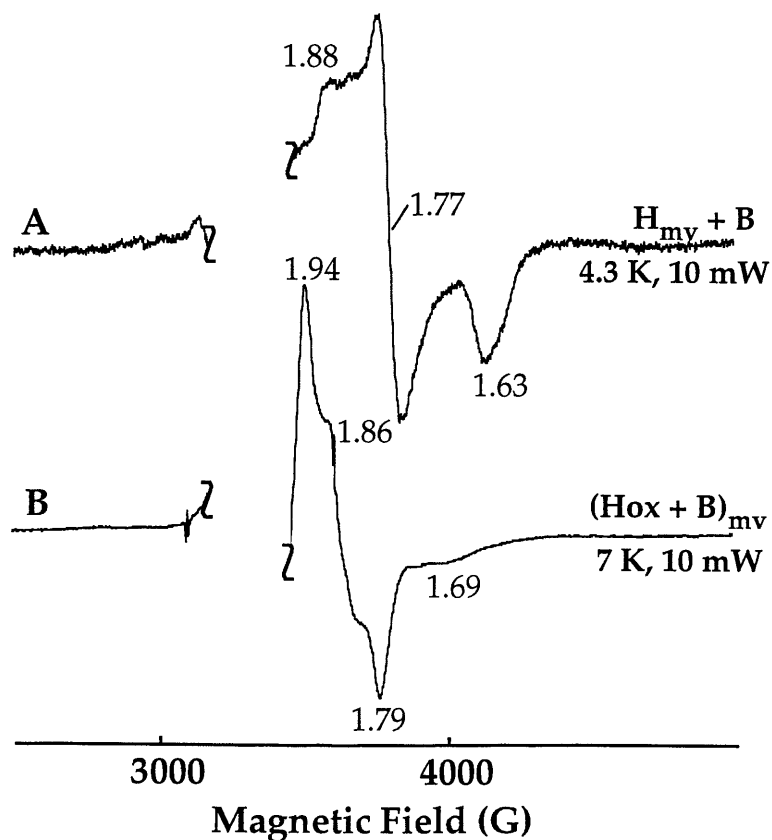


Figure 3.8. X-band EPR spectra of mixed-valent forms of the hydroxylase + component B complex produced by chemical reduction at room temperature (A) and by radiolytic reduction at 77 K (B). Instrument conditions were as in Figure 3.2 except for temperature and power as noted.

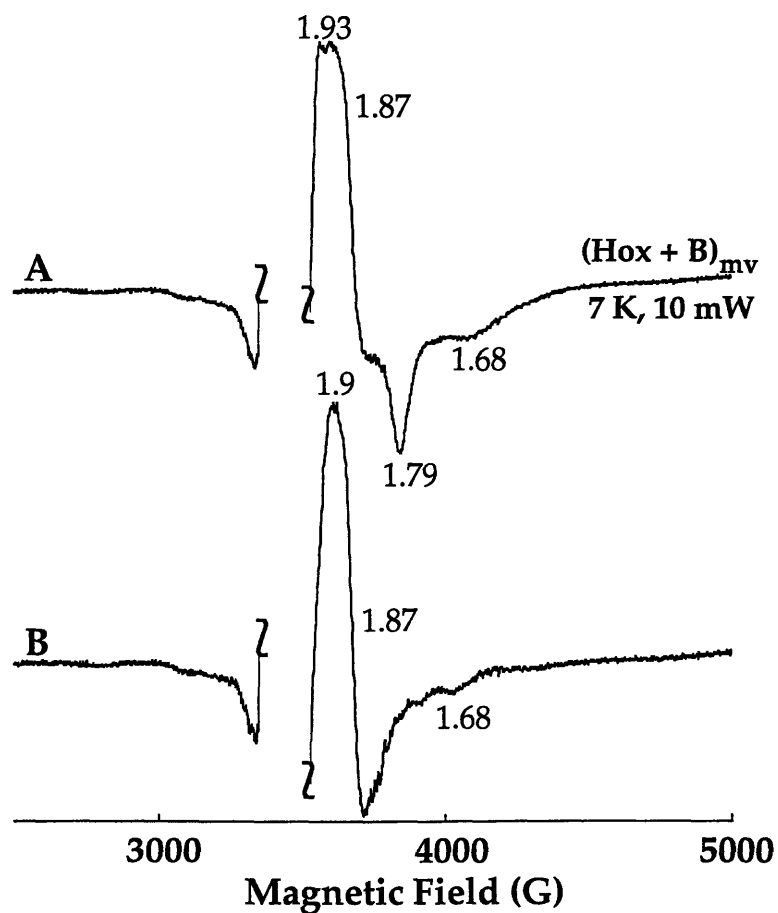


Figure 3.9. X-band EPR spectra of the $(\text{Hox}+\text{MMOB})_{\text{mv}}$ complex in 1:1 buffer-glycerol (A); (B) difference spectrum of signal HB2 obtained by subtraction of the spectrum of Figure 3.2B from spectrum (A). Instrument parameters were as in Figure 3.2 except for temperature and power as noted.

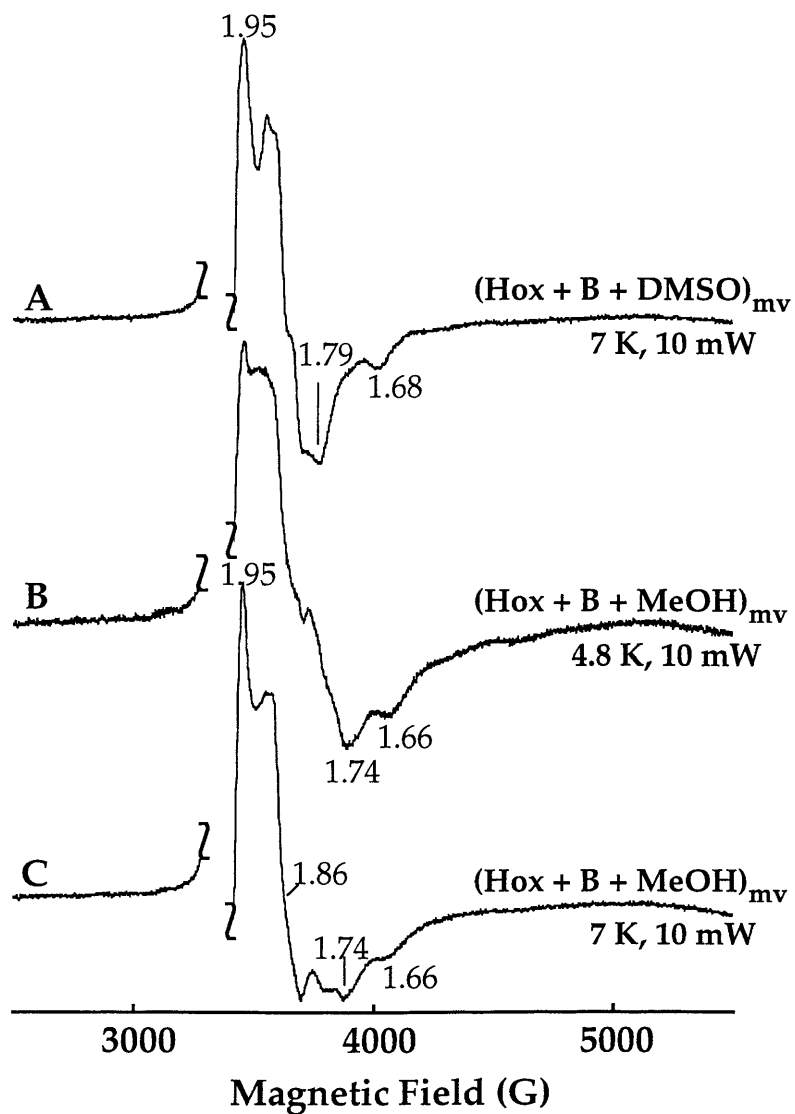


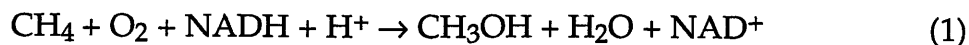
Figure 3.10. X-band EPR spectra of the $(\text{Hox} + \text{MMOB})_{\text{mv}}$ complex in the presence of 2% DMSO (A) and 2% methanol (B, C). Instrument parameters were as in Figure 3.2 except for temperature and power as noted.

Chapter Four:

An Investigation of the Reaction of Reduced Methane Monooxygenase Hydroxylase with Dioxygen and Substrates by Rapid Freeze-Quench and Stopped-Flow Spectroscopy

Introduction^{1,2}

The active site of the soluble methane monooxygenase (sMMO) hydroxylase effects the reductive activation of dioxygen and the oxidation of substrate molecules.^{3,4} The reaction for which the enzyme is named (eq 1)



is the physiologically relevant one and is impressive given the 104 kcal/mol C-H bond being activated and the kinetic inertness of methane. In methanotrophic organisms from which sMMO is isolated, this reaction represents the first step in the assimilation of carbon and energy for the cell.^{5,6} The protein system from *Methylococcus capsulatus* (Bath), which operates at 45 °C, consists of a 251 kD hydroxylase (MMOH)⁷⁻¹⁰ which is an $\alpha_2\beta_2\gamma_2$ homodimer containing one dinuclear non-heme iron center in each α subunit. A 38.5 kD reductase protein (MMOR) supplies reducing equivalents to these centers during catalytic turnover.^{7,11} Finally, a 15.8 kD component lacking cofactors (MMOB) acts as a coupling protein,¹²⁻¹⁴ linking electron consumption with hydrocarbon oxidation (eq. 1).

The first step in the catalytic cycle is the reduction of active site iron to the diferrous state by electrons from MMOR. Under steady state conditions, electron transfer is greatly accelerated by the presence of substrate.^{14,15} This control mechanism allows the protein to avoid futile cycles, in which oxygen-activated iron species are nonproductively generated in the absence of substrate, wasting reducing equivalents and possibly damaging the protein by oxidization of amino acid side chains. The diiron center can be chemically reduced and maintained anaerobically for reaction with dioxygen under rapid mixing conditions. Such single turnover studies of sMMO performed with

MMOH from *M. capsulatus* (Bath)^{13,16,17} and *Methylosinus trichosporium* (OB3b)^{18,19} have revealed the formation of intermediate species during the reaction cycle. These intermediates can be observed either by continuous or discontinuous techniques and in the presence or absence of substrates.

Figure 4.1 portrays intermediate species spectroscopically observed in the reaction of the diferrous MMOH (H_{red}) with dioxygen carried out in the presence of two equivalents of MMOB. In its absence, the oxidation of the diiron center is much slower than occurs during steady state turnover, and intermediate species are not observed. When MMOB is present, the first intermediate appears with a rate constant of 25 s^{-1} at $4\text{ }^{\circ}\text{C}$ when monitored by rapid freeze-quench (RFQ) Mössbauer or optical spectroscopy.^{13,16,17} Its properties, when referenced to well-characterized model compounds,²⁰⁻²² are characteristic of a diiron(III) peroxo intermediate, termed H_{peroxo} .

Several lines of evidence indicate that at least one intermediate precedes the formation of H_{peroxo} . In a RFQ electron paramagnetic resonance (EPR) study employing the *M. trichosporium* OB3b enzyme, the rate of disappearance of the integer spin signal was independent of dioxygen concentration.²³ This result suggests rapid formation of a complex between H_{red} and O_2 which retains the integer spin signal and decays with an observed rate constant of $\sim 22\text{ s}^{-1}$. This putative complex was designated intermediate O. In stopped-flow experiments with the *M. trichosporium* OB3b system, the H_{peroxo} optical signal appeared with a rate constant of $\sim 5\text{ s}^{-1}$, suggesting the presence of yet another intermediate designated P^* between H_{red} and H_{peroxo} .²⁴ Indirect support for the occurrence of rapid, stepwise oxidation of the dinuclear iron center was provided by studies with nitric oxide (NO). This reagent reacts with H_{red} producing optical changes that were best fit with two kinetic rate constants, $k \sim 100\text{ s}^{-1}$ and $k \sim 25\text{ s}^{-1}$ at $4\text{ }^{\circ}\text{C}$. This result suggests that

NO binds sequentially to the iron atoms to produce a dinitrosyl adduct.²⁵ The first addition would formally afford a Fe(II)Fe(III) mixed-valent species, the analog of a superoxo intermediate in the reaction of the H_{red} with dioxygen. We present here additional support for the existence of such a species prior to the formation of H_{peroxo}.

The H_{peroxo} intermediate subsequently converts to a formally high-valent, diiron(IV) intermediate Q, characterized by its relatively long evolution time, $k_{\text{form}} = 0.45 \text{ s}^{-1}$, $k_{\text{decay}} = 0.1 \text{ s}^{-1}$ at 4 °C for *M. capsulatus* (Bath), and intense yellow color.^{13,16,18,19} The Mössbauer parameters of Q indicate Fe(IV) centers which, in the *M. capsulatus* (Bath) hydroxylase, appear to be in slightly inequivalent environments.^{13,16} RFQ Extended X-ray Absorption Fine Structure (EXAFS) experiments on Q generated from *M. trichosporium* OB3b revealed a short (~2.45 Å) Fe...Fe distance.²⁶ The rate of decay of Q is greatly accelerated when substrate is present, leading to its assignment as the active oxidizing species.¹⁹ The spectroscopic characteristics of H_{peroxo} and Q suggest a range of possible structures,²⁷ which have been evaluated by theoretical studies employing extended Hückel and density functional theory.²⁸⁻³⁰

Additional intermediate species after Q have been suggested in reactions of the *M. trichosporium* OB3b enzyme with substrate molecules.¹⁹ In the presence of methane, and by analogy to the widely accepted mechanism for cytochrome P450 oxidations,³¹ a radical intermediate R was proposed comprising a ferric hydroxo center and a methyl radical. Some studies employing spin traps³² and a radical clock substrate probe³³ have supported the existence of such a substrate radical. Evidence against discrete substrate radical formation has been provided by experiments employing chiral tritiated alkanes^{34,35} and very fast radical clock substrate probes.^{36,37} The latter

investigations estimated the lifetime of a putative radical intermediate to be on the order of 100 femtoseconds. This value is considered to be too short to be ascribed to a discrete intermediate, and whether or not radicals are formed by sMMO is still a subject of debate. Single turnover experiments with nitrobenzene as a substrate afforded evidence for an iron-bound product species denoted intermediate T with the *M. trichosporium* OB3b enzyme.¹⁹ No such intermediate was observed for the analogous reaction with MMOH from *M. capsulatus* (Bath),^{13,38} although the binding of product molecules including methanol in the active site has been established for this enzyme.³⁹ The release of product regenerates the resting state of the hydroxylase which, in the absence of additional reducing equivalents, terminates the single turnover reaction (Figure 4.1).

In the above discussion, the oxidation of several substrates besides methane was mentioned. Hydroxylation is not the only reaction effected by sMMO. It can oxidize a wide variety of substrates, including alkanes, alkenes, alkynes, aromatic compounds, and heterocycles.^{6,40-42} Substrates can range in size from methane to 1,1-diphenyl-2-methylcyclopropane, one of the radical clock substrate probes.³⁶ Alkenes are epoxidized by sMMO, and some substrates such as 2-butene having both double bonds and alkyl functionalities yield mixtures of epoxides and alcohols. 1-Butene and propylene, however, are exclusively epoxidized.⁴⁰ Acetylene has been characterized as a suicide substrate for sMMO.⁴³ An interesting and unanswered question is whether and how the mechanisms for these oxidation processes might differ.

The work described in the present chapter was undertaken to define further the features of the observable intermediate species H_{peroxo} and Q and to characterize their reactions with a range of substrate molecules. Specifically, we provide new information about the following questions. Is H_{peroxo} the

first diiron reaction product when H_{red} is mixed with dioxygen? What is the chemical nature of the intermediates characterized spectroscopically? What drives the formation and decay of these species? How do they react with exogenous substrate molecules and in their absence? Finally, is the oxidation mechanism the same for all substrates? Such information is essential for a complete understanding of the sMMO system and pertinent to the more general subjects of dioxygen activation and hydrocarbon functionalization by metalloenzymes and biomimetic systems.

Experimental

Protein Isolation and Characterization. Native MMOH was purified by a modification of a published procedure⁴⁴ reported in detail elsewhere.³⁹ The purified enzyme was characterized according to methods previously described.^{36,45} Recombinant MMOB was expressed,⁴⁶ purified, and characterized according to published procedures.³⁶

Single Turnover Reactions. Preparation of H_{red} . Solutions of MMOH with two equivalents of MMOB were made anaerobic and were reduced as reported elsewhere.¹³ The excess dithionite and electron transfer mediator were removed by two 1 h anaerobic dialyses against 500 mL of 25 mM MOPS (pH 7) in a Vacuum Atmospheres wet box. The solution was diluted to a final MMOH concentration of 700 μ M for RFQ Mössbauer experiments and 100 μ M for single mixing and 200 μ M for double mixing stopped-flow optical studies. The protein is diluted by a factor of two in the single mixing experiments, including RFQ Mössbauer, and by a factor of four in those employing double mixing.

Rapid Freeze-Quench. Samples were prepared according to previously published procedures.¹³ In samples designated for radiolytic reduction, an

anaerobic solution of 0.7 mM MMOH_{red} and 1.4 mM MMOB in 25 mM MOPS (pH 7) was mixed rapidly at 4 °C with a dioxygen-saturated solution of 25 mM MOPS (pH 7) in 40% glycerol. The reaction mixture was allowed to age for 6 s before quenching into isopentane at -150 °C. The sample was packed either into a Mössbauer sample cell or a quartz Q band ENDOR tube for spectroscopic measurements.

Mössbauer Spectroscopy. RFQ Mössbauer samples were analyzed by the Huynh group at Emory University according to reported procedures.¹³

Radiolytic Reduction. Samples were irradiated by Roman Davydov of Northwestern University by using γ rays from a ⁶⁰Co source at a dose rate of 0.45 Mrad/hr to a total dose of 6 Mrad.

Stopped-Flow Spectroscopy. Both single and double mixing stopped-flow experiments were carried out by using a Hi-Tech Scientific (Salisbury, UK) SF-61 DX2 sample handling unit and a diode array spectrophotometer or photomultiplier assembly manufactured by Hi-Tech. The sample handling unit was made anaerobic by passing at least 20 mL of anaerobic dithionite-saturated buffer (25 mM MOPS, pH 7) through the system, followed by at least 20 mL of anaerobic buffer to rinse away the excess dithionite. Anaerobic buffers and protein solutions were transferred by using Hamilton gastight Samplelock syringes. The temperature was thermostatted with a circulating water bath. In experiments with varying temperature, solutions were allowed to equilibrate for at least 10 min before beginning the run. Matheson gas mixers were used as reported previously¹³ to prepare solutions of known dioxygen concentration.

In experiments employing gaseous substrates, buffer solutions were sparged at 25 °C with the appropriate substrate for 30 min or more, and the saturating substrate concentration calculated.⁴⁷ The solutions were diluted

with argon-saturated buffer solutions in gastight syringes by using three-way valves to achieve the desired substrate concentration.

In single mixing experiments, reduced anaerobic protein solutions were mixed rapidly with dioxygen-containing solutions with or without substrate. In double mixing experiments, the reduced protein was mixed with dioxygen-containing buffer in the first push, and then after a programmed delay time, substrate-containing buffer was introduced at the second push, filling the optical cell and initiating data collection. Data were collected with the KinetAsyst software package (Hi-Tech) and analyzed with this program as well as Specfit⁴⁸ for global analysis. The Specfit package performs a principal component analysis by singular value decomposition to yield orthogonal spectral and time axis eigenvectors. These vectors were examined and applied by global Marquardt least squares fits to the appropriate kinetic model. The spectra of intermediate species and rate constants were derived from such fits.

Quantitation of Hydrogen Peroxide. The production of hydrogen peroxide during a single turnover was investigated by a modification of the method of Hildebrandt and Roots.⁴⁹ A 50 μM sample of MMOH in 25 mM MOPS (pH 7) was reduced according to the usual procedure (vide supra) in the presence or absence of 100 μM MMOB, and the dithionite and methyl viologen were dialyzed away anaerobically. The solutions were diluted with an equal volume of dioxygen-saturated buffer. After 60 s, 100 μL of a 2 M solution of trichloroacetic acid was added to each 450 μL sample to quench the reaction. A 50 μL portion of 100 mM $\text{Fe}(\text{NH}_4)_2(\text{SO}_4)_2 \cdot 6\text{H}_2\text{O}$ and 500 μL of 2.5 M NaSCN were added, and the resulting absorbance at 480 nm was compared to a series of standard samples to quantitate the amount of hydrogen peroxide produced.

Detection of Products in the Propylene Reaction. The products of propylene oxidation in a single turnover reaction were determined by using gas chromatography (GC) with flame ionization detection as described elsewhere.⁴⁵ Authentic samples of propylene oxide and 3-hydroxy-1-propene were employed to construct calibration curves.

Results

Optical Spectra of Intermediate Species. Figure 4.2 depicts the optical spectra observed after mixing $H_{red}/2B$ with dioxygen in the absence of substrate at 20 °C. A total of 200 spectra were collected in a typical run. A shoulder resulting from the Soret band of a cytochrome impurity is visible at 420 nm in the starting spectrum. From the expected extinction coefficient of such a component, $115\text{-}230\text{ mM}^{-1}\text{cm}^{-1}$,⁵⁰ we estimate its concentration to be <1% of the hydroxylase concentration. In control experiments in the absence of MMOB, there is a slight shifting of the Soret band of this cytochrome to higher energy characteristic of heme iron oxidation. The magnitude of the optical change is very small compared to that of Q formation and decay, and it was therefore not identified as a separate process by global analysis in experiments with MMOB present. Fits of the data with the Specfit software package⁴⁸ yielded rate constants and spectra presented in Figure 4.3.

Dioxygen Dependence of H_{peroxo} Formation. The rates of formation and decay for the optical signal of H_{peroxo} at 4 °C under conditions of varying dioxygen concentration were investigated by using the reaction of Q with acetylene to remove its Q optical signal. Intermediate Q has significant absorbance in the region above 600 nm in which H_{peroxo} absorbs (Figure 4.3) At low temperatures, especially, the time course of formation and decay of these two intermediates overlap to a significant extent. These attributes made

it impractical to derive reliable rate constants for the formation and decay of H_{peroxo} unless a substrate was present to accelerate the decay of Q. For a given data set in the absence of substrate, reasonably good fits could be achieved by applying various combinations of rate constants and extinction coefficients where those constants varied by as much as a factor of two, an unacceptable margin of error. To determine the rate constants for H_{peroxo} formation and decay, experiments were therefore performed with 17.5 mM acetylene in the stopped-flow syringe containing dioxygen. This very soluble substrate reacts quickly with Q (*vide infra*), significantly improving our ability to observe the formation and decay of H_{peroxo} . The rate constants were unaffected by changes in acetylene concentration, indicating that H_{peroxo} does not react with acetylene. The results of a dioxygen concentration dependence study are listed in Table 4.1 and plotted in Figure 4.4. No dioxygen dependence was observed outside of experimental error.

Activation Parameters for the Formation and Decay of Intermediates.

Activation parameters for the formation and decay of H_{peroxo} were also measured in the presence of acetylene. The rate of reaction of Q with acetylene is expected to depend on temperature, but judging from the very small optical changes at 415 nm at each temperature, no Q was building up. The observed decay rate constant for H_{peroxo} agreed well the known rate constant for Q formation at each given temperature (*vide infra*). The resulting data appear in Table 4.2 and in the form of an Eyring plot in Figure 4.5A.

The temperature dependence of the rate constants for the formation and decay of intermediate species in the absence of substrate was also investigated in order to determine activation parameters for Q. Similar experiments were reported previously,¹³ but given the larger portion of active

enzyme in more recent preparations as determined by Mössbauer quantitations (vide infra) and the presence of greater quantities (up to 5 mol%) of cytochrome impurities in material used previously, we were interested to repeat the experiments. In the present study, activation parameters were determined by using both a xenon lamp with diode array detection and a quartz-halogen lamp and monochromator ($\lambda = 420$ nm) with a photomultiplier tube detector. In both cases, the data fit well to rate constants for a single exponential formation and a single exponential decay. The data are presented in Tables 4.3 and 4.4 and Figure 4.5B. From the Eyring plot were extracted the activation parameters listed in Table 4.5.

Photoreactivity of Intermediate Q. The decay of intermediate Q was much faster when a 75 W xenon lamp was employed to obtain diode array data as compared to the 30 W quartz-halogen lab used for single wavelength studies with a monochrometer placed in front of the optical cell (Figure 4.6). This photoreaction is reflected in the above Eyring plots and leads to different activation parameters for the decay of Q determined under the two different experimental conditions (Figure 4.5B and Table 4.5). The reaction of intermediate Q with substrates was faster than decay with any light source in the absence of substrate. Thus, whatever the photodecay processes may be, they are too slow to compete with the oxidation reactions as monitored by stopped-flow spectroscopy.

Decay of Q in the Absence of Substrate. The chemical reaction responsible for the decay of Q in the absence of substrate is not well understood. No covalent protein adducts have been detected which would indicate that an amino acid side chain had been oxidized.^{51,52} Quantitation of hydrogen peroxide formed after a single turnover showed that H₂O₂ was produced in an amount corresponding to about 30% of the protein active sites

in the presence of protein B and about 20% of those sites in its absence. This result suggests that, in the absence of substrate, at least some of the iron centers evolve hydrogen peroxide. It is also possible that the buffer is oxidized by Q, although no changes in the Q decay rate have been observed when using different buffers.

Generation of Q_X. Figure 4.7A depicts the Mössbauer spectrum of a RFQ sample containing intermediate Q (35% of total iron) as well as other protein species. Analysis of the Mössbauer data indicates that the sample contained 32% H_{red}, 10% H_{peroxo}, 35% Q, 14% H_{ox}, and 9% V. Spectral parameters for these species have been reported previously^{13,16} except for V (vide infra). The Mössbauer spectrum of the same sample after irradiation is shown in Figure 4.7B. The sample contained 40% H_{red}, 9.5% H_{peroxo}, 13.5% Q, 8.5% V and 6.5% H_{ox}. A difference spectrum (Figure 4.7C) illustrates that irradiation converts a portion of Q into a new paramagnetic species, designated Q_X. The amount of Q lost appears as a negative quadrupole doublet (pointing upward) and corresponds to approximately 22% of the total iron in the sample, while the new species accounting for the same portion appears as a magnetic spectrum in the positive direction (pointing downward). Detailed analysis of the spectra indicates that high-valent Q was reduced preferentially over other species during irradiation, except for a small portion (7.5% of the total iron) of H_{ox} which was apparently fully reduced to the diferrous form.

Because the Mössbauer parameters of the other components are known,^{13,16} their contributions can be removed from the spectrum of the irradiated sample to reveal the features of Q_X (Figure 4.8A). Its properties are very similar to those of R2-X (Figure 4.8B), formally a Fe(III)Fe(IV) species.⁵³ The close resemblance of the electronic structures of Q_X and R2-X is further revealed by the field direction dependence of their Mössbauer spectra. For an

isotropic $S = 1/2$ system, such as the exchange-coupled Fe(III)Fe(IV) state of R2-X, the weak-field spectrum depends strongly on the direction of the applied field in relation to the direction of the Mössbauer γ rays. The $\Delta m = 0$ transition lines acquire their minimum and maximum intensities, respectively, when the field is oriented in a parallel and perpendicular direction. In the irradiated sample, all species except for Q_X are either diamagnetic or have an integer spin, and their spectra do not change with the direction of a weak applied field. Consequently, a difference spectrum (Figure 4.8C) recorded with a 50 mT field applied parallel and perpendicular to the γ rays will cancel the contributions from all other species, revealing the field direction dependence of Q_X . Two sets of $\Delta m = 0$ lines (marked by brackets) corresponding to two distinct Fe sites are clearly visible. This difference spectrum is very similar to the analogous one of R2-X (Figure 4.8D).⁵³ Preliminary analysis of these Q_X spectra yields Mössbauer parameters comparable to those reported for R2-X and a related model compound (Table 4.6).^{53,54}

Identification of a New Species, V. In recent RFQ experiments in the absence of substrate, a new species named V is observed after Q. Its Mössbauer spectrum, prepared by subtracting contributions from other intermediate species (*vide supra*), is shown in Figure 4.9.

Reactions of Intermediate Species with Substrates. Rapid Freeze-Quench Mössbauer Spectroscopy. As in the absence of substrate,¹³ decay of H_{red} , the formation and decay of intermediate species, and the eventual formation of H_{ox} were followed by RFQ Mössbauer spectroscopy in the presence of methane. The results are displayed graphically in Figure 4.10. A portion of the active sites corresponding to 15% of the total iron was reduced only to the mixed valent Fe(II)Fe(III) form. This form of the protein reacts

with dioxygen only on a time scale of hours. It was present in all samples and is not shown in Figure 4.10. Approximately 50% of the diferrous active sites were not oxidized after 70 s of reaction time (Figure 4.10A). One possibility for this result is that a large percentage of the active sites were in the slowly converting, inactive form.¹³ A more likely explanation, however, is that the reaction was dioxygen-limited. The anaerobic syringe contained approximately 1.4 mM active sites, whereas the aerobic syringe contained approximately 1 mM dioxygen.

For material which did convert by forming intermediates, the formation and decay of H_{peroxo} were not obviously affected by the presence of methane.¹³ The best fit of the data of Figure 4.10B afforded formation and decay rate constants, respectively, of 25 s^{-1} and 0.4 s^{-1} for H_{peroxo} , the values determined previously for the reaction in the absence of substrate.¹³ Very little of intermediate Q builds up, which is consistent with its very fast reaction with methane. The data in Figure 4.10B were fit to a formation rate constant of 0.4 s^{-1} and a decay rate constant of 4 s^{-1} for Q, but so little of the species builds up that it was difficult to obtain a very accurate fit. No additional intermediates were observed.

Stopped-Flow Optical Spectroscopy. When single mixing stopped-flow experiments were performed with alkane or acetylene in the aerobic syringe, much less of intermediate Q accumulated (Figure 4.11A), and the rate of Q decay depended on the identity and concentration of substrate, in agreement with earlier reports.^{13,19} When olefins were used as substrates, the same effect was observed, but the apparent extinction coefficient of Q decreased with increasing olefin concentration. This result suggests that less of that intermediate is forming. At the highest concentrations of olefin, the rate of decay of H_{peroxo} also increases (Figure 4.11B). In single turnover experiments

with substrate, the final oxidized spectrum displays a shoulder at 480 nm. Addition of propylene oxide to H_{ox} in the presence of MMOB does not produce this shoulder.

Double mixing stopped-flow experiments were performed to allow buildup of intermediate species, followed by rapid initiation of their reaction with substrate. This technique has the added advantage that reaction of reduced protein with dioxygen takes place in an aging loop, where the protein is not irradiated to accelerate the rate of Q decay. More of that intermediate therefore accumulates than would normally happen in a single mixing experiment, even in the absence of substrate. Experiments were carried out at 20 °C with varying delay times. Typically, for reactions with H_{peroxo} the delay time was 35-40 ms at 20 °C and for reactions with Q the delay time was 400 ms.

In such a double mixing experiment, propylene caused the H_{peroxo} signal to disappear in a concentration-dependent manner (Figure 4.12A), whereas methane did not (Figure 4.12B). Analysis of the solution by GC after such a single turnover experiment with propylene revealed only propylene oxide formation, irrespective of the delay time before addition of propylene. No allylic alcohol was detected. All of the substrates tested caused the Q optical signal to decay in a concentration-dependent manner (Figure 4.13). This resulting data were fit to determine the reaction order with respect to substrate (Figures 4.14 and 4.15) and to provide second order rate constants for the reactions of some of the substrates with Q (Figure 4.14 and 4.15 and Table 4.7)

Discussion

Characterization of Intermediates. Optical Spectrum of H_{peroxo} Figure 4.3A depicts the optical spectrum of the H_{peroxo} intermediate. Like many diferric peroxo model compounds^{20-22,55-58} and the recently identified intermediates in an RNR mutant and in frog M ferritin,^{59,60} it exhibits a very broad absorbance ($\lambda_{\text{max}} \approx 725 \text{ nm}$, $\epsilon = 1500 \text{ M}^{-1} \text{ cm}^{-1}$) characteristic of a peroxo-to-iron(III) charge-transfer band.⁶¹ Its extinction coefficient was calculated based on total MMOH concentration and was not corrected for any protein heterogeneity. From RFQ Mössbauer time course experiments, we estimate that at most 70% of the protein forms the H_{peroxo} intermediate. Because there is no simple way to know the productive population for each stopped-flow experiment, however, the reported data have not been corrected. The extinction coefficient also does not take into account the fact that there are two active sites per protein molecule.

The Mössbauer parameters of H_{peroxo} ($\delta = 0.66 \text{ mm/s}$, $\Delta E_{\text{Q}} = 1.51 \text{ mm/s}$)^{13,16} most resemble those of the RNR mutant and frog M ferritin peroxo intermediates^{59,60} and a structurally characterized model compound.²⁰ In the model, $[\text{Fe}_2(\mu\text{-O}_2)(\mu\text{-O}_2\text{CCH}_2\text{Ph})_2\{\text{HBpz}'\}_3]_2$, where $\text{pz}' = 3,5\text{-bis(isopropyl)-pyrazolyl}$, the peroxide moiety bridges in a gauche $\mu\text{-}1,2$ fashion, with a Fe–O–O–Fe dihedral angle of 52.9° . Theoretical studies of H_{peroxo} suggest such a $\mu\text{-}\eta^1:\eta^1$ binding mode to be favored for the protein intermediate as well,^{28-30,62} and it remains the preferred model for its structure (Figure 4.1). In a spectroscopic and theoretical study of a diferric peroxo model compound, $[\text{Fe}_2(\mu\text{-O}_2)(\mu\text{-O}_2\text{CPh})_2\{\text{HBpz}'\}_3]_2$,⁵⁵ four ligand-to-metal charge-transfer bands were identified at 382 nm ($\epsilon = 3800 \text{ M}^{-1}\text{cm}^{-1}$), 406 nm ($\epsilon = 1600 \text{ M}^{-1}\text{cm}^{-1}$), 685 nm ($\epsilon = 3800 \text{ M}^{-1}\text{cm}^{-1}$), and 800 nm ($\epsilon = 400 \text{ M}^{-1}\text{cm}^{-1}$).⁶¹ Specific electronic transitions were assigned to the first three bands. In

the optical spectrum of H_{peroxo} , there is some intensity in the 400 nm region (Figures 4.3A and 4.3C), and bands similar to those in the model compound are probably present, but they are difficult to distinguish from one another and from the background protein absorption.

Reaction of H_{red} with O_2 . It has already been reported that the rates of Q formation and decay do not depend of dioxygen concentration.¹³ This result is expected because these processes occur later than the point of a presumably irreversible reaction of H_{red} with O_2 . If H_{peroxo} were the immediate product of the reaction of H_{red} with dioxygen, one would expect its formation rate to depend on O_2 concentration. As indicated in Figure 4.4, the formation and decay of H_{peroxo} ($\lambda_{\text{max}} = 725 \text{ nm}$) do not depend on O_2 concentration. This result differs from that obtained for structurally similar but sterically far less demanding diiron(II) model compounds, the O_2 reactions of which exhibit a first-order dependence on dioxygen concentration.^{57,58} This result reinforces the hypothesis that there is at least one intermediate species before H_{peroxo} in the reaction cycle (Figure 4.1), but does not address their identity or oxidation state. Such species could be a transient mixed-valent superoxo, a Michaelis complex similar to the postulated intermediate O, or perhaps the product of an outer sphere electron transfer reaction to dioxygen. The last occurs in the autoxidation of ferrous hemes and cyclidenes⁶³ and has recently been proposed for tyrosine hydroxylase.⁶⁴

The diferrous hydroxylase in the absence of MMOB reacts with NO at 4 °C to form a dinitrosyl species.²⁵ Two rate constants, $k = 100 \text{ s}^{-1}$ and 25 s^{-1} , were required to fit the formation of this species. These values are close to that for H_{peroxo} formation at the same temperature. The NO experiment may model the formation of a mixed-valent superoxo species in the dioxygen reaction, which might convert quickly to yield H_{peroxo} without accumulation

any $\{\text{Fe(II)Fe(III)(O}_2^-\}$ intermediate. Protein B is not required for the NO reaction as it is for H_{peroxo} formation. The role of MMOB in the latter reaction may be to induce carboxylate shifts or other ligand rearrangements to open adjacent coordination positions on the two iron atoms, allowing formation of a gauche μ -1,2-peroxo unit. In the putative dinitrosyl adduct, adjacent positions, and hence MMOB, would not be required.

One discrepancy between the published RFQ-Mössbauer time course¹³ and the current stopped-flow optical results is reflected in the rate constant for H_{peroxo} formation at 4 °C. When the single turnover reaction of $\text{H}_{\text{red}}/2\text{MMOB}$ with dioxygen was monitored by RFQ Mössbauer spectroscopy,¹³ the H_{red} signal disappeared and that for H_{peroxo} appeared with a rate constant of 25 s⁻¹. Previously,¹⁷ an optical signal for H_{peroxo} formed with a rate constant of 20 s⁻¹ as monitored by single wavelength stopped-flow spectroscopy at 625 nm. At the same temperature in the current study, the $\lambda_{\text{max}} = 725$ nm H_{peroxo} optical signal formed with a rate constant of 6 ± 2 s⁻¹ when studied by diode array stopped-flow spectroscopy. The rate constants for decay of this species and for Q formation, whether measured by diode array or by single wavelength techniques, agree quite well with the value determined in the previous the RFQ Mössbauer time course. The diode array methodology sacrifices time resolution (≥ 1.5 ms between spectra) and signal-to-noise ratio for the ability to collect data simultaneously at many wavelengths.

One explanation for the disparate H_{peroxo} formation rate constants is that an intermediate with different optical but indistinguishable Mössbauer spectral parameters forms prior to the species absorbing at 725 nm. In very recent preliminary work carried out by single wavelength stopped-flow spectroscopy, biphasic kinetics for the formation of an optical signal in the

region > 600 nm were observed.⁶⁵ The first phase occurred with a rate constant of approximately 25 s^{-1} and had a relatively small amplitude and the second with a rate constant of approximately $1\text{-}2 \text{ s}^{-1}$ and a significantly greater optical change at $4 \text{ }^\circ\text{C}$. To be consistent the current results, the two phases would have to be indistinguishable by diode array methods.

Several alternative explanations are possible. There is a sixfold difference in protein concentration between the optical and Mössbauer experiments, with the latter having more concentrated enzymes. The high viscosity of the solution might affect protein-protein interactions which may somehow alter the rate of H_{peroxo} formation. The previously published stopped-flow optical experiments employed more concentrated protein solutions, $\approx 180 \text{ } \mu\text{M}$ after mixing, than the current study ($\approx 50 \text{ } \mu\text{M}$), but still less concentrated than used in the RFQ Mössbauer time course ($\approx 300 \text{ } \mu\text{M}$). These concentrations correlate with the observed rate constants, with the more concentrated protein solutions affording faster H_{peroxo} formation. A pH dependence on the formation of H_{peroxo} from *M. trichosporium* OB3b has been reported,²⁴ and although preliminary experiments have not supported such a dependence for the *M. capsulatus* (Bath) system³⁸ subtle changes in pH or in proton transfer rates among the experiments might be the cause of the observed differences. Alternatively, changes in protein isolation methods to afford more active material (vide supra) may also have affected the kinetics of H_{peroxo} formation. It is difficult to imagine how Q formation and decay would not have been similarly affected, however. Finally, because RFQ Mössbauer is a discontinuous technique requiring spectral fitting and subtraction, it may be that the error has been underestimated and the true rate constant is on the order of 6 s^{-1} .

A similar situation occurs for the *M. trichosporium* sMMO, in which the $g = 16$ signal attributed to intermediate O (vide supra) decays with a rate constant of 22 s^{-1} as determined by RFQ-EPR spectroscopy but the H_{peroxo} formation rate constant is only 4.7 s^{-1} by stopped-flow optical methods.²⁴ Those results were rationalized by invoking another intermediate P^* between O and H_{peroxo} which was proposed to be closely related to H_{peroxo} , and possibly associated by a proton transfer step.

Activation Parameters. The optical signal for H_{peroxo} at $\lambda_{\text{max}} = 725 \text{ nm}$ forms with a modest enthalpy of activation and a positive entropy of activation (Table 4.5). The entropy change is inconsistent with a reaction involving bimolecular collision between H_{red} and dioxygen. Such a process would be expected to have a negative entropy of activation, unless accompanied by significant protein or solvent reorganization.

Activation parameters for the conversion of H_{peroxo} to Q are similar to those measured previously,¹³ both for decay of H_{peroxo} and formation of Q (Table 4.5). In the latter case, the determined parameters are independent of the light source used for detection. By contrast, parameters for Q decay in the absence of substrate depend on whether diode array or single wavelength techniques are used to observe the reaction, with the light-promoted reaction having a lower activation energy. Both have relatively small activation enthalpies and negative entropies of activation. The chemical reaction corresponding to this decay may involve hydrogen peroxide formation, although proton transfer does not seem to be involved in the rate determining step because Q decay is not pH-dependent.^{13,38}

Model for the Evolution of Intermediate Species in a Single Turnover Reaction Without Substrate. Figure 4.16 depicts possible species observed in the single turnover reaction in the absence of a hydrocarbon substrate. The

resting diferric enzyme, shown in the bis(μ -hydroxo) bridged form,²⁷ is converted to the diferrous state by addition of two electrons from dithionite and two protons. The structure depicted for the reduced hydroxylase is that recently observed by X-ray crystallography.⁶⁶ The initial reaction of the diferrous hydroxylase with dioxygen is rapid and not observed by any of the methods employed thus far. Formation of H_{peroxo} , however, is observed and might occur with the concomitant release of water to account for the positive entropy of activation determined for this step. A μ -1,2 gauche geometry is depicted for H_{peroxo} in agreement with the structure of a crystallographically characterized model compound (vide supra).²⁰

In the next step, H_{peroxo} converts to Q, which is represented as a bis(μ -oxo)bis(μ -carboxylato)diiron(IV) unit. This structure postulated based on recent synthetic model studies in which a bis(μ -carboxylato)diiron(II) model compound reacts with dioxygen to form a bis(μ -hydroxo)bis(μ -carboxylato)-diiron(III) product having just such a tetra-bridged geometry and a short Fe...Fe distance.⁶⁷ In sMMO, conversion to Q might require side chain movements to accommodate the short Fe...Fe distance observed in the EXAFS spectrum.²⁶ Such movements could account for the positive entropy of activation. MMOB is required to form the intermediate species, but during turnover it might dissociate, further contributing to the positive ΔS^\ddagger value.

In the absence of substrate, the electrophilic intermediate Q might be attacked by water as a nucleophile. The lower activation energy for the light-promoted Q decay reaction might reflect increased electrophilicity of a charge-transfer excited state created by irradiation. With or without such a photoactivation step, the bimolecular reaction would proceed with a negative entropy of activation and only a modest enthalpy of activation. Release of hydrogen peroxide would regenerate the diiron(III) form of the enzyme.

Precedent for this conversion is provided by the structurally similar ferroxidase center of ferritin, in which hydrogen peroxide forms in the reaction of the diferrous protein with dioxygen.⁶⁸⁻⁷⁰ The mechanism of hydrogen peroxide formation may involve either protonation of a diferric peroxo species or its conversion to a putative high valent intermediate which would react with water.⁶⁰ In the MMOH reaction, the oxo-bridged form on the left in Figure 4.16 would be expected to have a Mössbauer spectrum similar to that of the observed species V and the characteristic optical signature (*vide infra*). Intramolecular proton transfer and a carboxylate shift would regenerate the resting H_{ox} structure.

Generation of Q_x and Comparison to RNR-R2-X. Low temperature radiolytic reduction has been applied to the study of carboxylate-bridged diiron proteins^{71,72} and models.⁷³ In a solid matrix, a diamagnetic sample can be reduced by one electron to form a paramagnetic species while maintaining a geometry close to that of the diamagnetic form. Annealing the sample to temperatures above 200 K allows the sample to relax to an equilibrium conformation, with concomitant conversion of the electron paramagnetic resonance (EPR) signal to that observed following chemical reduction in solution at 25 °C. This technique has thus far been applied only to the diferric form of non-heme iron proteins and model compounds, generating the mixed-valent Fe(II)Fe(III) form. Intermediate Q, which is diamagnetic at 4 K, has now been made paramagnetic in this manner.

The structure of intermediate Q has been inferred from a variety of physical and theoretical studies,^{13,16,18,19,26,28} but owing in part to its diamagnetism, it is less well characterized than that of intermediate X of RNR-R2. The rhombic nature of the EPR spectrum of R2-X at 35 GHz (Q band) has been exploited by ENDOR spectroscopy to afford a very detailed picture of

the structure, as well as the fate of oxygen atoms incorporated during its formation from reduced R2 and O₂.^{53,74} Such studies on Q could prove invaluable in its characterization. The 35 GHz EPR spectrum of a RFQ sample of Q quenched into a sample tube and then irradiated exhibits an intense signal at $g = 2$ due to free radicals generated by the high energy γ rays (data not shown). This signal completely obscures the Q_X EPR features, as would be expected if its dispersion from $g = 2$ were as small as that of R2-X. The EPR spectrum also exhibits a signal with $g \leq 1.96$ corresponding to less than 2% of the total iron. This feature arises from a mixed valent Fe(II)Fe(III) species, which is not present in a sufficient population to be detected by Mössbauer spectroscopy. Efforts are underway to reduce the intensity of the free radical signal by annealing so that the EPR spectrum of Q_X can be revealed. Alternatively, the Q_X spectrum may be revealed at higher field.

This work, together with recent experiments on wild-type and mutant forms of R2,^{59,75} demonstrates the first spectroscopic link between intermediate Q of sMMO and RNR R2 intermediate X. As such it provides strong support for the supposition^{56,76,77} that the reaction chemistry of the diiron centers in the two proteins is quite analogous. The present application of the radiolytic reduction technique extends its utility to high-valent iron species and paves the way for detailed ENDOR studies of intermediate Q.

Species V. In the original RFQ Mössbauer time course experiments,^{13,16,17} only approximately 35% of the active sites turned over productively, forming the intermediate species on a catalytically relevant time scale. The remainder converted directly from H_{red} to H_{ox} without building up any intermediates. In more recent work with slightly different protein isolation and purification procedures, that active fraction was increased to 60 - 70%. The Mössbauer isomer shift of V ($\delta = 0.51$ mm/s and

$\Delta E_Q = 2.34$ mm/s) is similar to that of the resting state of the ribonucleotide reductase R2 subunit ($\delta = 0.53$ mm/s and $\Delta E_Q = 1.66$ mm/s)^{56,78} and characteristic of (μ -oxo)diiron(III) model complexes ($\delta = 0.35 - 0.60$ mm/s and $\Delta E_Q > 1$ mm/s).⁷⁹ The quadrupole splitting of V is quite large, an attribute which has been correlated to a short Fe–O distance.⁷⁹ We therefore assign V as an oxo-bridged diiron(III) species. An insufficient number of time points were collected to construct kinetic formation and decay curves for V, but it seems to persist for at least several minutes. Like oxidized RNR-R2 and model compounds, such a unit would be expected to have characteristic optical features, particularly in the 300-400 nm region.⁷⁹ The optical bands for the RNR-R2 protein occur at 325 nm ($\epsilon = 9400$ M⁻¹cm⁻¹), 370 nm ($\epsilon = 7200$ M⁻¹cm⁻¹), 500 nm ($\epsilon = 800$ M⁻¹cm⁻¹), and 600 nm ($\epsilon = 300$ M⁻¹cm⁻¹).^{56,78,79} The optical spectrum of reoxidized protein after a single turnover does exhibit similar features (Figures 4.2, 4.11, and 4.13A). In addition, the reduction/reoxidation/ radiolytic reduction/EPR experiments described in Chapter 3 indicate that a different distribution of oxidized species is present after a single turnover than before. An oxo-bridged diferric spectrum has also been observed in those experiments. A species apparently similar to V was reported in a footnote to a paper concerning sMMO from *M. trichosporium* OB3b.²⁶

Reactions of Intermediates With Substrates. The possibility that olefins can react directly with H_{peroxo} or a closely related species is supported by evidence from single and double mixing stopped-flow spectroscopy. In the single mixing experiment, significantly less Q accumulates when olefins are present (Figure 4.11B), and the H_{peroxo} decay rate increases with increasing olefin concentration. In the double mixing experiment, H_{peroxo} decay depends on olefin concentration. A plot of ln[substrate] vs. ln(k_{obs}) (not shown) affords

a reaction order in propylene of 0.48, significantly less than one, which suggests a more complicated mechanism than a direct bimolecular collision reaction with H_{peroxo} . Accelerated conversion of H_{peroxo} to Q in the presence of olefin does not explain the data, because the rate constants for reactions of olefins with Q are modest (vide infra) and this effect would not explain the decreased amount of Q which forms.

There are precedents for epoxidation of olefins by early transition metal peroxo species.⁸⁰ Usually, however, the metal requires a high oxidation state for O-atom transfer to olefins. Low-valent, late transition metal peroxo species are typically nucleophilic,^{81,82} and the H_{peroxo} intermediate in particular has been predicted to be a nucleophile.⁶¹ Protonation to form a hydroperoxide, however, would generate a more electrophilic oxidant. In a recent study of a cytochrome P450 mutant, proton delivery to the ferric hydroperoxo intermediate was blocked, preventing formation of an iron oxenoid intermediate. The result was increased epoxidation, compared to hydroxylation, for cyclohexene and 2-butene,⁸³ providing evidence that the ferric hydroperoxo species itself was competent to epoxidize olefins. In addition, alkene monooxygenases (AMO) have been identified which are similar to sMMO in protein components, sequence homology, and putative diiron active site.⁸⁴⁻⁸⁶ These enzymes epoxidize propylene but do not hydroxylate alkanes. They are not inhibited by acetylene, which is a suicide substrate for sMMO,⁴³ reacts with Q, and does not react with H_{peroxo} (vide supra). We suggest that AMO does not form more powerful an oxidant than is required for its biochemistry, and thus utilizes a diiron(III) hydroperoxo rather than a high valent iron-oxo species. Very preliminary stopped-flow studies with the AMO proteins provide no evidence for a Q-like intermediate

in the single turnover reaction. Optical bands in the low energy region, suggestive of a peroxo intermediate, were observed.⁸⁷

A possible mechanism for the reaction of propylene with a protonated form of H_{peroxo} is depicted in Figure 4.17.

Reactions of Substrates with Q. All of the substrates accelerate the decay of Q in a concentration-dependent manner. This result is consistent with the hypothesis that Q is the active oxidizing species. Plots of \ln [substrate] versus \ln (k_{obs}) (Figure 4.15) reveal that reaction to be approximately first order (1.0 ± 0.1) in substrate for methane, ethylene, and acetylene, but the order decreases with increasing substrate size, reaching 0.7 for propane. This result can be explained by postulating a two-step mechanism⁵⁷ for the larger substrates. For example, if Q were in equilibrium with a more reactive form that required conformational change, the result could be a partial order with respect to substrate. Alternatively, substrate binding to the enzyme followed by reaction with Q would lower the effective order. The importance of substrate size is illustrated by the rate of reaction of Q with ethane and propane at a given substrate concentration (Figure 4.15). If reaction of substrate with Q involved hydrogen atom abstraction, one would expect these two hydrocarbons, which have the same C-H bond energy (98 kcal/mol), to react at similar rates. Instead, the rate constant for the reaction of Q with propane is an order of magnitude slower at every substrate concentration. Clearly, the reaction is more complicated. Similarly, the reaction of Q with propylene is five- to sixfold slower than with ethylene. This difference is not electronic, because propylene should be a better substrate for an electrophilic oxidant.

Acetylene reacts most rapidly with Q among all the substrates tested. Acetylene is a suicide substrate for sMMO, covalently modifying the α subunit during steady state turnover.⁴³ The protein retains 95% of its activity

after a single turnover reaction with acetylene,³⁸ however, so the protein is not inactivated in every cycle. The probable mechanism of acetylene activation is electrophilic oxidation to yield the oxirene^{88,89} followed by product rearrangement^{90,91} to a reactive ketene which sometimes covalently modifies the protein and sometimes reacts with water to give acetic acid.⁴³

Figure 4.17 portrays possible mechanisms for oxidation of methane, propylene and acetylene by Q, depicted as a bis(μ -oxo)diiron(IV) species.

Conclusion

Rapid freeze-quench and stopped-flow experiments have provided new information about the intermediates in the catalytic cycle of sMMO as accessed through a single turnover reaction. The optical spectrum of H_{peroxo} and activation parameters for its formation are presented for the first time. The dioxygen independence of the rate constant for its formation supports the theory that H_{peroxo} is not the immediate product of the reaction of H_{red} with dioxygen. Differences in formation of H_{peroxo} as monitored optically and by RFQ Mössbauer are revealed and specific hypotheses to explain this variance set forth. Evidence is presented that H_{peroxo} or a closely related species such as a protonated ferric hydroperoxo form reacts directly with olefins.

Intermediate Q has been made paramagnetic by radiolytic reduction at 77K and the resulting paramagnetic species was characterized by Mössbauer spectroscopy. These experiments provide spectroscopic evidence to connect this species to RNR-R2 intermediate X. Activation parameters for Q formation and decay were reinvestigated. Photosensitivity of intermediate Q is reported, and a model for the evolution and fate of intermediates in the absence of exogenous substrate is proposed. The reaction of substrates with Q in double mixing stopped-flow experiments were studied, and support the

assignment of Q as an active oxidizing species. The reaction of Q with substrates is more complex than can be explained by a simple hydrogen atom abstraction, and probably involves protein conformational changes, especially for the larger substrates.

References

- (1) A preliminary account of a portion of this work has appeared. See reference 2.
- (2) Valentine, A. M.; Tavares, P.; Pereira, A. S.; Davydov, R.; Krebs, C.; Hoffman, B. M.; Edmondson, D. E.; Huynh, B. H.; Lippard, S. J. *J. Am. Chem. Soc.* **1998**, *120*, 2190-2191.
- (3) Liu, K. E.; Lippard, S. J. In *Advances in Inorganic Chemistry*; Sykes, A. G., Eds.; Academic Press: San Diego, 1995; Vol. 42; pp 263-289.
- (4) Wallar, B. J.; Lipscomb, J. D. *Chem. Rev.* **1996**, *96*, 2625-2657.
- (5) Anthony, C. *The Biochemistry of Methylotrophs*; Academic Press: New York, 1982, p 296-379.
- (6) Dalton, H. In *Adv. Appl. Microbiol.* Academic Press: 1980; Vol. 26; pp 71-87.
- (7) Colby, J.; Dalton, H. *Biochem. J.* **1978**, *171*, 461-468.
- (8) Woodland, M. P.; Dalton, H. *J. Biol. Chem.* **1984**, *259*, 53-59.
- (9) Rosenzweig, A. C.; Frederick, C. A.; Lippard, S. J.; Nordlund, P. *Nature* **1993**, *366*, 537-543.
- (10) Rosenzweig, A. C.; Nordlund, P.; Takahara, P. M.; Frederick, C. A.; Lippard, S. J. *Chem. Biol.* **1995**, *2*, 409-418.
- (11) Colby, J.; Dalton, H. *Biochem. J.* **1979**, *177*, 903-908.
- (12) Green, J.; Dalton, H. *J. Biol. Chem.* **1985**, *260*, 15795-15801.
- (13) Liu, K. E.; Valentine, A. M.; Wang, D.; Huynh, B. H.; Edmondson, D. E.; Salifoglou, A.; Lippard, S. J. *J. Am. Chem. Soc.* **1995**, *117*, 10174-10185.
- (14) Gassner, G. T.; Lippard, S. J. submitted for publication.
- (15) Green, J.; Dalton, H. *Biochem. J.* **1986**, *236*, 155-162.
- (16) Liu, K. E.; Wang, D.; Huynh, B. H.; Edmondson, D. E.; Salifoglou, A.; Lippard, S. J. *J. Am. Chem. Soc.* **1994**, *116*, 7465-7466.

- (17) Liu, K. E.; Valentine, A. M.; Qiu, D.; Edmondson, D. E.; Appelman, E. H.; Spiro, T. G.; Lippard, S. J. *J. Am. Chem. Soc.* **1995**, *117*, 4997-4998; Correction **1997**, *119*, 11134.
- (18) Lee, S.-K.; Fox, B. G.; Froland, W. A.; Lipscomb, J. D.; Münck, E. *J. Am. Chem. Soc.* **1993**, *115*, 6450-6451.
- (19) Lee, S.-K.; Nesheim, J. C.; Lipscomb, J. D. *J. Biol. Chem.* **1993**, *268*, 21569-21577.
- (20) Kim, K.; Lippard, S. J. *J. Am. Chem. Soc.* **1996**, *118*, 4914-4915.
- (21) Ookubu, T.; Sugimoto, H.; Nagayama, T.; Masuda, H.; Sato, T.; Tanaka, K.; Madea, Y.; Okawa, H.; Hayashi, Y.; Uehara, A.; Suzuki, M. *J. Am. Chem. Soc.* **1996**, *118*, 701-702.
- (22) Dong, Y.; S., Y.; Young, V. G. J.; Que, L. J. *Angew. Chem. Int. Ed. Engl.* **1996**, *35*, 618-620.
- (23) Liu, Y.; Nesheim, J. C.; Lee, S.-K.; Lipscomb, J. D. *J. Biol. Chem.* **1995**, *270*, 24662-24665.
- (24) Lipscomb, J. D.; Lee, S.-K.; Nesheim, J. C.; Jin, Y.; Wallar, B. J.; Zhang, X.-Y. In *Proceedings of the Symposium on Inorganic Biochemistry and Regulatory Mechanisms of Iron Metabolism*; Ferriera, G., Eds.; 1998.
- (25) Coufal, D. E.; Lippard, S. J. to be submitted for publication.
- (26) Shu, L.; Nesheim, J. C.; Kauffmann, K.; Münck, E.; Lipscomb, J. D.; Que, L., Jr. *Science* **1997**, *275*, 515-518.
- (27) Valentine, A. M.; Lippard, S. J. *J. Chem. Soc., Dalton Trans.* **1997**, *21*, 3925-3931.
- (28) Siegbahn, P. E. M.; Crabtree, R. H. *J. Am. Chem. Soc.* **1997**, *119*, 3103-3113.
- (29) Yoshizawa, K.; Hoffmann, R. *Inorg. Chem.* **1996**, *35*, 2409-2410.

- (30) Yoshizawa, K.; Yamabe, T.; Hoffmann, R. *New J. Chem.* **1997**, *21*, 151-161.
- (31) Ortiz de Montellano, P. R. In *Cytochrome P450: Structure, Mechanism, and Biochemistry*; 2nd ed.; Ortiz de Montellano, P. R., Eds.; Plenum Press: New York, 1995; pp 245-303.
- (32) Deighton, N.; Podmore, I. D.; Symons, M. C. R.; Wilkins, P. C.; Dalton, H. J. *Chem. Soc., Chem. Comm.* **1991**, 1086-1088.
- (33) Ruzicka, F.; Huang, D.-S.; Donnelly, M. I.; Frey, P. A. *Biochemistry* **1990**, *29*, 1696-1700.
- (34) Priestley, N. D.; Floss, H. G.; Froland, W. A.; Lipscomb, J. D.; Williams, P. G.; Morimoto, H. J. *Am. Chem. Soc.* **1992**, *114*, 7561-7562.
- (35) Valentine, A. M.; Wilkinson, B.; Liu, K. E.; Komar-Panicucci, S.; Priestley, N. D.; Williams, P. G.; Morimoto, H.; Floss, H. G.; Lippard, S. J. *J. Am. Chem. Soc.* **1997**, *119*, 1818-1827.
- (36) Liu, K. E.; Johnson, C. C.; Newcomb, M.; Lippard, S. J. *J. Am. Chem. Soc.* **1993**, *115*, 939-947.
- (37) Choi, S.-Y.; Eaton, P. E.; Hollenberg, P. F.; Liu, K. E.; Lippard, S. J.; Newcomb, M.; Putt, D. A.; Upadhyaya, S. P.; Xiong, Y. *J. Am. Chem. Soc.* **1996**, *118*, 6547-6555.
- (38) Valentine, A. M.; Lippard, S. J. unpublished results.
- (39) Willems, J.-P.; Valentine, A. M.; Gurbiel, R.; Lippard, S. J.; Hoffman, B. M. *J. Am. Chem. Soc.* **1998**, in press.
- (40) Colby, J.; Stirling, D. I.; Dalton, H. *Biochem. J.* **1977**, *165*, 395-402.
- (41) Green, J.; Dalton, H. *J. Biol. Chem.* **1989**, *264*, 17698-17703.
- (42) Fox, B. G.; Borneman, J. G.; Wackett, L. P.; Lipscomb, J. D. *Biochemistry* **1990**, *29*, 6419-6427.
- (43) Prior, S. D.; Dalton, H. *FEMS Microbiol. Lett.* **1985**, *29*, 105-109.

- (44) Fox, B. G.; Froland, W. A.; Jollie, D. R.; Lipscomb, J. D. In *Methods In Enzymology* Academic Press: New York, 1990; Vol. 188; pp 191-202.
- (45) DeWitt, J. G.; Bentsen, J. G.; Rosenzweig, A. C.; Hedman, B.; Green, J.; Pilkington, S.; Papaefthymiou, G. C.; Dalton, H.; Hodgson, K. O.; Lippard, S. J. *J. Am. Chem. Soc.* **1991**, *113*, 9219-9235.
- (46) Coufal, D. E.; Blazyk, J.; Whittington, D. A.; Lippard, S. J. manuscript in preparation.
- (47) Wilhelm, E.; Battino, R.; Wilcock, R. J. *Chem. Rev.* **1977**, *77*, 219-262.
- (48) Binstead, R. Specfit Global Analysis Package. 2.10M; Chapel Hill, NC, 1997.
- (49) Hildebrandt, A. G.; Roots, I. *Arch. Biochem. Biophys.* **1975**, *171*, 385-397.
- (50) Lemberg, R.; Barrett, J. *Cytochromes*; Academic Press: New York, 1973.
- (51) Salifoglou, A.; Lippard, S. J. unpublished data.
- (52) Coufal, D. E.; Wolf, S.; Biemann, K.; Lippard, S. J. unpublished data.
- (53) Sturgeon, B. E.; Burdi, D.; Chen, S.; Huynh, B. H.; Edmondson, D. E.; Stubbe, J.; Hoffman, B. M. *J. Am. Chem. Soc.* **1996**, *118*, 7551-7557.
- (54) Dong, Y.; Que, L. J.; Kauffmann, K.; Münck, E. *J. Am. Chem. Soc.* **1995**, *117*, 11377-11378.
- (55) Kitajima, N.; Tamura, N.; Amagai, H.; Fukui, H.; Moro-oka, Y.; Mizutani, Y.; Kitagawa, T.; Mathur, R.; Heerweigh, K.; Reed, C. A.; Randall, C. R.; Que, L. J.; Tatsumi, K. *J. Am. Chem. Soc.* **1994**, *116*, 9071-9085.
- (56) Feig, A. L.; Lippard, S. J. *Chem. Rev.* **1994**, *94*, 759-805.
- (57) Feig, A. L.; Becker, M.; Schindler, S.; Eldik, R. v.; Lippard, S. J. *Inorg. Chem.* **1996**, *35*, 2590-2601.
- (58) LeCloux, D. D.; Barrios, A. M.; Mizoguchi, T. J.; Lippard, S. J. *J. Am. Chem. Soc.* **1998**, in press.

- (59) Bollinger, J. M.; Krebs, C.; Vicol, A.; Chen, S.; Ley, B. A.; Edmondson, D. E.; Huynh, B. H. *J. Am. Chem. Soc.* **1998**, 1094-1095.
- (60) Periera, A. S.; Small, W.; Krebs, C.; Tavares, P.; Edmondson, D.; Theil, E. C.; Huynh, B. H. *Biochemistry* **1998**, 37, 9871-9876.
- (61) Brunold, T. C.; Tamura, N.; Kitajima, N.; Moro-oka, Y.; Solomon, E. I. *J. Am. Chem. Soc.* **1998**, 120, 5674-5690.
- (62) Yoshizawa, K.; Yokomichi, Y.; Shiota, Y.; Ohta, T.; Yamabe, T. *Chem. Lett.* **1997**, 1997, 587-588.
- (63) Dickerson, L. D.; Sauer-Masarwa, A.; Herron, N.; Fendrick, C. M.; Busch, D. H. *J. Am. Chem. Soc.* **1993**, 115, 3623-3626.
- (64) Francisco, W. A.; Tian, G.; Fitzpatrick, P. A.; Klinman, J. P. *J. Am. Chem. Soc.* **1998**, 120, 4047-4062.
- (65) Stahl, S. S.; Lippard, S. J. unpublished results.
- (66) Whittington, D. A.; Lippard, S. J. to be submitted for publication.
- (67) Lee, D.; Lippard, S. J. to be submitted for publication.
- (68) Xu, L. B.; Chasteen, N. D. *J. Biol. Chem.* **1991**, 266, 19965-19970.
- (69) Sun, S.; Arosio, P.; Levi, S.; Chasteen, N. D. *Biochemistry* **1993**, 32, 9362-9369.
- (70) Waldo, G. S.; Theil, E. C. *Biochemistry* **1993**, 32, 13262-13269.
- (71) Davydov, R.; Kuprin, S.; Gräslund, A.; Ehrenberg, A. *J. Am. Chem. Soc.* **1994**, 116, 11120-11128.
- (72) Davydov, A.; Davydov, R.; Gräslund, A.; Lipscomb, J. D.; Andersson, K. *J. Biol. Chem.* **1997**, 272, 7022-7026.
- (73) Davydov, R. M.; Menage, S.; Fontecave, M.; Gräslund, A.; Ehrenberg, A. *J. Bioinorg. Chem.* **1997**, 2, 242-255.
- (74) Willems, J.-P.; Lee, H.-I.; Burdi, D.; Doan, P. E.; Stubbe, J.; Hoffman, B. *M. J. Am. Chem. Soc.* **1997**, 119, 9816-9824.

- (75) Tong, W. H.; Chen, S.; Lloyd, S. G.; Edmondson, D. E.; Huynh, B. H.; Stubbe, J. J. *Am. Chem. Soc.* **1996**, *118*, 2107-2108.
- (76) Nordlund, P.; Eklund, H. *Curr. Opin. Struct. Biol.* **1995**, *5*, 758-766.
- (77) Que, L. J.; Dong, Y. *Acc. Chem. Res.* **1996**, *29*, 190-196.
- (78) Sanders-Loehr, J. In *Iron Carriers and Iron Proteins*; Loehr, T. M., Eds.; VCH: New York, 1989; Vol. 5; pp 373-466.
- (79) Kurtz, D. M. *Chem. Rev.* **1990**, *90*, 585-606.
- (80) Dussault, P. In *Active Oxygen in Chemistry*; Foote, C. S., Valentine, J. S., Greenberg, A. and Liebman, J. F., Eds.; Chapman & Hall: New York, 1995; pp 141-203.
- (81) Ho, R. Y. N.; Liebman, J. F.; Valentine, J. S. In *Active Oxygen in Biochemistry*; Valentine, J. S., Foote, C. S., Greenberg, A. and Liebman, J. F., Eds.; Chapman & Hall: New York, 1995; pp 1-36.
- (82) Selke, M.; Sisemore, M. F.; Ho, R. Y. N.; Wertz, D. L.; Valentine, J. S. *J. Mol. Cat. A* **1997**, *117*, 71-82.
- (83) Vaz, A. D.; McGinnity, D. F.; Coon, M. J. *Proc. Natl. Acad. Sci.* **1998**, *95*, 3555-3560.
- (84) Small, F. J.; Ensign, S. A. *J. Biol. Chem.* **1997**, *272*, 24913-24920.
- (85) Gallagher, S. C.; Cammack, R.; Dalton, H. *Eur. J. Biochem.* **1997**, *247*, 635-641.
- (86) Gallagher, S. C.; George, A.; Dalton, H. *Eur. J. Biochem.* **1998**, *254*, 480-489.
- (87) Valentine, A. M. Ph. D. Thesis, Massachusetts Institute of Technology, 1998 Appendix Three.
- (88) Lewars, E. G. *Chem. Rev.* **1983**, *83*, 519-533.
- (89) Ortiz de Montellano, P. R.; Kunze, K. L. *J. Am. Chem. Soc.* **1980**, *102*, 7373-7375.

- (90) Scott, A. P.; Nobes, R. H.; Schaefer, H. F.; Radom, L. *J. Am. Chem. Soc.* **1994**, *116*, 10159-10164.
- (91) Termath, V.; Tozer, D. J.; Handy, N. C. *Chem. Phys. Lett.* **1994**, *228*, 239-245.

Table 4.1. Rate Constants for Formation and Decay of H_{peroxo} Under Conditions of Varying Dioxygen Concentration at 4 °C.

[Dioxygen] (mM)	k_1 (s ⁻¹) ^a	error ^b	k_2 (s ⁻¹) ^a	error ^b
0.1875	5.6	2.3	0.61	0.04
0.375	7.3	2.8	0.61	0.07
0.5625	4.9	2.3	0.47	0.06
0.75	7.2	2.5	0.61	0.13
average	6.2	2.5	0.58	0.08

^a k_1 and k_2 refer to H_{peroxo} formation and H_{peroxo} decay/Q formation, respectively. ^b \pm one standard deviation.

Table 4.2. Rate Constants for Formation and Decay of H_{peroxo} Under Conditions of Varying Temperature in the Presence of 8.75 mM acetylene.

Temperature (K)	k_1 (s^{-1}) ^a	error ^b	k_2 (s^{-1}) ^a	error ^b
276.2	1.45	0.70	0.46	0.06
276.7	3.0	1.3	0.32	0.13
277.0	6	3	0.70	0.18
282.2	8	4	1.78	0.6
284.7	24	2	3.3	0.2
284.8	21	3	2.2	0.8
285.0	19	4	3.80	0.14
285.5	22	4	6.1	1.4
290.0	31	1.7	12.0	0.4
291.0	52	5	12.6	0.4
291.4	35	5	14.7	1.3
291.5	44	3	7.6	0.5
295.7	30	2	14	4
298.2	88	18	16	2
301.2	120	56	29	5

^a k_1 and k_2 refer to H_{peroxo} formation and H_{peroxo} decay/Q formation, respectively. ^b \pm one standard deviation.

Table 4.3. Rate Constants for Formation and Decay of Q at 420 nm Under Conditions of Varying Temperature in the Absence of Substrate and With Detection by a Photomultiplier Tube.^a

Temperature (K)	k_2 (s ⁻¹)	k_3 (s ⁻¹)
277.0	0.467	0.0274
277.0	0.592	0.0223
283.3	1.76	0.043
283.3	1.61	0.043
284.3	1.84	0.060
284.3	1.68	0.050
287.8	3.85	0.069
288.1	3.73	0.075
292.5	8.93	0.0936
292.5	8.85	0.0929
297.3	17.61	0.156
297.3	17.70	0.156
302.0	44.10	0.247
307.6	117.97	0.358

^a k_2 and k_3 refer to Q formation and decay, respectively.

Table 4.4. Rate Constants for Formation and Decay of Q With Varying Temperature in the Absence of Substrate With Detection by Diode Array.^a

Temperature (K)	k_2 (s ⁻¹)	k_3 (s ⁻¹)
274.6	0.299	0.155
274.6	0.276	0.083
274.6	0.324	0.140
274.6	0.272	0.086
277.0	0.489	0.263
277.0	0.458	0.180
277.0	0.470	0.176
281.0	1.43	0.320
281.0	2.49	0.170
281.0	1.71	-
281.0	1.32	0.291
283.2	2.48	0.430
283.2	2.20	0.63
283.2	3.40	0.344
283.2	2.98	0.334
285.2	5.39	0.359
285.2	3.80	0.339
285.2	3.83	0.390
285.2	3.80	-
285.2	3.05	0.450
285.2	4.17	-
290.9	7.97	0.362
290.9	7.63	0.430
290.9	10.40	0.412
290.9	8.61	0.395
296.4	16.4	0.514
296.4	16.50	0.590
296.4	15.10	0.550
296.4	15.40	0.740
301.8	32.00	0.580
301.8	33.10	0.491
301.8	28.30	1.44
301.8	36.30	0.426
301.8	38.10	1.07
301.8	38.00	0.540
301.8	40.10	0.48
307.8	51.00	1.36
307.8	43.80	0.740
307.8	82.70	1.33
307.8	67.00	1.17

^a k_2 and k_3 refer to Q formation and decay, respectively.

Table 4.5. Activation Parameters for the Formation and Decay of Intermediate Species.

Rate Constant ^a	ΔH^\ddagger (kcal/mol)	ΔS^\ddagger (cal/mol·K)
k_1^b	19	14
k_2^b	25	31
k_2^c	29	45
k_2^d	26	33
k_3^c	14	-15
k_3^d	9	-30

^a k_1 , k_2 , and k_3 refer to H_{peroxo} formation, H_{peroxo} decay/Q formation, and Q decay, respectively. ^bDetermined by mixing $H_{\text{red}}/2B$ with buffer containing 700 μM dioxygen and 17.5 mM acetylene. ^cDetermined in the absence of substrate by using 420 nm monochromatic light with detection by a photomultiplier tube. These values agree reasonably well with the previously reported values determined under similar conditions:¹³ $\Delta H^\ddagger = 27$ kcal/mol and $\Delta S^\ddagger = 35$ cal/mol·K for k_2 and $\Delta H^\ddagger = 18$ kcal/mol and $\Delta S^\ddagger = 2$ cal/mol·K for k_3 . ^dDetermined by using a Xe lamp and diode array detection.

Table 4.6. Mössbauer Parameters for Q_X and Related Species.^a

	Q_X		$R2-X^b$		$[Fe_2(6-Me-TPA)_2(\mu-O)_2]^{3+c}$	
	Fe _A	Fe _B	Fe _A	Fe _B	Fe _A	Fe _B
δ (mm/s)	0.48(6)	0.14(6)	0.56(3)	0.26(4)	0.48(3)	0.08(3)
ΔE_Q (mm/s)	-0.9(1)	-0.6(1)	-0.9(1)	-0.6(1)	1.6(2)	0.5(1)
η	0.2(5)	0.9(5)	0.5(2)	2.7(3)	1.0(3)	1.0(3)
A_{xx} (MHz)	-70(4)	26(4)	-74.2(2)	27.5(2)	-64.5(20)	20(3)
A_{yy} (MHz)	-75(4)	30(4)	-72.2(2)	36.8(2)	-64.5(20)	36.5(15)
A_{zz} (MHz)	-75(4)	32(4)	-73.2(2)	36.8(2)	-64.5(20)	36.5(15)

^a Numbers in parentheses are estimated standard deviations in the last significant digits. ^b Data from reference 53. ^c Data from reference 54. 6-Me-TPA = *N*-(6-methyl-2-pyridylmethyl)-*N,N*-bis(2-pyridylmethyl)amine.

Table 4.7. Reaction Order in Substrate and Second Order Rate Constants for the Reactions of Substrates with Intermediate Q at 20 °C.

Substrate	Reaction order in substrate	k (M ⁻¹ s ⁻¹)
methane	1.10	2.9 × 10 ⁴
ethane	0.73	-
propane	0.70	-
ethylene	0.90	6.3 × 10 ⁴
propylene	0.83	-
acetylene	0.90	8.4 × 10 ⁴

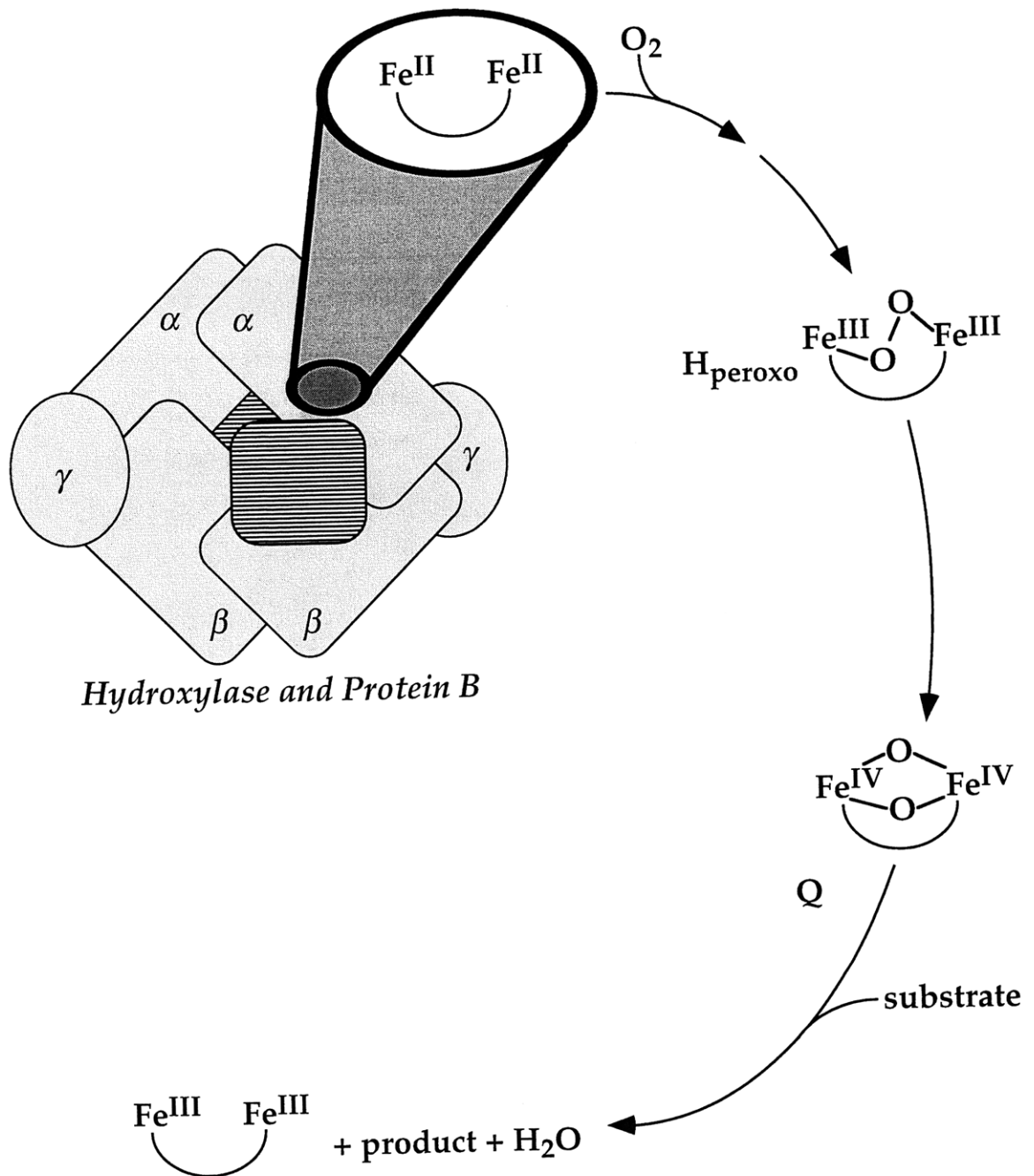


Figure 4.1. Single turnover reaction of H_{red} in the presence of two equivalents of MMOB with dioxygen. Two protons are also required and are not explicitly drawn. At least one intermediate species exists before H_{peroxo} .

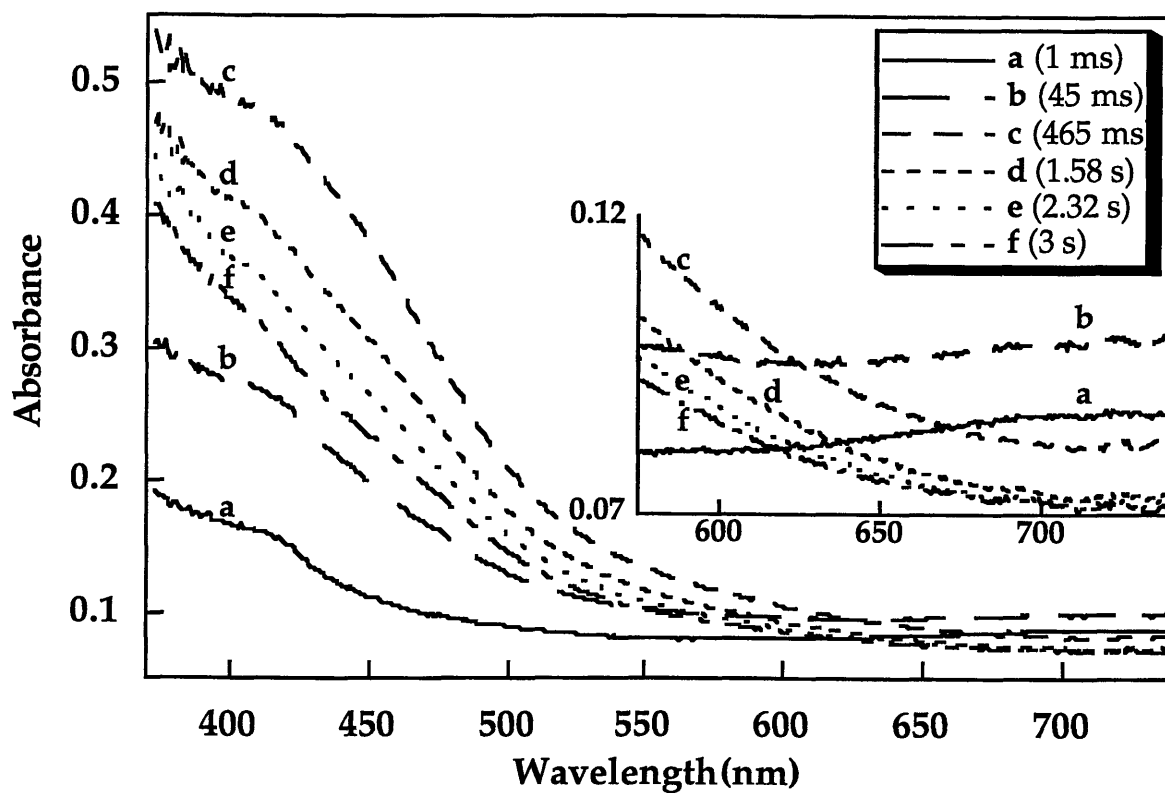


Figure 4.2. Diode array data collected after the rapid mixing of $H_{red}/2B$ with dioxygen at 20 °C. Two hundred spectra were collected in a typical experiment. Selected spectra are shown.

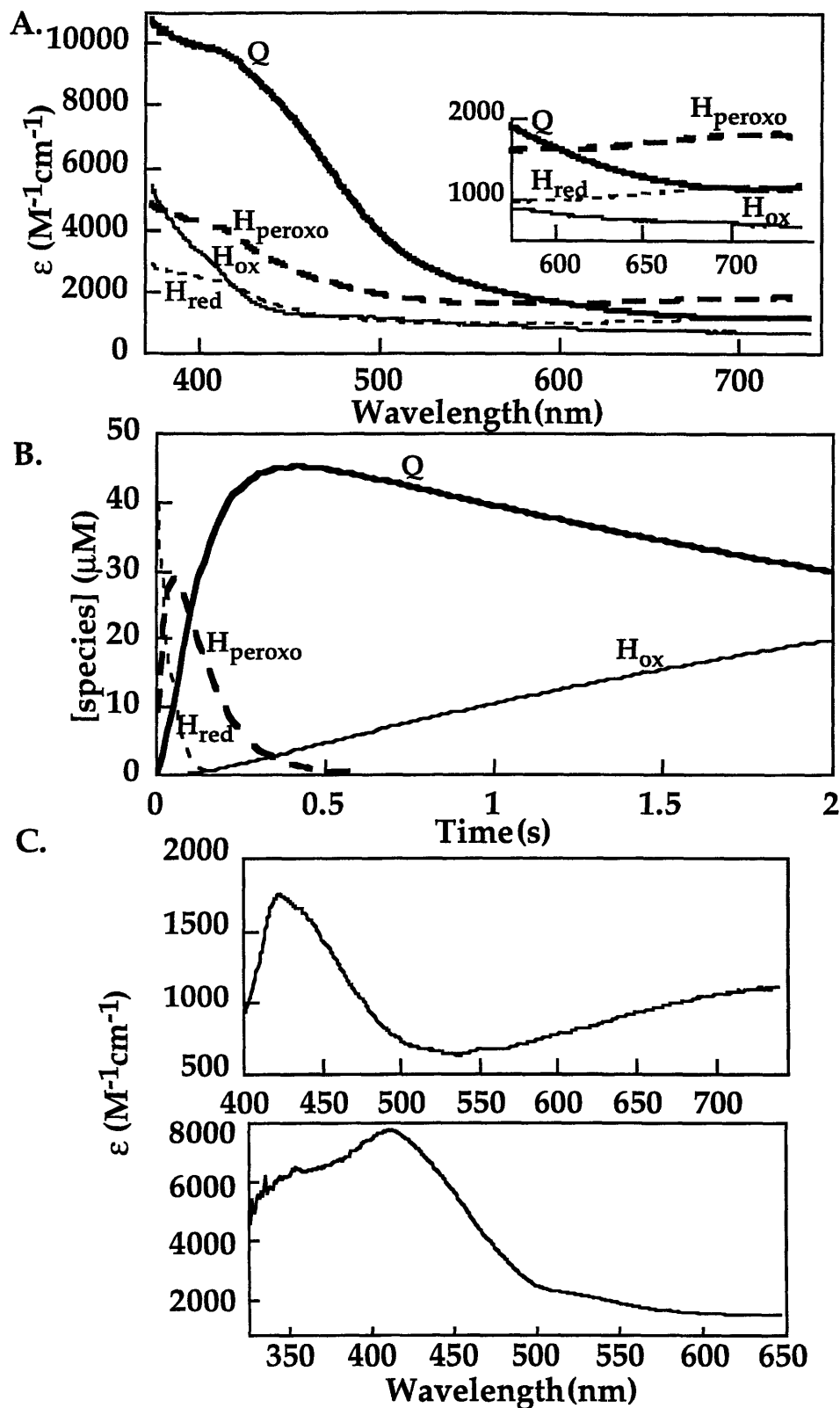


Figure 4.3. Fits of the data from Figure 4.2 with the global analysis package Specfit. The optical species (A) evolve with $k_1 = 40 s^{-1}$, $k_2 = 9.9 s^{-1}$ and $k_3 = 0.31 s^{-1}$ (B) where the rate constants describe H_{peroxo} formation, H_{peroxo} decay/ Q formation and Q decay, respectively. (C) Spectra prepared by subtracting the H_{ox} spectrum from that of H_{peroxo} (top) and Q (bottom).

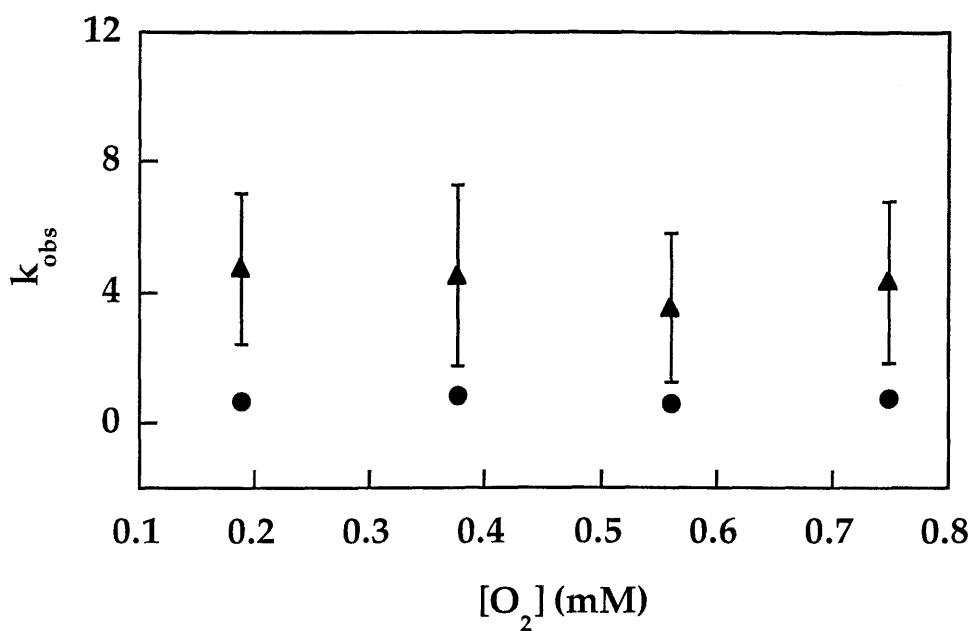


Figure 4.4. Oxygen concentration dependence of formation (triangles) and decay (circles) of the H_{peroxo} signal at 4 °C as determined by global analysis. Each point was determined at least in triplicate and error bars signify ± 1 standard deviation. Error bars for H_{peroxo} decay rate constants are contained within the symbols.

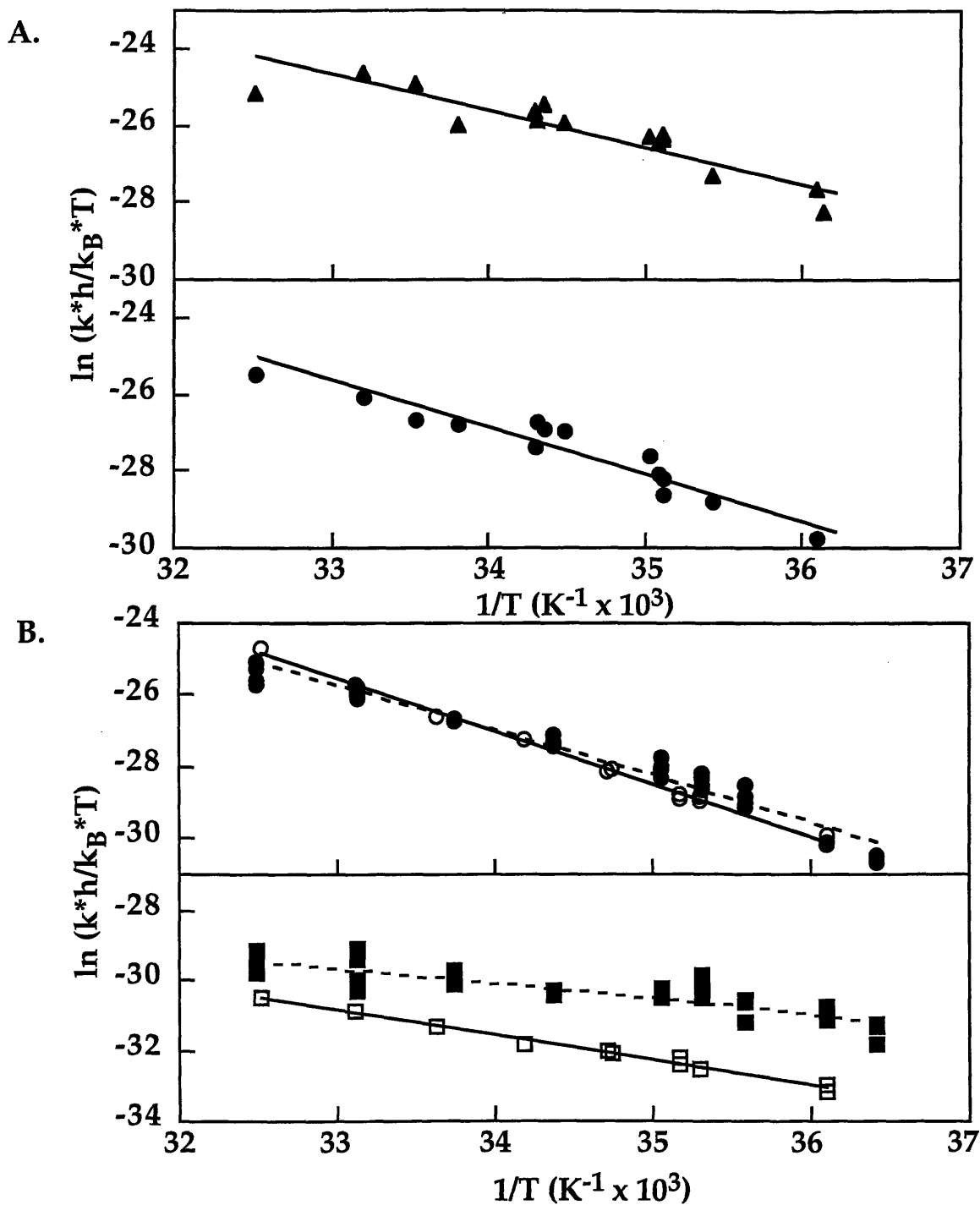


Figure 4.5. (A) Eyring plot describing the formation (triangles) and decay (circles) of H_{peroxo} in a single mixing experiment employing acetylene to prevent intermediate Q from building up. (B) Eyring plot of the formation (circles) and decay (squares) of intermediate Q under conditions of single wavelength (open symbols) and diode array (closed symbols) stopped-flow spectroscopy. The activation parameters are tabulated in Table 4.5.

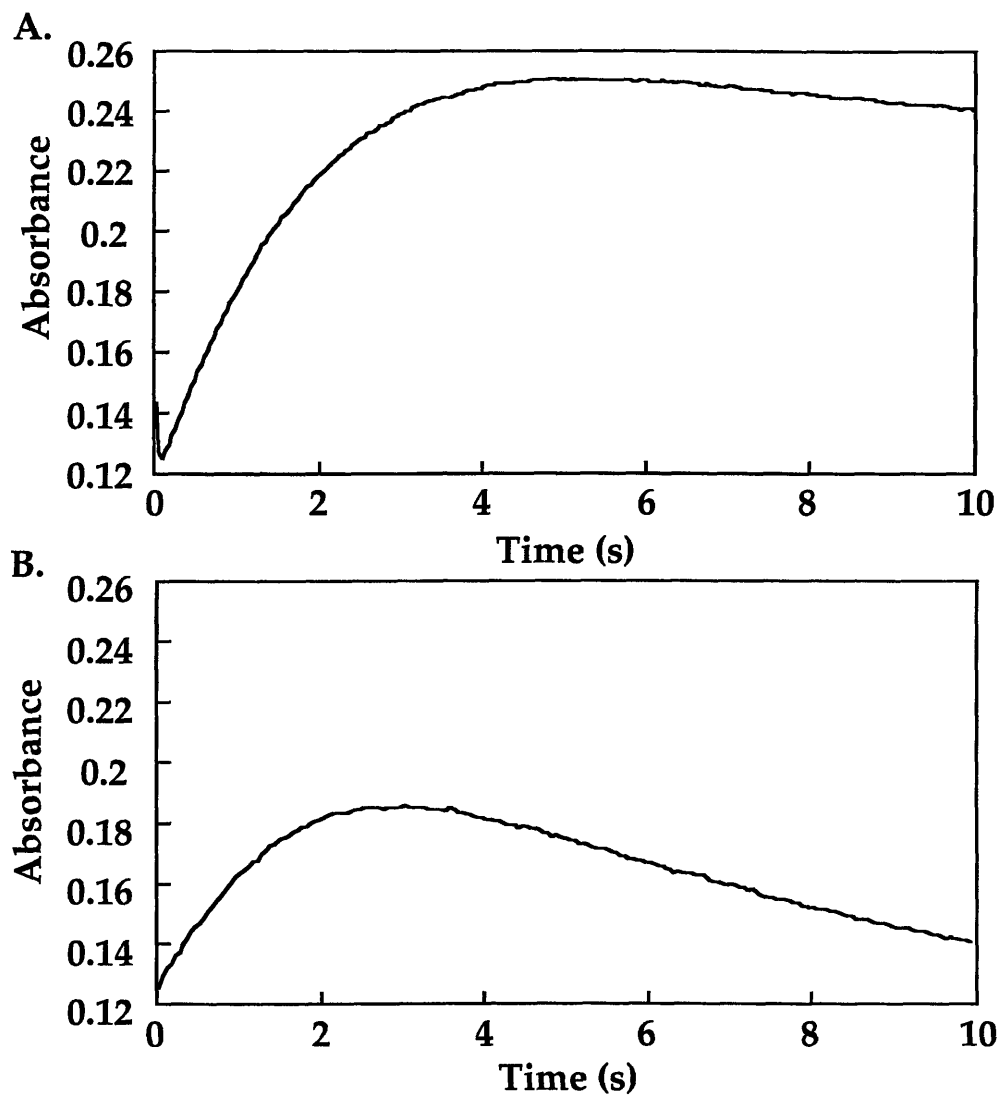


Figure 4.6. Formation and decay of Q at 4 °C when irradiated with (A) 420 nm light from a 30 W quartz-halogen lamp and (B) a 75 W xenon lamp. Rate constants of formation and decay are (A) $k_{\text{form}} = 0.43 \text{ s}^{-1}$ and $k_{\text{decay}} = 0.06 \text{ s}^{-1}$ and (B) $k_{\text{form}} = 0.43 \text{ s}^{-1}$ and $k_{\text{decay}} = 0.24 \text{ s}^{-1}$.

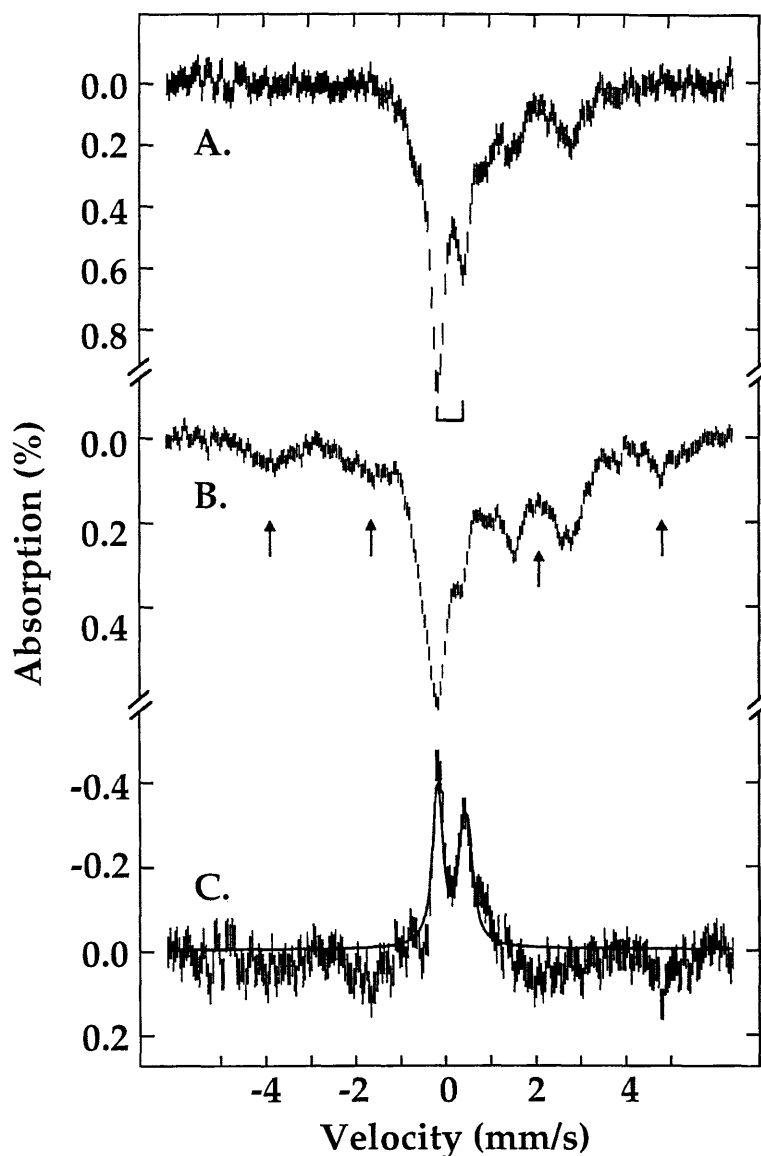


Figure 4.7. Mössbauer spectra of a rapid freeze quench sample from the reaction of $H_{red}/2B$ with dioxygen at 4 °C. The reaction was quenched at 6 s. Spectra were recorded at 4.2 K with a 50 mT magnetic field applied parallel to the Mössbauer low-energy γ rays. (A) The spectrum recorded before the sample was subjected to high-energy γ irradiation. The positions of the doublet attributed to intermediate Q is indicated by brackets. (B) The spectrum of the sample after high-energy γ irradiation. The signals due to the new paramagnetic species Q_X are designated by arrows. (C) A difference spectrum (B minus A) showing the conversion of a portion of the diamagnetic Q (upward pointing quadrupole doublet) into the paramagnetic Q_X (downward pointing absorption signals). The solid line is a theoretical simulation of Q using the previously reported parameters.^{13,16}

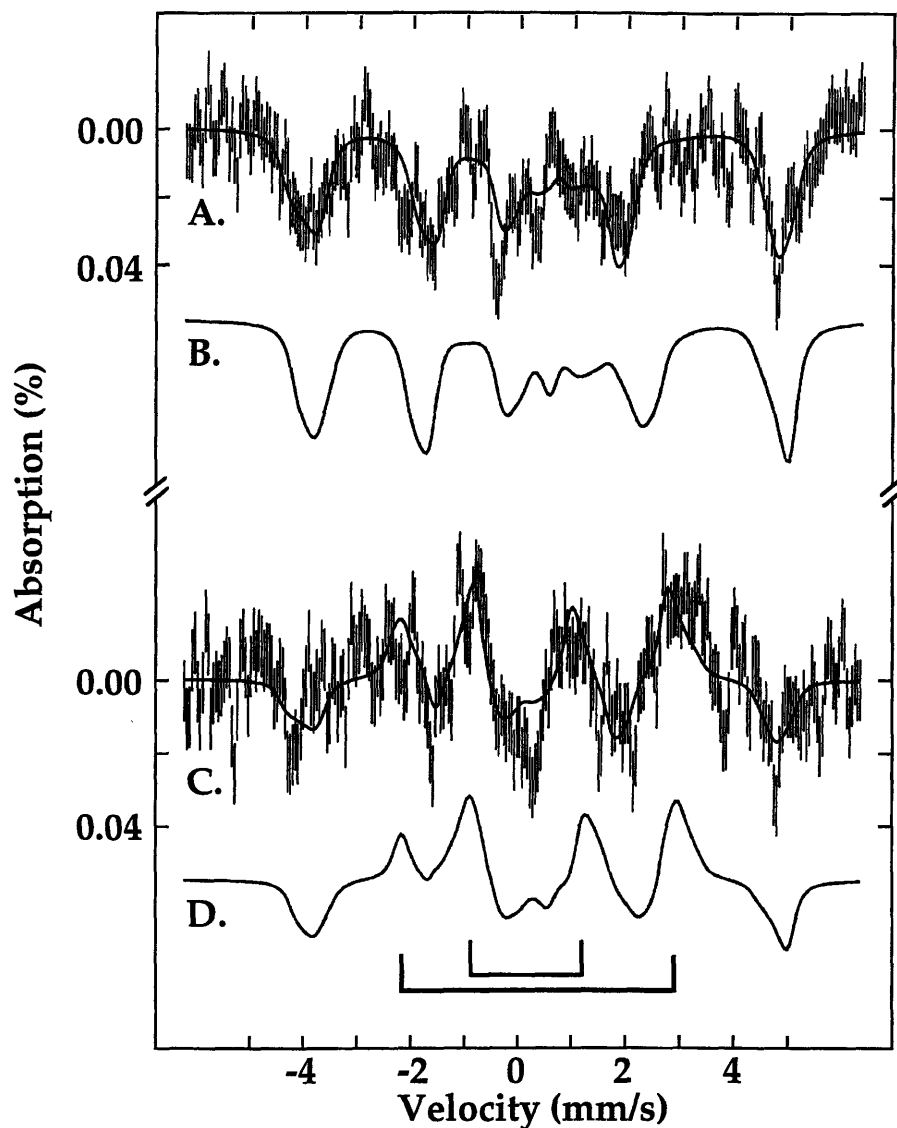


Figure 4.8. Mössbauer spectral comparison of Q_X and R2-X. (A) 4.2 K spectrum of Q_X prepared from the spectrum in Fig. 4.7B by removing the contributions of the other components. The solid line plotted through the experimental data is a theoretical simulation of Q_X obtained by using the parameters listed in Table 4.6. The corresponding theoretical spectrum of R2-X⁵³ is shown in (B). (C) A difference spectrum (parallel minus perpendicular) showing the field direction dependence of Q_X . The solid line plotted through the experimental data is a theoretical simulation of this dependence obtained by using the parameters listed in Table 4.6. The corresponding difference spectrum for the R2-X intermediate⁵³ is shown in (D). The positions for the two sets of $\Delta m = 0$ lines corresponding to the two Fe sites are indicated by brackets at the bottom of the figure.

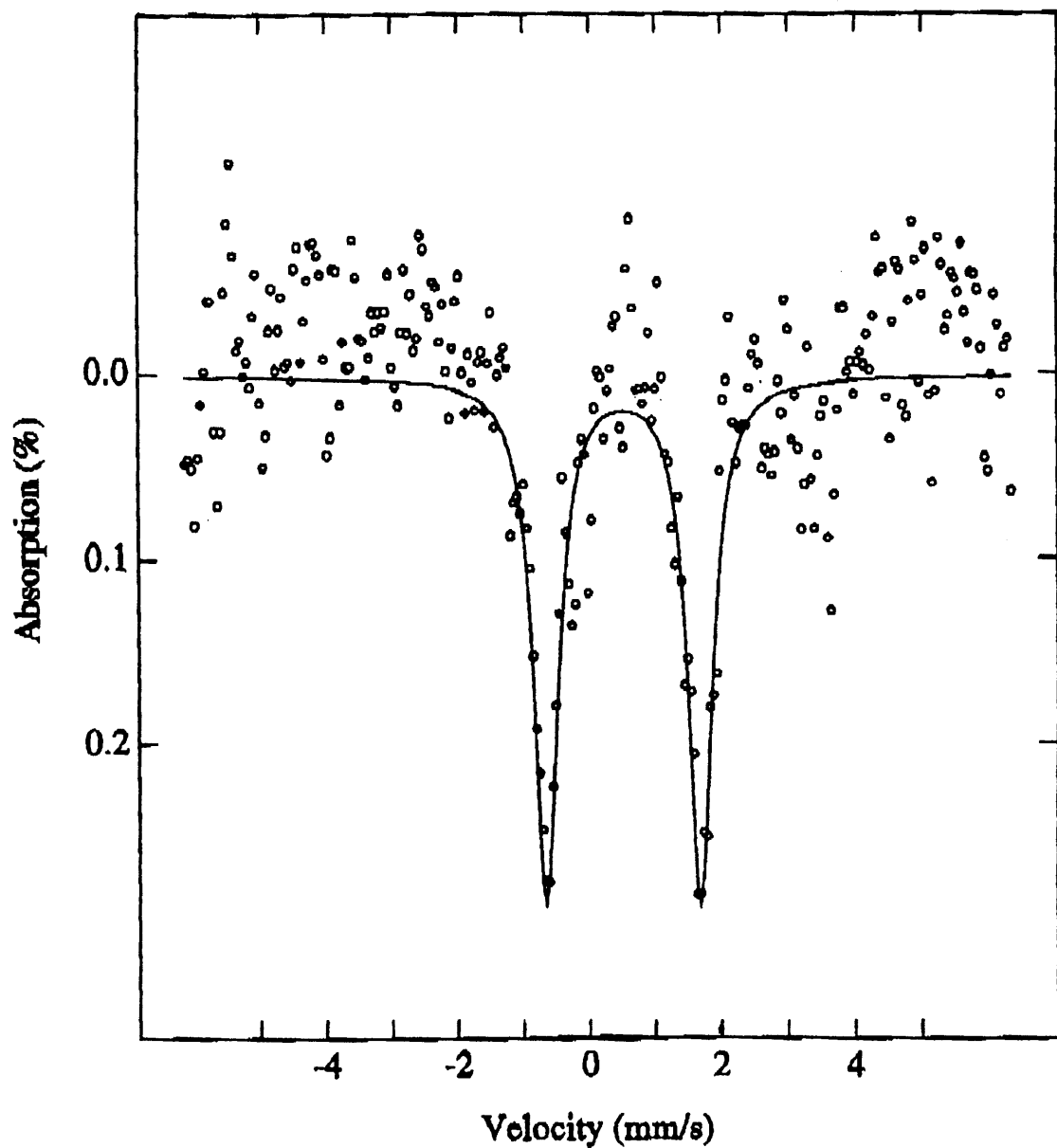


Figure 4.9. Mössbauer spectrum of intermediate V prepared by subtracting the known spectra of other components. The data were fit with a single quadrupole doublet with $\delta = 0.51$ mm/s and $\Delta E_Q = 2.34$ mm/s.

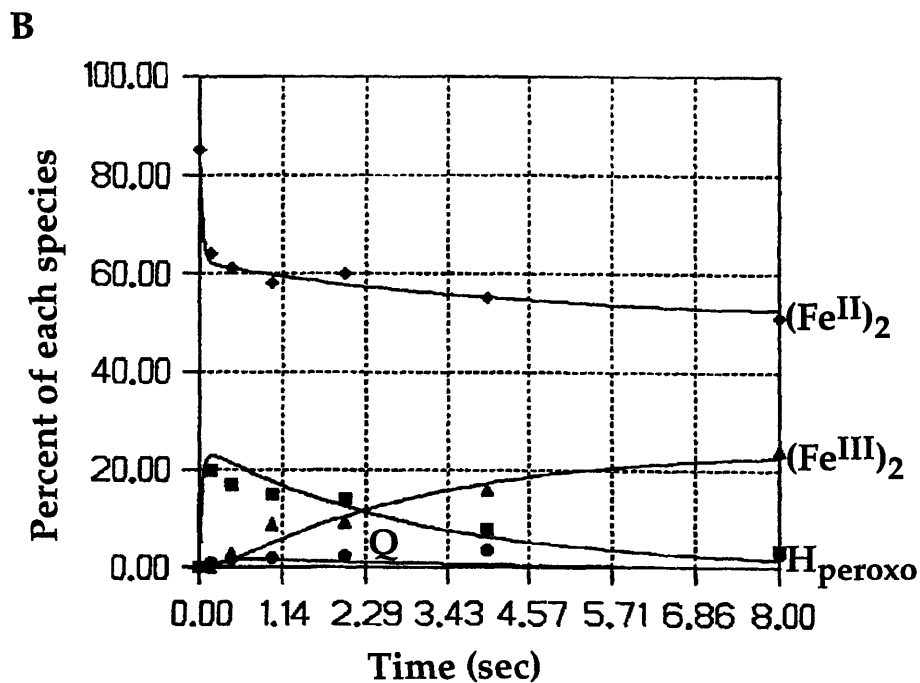
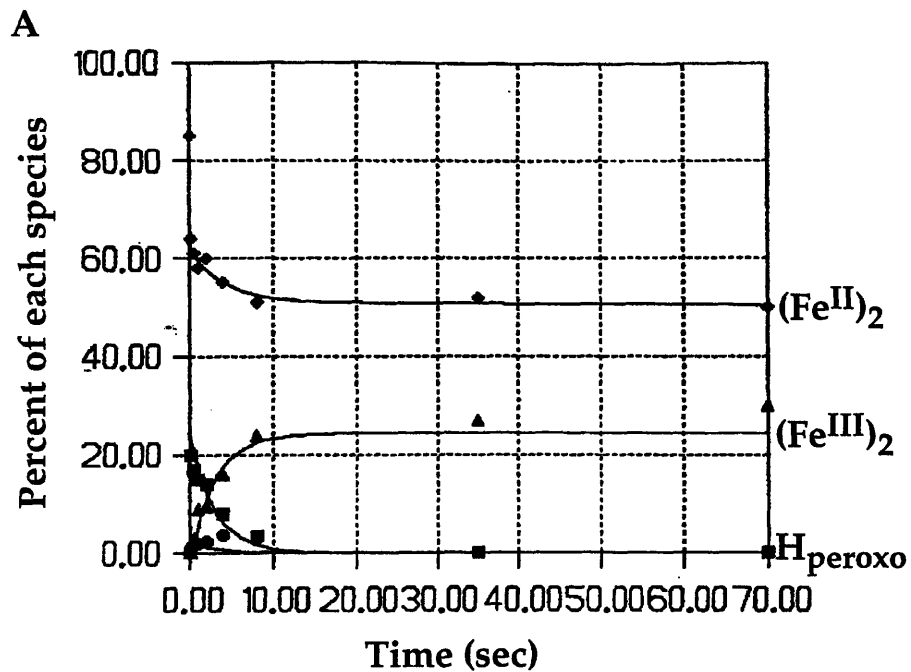


Figure 4.10. Mössbauer analysis of freeze-quench samples from the reaction of reduced hydroxylase with buffer containing dioxygen and methane. Diamonds, squares, circles, and triangles represent the diferrous species, the peroxo intermediate, Q, and the diferric species, respectively. Rate constants are given in the text.

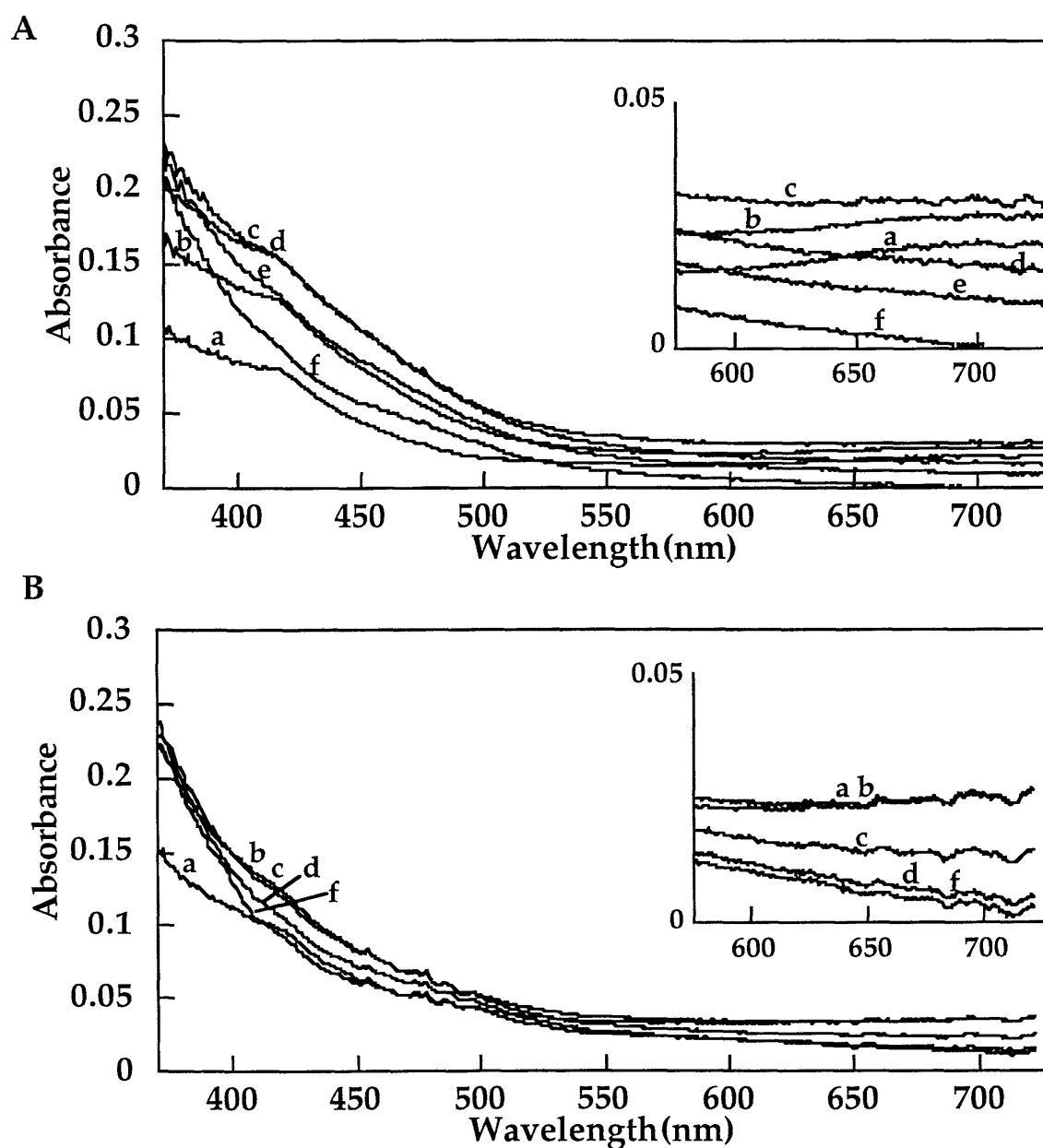


Figure 4.11. Diode array spectra after mixing $H_{red}/2B$ with dioxygen and 1 mM methane (A) or 3 mM propylene (B) and dioxygen at 20 °C. Spectra correspond to (a) 15 ms, (b) 45 ms, (c) 75 ms, (d) 135 ms, (e) 195 ms, and (f) 285 ms of reaction time.

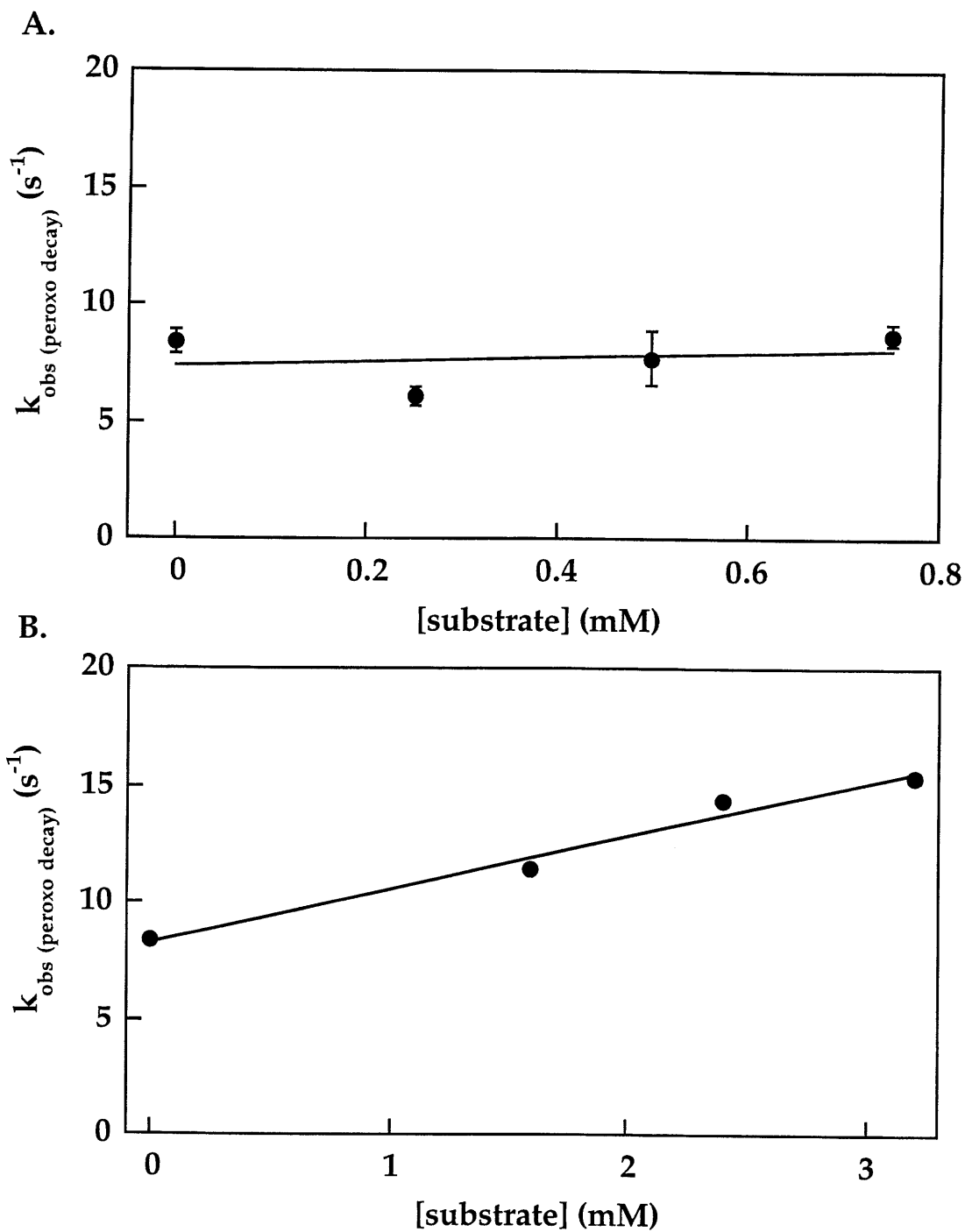


Figure 4.12. (A) A plot of k_{obs} for H_{peroxo} decay vs. [methane]. Error bars represent \pm one std. deviation. (B) A plot of k_{obs} for H_{peroxo} decay vs. [propylene]. Error bars represent \pm one std. deviation and are contained within the points.

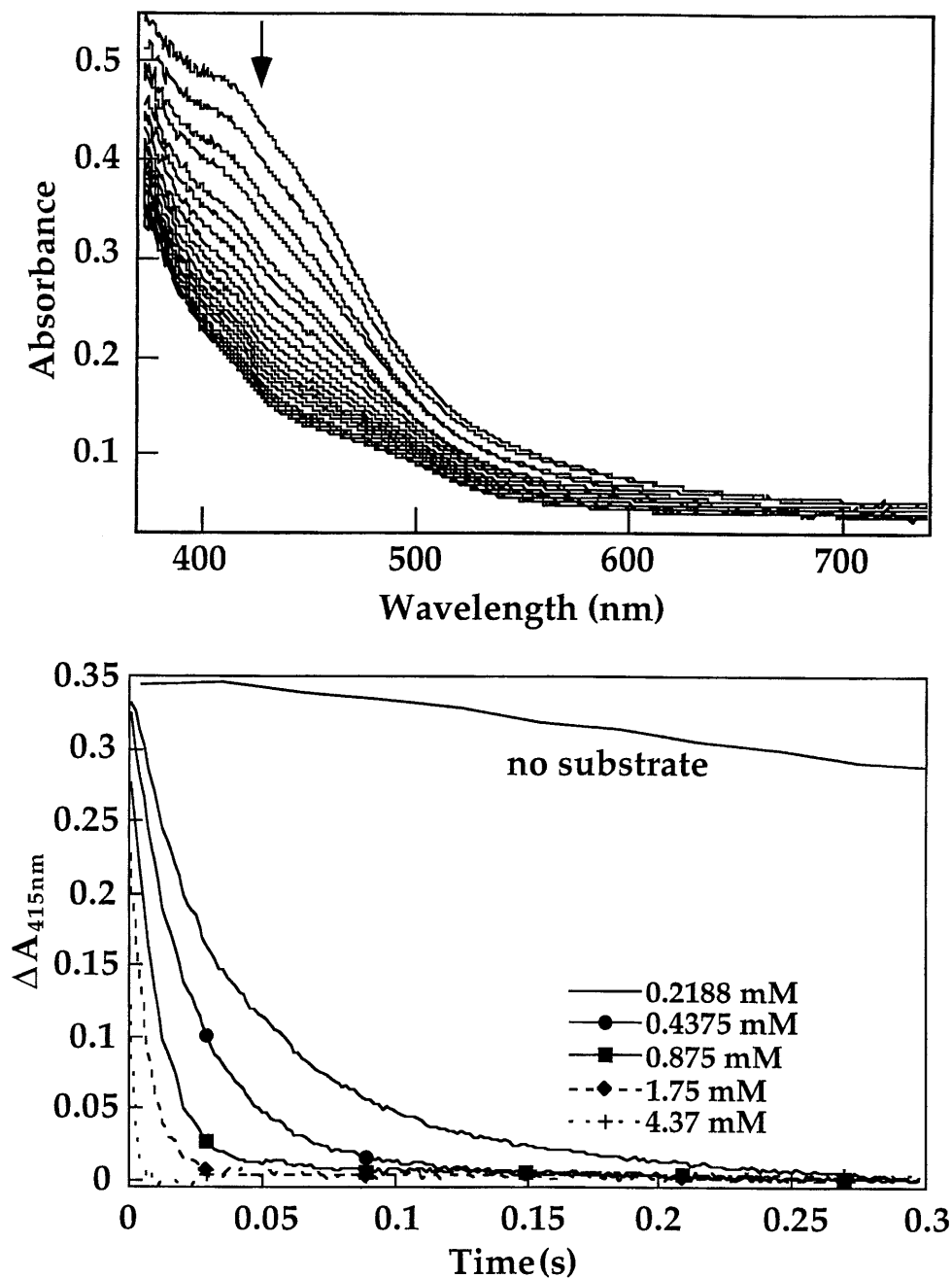


Figure 4.13. (A) Raw data resulting from mixing acetylene ($438 \mu\text{M}$ after mixing) with the evolving intermediates after a 0.4 s delay after mixing $\text{H}_{\text{red}}/2\text{B}$ with dioxygen. (B) Traces at 415 nm after similar experiments employing a range of concentrations of acetylene.

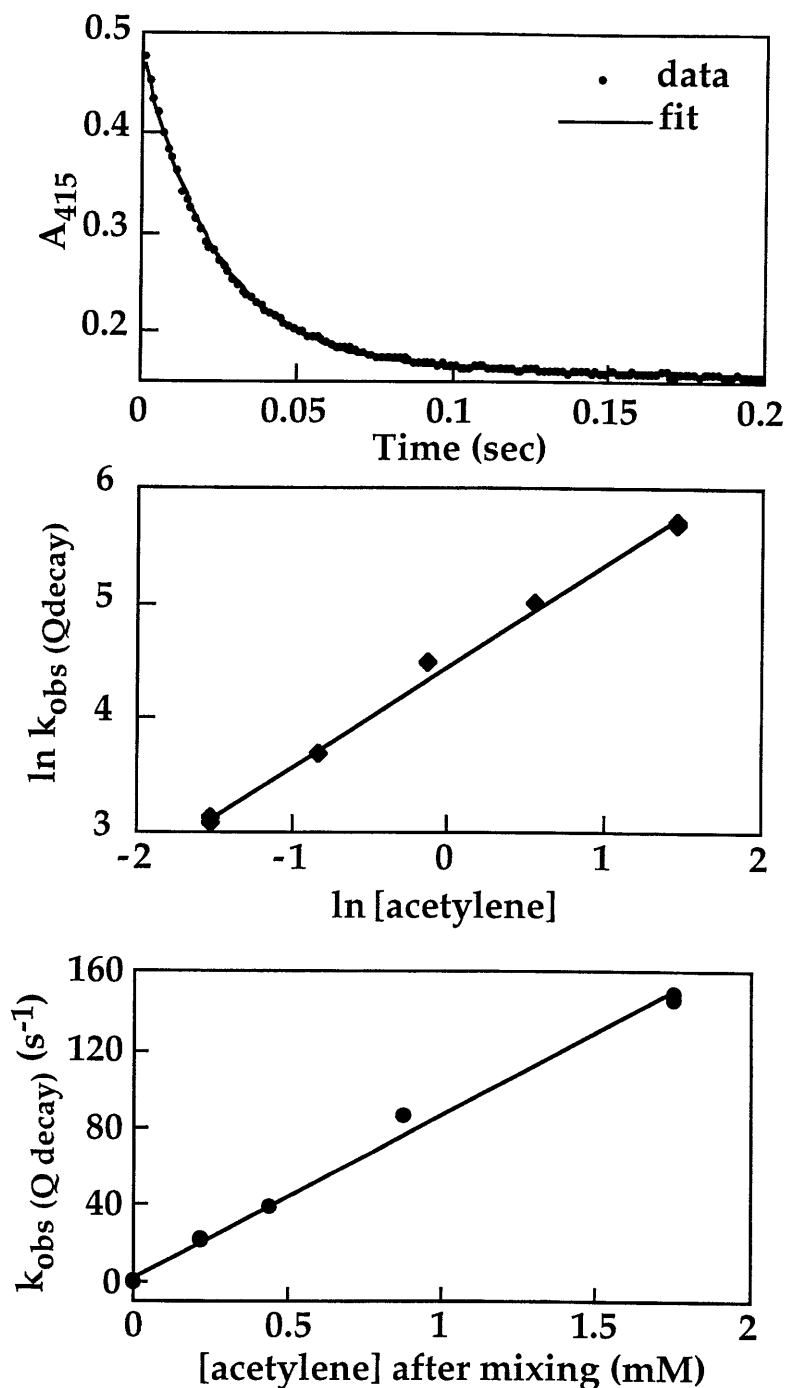


Figure 4.14. (A) The fit of a single exponential decay to the kinetic data at 415 nm describing the reaction of acetylene with intermediate Q pictured in Figure 4.13A. (B) A plot of $\ln(k_{\text{obs}})$ vs. $\ln([\text{acetylene}])$. The slope of the line is 0.9. (C) A plot of k_{obs} for Q decay vs. $[\text{acetylene}]$. The slope of the line, the second order rate constant for the reaction, is $8.4 \times 10^4 \text{ M}^{-1}\text{cm}^{-1}$.

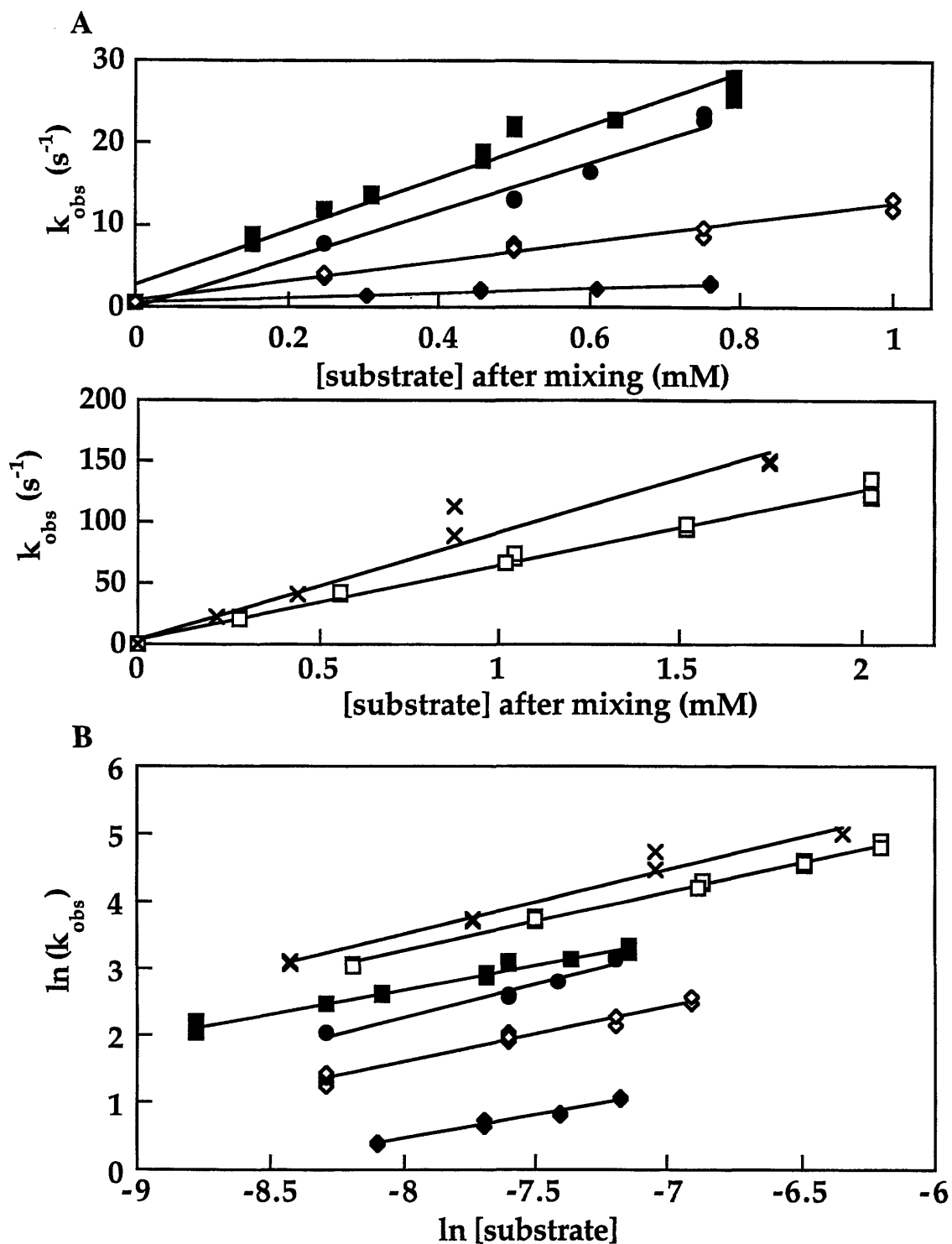


Figure 4.15. (A) Plot of k_{obs} vs. [substrate] for methane (closed circles), ethane (closed squares), propane (closed diamonds), ethylene (open squares), propylene (open diamonds), and acetylene (crosses). (B) Plot of $\ln(k_{\text{obs}})$ vs. $\ln[\text{substrate}]$ for the same substrates.

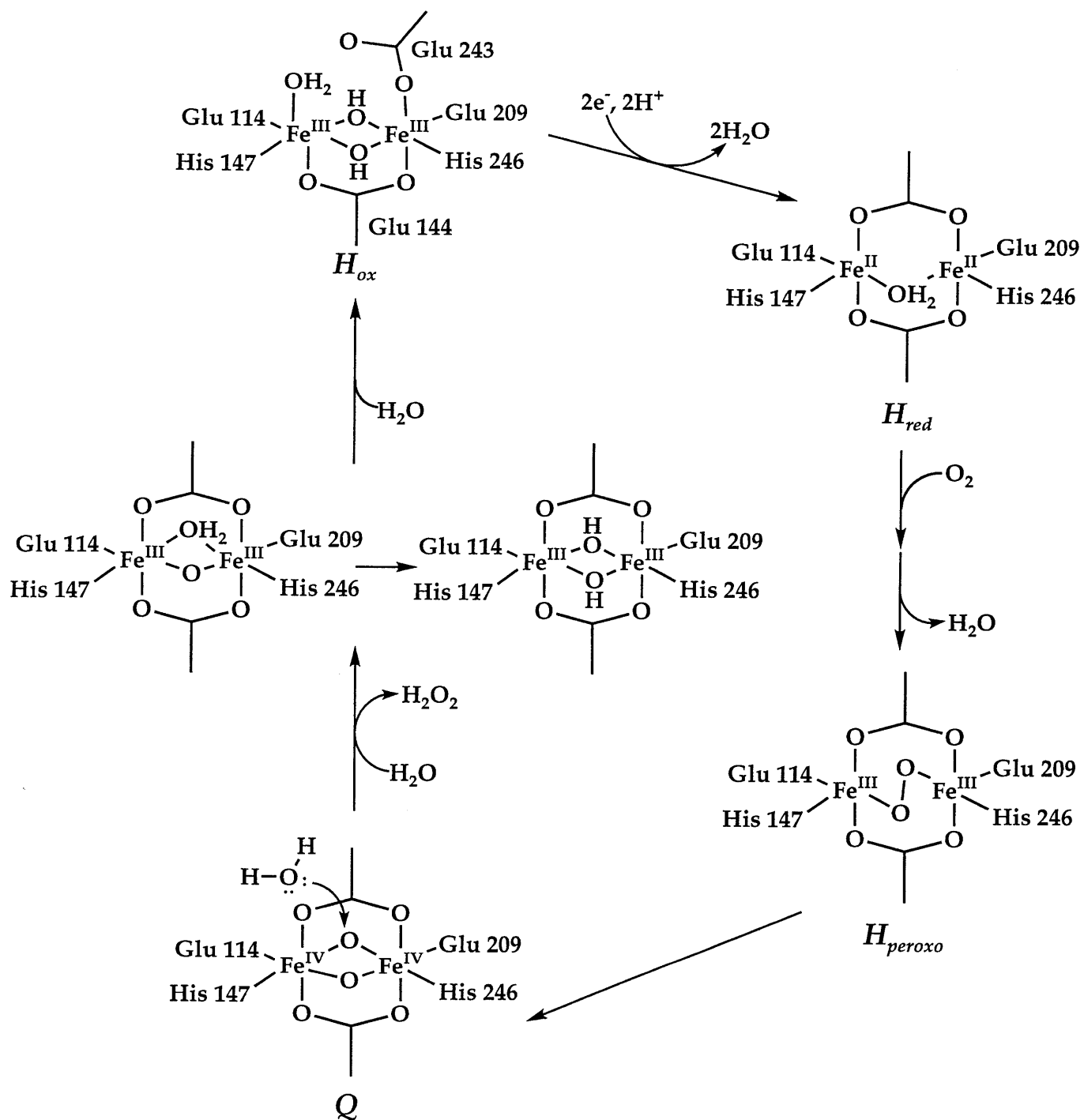


Figure 4.16. Proposal for the species observed in the single turnover reaction of $H_{red}/2B$ with O_2 in the absence of substrate.

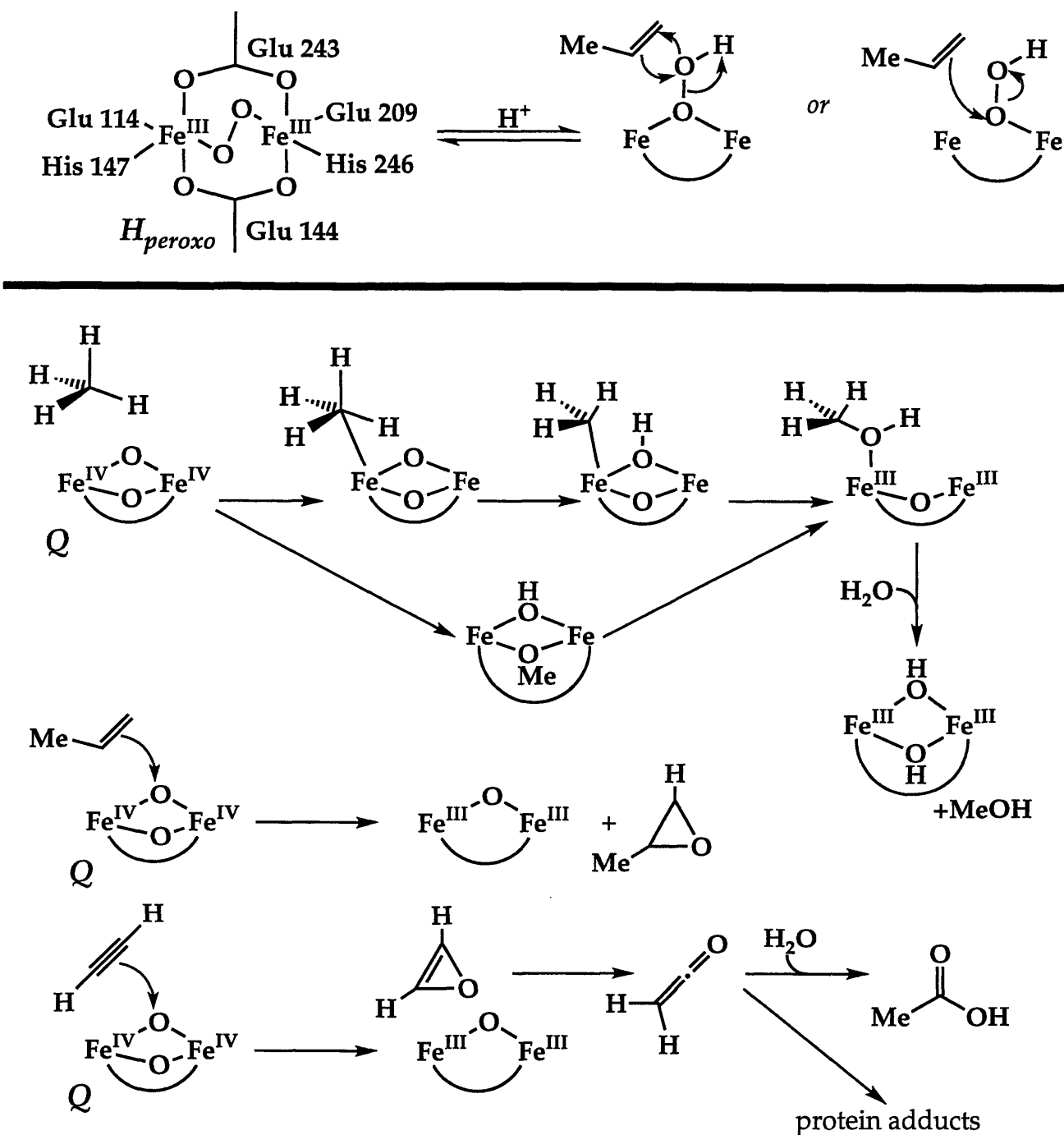


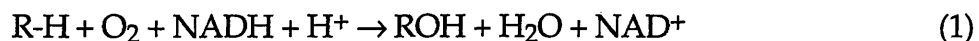
Figure 4.17. Possible mechanisms for the oxidation of substrates by sMMO. (Top) Oxidation of propylene by a putative diiron(III) hydroperoxide intermediate species. (Bottom) Oxidation of methane, propylene, and acetylene by intermediate Q.

Chapter Five:

**Oxidation of Radical Clock Substrate Probes by the
Soluble Methane Monooxygenase**

Introduction

The dinuclear iron-containing soluble methane monooxygenase (sMMO) from *Methylococcus capsulatus* (Bath) effects the mixed-function oxidation of substrate molecules according to eq. 1.¹⁻³ In methanotrophic



bacteria from which sMMO is isolated, methane is the native substrate and provides carbon and energy for the growth of the cell. This kinetically difficult transformation is carried out at the active site of a 251 kDa hydroxylase enzyme (MMOH),⁴⁻⁷ the structure of which has been determined by X-ray crystallography. Electrons are supplied from NADH via a 38.5 kDa reductase protein (MMOR),^{4,8} and the reactivity of the system is modulated by a 15.8 kDa coupling protein (MMOB).⁹⁻¹¹

In addition to methane, sMMO will oxidize a wide variety of substrates.¹²⁻¹⁵ This property has allowed the use of radical clock substrate probes to derive mechanistic information. These probes were first described in 1980¹⁶ as calibrated clocks¹⁷ which could be used in mechanistic studies of proteins^{18,19} and model compounds.^{20,21} Specifically, these substrates can reveal whether radical intermediates are formed during a reaction and, if so, establish their lifetime and the rate constant for radical rebound. Figure 5.1 depicts the oxidation of a radical clock substrate probe which employs the ring opening of a cyclopropyl carbinyl radical. If hydrogen atom abstraction from the probe occurs, the resulting radical can either rebound to form the unrearranged alcohol or undergo ring opening before rebound to afford the rearranged alcohol. If the ring opening rate has been determined,¹⁷ the rebound rate, $k_{\text{oxidation}}$, can be calculated according to eq. 2.

$$k_{\text{oxidation}} = k_{\text{ring opening}} (\text{unrearranged alcohol/rearranged alcohol}) \quad (2)$$

The hypothesis that radical intermediates form in the sMMO system has been tested by a variety of techniques. Nitroxyl spin traps detected radical species produced during the oxidation of methane, methanol, and acetonitrile.²² The respective $\cdot\text{CH}_3$, $\cdot\text{CH}_2\text{OH}$, and $\cdot\text{CH}_2\text{CN}$ radicals apparently were able to diffuse out of the protein and react with the spin traps. The products were not quantitated, however, so it is difficult to gauge the importance of these species in the bulk mechanism. Early radical clock results employing sMMO from *Methylosinus trichosporium* OB3b suggested both radical and cationic intermediates.²³ Later radical clock studies revealed no radical rearrangement for the *M. capsulatus* (Bath) system and very little for the enzyme from *M. trichosporium* OB3b.^{19,24} Hydroxylations of chiral tritiated alkanes proceeded with ~30% inversion of stereochemistry, an amount corresponding to putative radical lifetimes (< 100 fs) too short to be attributed to a discrete radical formation.^{25,26}

The possibility exists that substrate-dependent reactivity might invalidate the conclusions of research based on diagnostic substrate probes. In chapter four, evidence was presented that an intermediate other than Q is competent to oxidize olefins, demonstrating that substrate can indeed influence the reaction pathway. Even for hydroxylation reactions there is some indication that the substrate itself might dictate the mechanism. For sMMO from *M. trichosporium* OB3b, a kinetic isotope effect of 50-100 was reported for reaction of CH_4 vs. CD_4 with Q.²⁷ This value is far greater than that for any other substrate and might suggest that a different mechanism is at work. Experiments with the *M. capsulatus* (Bath) protein do not reproduce

these very large isotope effects.²⁸ Conversely, it is also possible that the protein, through steric constraints or other interactions, might alter the reactivity of the probe from that observed free in solution. If ring opening were impeded, the clocks would “run slow” in the enzyme active site. These concerns have been addressed by using probes that do not dramatically change shape upon rearrangement. The best examples of such behavior are the round trip probes.¹⁹ A radical formed by H-atom abstraction from the methyl group of methylcubane, for example, ends up on the same carbon, so there is no need for substrate translocation in the active site prior to rebound. The oxidation of methylcubane by sMMO from *Methylococcus capsulatus* (Bath) yielded no rearranged products.¹⁹

The results of the radical clock substrate probe studies have so far been in agreement with those employing chiral tritiated alkanes,^{25,26} the closest substrates to methane from which mechanistic information can be obtained. Nevertheless, we were interested to try the new hypersensitive radical clock substrate probes (Table 5.1), which have ring opening rates in excess of 10^{11} s^{-1} . Such values allow detection of rebound reactions occurring with rate constants up to 10^{13} s^{-1} , assuming a detection limit of 1% of ring-opened versus total product. This rate constant is at the limit for a barrierless decomposition of a transition state.²⁶ Probe 1²⁴ can be prepared in pure (R,R) and (S, S) form. Probe 2 is constrained to require minimal conformational change upon ring opening.²⁹ Probes 3 and 4 are substituted at the para position on the phenyl ring, eliminating the presence of “uninformative” product (1b). These substitutions also increase the ring opening rate constant. Probe 5 discriminates between radical and carbocationic intermediates (Figure 5.2).¹⁸ In this chapter, we report the results of oxidation of these substrate

probes by the reconstituted sMMO catalytic system. These and other data are used to assess some recent mechanistic proposals for catalysis.

Experimental

Protein Preparation and Characterization. Native MMOH^{24,30,31} and MMOR²⁶ and recombinant MMOB^{24,32} were purified and characterized as previously reported.

Radical Clock Substrate Probes and Products. All probes and authentic samples of the anticipated products were provided as neat liquids or solids by Marie Helene Le Tadic-Biadatti and Patrick Toy of the Professor Martin Newcomb's laboratory at Wayne State University.

Enzymatic Oxidations and Product Characterization. Typically, 15 nmol of MMOH, 15 nmol of MMOB, and 5.25 nmol of MMOR were combined in a 20 mL glass scintillation vial. Probes 1-4 were added as neat liquids, typically as 1 μ L aliquots. Probe 5 was added as 2 mL of a saturated solution in 25 mM MOPS (pH 7). The solution was incubated for 2 min at 45 °C. A 100 μ L aliquot of 0.1 M ethanol-free NADH was added to initiate the reaction and bring the total volume to 5 mL, and the reaction was allowed to proceed at 45 °C for 15 min with gentle agitation. The mixture was extracted with methylene chloride (5 x 4 mL), and the solution was spun in an analytical centrifuge for 10 min after each extraction. The combined extracts (20 mL) were dried over MgSO₄ and concentrated to ~100 μ L by using a rotary evaporator. A 10 μ L aliquot of a 10 mM solution of an internal standard, methyl benzoate or ethyl benzoate, was added. The products were analyzed by parallel gas chromatography (GC) and gas chromatography with mass spectrometry (GC/MS) methods on 50 m HP-1 methyl silicone columns. A Hewlett-Packard 5890A gas chromatograph equipped with a Hewlett-Packard 5971A mass

spectrometer was employed. A typical trace is shown in Figure 5.3. Standard curves (Figure 5.4) were generated by analyzing a range of concentrations of each substrate and product referenced to the same internal standard added to the reaction mixture. To determine whether products were consumed during the reaction or lost during workup, reaction solutions were spiked with small known amounts of these species and the resulting product mixtures analyzed for their presence. No such loss of consumption was observed.

To test for possible enzyme inhibition by probe 5, the reconstituted protein system was incubated with NADH and this probe for 5 min prior to addition of a second substrate. In some cases, the 5 was removed by transferring the solution following preincubation to Centriplus 100 centrifugal concentrators (Amicon) and repeatedly concentrating and diluting it with 25 mM MOPS (pH 7). MMOB, MMOR, NADH, and free probe 5 were removed by this procedure. The concentration of the resulting hydroxylase solution was determined and the absence of NADH was established by UV/vis spectroscopy. Removal of the other proteins was verified by sodium dodecyl sulfate polyacrylamide gel electrophoresis (SDS-PAGE). The system was reconstituted with the MMOB and MMOR, substrate, and NADH, and oxidation of a second probe was attempted as described above for radical clock probe substrates or by standard methods when propylene or nitrobenzene was used.²⁴

Results and Discussion

Characterization of Oxidation Products. The products of oxidation of the radical clock substrate probes are shown in Table 5.2. Typically, less than 10% of the substrate was oxidized and more than 85% of added material was recovered as products or unreacted probe. None of the products were consumed during the course of the reaction. In no case was a rearranged or

ring opened product detected. Less conversion was observed for probes 3 and 4 than for the unfluorinated analog 1, most probably due to their decreased solubility. Only the primary alcohol products were observed for these substrates.

In previous work reporting hydroxylation of racemic 1, there was a slight preference for forming of the primary alcohol over the phenol.²⁴ It was hypothesized that this preference might reflect the conformation of the substrate molecule, such that one diastereomer might afford predominantly phenol and the other, the primary alcohol. A comparison of the hydroxylation products of (S,S)- and (R,R)-1-phenyl-2-methylcyclopropane (Table 5.3) reveals that, when (R,R)-1 was employed as the substrate, the primary alcohol was formed preferentially. When the (S,S)-diastereomer was used, the phenol was predominantly formed. This result supports the hypothesis that each diastereomer has a favored orientation within the MMOH active site.

In order to understand these stereochemical preferences, a model of the enzyme active site was generated by using the 1.7 Å resolution MMOH x-ray crystallographic coordinates.³³ The (R,R) and (S,S) diastereomers were docked into the active site, positioning either the methyl or phenyl group near the iron atoms and extending the remainder of the substrate into the hydrophobic cavity 1 at the active site. When the para position of the phenyl ring for either substrate was positioned near the iron atoms, steric interactions were minimized by directing the methylcyclopropyl group out towards the neighboring hydrophobic cavity, cavity 2, in the vicinity of a mobile leucine residue, Leu110 (Figure 5.5A and B).³⁴ Attempts to position the phenyl ring near this leucine residue were unfavorable and did not orient the methyl group of the substrate near positions at the diiron center

previously identified as the most likely to generate activated oxygen species.³⁵ Instead, the phenyl group was more readily accommodated when positioned toward helices E and F, which help form the canyon walls of MMOH. When the substrate was so oriented, the methyl group of the (R,R) diastereomer was positioned directly over the diiron center (Figure 5.5C), whereas the methyl group of the (S,S) diastereomer (Figure 5.5D) was directed away from it. If the substrate does indeed bind in these two alternative modes, this model explains the more favorable methyl oxidation with respect to phenyl oxidation observed for the (R,R) probe. The internal packing differences for the (S,S) substrate are less disparate, however, and might reflect protein side chain movements induced by MMOB not observed in the structure of oxidized MMOH alone.

Attempts to oxidize **5** failed to yield any product alcohol. This result suggested that this molecule might be a mechanism-based inhibitor. Probe **5** did inhibit the ability of the sMMO to oxidize **1**, the largest of the substrates employed, and the inhibition could be reversed by removal of the probe. Propylene and nitrobenzene oxidation were not affected by the presence of **5**. Thus, **5** does not covalently modify the protein, but may be difficult to dislodge from the series of hydrophobic cavities leading to the enzyme active site cavity which lie along the proposed path of substrate access.^{6,33,35} Several such cavities have been identified in the MMOH structure, and the path taken by a given substrate may depend on its steric requirements. The fact that activity toward small substrates is unaffected suggests that **5** cannot access the enzyme active site, which explains the observed lack of activity for that probe. Probe **5** did not fit well when modeled into the enzyme active site (Figure 5.6). Attempts to bring either the methyl or phenyl group near the iron center resulted in steric clashes between the *t*-butoxy group and protein side chains.

The orientation shown, with the *t*-butoxy group pointing toward the iron center, was the most favorable, and still would require some protein side chain movements.

Calculation of a Lower Limit for the Rebound Rate Constant of a Putative Radical Intermediate. Detection of any rearranged products would have provided evidence for the intermediacy of a substrate radical. In the absence of such products, eq. 2 can be used to calculate the lower limit on the rate constant such a process would require in order to occur without ring opening. Assuming a 1% detection limit for the oxidation of 4, the fastest probe tested, the corresponding rebound rate would be greater than $9 \times 10^{12} \text{ s}^{-1}$ and the lifetime of the putative radical would be at most 11 femtoseconds. Thus the present results strongly reinforce our previous conclusions that a radical rebound mechanism does not occur for sMMO and that a non-synchronous concerted process better explains the experimental data.^{18,26,36} Some possible oxidation mechanisms are depicted in Figure 5.7 and discussed in more detail below.

Mechanistic Implications and Comparisons to Literature Results. Many possible mechanisms for the catalytic cycle in MMOH have been compiled in review and opinion articles regarding sMMO.^{2,24,37} These mechanisms are supported in part by the detection of intermediate species in single turnover studies of the enzyme.^{10,38-40} The oxidation step typically involves reaction of an electrophilic intermediate Q, postulated to be a bis(μ -oxo)diiron(IV)⁴¹ or related species, with the hydrocarbon substrate. Some agreement has been reached that freely diffusing substrate radicals are not a hallmark of sMMO oxidation chemistry, although some workers still draw a discrete radical intermediate (R).^{42,43} How best to explain the available mechanistic information remains a contested topic.

Recently, a set of commentaries appeared which speculated on the hydrocarbon oxidation mechanism.⁴⁴ Some common questions which emerged: What is the structure of Q? Is Q the active species? Is the oxygen transferred to substrate bridging the iron atoms⁴⁵ or terminal^{46,47} in the active species? Are Fe-C bonds formed and, if so, before^{48,49} or after^{42,43,46,47} C-H bond cleavage?³⁶

Some favor a ferryl species for Q as the active intermediate,⁴² with concerted addition of the C-H bond across the Fe(IV)=O unit and some component of Fe-C bonding. Radical traps are claimed to be able to intercept the C-OH bond as it forms in the transition state. The presence of terminal Fe=O bonds in Q remains a viable possibility, although it is not supported by EXAFS spectroscopy⁴¹ and modeling chemistry.⁵⁰ Perhaps Q is in dynamic equilibrium with such a species, as we have previously suggested. The lack of quantitation in the radical trap experiments has already been noted. In recent work,⁵¹ inhibition of cyclohexane oxidation by H₂, D₂, and CH₄ provided evidence for an agostic interaction of these molecules involving a porphyrin Fe(IV)=O unit. Both steady-state⁵² and single turnover²⁸ sMMO oxidations are unaffected by the presence of H₂, as would be expected if such an interaction were taking place.

Others⁴⁵ prefer a "bridge mechanism," or oxidation by a di- μ -oxo-diiron(IV) active species. Such an intermediate structure has been combined with the above oxidation mechanism in an extended Hückel theory analysis of the oxidation of methane by a ferryl species.⁵³ When applied to sMMO,⁴⁹ drawn for the general substrate R-H in the upper pathway of Figure 5.7, methane undergoes a C_{3v} distortion and coordinates to the iron atom of a bis(μ -oxo)diiron(IV) active species. The resulting five-coordinate carbon could undergo pseudorotation, which was one of the explanations offered to

account for the chiral ethane results.²⁶ This process would invert the chiral ethane molecule without forming a discrete radical. A hydrogen shift to the bridging oxygen atom followed by a methyl shift would yield the product complex.⁵⁴

Others bring to the debate a combination of computational and structural insights.^{46,47} According to density functional theory, the active intermediate is an Fe(III)-O-Fe(IV)-O· species which reacts by hydrogen atom abstraction to afford a caged radical. Rapid formation of an Fe(V)-C bond ensues. The very short lifetime limit determined in the radical clock and chiral ethane experiments would correspond to the period between hydrogen atom abstraction and iron-carbon bond formation. These translational motions could not take place in less than the 11 fs limit set by our current results, however. The authors postulate that the Fe-C bond could be very weak and that the alkyl could still be intercepted by spin traps, but again the time scales seem incommensurate. Still others⁴³ support an oxo-bridged Q structure, which generates an intermediate having radical character, perhaps according to one of the mechanisms described above, but without forming discrete free radicals.

The current proposals for the structure of the oxidizing intermediate thus fall into three classes: a bis(μ -oxo)diiron(IV), a diferryl, and a Fe(III)-O-Fe(IV)-O· species. Iron-carbon bonds are usually invoked, either before or after C-H bond cleavage despite the fact that there is so far no experimental evidence to support them. The reaction itself must proceed by some version of a nonsynchronous concerted pathway in order to allow partial inversion of chiral ethane without generating free substrate radicals. One such mechanism depicting oxidation by the form of Q we currently favor is given in the middle pathway of Figure 5.7. This mechanism is similar to that proposed previously

(also Figure 6.7) except that the active species drawn was a diferryl rather than a bridged structure.²⁶ In this model, reaction of substrate with the active species affords hydroxide and alkoxide, which are protonated to release the products.

At the bottom of Figure 5.7 is a mechanism which invokes participation of the nearby cysteine sulfhydryl group. Its involvement has been proposed previously.³⁷ In this mechanism, hydrogen atom transfer from the cysteine to Q affords a mixed-valent, hydroxo-bridged species. This species would have to be very short-lived, because no such compound has been detected in RFQ Mössbauer time course studies without substrate or with methane. In a concerted reaction, the cysteine radical and iron center would cleave the C–H bond in a non-synchronous fashion, during which time some radical character in the substrate might develop without formation of a discrete substrate radical species. Alternatively, if either bridging (or terminal) oxygen atom were able to attack the substrate, hydroxylation would occur on one face or the other of the RCH₃ molecule, accounting for the partial inversion of the chiral ethane probe.

Conclusions

Results from oxidations of hypersensitive radical clock substrate probes continue to refute the notion that a discrete substrate radical species forms in sMMO oxidations. For probe **1**, which can be prepared in diastereomerically pure form, the predominant oxidation product depends on the diastereomer used, providing evidence that the substrate assumes a preferred binding mode in the enzyme active site. Although probe **5** is not oxidized by sMMO, it inhibits oxidation of **1** but not of propylene or nitrobenzene. This inhibition is reversed upon removal of **5**, suggesting that it sterically blocks access to the

active site for the large substrate **1**. Several recent mechanistic proposals incorporate aspects of a nonsynchronous concerted mechanism and attempt to reconcile all the existing spectroscopic and mechanistic data regarding sMMO. Additional mechanistic experimental and theoretical work is clearly warranted.

References

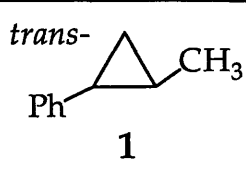
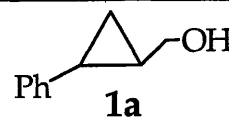
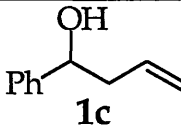
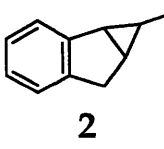
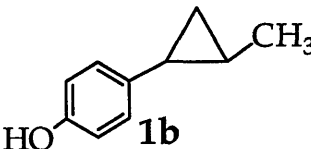
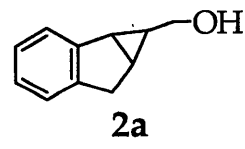
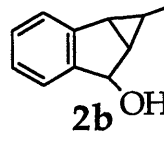
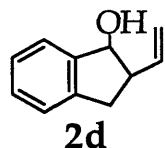
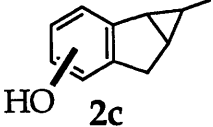
- (1) Liu, K. E.; Lippard, S. J. In *Advances in Inorganic Chemistry*; Sykes, A. G., Eds.; Academic Press: San Diego, 1995; Vol. 42; pp 263-289.
- (2) Wallar, B. J.; Lipscomb, J. D. *Chem. Rev.* **1996**, *96*, 2625-2657.
- (3) Valentine, A. M.; Lippard, S. J. *J. Chem. Soc., Dalton Trans.* **1997**, *21*, 3925-3931.
- (4) Colby, J.; Dalton, H. *Biochem. J.* **1978**, *171*, 461-468.
- (5) Woodland, M. P.; Dalton, H. *J. Biol. Chem.* **1984**, *259*, 53-59.
- (6) Rosenzweig, A. C.; Frederick, C. A.; Lippard, S. J.; Nordlund, P. *Nature* **1993**, *366*, 537-543.
- (7) Rosenzweig, A. C.; Nordlund, P.; Takahara, P. M.; Frederick, C. A.; Lippard, S. J. *Chem. Biol.* **1995**, *2*, 409-418.
- (8) Colby, J.; Dalton, H. *Biochem. J.* **1979**, *177*, 903-908.
- (9) Green, J.; Dalton, H. *J. Biol. Chem.* **1985**, *260*, 15795-15801.
- (10) Liu, K. E.; Valentine, A. M.; Wang, D.; Huynh, B. H.; Edmondson, D. E.; Salifoglou, A.; Lippard, S. J. *J. Am. Chem. Soc.* **1995**, *117*, 10174-10185.
- (11) Gassner, G. T. personal communication.
- (12) Colby, J.; Stirling, D. I.; Dalton, H. *Biochem. J.* **1977**, *165*, 395-402.
- (13) Green, J.; Dalton, H. *J. Biol. Chem.* **1989**, *264*, 17698-17703.
- (14) Dalton, H. In *Adv. Appl. Microbiol.* Academic Press: 1980; Vol. 26; pp 71-87.
- (15) Fox, B. G.; Borneman, J. G.; Wackett, L. P.; Lipscomb, J. D. *Biochemistry* **1990**, *29*, 6419-6427.
- (16) Griller, D.; Ingold, K. U. *Acc. Chem. Res.* **1980**, *13*, 317-323.
- (17) Newcomb, M. *Tetrahedron* **1993**, *49*, 1151-1176.
- (18) Newcomb, M.; Le Tadic-Biadatti, M.-H.; Chestney, D. L.; Roberts, E. S.; Hollenberg, P. F. *J. Am. Chem. Soc.* **1995**, *117*, 12085-12091.

- (19) Choi, S.-Y.; Eaton, P. E.; Hollenberg, P. F.; Liu, K. E.; Lippard, S. J.; Newcomb, M.; Putt, D. A.; Upadhyaya, S. P.; Xiong, Y. *J. Am. Chem. Soc.* **1996**, *118*, 6547-6555.
- (20) Castellino, A. J.; Bruice, T. C. *J. Am. Chem. Soc.* **1988**, *110*, 7512-7519.
- (21) Vanni, R.; Garden, S. J.; Banks, J. T.; Ingold, K. U. *Tet. Lett.* **1995**, *36*, 7999-8002.
- (22) Deighton, N.; Podmore, I. D.; Symons, M. C. R.; Wilkins, P. C.; Dalton, H. *J. Chem. Soc., Chem. Comm.* **1991**, 1086-1088.
- (23) Ruzicka, F.; Huang, D.-S.; Donnelly, M. I.; Frey, P. A. *Biochemistry* **1990**, *29*, 1696-1700.
- (24) Liu, K. E.; Johnson, C. C.; Newcomb, M.; Lippard, S. J. *J. Am. Chem. Soc.* **1993**, *115*, 939-947.
- (25) Priestley, N. D.; Floss, H. G.; Froland, W. A.; Lipscomb, J. D.; Williams, P. G.; Morimoto, H. *J. Am. Chem. Soc.* **1992**, *114*, 7561-7562.
- (26) Valentine, A. M.; Wilkinson, B.; Liu, K. E.; Komar-Panicucci, S.; Priestley, N. D.; Williams, P. G.; Morimoto, H.; Floss, H. G.; Lippard, S. J. *J. Am. Chem. Soc.* **1997**, *119*, 1818-1827.
- (27) Nesheim, J. C.; Lipscomb, J. D. *Biochemistry* **1996**, *35*, 10240-10247.
- (28) Stahl, S. S.; Lippard, S. J. unpublished results.
- (29) Martin-Esker, A. A.; Johnson, C. C.; Horner, J. H.; Newcomb, M. *J. Am. Chem. Soc.* **1994**, *116*, 9174-9181.
- (30) Valentine, A. M. Ph. D. Thesis, Massachusetts Institute of Technology, 1998, Chapter Two.
- (31) DeWitt, J. G.; Bentsen, J. G.; Rosenzweig, A. C.; Hedman, B.; Green, J.; Pilkington, S.; Papaefthymiou, G. C.; Dalton, H.; Hodgson, K. O.; Lippard, S. J. *J. Am. Chem. Soc.* **1991**, *113*, 9219-9235.

- (32) Coufal, D. E.; Blazyk, J.; Whittington, D. A.; Lippard, S. J. manuscript in preparation.
- (33) Rosenzweig, A. C.; Lippard, S. J. *Acc. Chem. Res.* **1994**, *27*, 229-236.
- (34) Rosenzweig, A. C.; Brandstetter, H.; Whittington, D. A.; Nordlund, P.; Lippard, S. J.; Frederick, C. A. *Proteins* **1997**, *29*, 141-152.
- (35) Whittington, D. A.; Lippard, S. J. In *ACS Symposium Series*; Hodgson, K. O. and Solomon, E. I., Eds.; 1998.
- (36) Whittington, D. A.; Valentine, A. M.; Lippard, S. J. *JBIC* **1998**, *3*, 307-313.
- (37) Feig, A. L.; Lippard, S. J. *Chem. Rev.* **1994**, *94*, 759-805.
- (38) Lee, S.-K.; Fox, B. G.; Froland, W. A.; Lipscomb, J. D.; Münck, E. *J. Am. Chem. Soc.* **1993**, *115*, 6450-6451.
- (39) Lee, S.-K.; Nesheim, J. C.; Lipscomb, J. D. *J. Biol. Chem.* **1993**, *268*, 21569-21577.
- (40) Liu, K. E.; Wang, D.; Huynh, B. H.; Edmondson, D. E.; Salifoglou, A.; Lippard, S. J. *J. Am. Chem. Soc.* **1994**, *116*, 7465-7466.
- (41) Shu, L.; Nesheim, J. C.; Kauffmann, K.; Münck, E.; Lipscomb, J. D.; Que, L., Jr. *Science* **1997**, *275*, 515-518.
- (42) Deeth, R. J.; Dalton, H. *JBIC* **1998**, *3*, 302-306.
- (43) Lipscomb, J. D.; Que, L. J. *JBIC* **1998**, *2*, 331-336.
- (44) Nordlander, E.; Andersson, K. K. *JBIC* **1998**, *3*, 300-301.
- (45) Shteinman, A. A. *JBIC* **1998**, *3*, 325-330.
- (46) Siegbahn, P. E. M.; Crabtree, R. H. *J. Am. Chem. Soc.* **1997**, *119*, 3103-3113.
- (47) Siegbahn, P. E. M.; Crabtree, R. H.; Nordlund, P. *JBIC* **1998**, *3*, 314-317.
- (48) Yoshizawa, K.; Shiota, Y.; Yamabe, T. *Chem. Eur. J.* **1997**, *3*, 1160-1169.
- (49) Yoshizawa, K. *JBIC* **1998**, *3*, 318-324.
- (50) Lee, D.; Lippard, S. J. to be submitted for publication.

- (51) Collman, J. P.; Chien, A. S.; Eberspacher, T. A.; Brauman, J. I. *J. Am. Chem. Soc.* **1998**, *120*, 425-426.
- (52) Valentine, A. M.; Lippard, S. J. unpublished results.
- (53) Yoshizawa, K.; Shiota, Y.; Yamabe, T. *Organometallics* **1998**, *17*, 2825-2831.
- (54) Willems, J.-P.; Valentine, A. M.; Gurbiel, R.; Lippard, S. J.; Hoffman, B. M. *J. Am. Chem. Soc.* **1998**, in press.
- (55) Newcomb, M.; Johnson, C. C.; Manek, M. B.; Varick, T. R. *J. Am. Chem. Soc.* **1992**, *114*, 10915-10921.
- (56) Toy, P. H.; Dhanabalasingam, B.; Newcomb, M.; Hanna, I. H.; Hollenberg, P. H. *J. Org. Chem.* **1997**, *62*, 9114-9122.

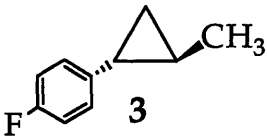
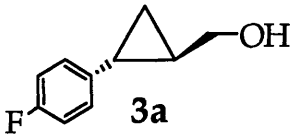
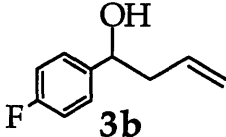
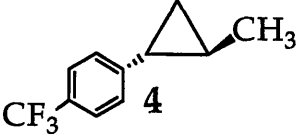
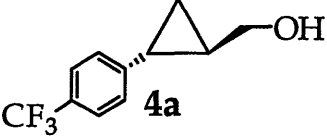
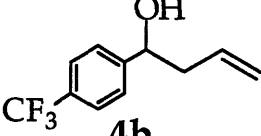
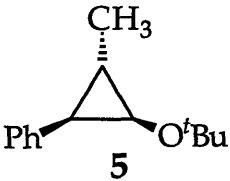
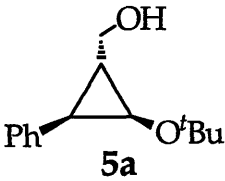
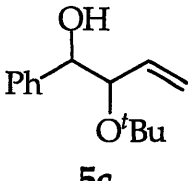
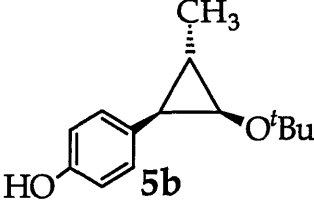
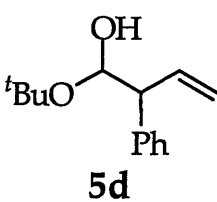
Table 5.1. Radical Clock Substrate Probes Used in the Current Study and the Ring Opening Rate of the Cyclopropylcarbinyl Radical Derived From the Probes.

Substrate	Unrearranged Products	Rearranged Product(s)	Ring Opening Rate Constant (s ⁻¹)
 <p><i>trans</i>-1</p>	 <p>1a</p>	 <p>1c</p>	3×10^{11} ^a 4×10^{11} ^b Ref. ^{24,55}
 <p>2</p>	 <p>1b</p>	 <p>2a</p>	3×10^{11} ^a Ref. ²⁹
	 <p>2b</p>	 <p>2d</p>	
	 <p>2c</p>		

^a Measured at 25°C by using benzeneselenol trapping as a competing reaction.

^b Measured at 45°C.

Table 5.1 Continued. Radical Clock Substrate Probes Used in the Current Study and the Ring Opening Rate of the Cyclopropylcarbinyl Radical Derived From the Probes.

Substrate	Unrearranged Products	Rearranged Product(s)	Ring Opening Rate Constant (s ⁻¹)
 3	 3a	 3b	-
 4	 4a	 4b	9 x 10 ¹¹ ^c Ref. ⁵⁶
 5	 5a	 5c	6 x 10 ¹¹ ^c Ref. ¹⁸
 5b		 5d	


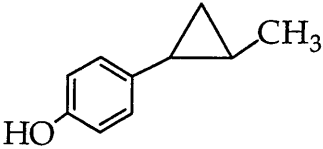
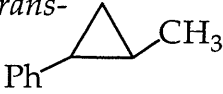

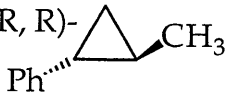
^c Measured at 37°C by using benzeneselenol trapping as a competing reaction.

Table 5.2. Products from Oxidation of Radical Clock Substrate Probes by sMMO.

Probe	Relative Product Yields ^a	Avg. Conversion
1	1a : 1b : 1c 1.1 : 1 : 0	6.4%
2	2a : 2b : 2c : 2d 0.48 : 0.12 : 1 : 0	10.5%
3	3a:3b 1 : 0	3.8%
4	4a : 4b 1 : 0	2.5%
5	-	-

^a See Table 5.1.

Table 5.3. Products from Oxidation of Racemic *trans*-1-Phenyl-2-methylcyclopropane and of Each Diastereomer.

Substrate		
racemic <i>trans</i> - 	1.1	1
(S, S)- 	0.70	1
(R, R)- 	1.36	1

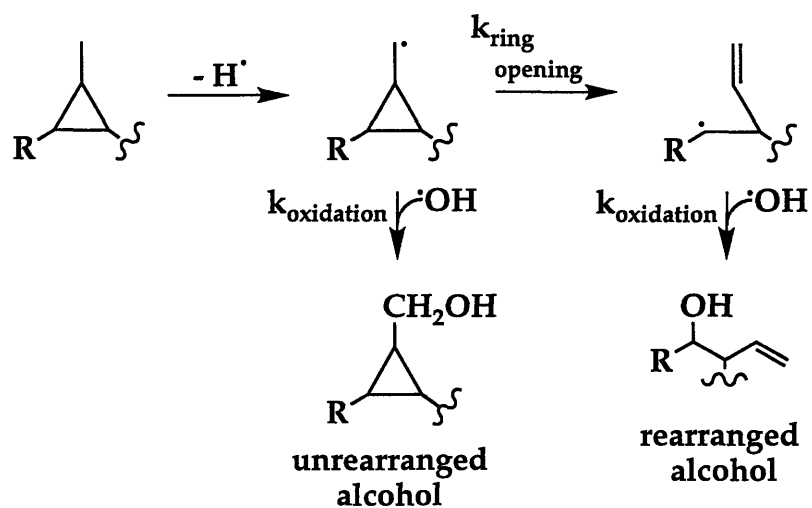


Figure 5.1. Ring opening of cyclopropylcarbinyl radicals resulting from hydrogen atom abstraction from a radical clock substrate probe.

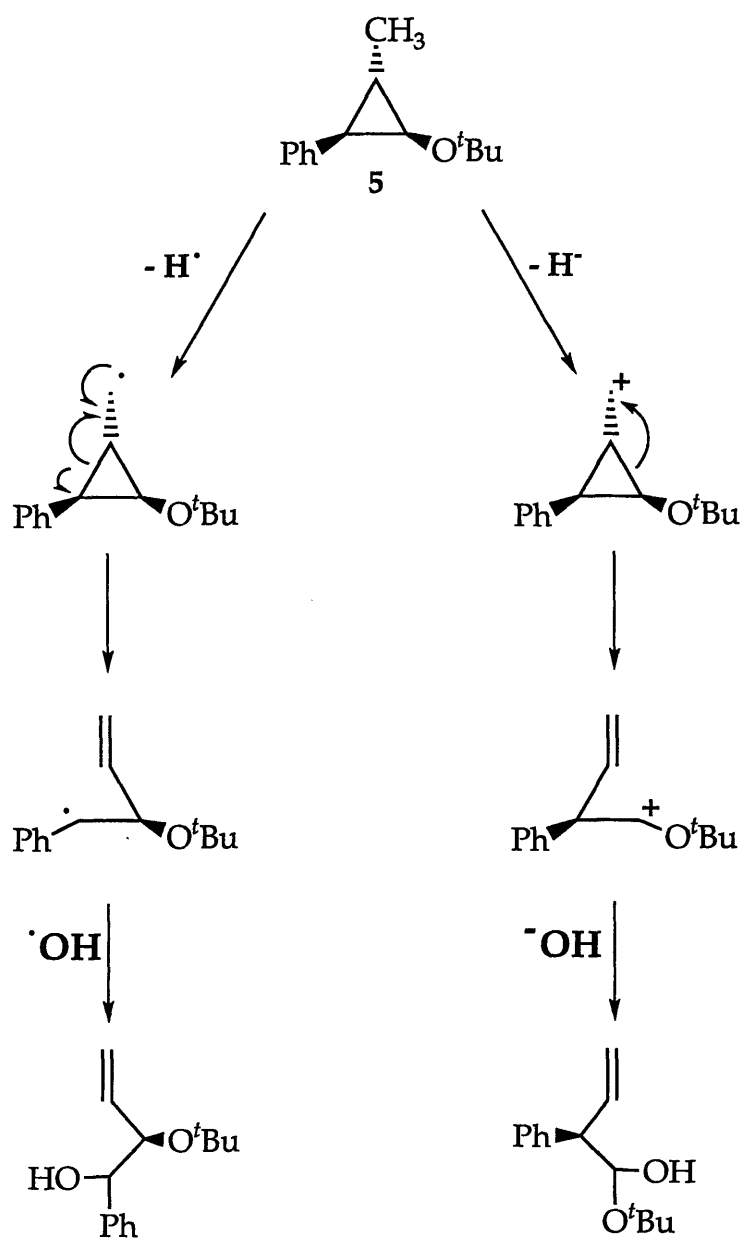


Figure 5.2. Ring opening of probe 5. This probe was designed to discriminate between radical and cationic intermediates.¹⁸

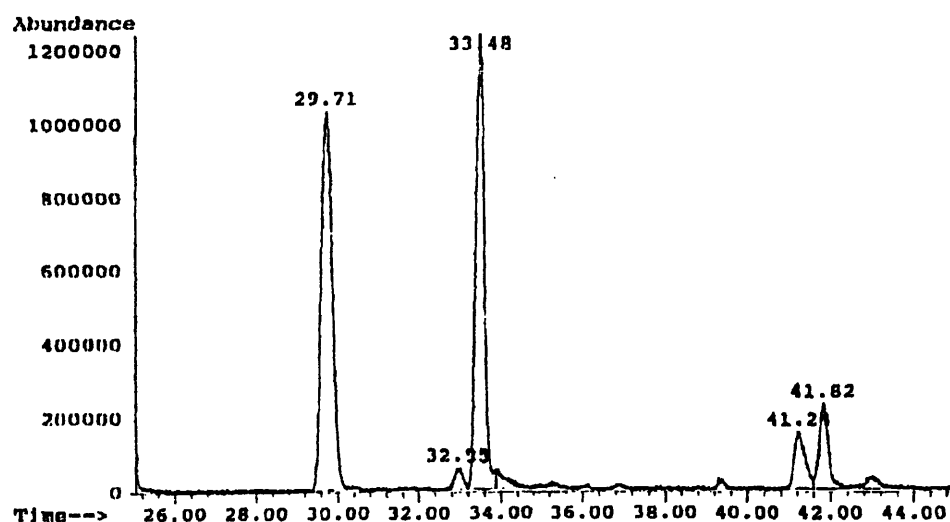


Figure 5.3. GC analysis of products from the hydroxylation of racemic **1** by a reconstituted sMMO system. Identities of the components were verified by MS. R_T (probe **1**) = 29.71 min, R_T (ethyl benzoate) = 33.48 min, R_T (**1a**) = 41.24 min, R_T (**1b**) = 41.82 min. Ethyl benzoate was used as an internal standard. The rearranged product has a retention time of 35.8 min and is not observed by using GC/MS. The feature at 32.95 min was identified as camphor, and it and all other impurities were present in control experiments in the absence of substrate.

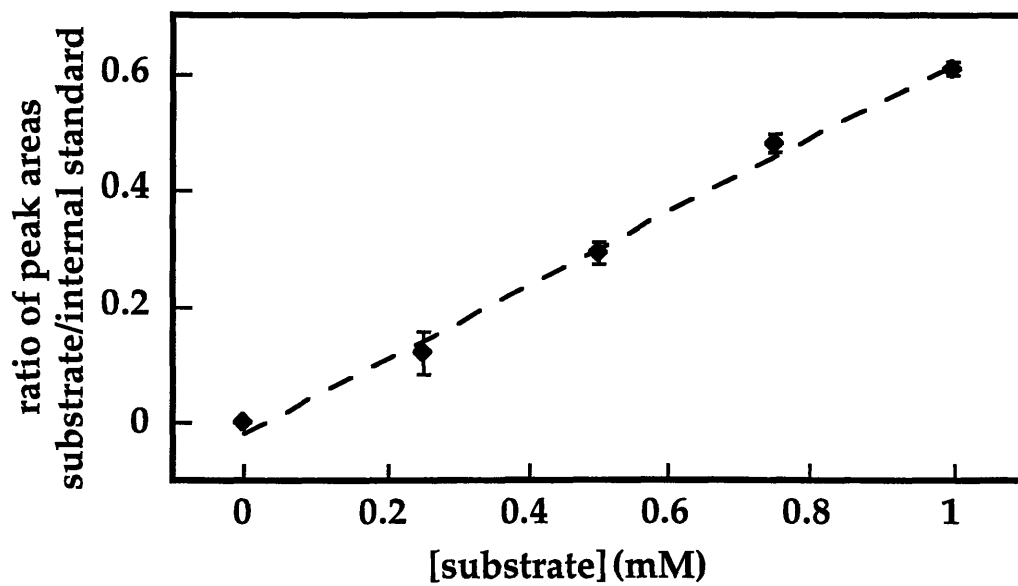


Figure 5.4. Calibration curve for racemic *trans*-1-phenyl-2-methyl-cyclopropane with reference to 1 mM ethylbenzoate as an internal standard. Error bars represent \pm one standard deviation for three measurements.

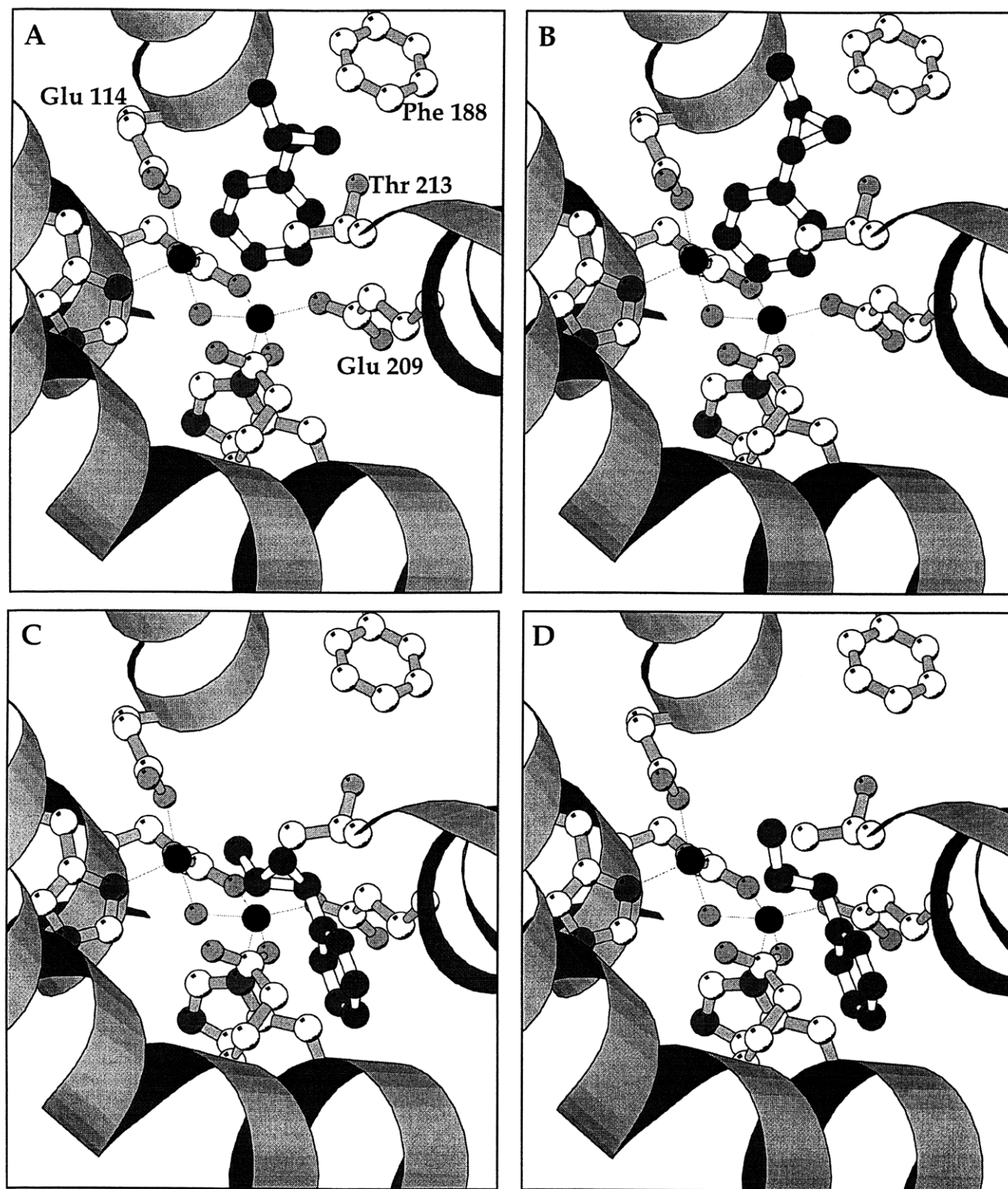


Figure 5.5. Binding of probe 1 in the MMOH active site with the phenyl ring (A, B) or the methyl group (C, D) pointing toward the presumed location of the activated oxygen species. (A) and (C) depict the (R,R) diastereomer, whereas (B) and (D) depict the (S,S) diastereomer.

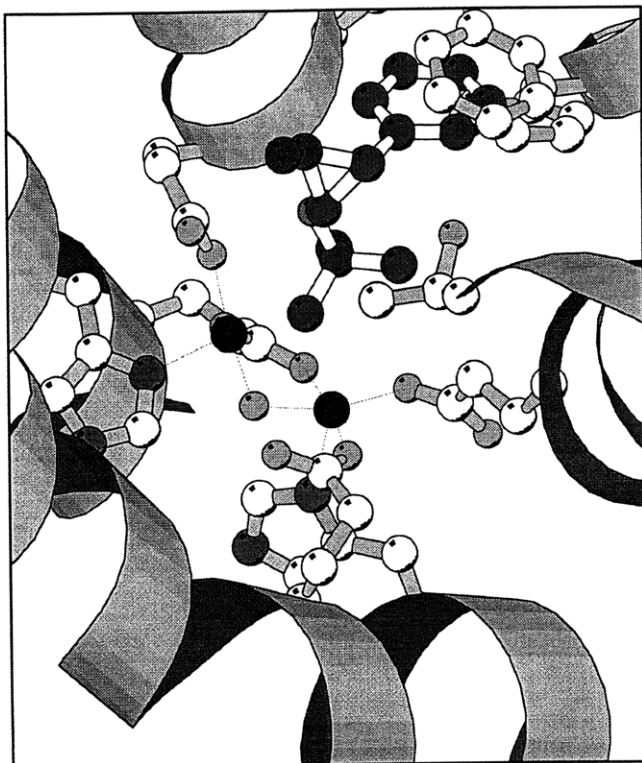


Figure 5.6. Binding of probe 5 in the MMOH active site.

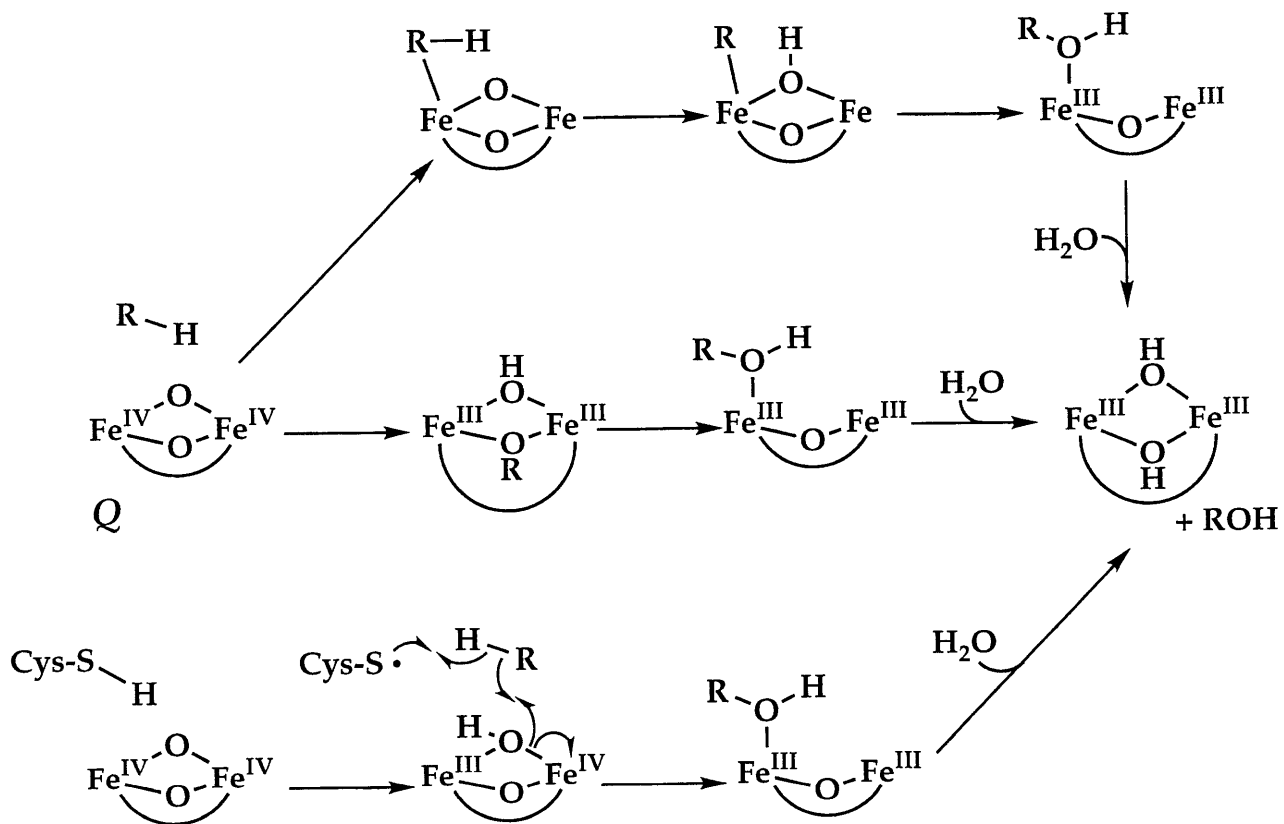


Figure 5.7. Possible mechanisms for the oxidation of substrates by sMMO.

Chapter Six:

**Tritiated Chiral Alkanes as Substrates for Soluble Methane
Monooxygenase from *Methylococcus capsulatus* (Bath):
Probes for the Mechanism of Hydroxylation**

Introduction^{1,2}

The methanotrophic bacteria *Methylococcus capsulatus* (Bath) and *Methylosinus trichosporium* OB3b rely on a methane monooxygenase (MMO) system to convert methane into methanol in the first step of their biosynthetic pathways.³⁻⁵ This reaction provides the organisms with their sole source of carbon and energy according to eq 1. MMO exists in both



particulate and soluble forms.⁶ The membrane-bound form contains copper and is active under normal growth conditions.⁷⁻⁹ When grown in media deficient in copper, methanotrophs express the soluble MMO system.^{10,11} Soluble MMOs from both *Methylococcus capsulatus* (Bath)¹² and *Methylosinus trichosporium* OB3b^{13,14} comprise three proteins, an iron-containing hydroxylase component (H) which binds the hydrocarbon substrate and dioxygen,¹⁰ a reductase (R) containing Fe₂S₂ and FAD cofactors which enable it to accept electrons from NADH and transfer them to the hydroxylase,^{12,15} and a regulatory or coupling component, protein B.^{16,17} In addition to methane, the sMMO system can oxidize a wide variety of substrates.¹⁸⁻²⁰

X-ray crystallographic studies of the resting, diferric form of the *M. capsulatus* (Bath) hydroxylase,^{21,22} EPR and ENDOR spectroscopy of the mixed-valent state,²³⁻²⁶ and other physical methods^{14,24} indicate that the hydroxylase active site contains a non-heme dinuclear iron center.²⁷ Crystal structures of the protein in several other forms provide clues about the nature of species formed during turnover.²⁸ In addition, the catalytic cycle has been explored by using freeze-quench and stopped-flow methodology, which

allowed intermediate species to be detected.^{17,29,30} The diferric resting center is reduced by the reductase to give a diferrous center, the structure of which in the absence of the other components is known.²⁸ This moiety binds dioxygen, forming a diiron(III) peroxo species, which then converts to the active oxidizing intermediate known as compound Q. Intermediates before the peroxo, and after Q, have been postulated but not directly observed for the *M. trichosporium* OB3b enzyme.^{31,32} One intermediate termed T, occurring after Q, has been observed only with the substrate nitrobenzene and has been assigned as protein-bound product.³³ The exact formulation of Q has not been elucidated, although it has been suggested to be a high valent iron-oxo species.^{4,5,34} The mechanism by which Q oxidizes substrate is also not known, and some facets of the mechanism have been postulated by analogy to cytochrome P-450.

The heme enzyme cytochrome P-450 displays similar reactivity to sMMO with the exception that it will not hydroxylate methane.³⁵ Cytochrome P-450 oxidations are thought to proceed through a high valent iron oxo, or ferryl, intermediate.³⁵⁻³⁸ This species is postulated to abstract a hydrogen atom from the hydrocarbon substrate, resulting in a substrate radical and an iron-coordinated hydroxyl radical. The hydroxyl radical and substrate radical recombine in a "rebound" reaction to afford the product alcohol, which dissociates from the active site leaving the resting state of the enzyme. Radical clock substrate probes which rearrange upon formation of a substrate radical provided early support for the presence of substrate radicals in the reaction cycle of cytochrome P-450.³⁹⁻⁴¹

Recently, some investigators have questioned the validity of the rebound model for cytochrome P-450. In one study employing a very fast radical clock substrate probe, the calculated radical rebound rate was too fast to be

rationalized on the basis of a discrete radical intermediate.⁴² In the same study, no correlation was observed between the ring opening rate of a range of probes and the amount of ring-opened products observed after oxidation of those probes by cytochrome P-450. Later work employing a probe designed to discriminate between radical and cation intermediates led to the proposal of a nonsynchronous concerted mechanism for the P-450 reaction.⁴³ A study of this enzyme activated by H₂O₂ concluded that an Fe(III) peroxo, not a ferryl, was responsible for hydroxylation of lauric acid.⁴⁴ Theoretical calculations indicate that a more likely scenario than radical rebound, at least for quadricyclane oxidation, might involve HO⁺ insertion into a C-C bond rather than radical rebound.⁴⁵

Radical clock substrate probe studies with sMMO isolated from *M. capsulatus* (Bath) afforded no evidence for the formation of substrate radicals.^{46,47} Based on the known rate constants for rearrangement of the various probes, a lower limit of 10¹³ s⁻¹ at 45 °C was estimated for a putative rebound reaction rate constant. For enzyme isolated from *M. trichosporium* OB3b, however, evidence for a substrate radical was detected in the form of 3 - 6% rearranged product alcohols.^{46,48} Based on the amount of rearrangement observed, a rate constant of 6 to 9 x 10¹² s⁻¹ at 30 °C was estimated for a putative rebound reaction for this enzyme.⁴⁶ In parallel work, information about the nature of possible intermediate substrate radicals was obtained by allowing sMMO from *M. trichosporium* OB3b to hydroxylate both (R)- and (S)-[1-²H₁,1-³H]ethane.⁴⁹ As illustrated in Figure 6.1, if the reaction were to proceed through a radical rebound mechanism, some inversion at the chiral carbon atom would be expected. In the figure, intermediate Q is depicted as a bis(oxo)iron(IV) or diferryl species, although this formulation is only one alternative.¹⁷ Following abstraction of a hydrogen atom from the chiral sub-

strate, an alkyl radical results. This substrate radical can rebound, forming the unrearranged product alcohol. Alternatively, because the carbon radical is planar, rotation about the C-C bond might occur prior to recombination, affording a product alcohol with the opposite configuration. The alcohol products were derivatized with a chiral acid, and tritium nuclear magnetic resonance (NMR) analysis of the resulting diastereomeric esters was used to quantify the amount of inversion that occurred during the hydroxylation reaction. For both (R)- and (S)-chiral ethane substrates, $\approx 65\%$ of the product alcohols retained their stereochemistry whereas $\approx 35\%$ were inverted.⁴⁹ Taking the energy barrier for rotation about the C-C bond to be 0.15 kcal/mol,^{50,51} we compute the rate constant for this process to be $4.9 \times 10^{12} \text{ sec}^{-1}$ at 30°C (eq 2). From the amount of retention of stereochemistry in the chiral alcohol products, a value of $3 \times 10^{12} \text{ s}^{-1}$ was calculated for the rebound reaction rate constant (eq 3). This value agrees well with that estimated from the radical clock work.⁴⁶

$$k_{\text{rotation}} = (kT/h)(\exp(-\Delta G^\ddagger/RT)) \quad (2)$$

$$k_{\text{rebound}} = k_{\text{rotation}}(\% \text{ retention}/\% \text{ inversion} - 1) \quad (3)$$

In view of the slight differences in reactivity toward radical clock substrate probes exhibited by sMMO from the different organisms, we were interested to determine how the *M. capsulatus* (Bath) enzyme would perform in the chiral ethane experiment.⁴⁹ Accordingly, the substrates (S)-[1-²H₁,1-³H]ethane, (R)-[1-²H₁,1-³H]ethane, (S)-[1-²H₁,1-³H]butane, (R)-[1-²H₁,1-³H]butane, (S)-[2-³H]butane and (R)-[2-³H]butane and racemic [2-³H]butane were hydroxylated with sMMO from *M. capsulatus* (Bath), the results and analysis of which are reported here.

Experimental

Bacterial Growth and Protein Purification. *Methylococcus capsulatus* (Bath) cells were grown as described previously.⁵² Hydroxylase and recombinant protein B were purified as reported elsewhere, and the iron content for hydroxylase and specific activities were in the usual ranges.^{24,46} In some reactions, an unresolved mixture of protein B, reductase and other cellular proteins (B/R mix) from the initial DEAE cellulose column (0.05 - 0.5 M NaCl fraction) was used with purified hydroxylase to reconstitute the enzymatic system.²⁰ In all other experiments, purified recombinant B^{24,46} and purified native reductase (vide infra) were employed.

Isolation of sMMO Reductase from Soluble Cell Extract. Protein purification procedures were performed at 4 °C or on ice. Cell lysis with a French pressure cell (American Instrument Co.) and the preparation of soluble cell extract were carried out as previously described⁴⁶ except for the buffer composition, which followed a published procedure.⁵³ Frozen cells (~100 g) were suspended in 200 mL of 25 mM N-morpholinopropane sulfonic acid (MOPS) buffer (pH 7.0) which contained 200 μ M of $\text{Fe}(\text{NH}_4)_2(\text{SO}_4)_2 \cdot 6\text{H}_2\text{O}$ and 2 mM cysteine (Buffer A), as well as 0.01 mg/mL of DNase 1 and 2 mM phenylmethylsulfonyl fluoride (PMSF). Buffers containing iron and cysteine were prepared just prior to use. After the cells were lysed, sodium thioglycolate (NaTG) was added to a final concentration of 8 mM, which was maintained in all subsequent steps of the reductase purification. The lysed cells were centrifuged in a Beckman L-70 ultracentrifuge at 32,000 x g for 10 min. The supernatant was centrifuged at 90,000 x g for 1 h. An additional 10 min centrifugation (90,000 x g) of the supernatant removed residual particles, allowing the supernatant to be filtered with a 0.2 μ m syringe filter. The soluble cell-free extract was diluted with an equal volume of buffer A and the sMMO protein

components were separated on a DEAE Sepharose fast flow (Pharmacia LKB Biotechnology Inc.) column which was packed (5.0 x 22 cm) and equilibrated in buffer A by using a Pharmacia FPLC chromatographic system. All buffers were filtered and degassed prior to use. The sample was loaded at approximately 4 mL/min by using an in-line peristaltic pump. The loaded sample was washed at the same flow rate with 800 mL of buffer A. An eight column volume gradient of 0 to 0.4 M NaCl in buffer A was employed to elute bound protein. The flow rate applied during the salt gradient was 3.5 mL/min. Native polyacrylamide gel electrophoresis (PAGE) and SDS-PAGE analysis were used to evaluate the protein fractions.

Fractions which contained protein of the correct molecular weight according to SDS-PAGE analysis, and which reduced dichlorophenol indophenol at a rate which was greater than 30% of the most active fraction,⁵⁴ were pooled as crude reductase protein. The crude reductase sample was diluted with an equal volume of 20 mM Tris (pH 7.1) with 8 mM NaTG (Tris buffer) and 50 mM NaCl, and was loaded at a flow rate of 3 mL/min on a DEAE Sepharose CL-6B column (2.6 x 8.0 cm). The loaded sample was washed with 2.8 column volumes of Tris buffer with 100 mM NaCl. The bound protein was eluted with a 10 column volume gradient of Tris buffer from 100 mM to 500 mM NaCl. Fractions from DEAE Sepharose CL-6B chromatography were pooled which had an $A_{458\text{nm}}/A_{340\text{nm}}$ ratio of greater than 1.0. The pooled material was applied to a 5'AMP Sepharose 4B affinity (Pharmacia) column (2.5 x 11 cm). The affinity column had been regenerated and equilibrated in Tris buffer, 50 mM NaCl.

The loaded sample was washed with 1.3 column volumes of Tris buffer, 95 mM NaCl. This wash eluted nonadsorbed proteins from the column. One column volume of Tris buffer, 410 mM NaCl followed by a 3 col-

umn volume rinse of Tris buffer, 50 mM NaCl eluted nonspecifically bound protein. Reductase fractions were eluted with Tris buffer and 50 mM NaCl containing 1.4 mM ethanol-free NADH. SDS-PAGE analysis was performed to confirm the absence of any contaminating protein in the purified reductase. The NADH was removed from purified reductase by concentrating the sample to ~10% of the original volume with an Amicon concentrating cell equipped with an ultrafiltration PM30 membrane, which was run under 30 psi of N₂ pressure. The reductase was rediluted in Tris buffer containing 50 mM NaCl and reconcentrated. This procedure was repeated until no NADH was detected spectrophotometrically in the eluate. A typical yield of 20-30 mg of purified reductase was obtained from 100 g of cell paste, and specific activities were in the range of 1200-1600 mU/mg under the conditions necessary to generate a high product concentration (vide infra). In a standard propylene assay, activities ranged from 3500 - 3800 mU/mg.^{24,46}

Determination of Conditions for Oxidizing Labeled Alkanes.

Preliminary assays with unlabeled ethane, butane, and propylene were carried out to determine conditions which afforded 1 to 2 μ mol of product alcohol. Hydroxylase was concentrated to \approx 300 μ M and incubated with the B/R mixture or the purified components in varying ratios in a 5 mL reaction flask capped with a septum. The total volume was adjusted to 400 μ L with 25 mM MOPS, pH 7.0 buffer. A syringe was inserted through the septum and 2 mL of the head space gas was removed and replaced with 2 mL of the substrate gas. The mixture was incubated for 30 s at 45 °C in a shaking incubator, after which time 100 μ L of a 0.1 M ethanol-free solution of NADH was added to initiate the reaction. The flask was returned to the incubator and the reaction was allowed to proceed for 5 min. A 5 μ L portion of the solution was injected into a gas chromatograph equipped with a Porapak Q column to quantitate

the alcohol product present in the reaction solution.⁴⁶ The area of the product peak was compared to a calibration curve of alcohol peak area versus the concentration of sample injected. Conditions which afforded at least 1 μmol of alcohol product per 1 mL of reaction volume were subsequently employed at the National Tritium Labeling Facility. Typically 50-80 nmol each of H and B and 42-68 nmol of R were employed. Under these conditions, the specific activity calculated for the hydroxylase is low, ≈ 40 mU/mg, owing to product inhibition.

Reagent Synthesis. Chiral tritiated alkanes were prepared, the stereochemistry was verified, and the product alcohols were derivatized and analyzed by Dr. Barrie Wilkinson of Washington University. Details appear elsewhere² and a summary of the synthetic strategy is included in the Results section.

Enzymatic Reactions. A round bottom flask equipped with a stopcock, sidearm, and septum was fitted to the reaction apparatus² and evacuated. Buffer (25 mM MOPS, pH 7.0, 100 to 500 μL) was added through a septum and cooled to -78 °C. Substrate gas was transferred to the flask from a charcoal bed by opening both stopcocks and bringing the charcoal bed to room temperature by warming with hot air. After 60 s the stopcocks were closed and the buffer was brought to room temperature. The protein solution was added through the septum. A quantity of NADH (50 or 100 μL of a 0.1 M solution) was also added. Pure O_2 gas (1 mL) was added by syringe through the septum and the mixture was incubated at 45 ± 2 °C with constant stirring for 30 min. Cooling the flask to -78 °C terminated the reaction. Excess substrate gas was transferred from the reaction flask back to the charcoal bed. Transfer was allowed to proceed for 60 s and then the stopcocks were closed. A 10 μL aliquot of the expected product alcohol (unlabeled) was added to the reaction flask to act as a

carrier in subsequent manipulations. This flask was removed from the apparatus and transferred to a vacuum line where the volatile reaction products were collected by lyophilization.

Oxidation of C₂D₆. Perdeuteroethane (Cambridge Isotope Labs, 99%) was oxidized by a reconstituted sMMO system as reported above for unlabeled substrates except that the incubation time was 30 min. The product alcohol was isolated from the aqueous reaction mixture by extraction with 1 mL of methylene chloride and the extract was dried over MgSO₄. A 1 μL aliquot of distilled pyridine and 1 μL benzoyl chloride were added. The esterification reaction was allowed to proceed for 1 h at room temperature and the mixture was analyzed by gas chromatography with mass spectrometric detection (GC/MS) on a Hewlett-Packard 5890A gas chromatograph equipped with a Hewlett Packard 5971A mass spectrometer. An HP-1 (methyl silicone gum) column (50 m x 0.2 mm x 0.5 μm film thickness) was employed for the separation.

Exchange Reactions. A 2 μL sample of CD₃CD₂OH or CH₃CD₂OH (Cambridge Isotope Labs, 99%) was added to 0.9 mL of B/R mix, a reconstituted system consisting only of purified H, B, and R components, or to buffer (25 mM MOPS, pH 7). A 100 μL portion of 0.1 M NADH was added. In some experiments, 1 μL of 0.1 M NAD⁺ was also added. The mixture was incubated at 45 °C with shaking for 30 min. The ethanol was isolated as described above and analyzed by GC/MS.

Results

Synthesis of Chiral Tritiated Alkanes. The method for preparing chiral tritiated alkanes applied known and unambiguous chemistry developed for the synthesis of chiral methyl tritiated acetates in high yield, activity, and

enantiomeric purity. [1- $^2\text{H}_1$]Acetaldehyde was reduced to (S)- or (R)-[1- $^2\text{H}_1$]ethanol by (R)- or (S)-Alpine Borane,[®] respectively. The ethanols were isolated by distillation and converted to their tosylates by treatment with tosyl chloride in pyridine. An aliquot was also converted to the (R)-O-acetyl mandelic acid ester derivative in the presence of DCC-DMAP. ^2H NMR analysis of the products demonstrated that the alcohols had been synthesized in $88 \pm 4\%$ ee. Experiments with standard materials were carried out to assure that the C-1 center in the alcohol does not racemize when this reaction is carried out below $-10\text{ }^\circ\text{C}$.⁵⁵ Treatment of the ethyl tosylates with (R)-O-acetyl mandelic acid and K_2CO_3 in DMF converted them to their mandelate derivatives with inversion at C-1. ^2H NMR experiments again demonstrated that the ethanols had been prepared in $88 \pm 4\%$ ee and confirmed the stereochemical fidelity of the derivatization procedure. For the final generation of chiral tritiated ethane, the tosylate group was converted to tritide by using the reagent $\text{LiEt}_3\text{B}^3\text{H}$ at maximum specific activity.⁵⁶ This reaction proceeds via a direct $\text{S}_\text{N}2$ displacement, affording ethane of unambiguous stereochemistry.

Primary tritiated butanes were generated in a similar manner. The [1- $^2\text{H}_1$]butyraldehyde was prepared by LiAl^2H_4 (>98 atom % ^2H) treatment of methyl butyrate to produce [1- $^2\text{H}_2$]butanol, which was converted to the aldehyde by treatment with $\text{K}_2\text{Cr}_2\text{O}_7$ in H_2SO_4 . This method takes advantage of the primary KIE for this process, yielding product with enriched deuterium content. No [1- $^1\text{H}_2$]butanol species were formed, as verified by ^{13}C NMR spectroscopy. Butanes carrying tritium in the secondary position were prepared initially from (S)- and (R)-2-butanol of $>99\%$ ee.

Analysis of Lyophilizates. For each alkane enantiomer, hydroxylation can take place either at the hydrogen atom or deuterium atom of the chiral carbon, at the tritium atom, or at an unlabeled carbon. Products that arise

from hydroxylation of the C-T bond are not detected because ^3H NMR spectroscopy is the analytical method. Intramolecular kinetic isotope effects, $k_{\text{H}}/k_{\text{D}}$, were calculated from the relative amounts of C-H versus C-D hydroxylation products. The ^3H NMR data also afforded information about the distribution of hydroxylation at each carbon atom of the substrate. These ratios of products, C2/C1 and C4/C1, for ethane and butane respectively, were also determined. In alkanes labeled at the primary position, the tritiated carbon is designated as C1. In the butanes labeled at a secondary carbon, that carbon is referred to as C2.

The possible alcohol products of the reaction of (S)-[1- $^2\text{H}_1$,1- ^3H]ethane with sMMO are depicted in Figure 6.2, and the observed ^3H NMR spectra are given in Figure 6.3. The ^3H NMR spectrum of the reaction products in Figure 6.3A contains four major resonances at $\delta = 1.19$ (s), $\delta = 3.65$ (s), $\delta = 3.67$ (s), and $\delta = 4.84$ (s) ppm. The resonance at $\delta = 4.84$ ppm was assigned to ^3HHO , and the singlet at $\delta = 1.19$ ppm to the product of oxidation occurring at the unlabeled carbon atom. The inset in Figure 6.3 shows an expansion of the two signals at $\delta = 3.65$ and 3.67 ppm. The narrower, more downfield resonance is attributed to the products of oxidation at the C-D bond (RCHTOH products, where R = CH_3), whereas the broader, more upfield signal is assigned as arising from oxidation at the C-H bond (RCDTOH products). The splitting of the latter signal is due to coupling to the deuterium atom present in the molecule. A kinetic isotope effect can be calculated from the ratio of alcohol products for hydroxylation of the C-H bond versus products hydroxylated at the C-D bond. The sum of the areas of these two peaks can be compared to the area at $\delta = 1.19$ ppm to obtain information about the relative hydroxylation rates at the two different carbon atoms. This value may reflect the relative reactivities of the C-H versus C-D bonds under the assumption that, once bound to the active

site, ethane is free to rotate and present either of its carbon atoms to the active hydroxylating species. Reaction at the tritium atom will not be revealed in the ^3H NMR spectrum, but is expected to be much slower. These experiments were carried out under V_{max} conditions, in which a saturating amount of substrate was added to the enzyme, conditions which could lead to an artificially low estimate of intermolecular isotope effects.

The ^3H NMR spectrum of the alcohol products formed by hydroxylation of (S)-[1- $^2\text{H}_1$,1- ^3H]butane with sMMO is given in Figure 6.4A. The downfield singlet again corresponds to tritiated water. The peaks at $\delta = 3.6$ ppm arise from hydroxylation at the labeled carbon atom. The far upfield peaks correspond to hydroxylation at C2, C3, and C4. Oxidation of (S)-[2- ^3H]butane by H + B/R mix leads to the product spectrum in Figure 6.5A. Tritiated water appears far downfield. The signal at $\delta = 3.8$ ppm arises from hydroxylation at the labeled carbon ($\text{CH}_3\text{CT}(\text{OH})\text{CH}_2\text{CH}_3$). The inset in Figure 6.5A shows the remaining alcohol products. The resonance at $\delta = 1.54$ ppm arises from hydroxylation at the primary carbon next to the tritium label ($\text{CH}_2(\text{OH})\text{CHTCH}_2\text{CH}_3$). The two signals at $\delta = 1.47$ ppm correspond to the diastereomeric products formed from hydroxylation at the unlabeled secondary carbon. The farthest upfield resonance is due to hydroxylation of the primary carbon more distant from the tritium label.

Analysis of Derivatives. Conversion of the ethanol products⁵⁷ to their ethyl mandelates can afford five ^3H NMR resonances, two sets arising from diastereomers and one from another product. These signals are shown in Figure 6.3B. The products arising from stereochemical inversion of (S)-ethane are labeled 2m and 4m, those with retention are labeled 1m and 3m. The peaks correspond to mandelates of the alcohols with the same number designations in Figure 6.2. The loss of stereochemistry was calculated by adding the

areas of peaks 2m and 4m and dividing by the combined areas of all four peaks. The value determined was corrected for the %ee of the substrate, $88 \pm 2\%$ for ethanes, 95% for primary labeled butanes, and 99% for butanes labeled at the 2° carbon.⁵⁸ The corrected percent inversion is given by eq 4, where x is the true fraction which has undergone inversion, e is the percent of the major substrate enantiomer, f is the observed percent of products displaying retention, and ee is the percent enantiomeric excess of the substrate (e minus the percent of the minor substrate enantiomer).

$$x = (e - f)/ee \quad (4)$$

The ³H NMR spectrum of the mandelate derivatives of the hydroxylation products of (S)-[1-²H₁,1-³H]butane are given in Figures 6.4B (whole spectrum) and inset (expanded version). The mandelates of the diastereomeric esters have ³H NMR signals at $\delta = 3.8-3.9$ which were analyzed analogously to the ethane products above. The ³H spectrum of the mandelate derivatives of alcohols formed with (S)-[2-³H]butane is given in Figure 6.5B. The signal at $\delta = 4.82$ ppm comes from the mandelate of (R)-2-butanol, which indicates retention of stereochemistry. The $\delta = 4.86$ ppm peak is indicative of inversion to form (S)-2-butanol. Table 6.1 summarizes the results for ethane hydroxylations and Table 6.2 reports results for oxidations of (R) and (S)-[1-²H₁,1-³H]butane, both by purified components. Tables 6.3 and 6.4 tabulate the results of oxidations of the same substrates by MMOH and a B/R mixture. Table 6.5 lists the findings for butane substrates labeled at the C2 position.

Oxidation by Purified Components. Hydroxylations of chiral ethane took place with an intramolecular k_H/k_D ratio of 3.4 ± 0.4 and a C2/C1 ratio, reflecting relative hydroxylation rates at the unlabeled versus the labeled car-

bon atom, of 3.3:1. The ethanol products displayed 72% retention of stereochemistry. For butanes labeled at the primary position, smaller intramolecular isotope effects were observed, together with a slightly higher ratio of hydroxylation at the unlabeled primary carbon to the one bearing the tritium atom. The amount of retention of stereochemistry was slightly larger for these alcohols than for the ethanes. The differences between results from oxidations of the (R)- and (S)- enantiomers of each substrate were within experimental error.

Oxidation by Hydroxylase and B/R Mix. When H and a mixture of B and R which contained other cellular proteins were used to hydroxylate the chiral alkanes, very low or even inverse (<1) intramolecular kinetic isotope effects were observed. This phenomenon was determined to occur not because the protein preferentially oxidized the C-D over the C-H bond, but because the product distributions were disturbed by a second enzymatic process which was acting on, and even interconverting, the product alcohols. Several factors were diagnostic of this secondary process. In multiple trials, the results were more variable than when purified proteins were used. A sign that the product distributions from H + B/R mix suffered from a process that masked their true values was that the amount of retention of stereochemistry in products arising from oxidation of the C-H bond was not the same as the amount of retention in products from oxidation of the C-D bond (*vide infra*).

Retention of stereochemistry was primarily seen with both (R)-[2- ^3H]butane and (S)-[2- ^3H]butane (Table 6.5). Products obtained from a racemic mixture of (R)-[2- ^3H]butane and (S)-[2- ^3H]butane showed only a slight preference for hydroxylation of one enantiomer over the other (Table 6.5). The product ratios were 1 : 1.3.

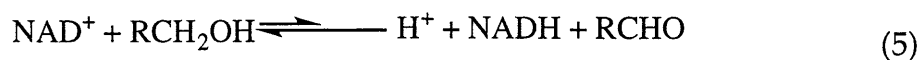
Oxidations of C₂D₆ and Exchange Reactions. In order for an exchange reaction of hydrogen atoms at the α carbon atom to explain the anomalous results obtained with H + B/R mix, the process would have to be stereoselective and reversible, properties characteristic of an enzymatic reaction. The possibility that such an exchange could occur was tested by oxidizing C₂D₆ both with H + B/R mix and with purified component proteins. When the latter were used, less than 2% of the ethanol was detected by GC/MS to be CD₃CDHOH, the rest being CD₃CD₂OH. Oxidation with H + B/R mix resulted in ~12-13% CD₃CDHOH in the product mixture. The exchange reaction is thus independent of the hydroxylation reaction. Incubation of CD₃CD₂OH in a solution containing cellular extract, NAD⁺, and NADH resulted in as much as 25% exchange of deuterons for protons at the α carbon. Much less exchange (~5%) was observed when NAD⁺ was not added, and the presence or absence of hydroxylase did not affect the amount of exchange.

Discussion

The present results indicate that hydroxylation of both chiral ethane and butane substrates by sMMO from *M. capsulatus* (Bath) affords products which retain their stereochemistry to a large degree (71-96%). These data, together with other results in the literature, can be explained by a simple unifying mechanism for the hydroxylation step, as described in the following analysis.

Differences Between H + B/R Mix and Purified Protein Components. A comparison of the results summarized in Tables 6.1 and 6.2 with those obtained by using crude cell extracts (Tables 6.3 and 6.4) clearly indicates the disparity between oxidations performed using purified sMMO component proteins versus partially purified cellular extracts. Control oxidations of C₂D₆

by these two systems as well as the C-H/C-D exchange reactions observed with C_2D_5OH support the hypothesis that a cellular protein other than sMMO hydroxylase catalyzes exchange of the hydrogen atoms at the α carbon of the product alcohol. One likely such enzyme is an alcohol dehydrogenase (ADH), which catalyzes the reaction given in eq 5.



Much is known about microbial ADHs, which have multiple isozymes in many organisms.⁵⁹ One major class of ADHs is NAD(P)-dependent, and all act reversibly to interconvert alcohol and aldehyde. Under the experimental conditions described here, the large excess of NADH would drive the reaction to favor the alcohol, but a portion of the alcohol produced in the sMMO reaction might be oxidized by NAD^+ formed during the hydroxylation of substrate. Alcohol dehydrogenases are highly stereospecific.^{60,61} Over the time course of the experiment, and depending on the alcohol being oxidized, this property can effect several transformations, as illustrated in Figure 6.6A. In this figure are traced the fate of products from oxidation of (R)-ethane, the substrate for which the most anomalous results were obtained when using H + B/R mix. The product distribution shown was calculated by assuming an intramolecular k_H/k_D isotope effect of 3 and 72% retention of stereochemistry, approximately the values obtained for the oxidation by purified components. This distribution is then perturbed by an ADH reaction which removes the pro-R hydrogen atom, protium, deuterium, or tritium, replacing it with a proton. Half of product A is converted to product D. Half of product B is lost to tritium "washout" and the product is not detected by 3H NMR. Half of product C is lost to washout. Finally, exchange of the pro-R hydrogen in D

leaves the molecule unaltered and, because of a significant amount of A conversion to D, a very large amount of D is detected. Kinetic isotope effects on the exchange might further complicate this picture, but the foregoing scenario is presented to show how such a process would explain the otherwise confusing resulting product distribution (Table 6.3).

One telling sign that such a process was occurring was the fact that different amounts of retention of stereochemistry were observed in the alcohols resulting from oxidation at the C-H bond versus the C-D bond (Table 6.3). In the scenario of Figure 6.6A, products A and B reflect 70% retention of stereochemistry, but C and D together show 79% *inversion* after exchange. It should be noted that, in the absence of an isotope effect on the exchange reaction, the ratio of the amount of product A to the total of A and B yields the true amount of retention of stereochemistry. Whereas differences in the amount of retention in H,T and D,T products were observed for all oxidations, they were within experimental error for the oxidations carried out using purified proteins. Finally, additional evidence for the exchange phenomenon was the large amount of tritiated water formed in many of the oxidations employing H + B/R mix. This water presumably arose from the tritium washed out of the product alcohols.

Alkanes are Not Highly Constricted in the Active Site Prior to Hydroxylation. The reaction products obtained with racemic [2-³H]butane indicate clearly that the active site does not rigidly constrain the substrate, since there was only a slight discrimination between the two enantiomers of this probe. The exchange reaction described above would not affect secondary alcohols. An extremely crowded active site would most likely readily distinguish between an ethyl and a methyl substituent at the reacting carbon atom.

Kinetic Isotope Effects. When chiral alkanes were hydroxylated by the sMMO system reconstituted from the purified components, intramolecular isotope effects in the range of 3-4 were determined, values similar to those obtained with other substrates.⁴⁶ Intramolecular kinetic isotope effects of ≈ 4 with these chiral substrates are similarly observed with sMMO from *M. trichosporium* OB3b.⁴⁹ In the radical clock experiments with *M. capsulatus* (Bath), an intramolecular isotope effect of ≈ 5 was interpreted as indicating that substantial C-H bond breakage is involved in the hydroxylation step.⁴⁶ With cytochrome P-450 hydroxylations, k_H/k_D values of 7 to 10 have been reported.³⁵ Such an isotope effect is expected to be ≥ 1 , the precise value depending on the linearity of the O \cdots H-C unit in the transition state⁶² and on whether the transition state is early or late.⁶³

The C2:C1 hydroxylation ratio depends upon the magnitude of the intramolecular kinetic isotope effect at C1, referred to as k_H/k_D , assuming that the hydroxylating species has equal access to hydrogen atoms on both the C1 and C2 positions of chiral ethane. In other words, ethane rotation would occur in the active site, rendering both ends of the molecule accessible to the active hydroxylating species. The ratio of C2/C1 products would thus reflect the relative ability to hydroxylate C-H versus C-D bonds, statistically corrected for the numbers of such bonds. From the observed k_H/k_D ratios for the chiral ethanes, 3.8 and 3.0 (Table 6.1), we compute a C2:C1 ratios of 2.38 and 2.25, respectively, smaller than the observed values of 3.3 and 3.4. This difference might reflect secondary kinetic isotope effects or some other factor not yet identified.

Calculation of an Apparent Rebound Rate Constant. The use of many calibrated radical probes has led to several varying values for the rate of the consensus oxygen rebound mechanism in C-H bond functionalization pro-

cesses. For chiral ethane probes, the known barrier to rotation for an ethyl radical can be used to calibrate the probe at different temperatures. These data can be applied to the ratio of retention and inversion to yield an apparent rebound rate constant. No racemization occurs in the derivatization of the alcohols when the reaction takes place below $-10\text{ }^{\circ}\text{C}$.⁵⁵

Equation 2 yields a calculated value of $k_{\text{rotation}} = 1 \times 10^{13}\text{ sec}^{-1}$ at $45\text{ }^{\circ}\text{C}$ for the ethyl radical. Therefore, when we include the data for our %retention/%inversion in equation 3, we calculate that any radical capture process must occur at approximately $k_{\text{rebound}} = 1 \times 10^{13}\text{ sec}^{-1}$. This value indicates that the process is occurring on a time scale approaching that of a single bond vibration. Such an interpretation appears impossible, however, if it corresponds to the lifetime of a discrete intermediate species. We can calculate the maximum rate for any process of this type, in which $\Delta G^{\ddagger} = 0$, i.e., the decomposition of a transition state, to be $6.3 \times 10^{12}\text{ s}^{-1}$ at 318 K. This result leads us to conclude either that our approach to calculating the rebound rate is not a good approximation as believed, or that the present consensus oxygen rebound mechanism for C-H bond functionalization is insufficient to account for hydroxylation of ethane by sMMO.

Comparisons with Literature. Very similar stereochemical results were obtained when chiral alkane was converted to product alcohols with sMMO from *M. trichosporium* OB3b.⁴⁹ The products consistently had $\approx 2:1$ retention versus inversion of stereochemistry observed for both substrate enantiomers and for both ethane and butane substrates.^{49,64} With sMMO from *M. capsulatus* (Bath), greater retention of configuration was observed and at a higher temperature, where the putative ethyl radical would rotate even more rapidly. The hydroxylase proteins from the two organisms are very similar in amino acid sequence and structure, the main differences between the two sys-

tems apparently being the rates of formation and decay of intermediates in the reaction cycle, *M. trichosporium* OB3b being the faster of the two.^{17,33} Our work with the radical clock substrate probes implied a putative rebound rate constant $> 10^{13} \text{ s}^{-1}$ for sMMO from *M. capsulatus* (Bath) and $3 - 6 \times 10^{12} \text{ s}^{-1}$ for sMMO from *M. trichosporium* OB3b,⁴⁶ and the results have been interpreted in terms of a nonsynchronous radical-like mechanism,⁴⁷ which is further elaborated below. Because some of the experiments with the *M. trichosporium* OB3b enzyme were carried out with identical batches of substrates reported here, it is unlikely that the different results are due to variations in the substrates or analytical procedures. When the copper-containing particulate MMO was studied by using the same methodology, hydroxylation was found to proceed with complete retention of configuration at the chiral atom.⁶⁵

An extremely large intermolecular isotope effect (50 - 100) has recently been reported for the decay of the oxidizing intermediate Q in the presence of CD₄ versus CH₄ for hydroxylase from *M. trichosporium* OB3b.³² This very large isotope effect was accompanied by intermolecular isotope effects in product distributions of ~20 and intramolecular isotope effects of 4-13. The results were interpreted as signifying that, following hydrogen atom abstraction as depicted in Figure 6.1, the methyl radical reabstracts the protium or deuterium from the iron-bound hydroxyl group, regenerating a different form of the original high-valent intermediate. If the abstraction but not the radical recombination step displays a large isotope effect, this pathway might account for the discrepancy between kinetic isotope effects for reactivity of the intermediate Q towards these substrates versus the resulting product alcohols. No evidence was presented that such a complicated process exists when ethane or butane is used as substrate, and the implications of such a process on the chiral ethane results were not addressed. A mechanism involving the

Cys151 residue might also explain the very large isotope effect.²⁷ In the absence of a fourth isotope of hydrogen, chiral ethanes are the closest analogs to methane for which absolute stereochemistry can be determined.

Mechanistic Implications. We now inquire what, given the foregoing analysis, the experimental results would indicate if the hydroxylation step were to occur with complete retention, with racemization, or with complete inversion of stereochemistry. None of the manipulations, including the derivatization procedures, scrambles the stereochemistry.⁵⁵ In hydroxylations of chiral ethane by pMMO,⁶⁵ the products were treated by the same methodology and 100% retention of configuration was observed, providing evidence against scrambling during the workup. Total inversion of stereochemistry would suggest a concerted reaction mechanism in which the C-O bond was formed on the face opposite to the C-H bond being broken, inverting the remaining three C-X bonds (where X = C or H). Total retention would indicate that the hydroxylation proceeds in a concerted manner with formal oxygen atom insertion into a C-H bond or occurs in two successive steps: C-O or C-metal bond formation at the alkyl carbon atom followed by C-H bond cleavage or reductive elimination. Racemization at the chiral carbon atom would be indicative of a process involving a radical which had sufficient time to rotate freely before the relatively slow recombination. Branched pathways would complicate any of these interpretations.

Given the above analysis, it is necessary to delineate a mechanism for sMMO hydroxylation of small alkanes in such a manner as to produce predominant, but not complete, retention of stereochemistry at the oxidized center. It is possible that there exists some radical or possibly carbocation character in the substrate during the hydroxylation step which inverts to a limited degree. This scenario might be interpreted in several ways. There could be

parallel reaction pathways, one involving a substrate radical (as in Figure 6.1) and one, or more, not (as in Figure 6.7). The degree to which a radical versus non-radical mechanism is followed may be determined by how snugly the substrate fits into the active site. Parallel mechanistic pathways have similarly been invoked in porphyrin model systems to explain the stereochemical consequences of hydroxylation chemistry depending on steric interactions of the substrate with the catalyst.⁶⁶⁻⁶⁸ Alternatively, abstraction of a hydrogen atom to form a substrate radical might occur in every reaction. The rate constant for the rebound reaction may be so large that only a small quantity of the substrate radical has sufficient lifetime for rotation about the C-C bond to occur before recombination with the bound hydroxyl group. Results with radical clock substrate probes were consistent with either no substrate radical formation or an extremely fast rebound step having a rate constant on the order of 10^{13} s^{-1} , too large really for formation of a discrete radical intermediate.

One proposal for the mechanism by which the oxidizing intermediate in sMMO reacts with substrate is depicted in the upper pathway of Figure 6.7. This scheme should result in complete retention of stereochemistry at the chiral carbon and is therefore not supported by the current results as the only mechanism at work.

Another explanation, perhaps the most satisfactory one, for the observed product distributions is that the reaction proceeds through a nonsynchronous concerted mechanism,^{43,47} as presented in the lower part of Figure 6.7. In this representation, intermediate Q is depicted as a diiron(IV) dioxo species, although other formulations are possible. The hydrocarbon substrate is doubly activated by two iron-bound oxo groups, either one of which could evolve into the hydroxyl group of the product alcohol. In this scenario, O-H bond formation, C-H bond breaking, and C-O bond formation occur in a con-

certed but not totally synchronous manner. For the pathway shown on the upper arrow, preferential C-O bond formation at the oxygen atom that takes the hydrogen would lead to predominant (1+2) retention of stereochemistry at the labeled carbon. As shown on the bottom arrow, C-O bond formation at the other oxygen atom would invert the stereochemistry (1+3). Formation of a pentavalent transition state and pseudorotation could also cause inversion [bottom arrow, 1 + (2 or 3) + 4]. This mechanism is consistent with the observed kinetic isotope effects and explains the lack of ring-opened products in the radical clock studies, since a free substrate radical is never formed. It also explains the greater retention of stereochemistry for the C2 chiral butane hydroxylation; steric bulk limits back-side attack and inversion of stereochemistry and it would also retard pseudorotation. Oxidation of primary carbons preferentially over secondary over tertiary ones, the opposite trend to that expected for a radical reaction, is also explained by this mechanism, because a primary carbon atom would have the least steric restrictions to formation of such a highly ordered transition state. In the absence of direct observation of substrate intermediates, diagnostic substrates such as the tritiated chiral alkanes described here offer the most information thus far about the characteristics of the transition state.

References

- (1) This work was already published in a slightly different form. See reference 2.
- (2) Valentine, A. M.; Wilkinson, B.; Liu, K. E.; Komar-Panicucci, S.; Priestley, N. D.; Williams, P. G.; Morimoto, H.; Floss, H. G.; Lippard, S. J. *J. Am. Chem. Soc.* **1997**, *119*, 1818-1827.
- (3) Anthony, C. *The Biochemistry of Methylotrophs*; Academic Press: New York, 1982, p 296-379.
- (4) Liu, K. E.; Lippard, S. J. In *Advances in Inorganic Chemistry*; Sykes, A. G., Eds.; Academic Press: San Diego, 1995; Vol. 42; pp 263-289.
- (5) Lipscomb, J. D. *Annu. Rev. Microbiol.* **1994**, *48*, 371-399.
- (6) Stanley, S. H.; Prior, S. D.; Leak, D. J.; Dalton, H. *Biotech. Lett.* **1983**, *5*, 487-492.
- (7) Nguyen, H.-H. T.; Shiemke, A. K.; Jacobs, S. J.; Hales, B. J.; Lidstrom, M. E.; Chan, S. I. *J. Biol. Chem.* **1994**, *269*, 14995-15005.
- (8) Zahn, J. E.; DiSpirito, A. A. *J. Bacteriol.* **1996**, *178*, 1018-1029.
- (9) Cook, S. A.; Shiemke, A. K. *J. Inorg. Biochem.* **1996**, *63*, 273-284.
- (10) Dalton, H.; Leak, D. J. In *Gas Enzymol.*; al., H. D. e., Eds.; D. Reidel Publishing Co.: London, 1985; pp 169-186.
- (11) Nielsen, A. K.; Gerdes, K.; Degn, H.; Murrell, J. C. *Microbiology* **1996**, *142*, 1289-1296.
- (12) Colby, J.; Dalton, H. *Biochem. J.* **1978**, *171*, 461-468.
- (13) Fox, B. G.; Lipscomb, J. D. *Biochem. Biophys. Res. Comm.* **1988**, *154*, 165-170.
- (14) Fox, B. G.; Froland, W. A.; Dege, J. E.; Lipscomb, J. D. *J. Biol. Chem.* **1989**, *264*, 10023-10033.
- (15) Colby, J.; Dalton, H. *Biochem. J.* **1979**, *177*, 903-908.

- (16) Green, J.; Dalton, H. *J. Biol. Chem.* **1985**, *260*, 15795-15801.
- (17) Liu, K. E.; Valentine, A. M.; Wang, D.; Huynh, B. H.; Edmondson, D. E.; Salifoglou, A.; Lippard, S. J. *J. Am. Chem. Soc.* **1995**, *117*, 10174-10185.
- (18) Green, J.; Dalton, H. *J. Biol. Chem.* **1989**, *264*, 17698-17703.
- (19) Dalton, H. In *Adv. Appl. Microbiol.* Academic Press: 1980; Vol. 26; pp 71-87.
- (20) Colby, J.; Stirling, D. I.; Dalton, H. *Biochem. J.* **1977**, *165*, 395-402.
- (21) Rosenzweig, A. C.; Frederick, C. A.; Lippard, S. J.; Nordlund, P. *Nature* **1993**, *366*, 537-543.
- (22) Rosenzweig, A. C.; Lippard, S. J. *Acc. Chem. Res.* **1994**, *27*, 229-236.
- (23) Woodland, M. P.; Patil, D. S.; Cammack, R.; Dalton, H. *Biochim. Biophys. Acta* **1986**, *873*, 237-242.
- (24) DeWitt, J. G.; Bentsen, J. G.; Rosenzweig, A. C.; Hedman, B.; Green, J.; Pilkington, S.; Papaefthymiou, G. C.; Dalton, H.; Hodgson, K. O.; Lippard, S. J. *J. Am. Chem. Soc.* **1991**, *113*, 9219-9235.
- (25) DeRose, V. J.; Liu, K. E.; Kurtz, D. M., Jr.; Hoffman, B. M.; Lippard, S. J. *J. Am. Chem. Soc.* **1993**, *115*, 6440-6441.
- (26) Liu, K. E.; Lippard, S. J. *J. Biol. Chem.* **1991**, *266*, 12836-12839.
- (27) Feig, A. L.; Lippard, S. J. *Chem. Rev.* **1994**, *94*, 759-805.
- (28) Rosenzweig, A. C.; Nordlund, P.; Takahara, P. M.; Frederick, C. A.; Lippard, S. J. *Chem. Biol.* **1995**, *2*, 409-418.
- (29) Liu, K. E.; Wang, D.; Huynh, B. H.; Edmondson, D. E.; Salifoglou, A.; Lippard, S. J. *J. Am. Chem. Soc.* **1994**, *116*, 7465-7466.
- (30) Liu, K. E.; Valentine, A. M.; Qiu, D.; Edmondson, D. E.; Appelman, E. H.; Spiro, T. G.; Lippard, S. J. *J. Am. Chem. Soc.* **1995**, *117*, 4997-4998; Correction **1997**, *119*, 11134.

- (31) Liu, Y.; Nesheim, J. C.; Lee, S.-K.; Lipscomb, J. D. *J. Biol. Chem.* **1995**, *270*, 24662-24665.
- (32) Nesheim, J. C.; Lipscomb, J. D. *Biochemistry* **1996**, *35*, 10240-10247.
- (33) Lee, S.-K.; Nesheim, J. C.; Lipscomb, J. D. *J. Biol. Chem.* **1993**, *268*, 21569-21577.
- (34) Shu, L.; Nesheim, J. C.; Kauffmann, K.; Münck, E.; Lipscomb, J. D.; Que, L., Jr. *Science* **1997**, *275*, 515-518.
- (35) Ortiz de Montellano, P. R. In *Cytochrome P450: Structure, Mechanism, and Biochemistry*; 2nd ed.; Ortiz de Montellano, P. R., Eds.; Plenum Press: New York, 1995; pp 245-303.
- (36) Groves, J. T.; Han, Y.-Z. In *Cytochrome P450: Structure, Mechanism, and Biochemistry*; 2nd ed.; Ortiz de Montellano, P. R., Eds.; Plenum Press: New York, 1995; pp 3-48.
- (37) Mansuy, D.; Battioni, P. In *Activation and Functionalization of Alkanes*; Hill, C. L., Eds.; Wiley: New York, 1989; pp 195-218.
- (38) Guengerich, F. P. In *Biological Oxidation Systems, Vol 1*; Reddy, C. C., Hamilton, G. A. and Madyastha, K. M., Eds.; Academic Press: San Diego, 1990; pp 51-67.
- (39) Ortiz de Montellano, P. R.; Stearns, R. A. *J. Am. Chem. Soc.* **1987**, *109*, 3415-3420.
- (40) Bowry, V. W.; Ingold, K. U. *J. Am. Chem. Soc.* **1991**, *113*, 5699-5707.
- (41) Bowry, V. W.; Luszyk, J.; Ingold, K. U. *J. Am. Chem. Soc.* **1991**, *113*, 5687-5698.
- (42) Newcomb, M.; Le Tadic, M.-H.; Putt, D. A.; Hollenberg, P. F. *J. Am. Chem. Soc.* **1995**, *117*, 3312-3313.
- (43) Newcomb, M.; Le Tadic-Biadatti, M.-H.; Chestney, D. L.; Roberts, E. S.; Hollenberg, P. F. *J. Am. Chem. Soc.* **1995**, *117*, 12085-12091.

- (44) Pratt, J. M.; Ridd, T. I.; King, L. J. *J. Chem. Soc., Chem. Comm.* **1995**, 2297-2298.
- (45) Bach, R. D.; Mintcheva, I.; Estevez, C. M.; Schlegel, H. B. *J. Am. Chem. Soc.* **1995**, *117*, 10121-10122.
- (46) Liu, K. E.; Johnson, C. C.; Newcomb, M.; Lippard, S. J. *J. Am. Chem. Soc.* **1993**, *115*, 939-947.
- (47) Choi, S.-Y.; Eaton, P. E.; Hollenberg, P. F.; Liu, K. E.; Lippard, S. J.; Newcomb, M.; Putt, D. A.; Upadhyaya, S. P.; Xiong, Y. *J. Am. Chem. Soc.* **1996**, *118*, 6547-6555.
- (48) Ruzicka, F.; Huang, D.-S.; Donnelly, M. I.; Frey, P. A. *Biochemistry* **1990**, *29*, 1696-1700.
- (49) Priestley, N. D.; Floss, H. G.; Froland, W. A.; Lipscomb, J. D.; Williams, P. G.; Morimoto, H. *J. Am. Chem. Soc.* **1992**, *114*, 7561-7562.
- (50) Pacansky, J.; Dupuis, M. *J. Am. Chem. Soc.* **1982**, *104*, 415-421.
- (51) Suter, H. U.; Ha, T.-K. *Chem. Phys.* **1991**, *154*, 227-236.
- (52) Pilkington, S. J.; Dalton, H. In *Methods In Enzymology* Academic Press: New York, 1990; Vol. 188; pp 181-190.
- (53) Fox, B. G.; Froland, W. A.; Jollie, D. R.; Lipscomb, J. D. In *Methods In Enzymology* Academic Press: New York, 1990; Vol. 188; pp 191-202.
- (54) Hultquist, D. E. In *Methods in Enzymology* Academic Press: New York, 1978; Vol. 52; pp 463-473.
- (55) Priestley, N.; Wilkinson, B.; Floss, H. G. unpublished results.
- (56) Andres, H.; Morimoto, H.; Williams, P. G. *J. Chem. Soc., Chem. Commun.* **1990**, 627-628.
- (57) Parker, D. *J. Chem. Soc. Perkin Trans. 2* **1983**, 83-88.
- (58) Floss, H. G.; Tsai, M. D. *Adv. Enzymol.* **1979**, *50*, 243-302.
- (59) Reid, M. F.; Fewson, C. A. *Crit. Rev. Microbiol.* **1994**, *20*, 13-56.

- (60) Santaniello, E.; Ferraboschi, P.; Grisenti, P.; Manzocchi, A. *Chem. Rev.* **1992**, *92*, 1071-1140.
- (61) Shapiro, S.; Piper, J. U.; Caspi, E. *J. Am. Chem. Soc.* **1982**, *104*, 2301-2305.
- (62) O'Ferrall, R. A. M. *J. Chem. Soc. (B)* **1970**, 785-790.
- (63) Ritchie, C. D. In *Physical Organic Chemistry: The Fundamental Concepts* Marcel Dekker: New York, 1990; pp 289-307.
- (64) Froland, W. A.; Wilkinson, B.; Priestley, N. D.; Morimoto, H.; Williams, P. G.; Lipscomb, J. D.; Floss, H. G. manuscript in preparation.
- (65) Wilkinson, B.; Zhu, M.; Priestley, N. D.; Nguyen, H.-H. T.; Morimoto, H.; Williams, P. G.; Chan, S. I.; Floss, H. G. *J. Am. Chem. Soc.* **1996**, *118*, 921-922.
- (66) Groves, J. T.; Viski, P. *J. Org. Chem.* **1990**, *55*, 3628-3634.
- (67) Groves, J. T.; Viski, P. *J. Am. Chem. Soc.* **1989**, *111*, 8537-8538.
- (68) Groves, J. T.; Stern, M. K. *J. Am. Chem. Soc.* **1987**, *109*, 3812-3814.

Table 6.1. Results of Oxidizing (R)- and (S)-[1-²H₁,1-³H]Ethane with Purified H, B, and R.

Substrate	(R)-ethane	(S)-ethane
k_H/k_D^a	3.8	3.0
C2/C1 ^a	3.3	3.4
% retention	72	71

^aCalculated from the product alcohol ³H NMR spectra.

Table 6.2. Results of Oxidizing (R)- and (S)-[1-²H₁,1-³H]Butane with Purified H, B, and R.

Substrate	(R)-butane	(S)-butane
k_H/k_D^a	2.5	1.8
C4/C1 ^a	3.8	3.3
% retention	76	78

^aCalculated from the product alcohol ³H NMR spectra.

Table 6.3. Results of Oxidizing (R)- and (S)-[1-²H₁,1-³H]Ethane with a Mixture Containing sMMO and Other Cellular Proteins.

Substrate	(R)-ethane	(S)-ethane
k_H/k_D^a	1.1	0.5
C2/C1 ^a	4.2	4.2
% retention CH ₃ CHTOH	14 ± 9	80 ± 18
% retention CH ₃ CDTOH	80 ± 4	85 ± 22
% retention	30 ± 8	76 ± 11

^aCalculated from the product alcohol ³H NMR spectra.

Table 6.4. Results of Oxidizing (R)- and (S)-[1-²H₁,1-³H]Butane with a Mixture Containing sMMO and Other Cellular Proteins.

Substrate	(R)-butane	(S)-butane
k_H/k_D^a	<0.5	0.8
C4/C1 ^a	3.0	3.0
% retention	84	51

^aCalculated from the product alcohol ³H NMR spectra.

Table 6.5. Results of Oxidizing (R)-, (S)-, and Racemic [2-³H]Butane with a Mixture of H, B, and R Containing Other Cellular Proteins.

Substrate	(R)-[2- ³ H]butane	(S)-[2- ³ H]butane	racemate
% (S) alcohol	86.5 (retention)	4.3 (inversion)	42.8
% (R) alcohol	13.5 (inversion)	95.7 (retention)	57.2
C3/C2 ^a	2.6	2.2	2.3
C1/C2 ^a	5.4	4.6	4.8

^aCalculated from the product alcohol ³H NMR spectrum.

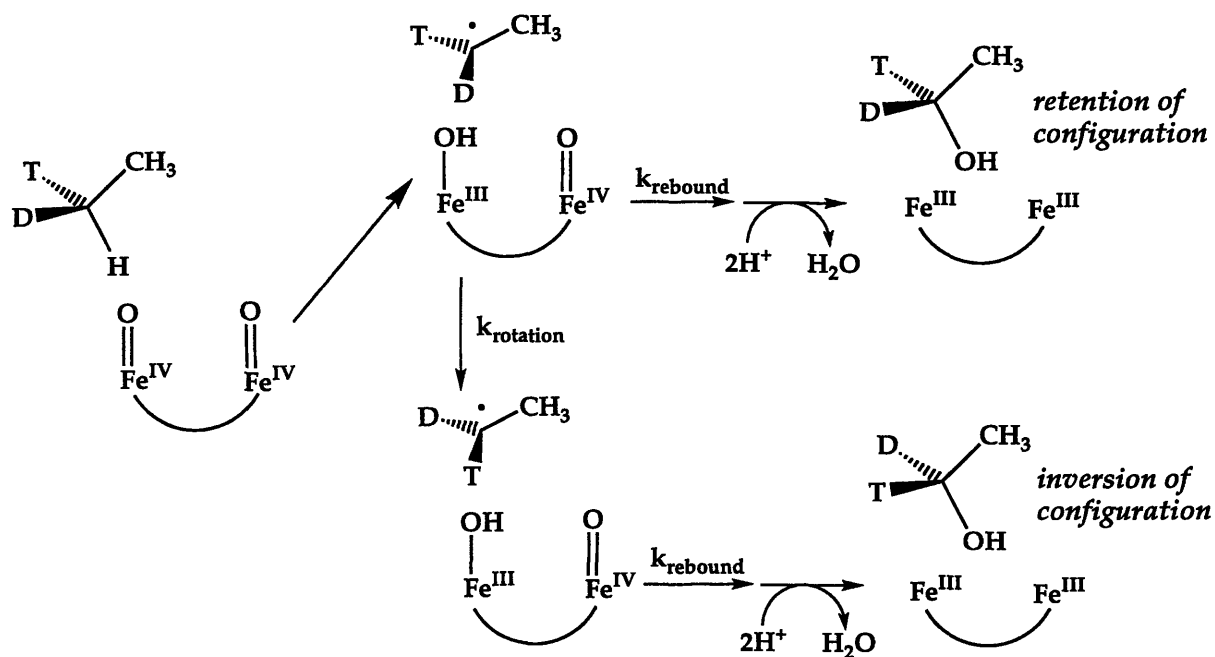


Figure 6.1. Oxidation of (S)-[1-²H₁,1-³H]ethane at the C-¹H bond via a proposed substrate radical intermediate. Radical rebound before rotation about the C-C bond in the resulting planar intermediate would lead to products displaying retention of configuration, as shown. Rotation before rebound would lead to inverted products.

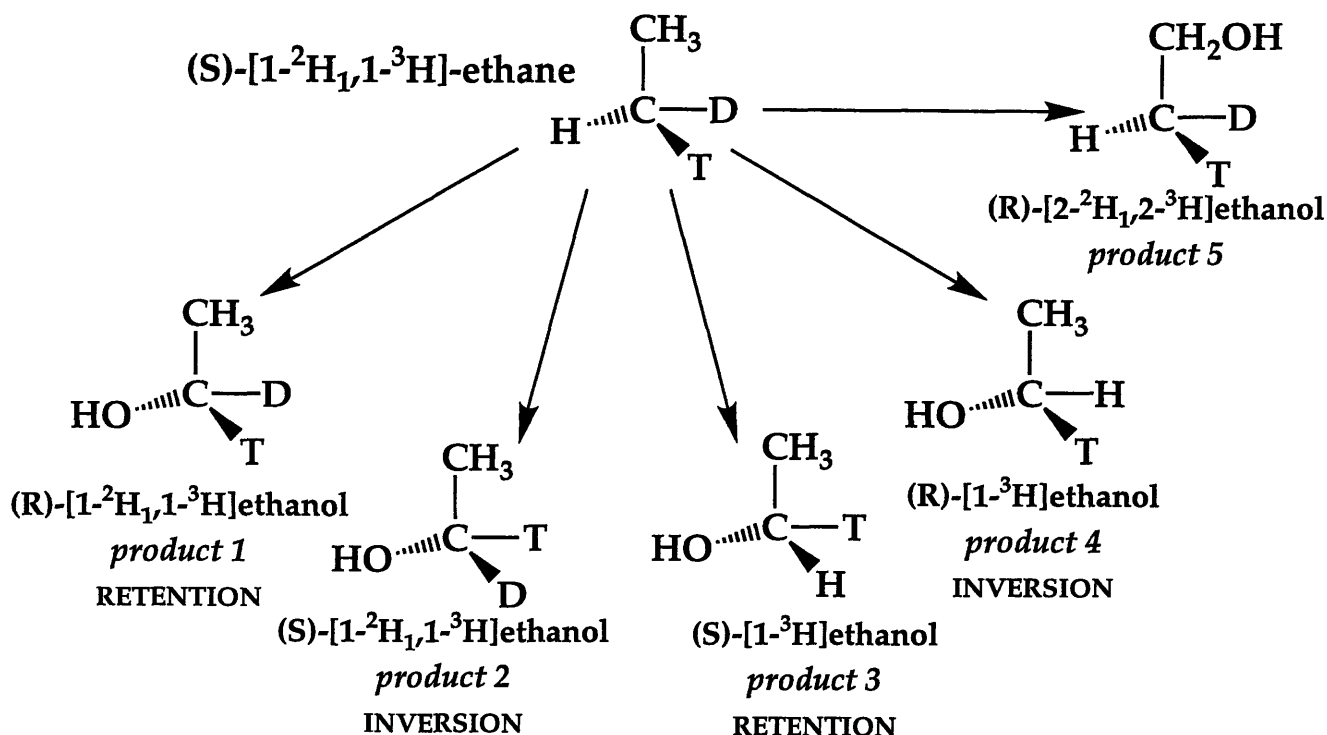


Figure 6.2. Possible reaction products from the oxidation of $(S)\text{-}[1\text{-}^2\text{H}_1, 1\text{-}^3\text{H}]\text{ethane}$. Products 1 and 2 arise from reaction at the C-H bond, products 3 and 4 from reaction at the C-D bond, and product 5 from reaction at the unlabeled carbon. Alcohols arising from hydroxylation of the C-T bond are not detected by ^3H -NMR spectroscopy. The ratio of the sum of products 1 and 2 to the sum of products 3 and 4 yields the intramolecular $k_{\text{H}}/k_{\text{D}}$ isotope effect. After derivatization, the products displaying retention of stereochemistry (1 and 3) can be distinguished from those exhibiting inversion (2 and 4), and the total percent retention can be determined.

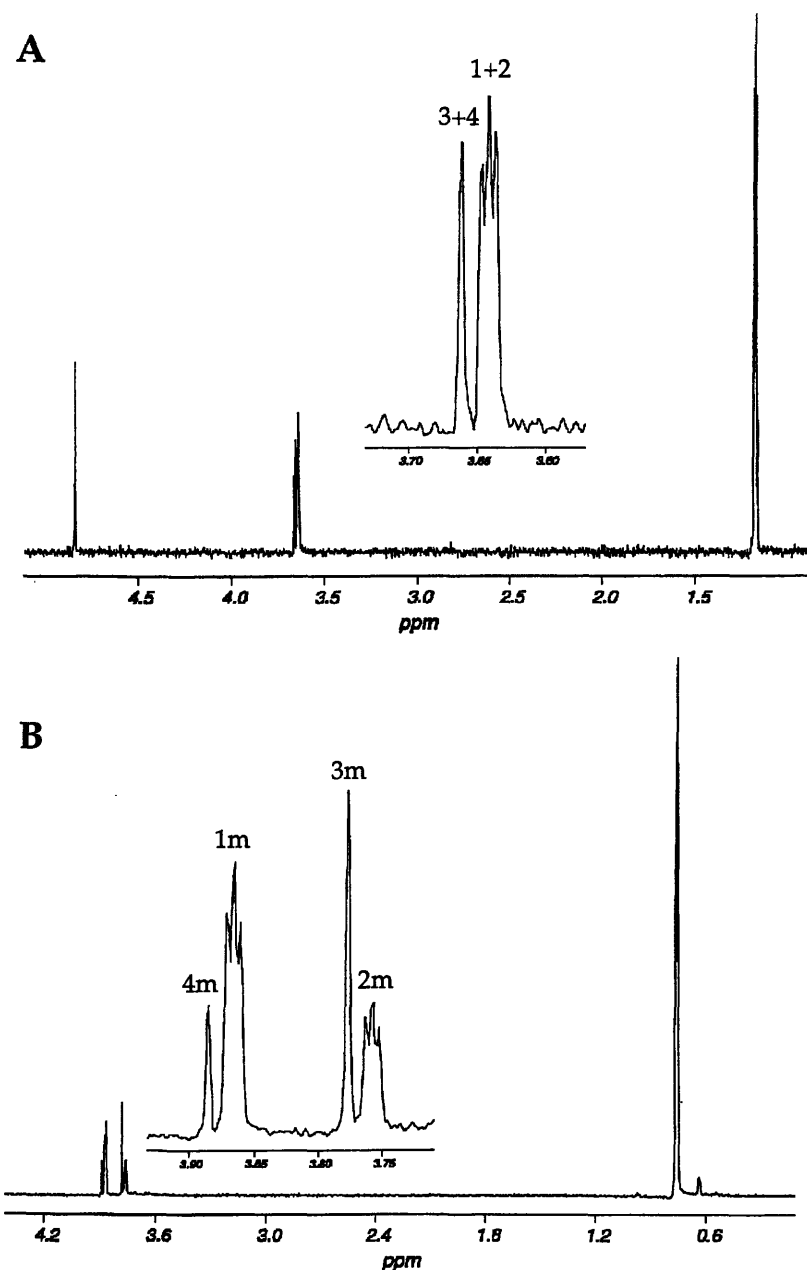


Figure 6.3. ^3H NMR analyses of the oxidation products of (S)-[1- $^2\text{H}_1$,1- ^3H]ethane. (A) Spectrum of the underivatized alcohols. The far upfield peak corresponds to oxidation at the unlabeled carbon (product 5 from Figure 6.2). The narrower downfield peak at ~ 3.65 ppm (inset) arises from alcohols 3 and 4 from Figure 6.2. The upfield peak, split by the integer-spin deuterium atom, originates from alcohols 1 and 2. The far downfield peak is assigned to tritiated water. (B) Spectrum of the mandelate derivatives. Resonances 1-4 (inset) correspond to the mandelates of the like-numbered products in Figure 6.2. The large upfield peak results from the mandelate of product 5.

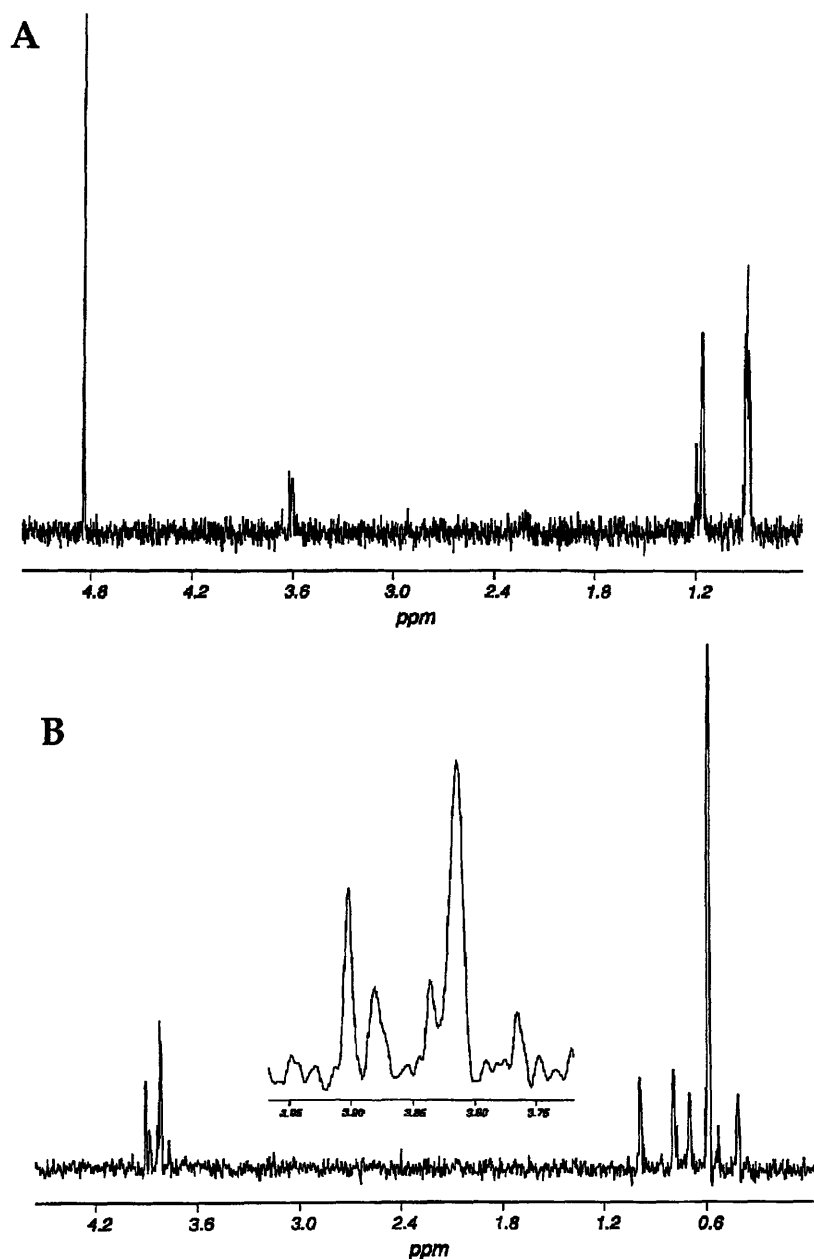


Figure 6.4. ^3H NMR analyses of the oxidation products of (S)-[1- ^3H ,1- $^2\text{H}_1$]butane. (A) Spectrum of the alcohol products. Tritiated water appears far downfield. The signal at $\delta = 3.7$ ppm corresponds to the primary alcohols $\text{CH}_3\text{CH}_2\text{CH}_2\text{CHT}(\text{OH})$ and $\text{CH}_3\text{CH}_2\text{CH}_2\text{CDT}(\text{OH})$. Other signals are identified in the text. (B) The spectra of corresponding mandelate derivatives. The inset is an expansion of the region of the diastereomeric esters of the products arising from oxidation at the labeled carbon.

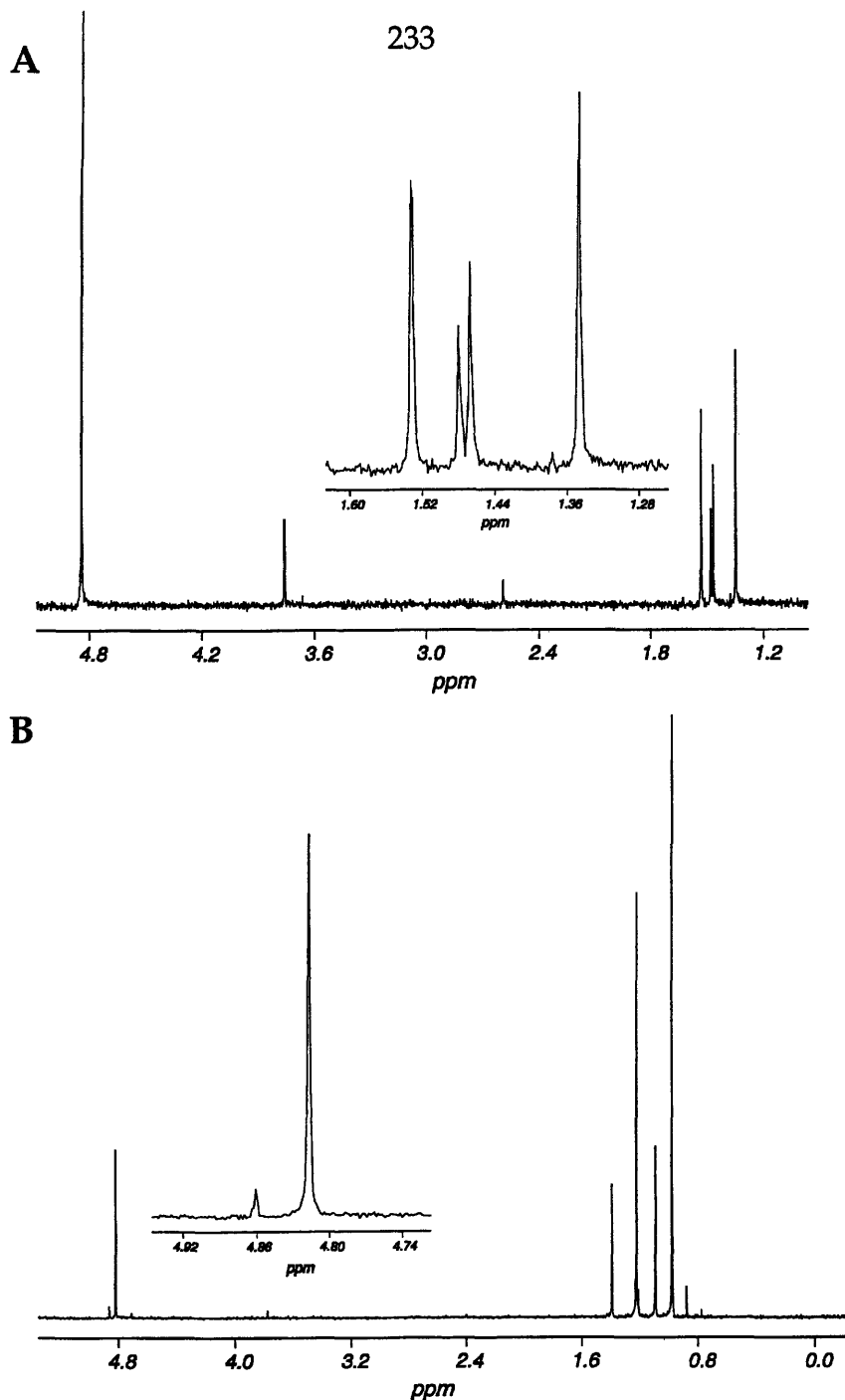


Figure 6.5. ³H NMR analyses of the oxidation products of (S)-[2-³H]butane. (A) Spectrum of the alcohol products. Tritiated water appears far downfield. The product of hydroxylation at the labeled carbon appears at $\delta = 3.8$ ppm. The inset is an expansion of the upfield region, as described in the text. (B) The spectra of corresponding mandelate derivatives. The inset is an expansion of the region of the esters of the products arising from oxidation at the labeled carbon. The peak at $\delta = 4.86$ ppm corresponds to the mandelate of (S)-2-butanol, signifying inversion of stereochemistry of the starting alkane. The signal at $\delta = 4.82$ ppm arises from the (R)-2-butanol which results from retention of stereochemistry.

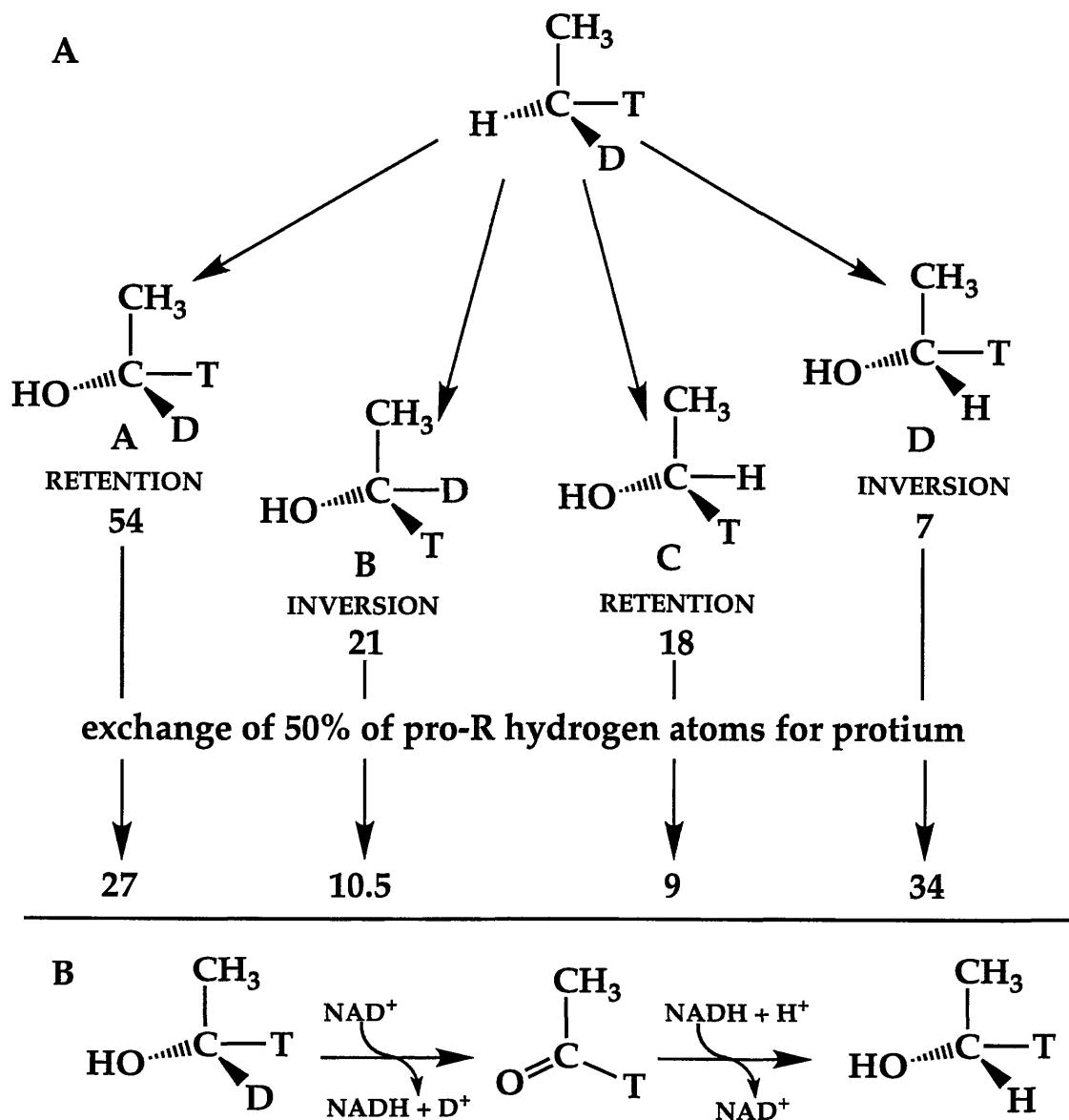


Figure 6.6. A scenario in which an alcohol dehydrogenase exchange reaction would cause inverted kinetic isotope effects and apparent inversion of stereochemistry in the products of oxidation of chiral (R)-ethane. The initial products in (A) are the theoretical distribution based on a $k_{\text{H}}/k_{\text{D}}$ of 3.0 and 72% retention of stereochemistry. Each product then exchanges 50% of the pro-R hydrogen atoms for protium, giving rise to the final product distribution shown. The apparent $k_{\text{H}}/k_{\text{D}}$ is then 0.87 and the apparent stereochemistry reflects only 45% retention. (B) Exchange of the pro-R hydrogen atom (in this case, a deuteron) from product A in Figure 6.6A to form product D in a NAD^+/NADH dependent process.

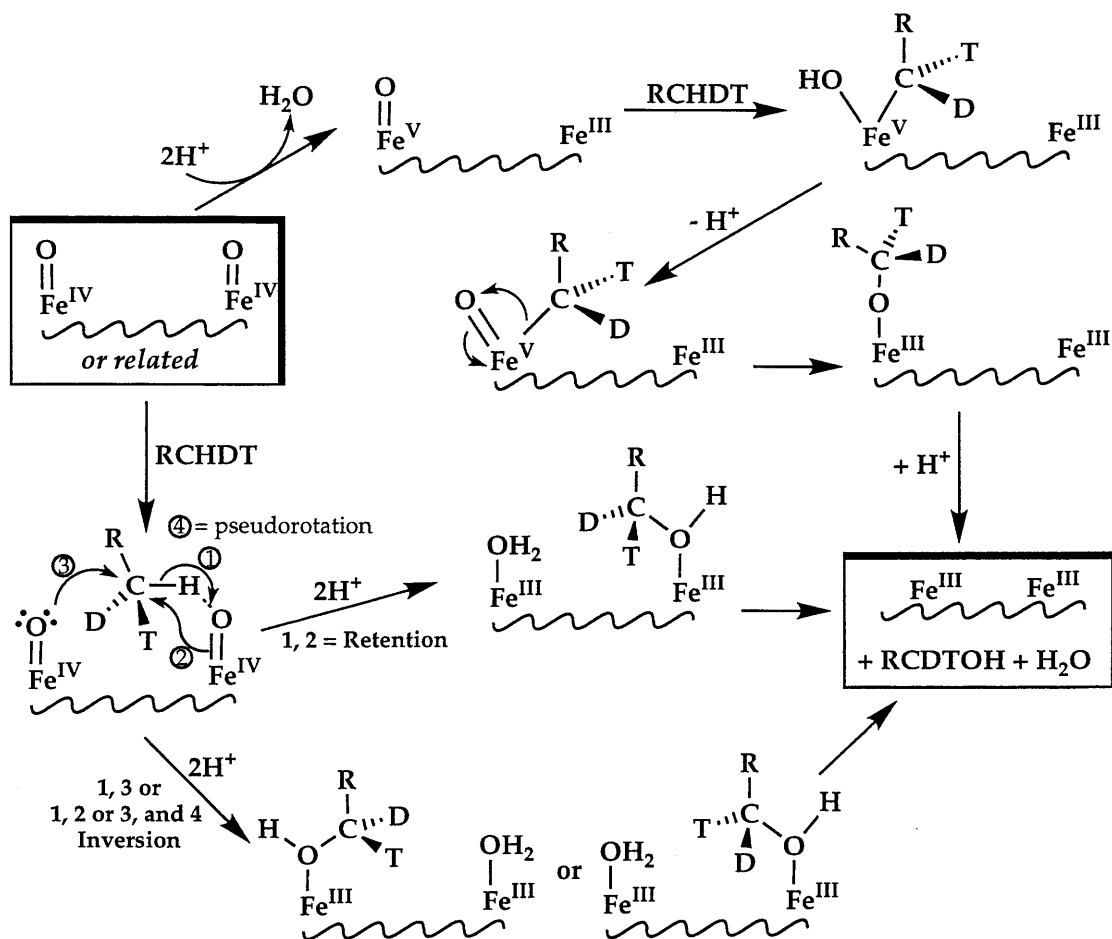


Figure 6.7. (Top) One alternative for the oxidation of alkane by a high valent iron-oxo intermediate without formation of a free substrate radical. This mechanism features oxygen atom insertion into an iron-bound alkane. In this scheme, protonation of one oxygen atom to form water occurs before substrate activation. It is unclear how inverted products could occur via this mechanism. (Bottom) A nonsynchronous concerted mechanism for oxidation of an alkane by sMMO.⁴⁶ In one manifestation of this mechanism (upper arrow), the alkane molecule is doubly activated by one iron and its bound oxygen atom, leading to retention. Inversion can occur (bottom arrow) either by backside attack from the other oxygen atom (1 + 3) or by pseudorotation in the transition state [1 + (2 or 3) + 4]. This mechanism currently has no precedence in non-heme iron model chemistry, in which primary alkane hydroxylation by dioxygen does not occur. Instead, non-productive decomposition pathways result.

Appendix One:

Attempts to Inhibit sMMO Activity by using Small Molecules

Introduction

This study was begun when the x-ray crystal structure of the sMMO hydroxylase¹ was determined. The molecular geometry of the active site provided several suggestions for the design of mechanism-based inhibitors of sMMO activity. Two of the compounds employed to prepare heavy atom derivatives, tetrakis(acetoxymethyl)mercuric methane (TAMM) and ethylmercurithiosalicylate (EMTS), bound in the active site and coordinated to Cys 151. This residue was correctly postulated, based on sequence alignments, to be in the same position as the tyrosine residue in RNR-R2 which is converted to a tyrosyl radical.²⁻⁴ It seemed likely that these mercury reagents be useful as inhibitors of activity, either by sterically blocking access to iron in the active site or perhaps by specific inactivation of a potentially catalytically important cysteine residue. In addition, in the x-ray crystal structure, electron density between the iron atoms was best fit as exogenous acetate from the crystallization buffer. Because formate is a downstream product of methane oxidation in methanotrophs, we speculated that exogenous carboxylate binding and inhibition of sMMO activity might provide a mechanism for feedback inhibition.

Experimental

At the time these experiments were undertaken, purified MMOR was not available,⁵ and a cell extract containing a mixture of proteins MMOB and MMOR (B/R mix) was used instead. The activity of these B/R mixtures was quite sensitive to temperature and irreproducible from batch to batch. MMOH activity was assayed by a standard propylene to propylene oxide conversion at 45 °C after treatment with a potential inhibitor.⁶ The inhibitor was added to MMOH just prior to the assay unless otherwise noted. For experiments employing hydrogen gas, 2 cc of the headspace gas in the reaction vessel were removed by using a gastight syringe. Through a septum, 1 cc of propylene gas, a volume of hydrogen gas, and air to make

up 2 cc were added and the mixture was allowed to equilibrate for 5 min with shaking to dissolve the gases. In the time course experiments, MMOH was incubated with the potential inhibitor at ambient temperature, and then freshly thawed B/R mix was added and the protein assayed in the usual manner.⁶ In the attempted reactivation experiments, samples containing 10 μ M MMOH were incubated in the presence or absence of 0.5 mM MeHgNO₃ for 4 h, followed by two 4 h dialyses against buffer with or without 1mM β -mercaptoethanol. Assays were carried out before and after dialysis with freshly thawed B/R mix.

Results and Discussion

The mercury compound EMTS inhibited MMOH activity in a concentration- and time-dependent manner (Figure A1.1). One unit of activity is defined as a millimole of product produced per minute. The scatter in the plots may be due to the irreproducibility of the activity of the B/R mixture. Still more dramatic inhibition was observed with methylmercury salts, including methylmercury nitrate (Figure A1.2) and methylmercury chloride (data not shown). Dialyses against β -mercaptoethanol did not restore the activity. Some compounds which did not inhibit sMMO activity were methylmethanethiolsulfonate (MMTS), sodium formate and sodium acetate, and hydrogen gas.

One conclusion from these experiments is that mercury compounds are inhibitors of sMMO activity, possibly by covalent modification of the cysteine residue at the active site. An unresolved question is whether the inhibition is due to inactivation of a functionally important Cys residue or simple blockage of access to iron in the active site. The smaller methylmercury salts also inhibit activity. We know from both the crystal structure and later ENDOR work⁷ that acetate can bind in active site. In the ENDOR work, however, acetate did not compete for binding with other small molecules, and the failure of this anion to inhibit activity further

suggests that it is easily expelled from the active site, perhaps upon reduction to the diferrous form. Inhibition by dihydrogen, which was used to invoke an agostic interaction for cytochrome P-450,⁸ is not indicated in the case of sMMO. No inhibition by dihydrogen was observed.

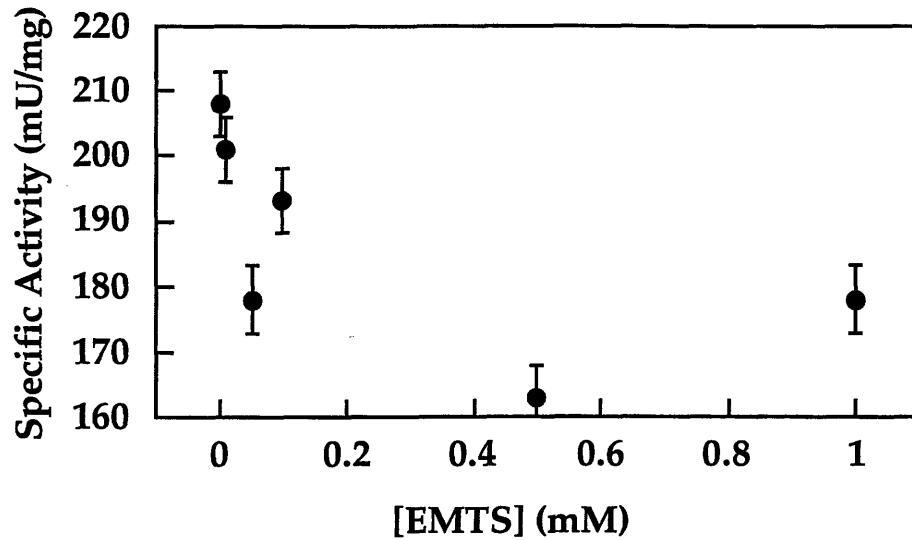
References

- (1) Rosenzweig, A. C.; Frederick, C. A.; Lippard, S. J.; Nordlund, P. *Nature* **1993**, *366*, 537-543.
- (2) Bollinger, J. M., Jr.; Edmondson, D. E.; Huynh, B. H.; Filley, J.; Norton, J. R.; Stubbe, J. *Science* **1991**, *253*, 292-298.
- (3) Nordlund, P.; Dalton, H.; Eklund, H. *FEBS Lett.* **1992**, *307*, 257-262.
- (4) Stubbe, J.; van der Donk, W. A. *Chem. Biol.* **1995**, *2*, 793-801.
- (5) Valentine, A. M.; Wilkinson, B.; Liu, K. E.; Komar-Panicucci, S.; Priestley, N. D.; Williams, P. G.; Morimoto, H.; Floss, H. G.; Lippard, S. J. *J. Am. Chem. Soc.* **1997**, *119*, 1818-1827.
- (6) DeWitt, J. G.; Bentsen, J. G.; Rosenzweig, A. C.; Hedman, B.; Green, J.; Pilkington, S.; Papaefthymiou, G. C.; Dalton, H.; Hodgson, K. O.; Lippard, S. J. *J. Am. Chem. Soc.* **1991**, *113*, 9219-9235.
- (7) Willems, J.-P.; Valentine, A. M.; Lippard, S. J.; Hoffman, B. M. *J. Am. Chem. Soc.* **1998**, in press.
- (8) Collman, J. P.; Chien, A. S.; Eberspacher, T. A.; Brauman, J. I. *J. Am. Chem. Soc.* **1998**, *120*, 425-426.

Table A1.1. Attempts to reactivate MeHgNO₃-inhibited MMOH by dialysis against β-mercaptoethanol.

MeHgNO ₃	β-ME	before dialysis	after dialysis
-	-	326	155
-	+	238	160
+	-	82	56
+	+	133	81

A.



B.

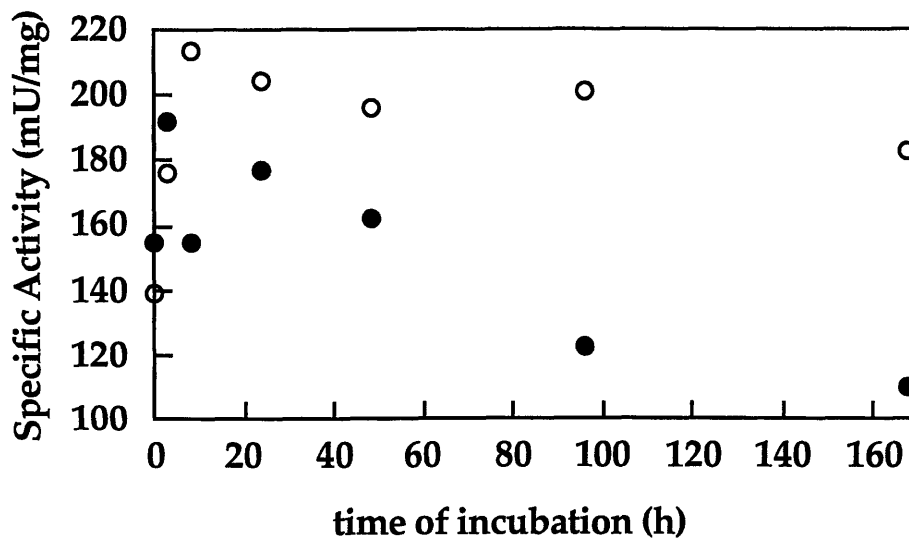


Figure A1.1. (A) Concentration-dependent inhibition of sMMO activity by EMTS. (B) Time-dependent inhibition by 0.5 mM EMTS (closed circles) compared to a control with no inhibitor (open circles). Hydroxylase was incubated with or without EMTS at room temperature and aliquots were removed periodically for activity determination. Freshly thawed B/R mix was used for each time point. The hydroxylase concentration in both experiments was 10 μ M.

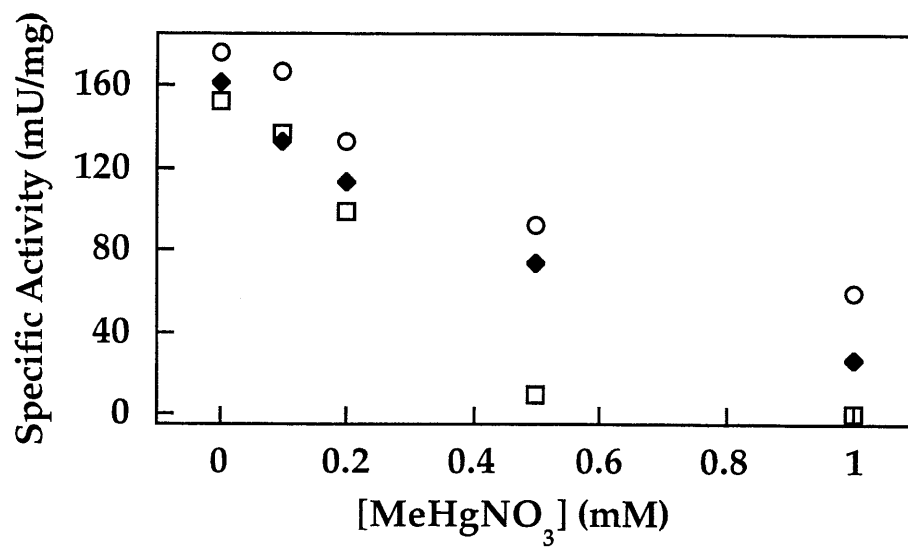


Figure A1.2. Concentration- and time- dependent inhibition of sMMO activity by MeHgNO₃. Samples were incubated for 2 h (open circles), 3 h (closed diamonds), or 24 h (open squares) before activity determination. Freshly thawed B/R mix was used for each time point. The hydroxylase concentration was 10 μ M.

Appendix Two:

**Binding of Fluorinated Small Molecules to the Mixed-Valent Diiron Center of
Methane Monooxygenase Hydroxylase from *Methylococcus capsulatus* (Bath) as
Revealed by ENDOR Spectroscopy**

This project was undertaken as an extension of the successful studies of small molecule substrate analogs and inhibitors binding to the active site of sMMO.¹⁻³ The advantage of using fluorinated probes in electron nuclear double resonance (ENDOR) experiments is that the distance from the paramagnetic center at which a ¹⁹F atom can be detected by ENDOR⁴ is about 10 Å,⁵ about twice as far as that for a proton. In the hydroxylase from *M. capsulatus* (Bath), this distance extends the range of detection out of the active site hydrophobic cavity⁶ and into the inside surface of the hydrophobic cavity beyond Leu110.⁷

Samples were prepared in the mixed-valent oxidation state by chemical reduction at room temperature and also by the radiolytic reduction technique described in Chapter 3.³ The latter method allows the interaction of the fluorinated molecule with the diferric state of the protein to be studied as well as any changes which might occur upon annealing. The two substrates chosen for exploratory work were CCl₃F and CF₃CH₂OH. Both are liquids and therefore easily handled. The CCl₃F molecule might model the substrate methane and CF₃CH₂OH might mimic the product alcohol.

No fluorine ENDOR signals were detected for samples prepared with CCl₃F. In a radiolytically reduced sample prepared with CF₃CH₂OH, however, fluorine ENDOR signals were observed (Figure A2.1). Most of the signals in the spectrum are centered at the proton Larmor frequency and split by hyperfine values up to a few MHz, but the asymmetry in the spectrum suggests that other nuclei contribute to the observed pattern. In particular, signals centered at the ¹⁹F Larmor frequency are marked on the figure. These signals could be selectively suppressed because the ENDOR response (R) is proportional to the hyperfine coupling (A) and the interval between pulses (τ) according to expression 1. The condition with τ = 1000 ns should

$$R \propto [1 - \cos(2\pi A\tau)] \quad (1)$$

suppress peaks split by 1 MHz, and the putative fluorine peaks are suppressed. The doublet moves with changing field (Figure A2.2). This result is promising for obtaining information about the position of the fluorinated ethanol molecule. Such an anisotropic interaction was observed for the binding of the DMSO molecule¹ and enabled the position of the substrate in the active site to be modeled.

The signal-to-noise ratio, however, was severely compromised by the presence of strongly coupled protons, and so the protein was exchanged into D₂O by an overnight dialysis and d⁸-glycerol was used to mitigate the contribution of protons. The ENDOR spectrum of the resulting sample reveals at least two sets of fluorine signals (Figure A2.3), the more strongly coupled of which appears only at g values near g₃. Analysis is in progress.

References

- (1) DeRose, V. J.; Liu, K. E.; Lippard, S. J.; Hoffman, B. M. *J. Am. Chem. Soc.* **1996**, *118*, 121-134.
- (2) Willems, J.-P.; Valentine, A. M.; Lippard, S. J.; Hoffman, B. M. *J. Am. Chem. Soc.* **1998**, in press.
- (3) Davydov, R.; Valentine, A. M.; Komar-Panicucci, S.; Hoffman, B. M.; Lippard, S. J. manuscript in preparation.
- (4) DeRose, V. J.; Hoffman, B. M. In *Methods in Enzymology*; ??, Eds.; Academic Press: New York, 1995; Vol. 246; pp 554-589.
- (5) Hoffman, B. M. personal communication.
- (6) Rosenzweig, A. C.; Frederick, C. A.; Lippard, S. J.; Nordlund, P. *Nature* **1993**, *366*, 537-543.
- (7) Rosenzweig, A. C.; Brandstetter, H.; Whittington, D. A.; Nordlund, P.; Lippard, S. J.; Frederick, C. A. *Proteins* **1997**, *29*, 141-152.

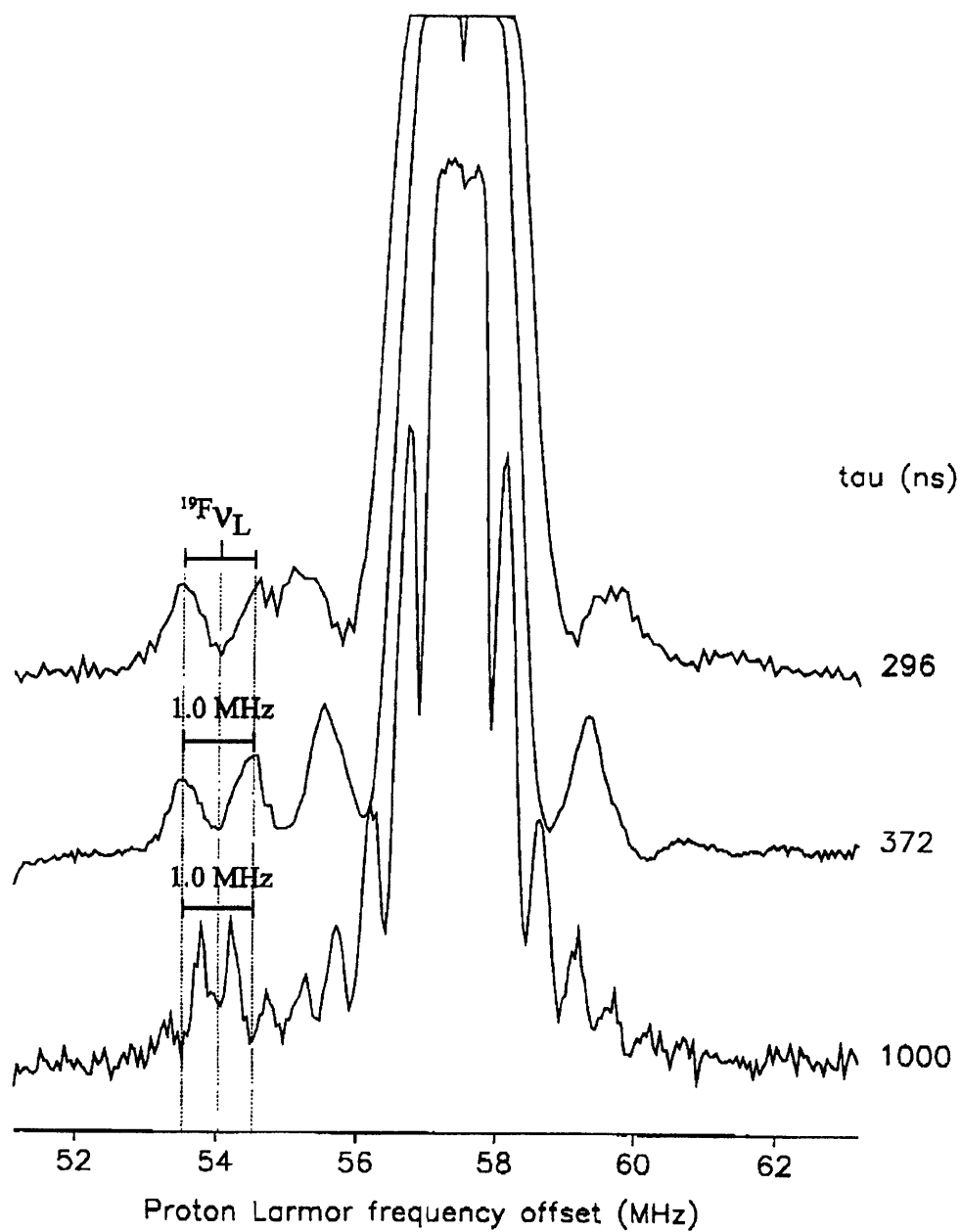


Figure A2.1. Interval-dependent ENDOR spectra of $(\text{MMOH}+\text{CF}_3\text{CH}_2\text{OH})_{\text{mv}}$.

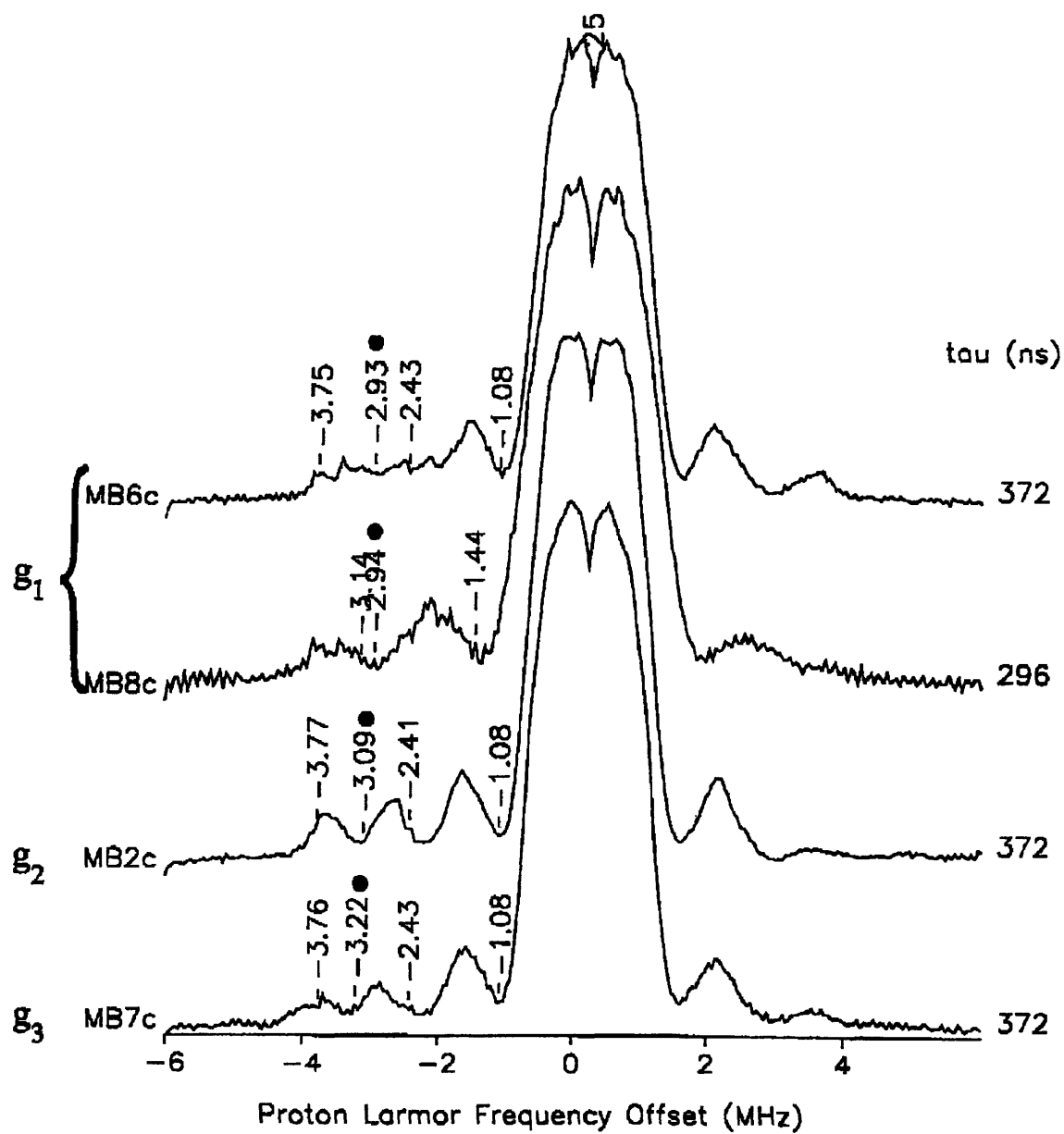


Figure A2.2. Field-dependent ENDOR spectra of $(\text{MMOH}+\text{CF}_3\text{CH}_2\text{OH})_{\text{mv}}$.

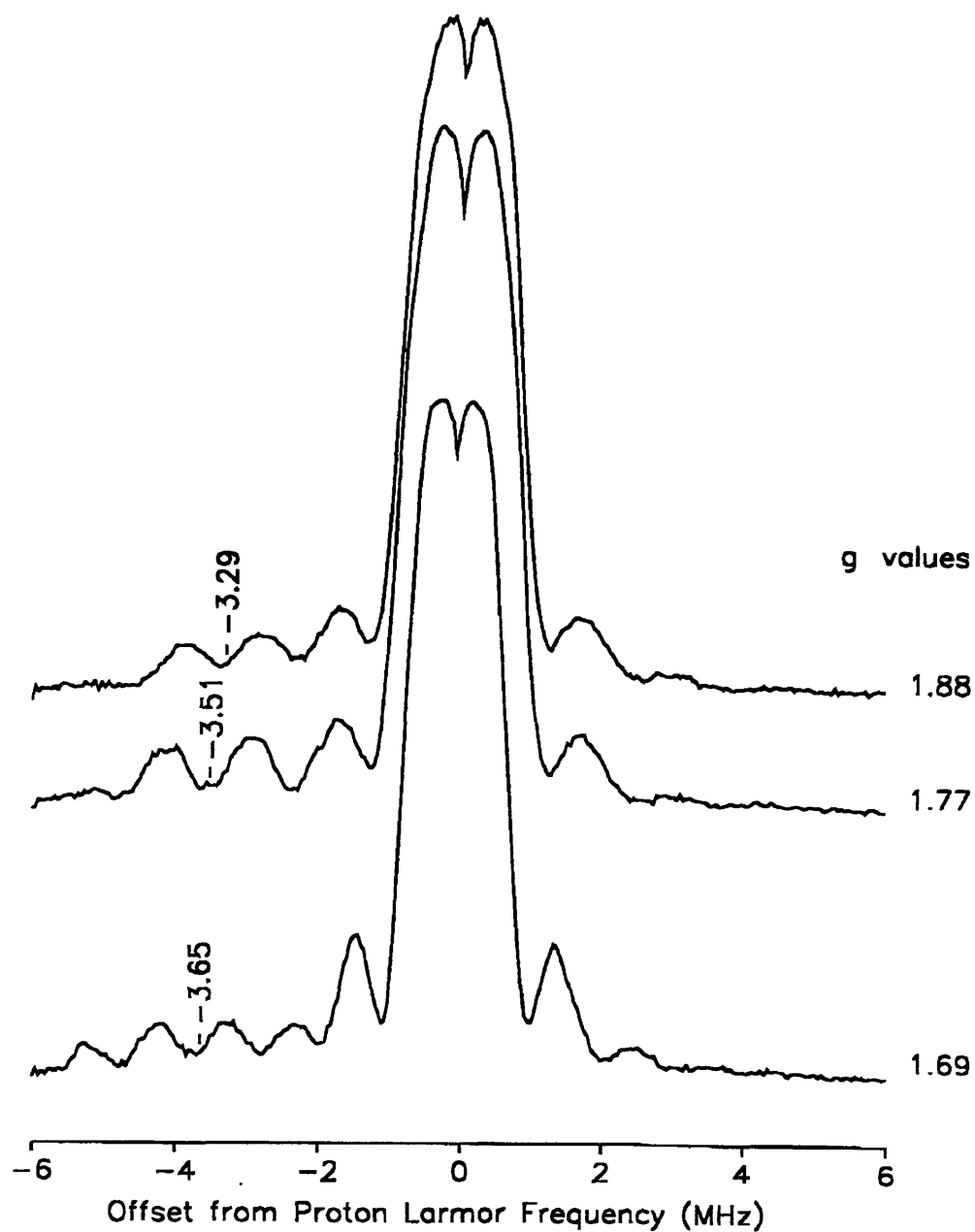


Figure A2.3. Field-dependent ENDOR spectra of a $(\text{MMOH} + \text{CF}_3\text{CH}_2\text{OH})_{\text{mv}}$ sample prepared in D_2O and d^8 -glycerol.

Appendix Three:

**Isolation of Two Components of the Alkene Monooxygenase System from
Xanthobacter Py2 and Preliminary Stopped-Flow Studies**

The purpose of this investigation was to look for intermediate species in the single turnover reaction of reduced alkene monooxygenase oxygenase with dioxygen in the presence and absence of olefin substrate.

Xanthobacter Py2 cells, together with instructions for their culture, were provided by Professor Scott Ensign of Utah State University. The cells grew well on plates and in glucose culture. A glucose culture (3% by volume) was used to inoculate a 13 L fermentation employing propene as the carbon source. The first fermentation succeeded but the cells failed to grow after rebatching. From 11.5 L of culture medium, 125 g of wet cells were obtained.

The oxygenase protein (AMO-O) and the small protein (AMO-SP) were purified by a procedure slightly modified from that of Small and Ensign.¹ The cells were lysed by ultrasonication and the cell-free extract applied to a DEAE Sepharose Fast Flow column. AMO-O and AMO-SP were resolved from many other cellular proteins on this column. The coeluting AMO-O and AMO-SP were separated on a Q Sepharose column and each was further purified by gel filtration by using Superdex 200 and Superdex 75 resin, respectively. The major contaminant in the crude fractions was a yellow protein which ran by SDS-PAGE just above the α subunit of AMO-O. An SDS-PAGE gel of the purified proteins is included as Figure A3.1. The AMO-O contained approximately 3.2 mol Fe/mol protein as determined by a ferrozine complexation assay. A total of ~10 mg of AMO-O and ~1 mg of AMO-SP were purified.

The scarcity of material limited the number of stopped-flow experiments that could be performed. For methane monooxygenase (MMO), the small coupling protein (MMOB) is required for intermediate species formation in single turnover reactions of the hydroxylase (MMOH), and is optimal at a ratio of about 2:1 MMOB:MMOH. This ratio of small protein to oxygenase was used for the AMO system. The oxygenase protein was reduced anaerobically by sodium dithionite with

methyl viologen as a mediator for electron transfer. These additives were removed by anaerobic dialysis and stopped-flow experiments were carried out at 4 °C with the reduced anaerobic protein solution in one syringe and dioxygen-saturated buffer in the other. The concentration of AMO-O after mixing was 20 μM .

Figure A3.2A depicts the spectral changes after one such experiment. Single wavelength fits (Figure A3.2B) revealed an increase in absorbance at greater than 650 nm with a rate constant of approximately 11 s^{-1} . At 450 nm, an increase at 4 s^{-1} was followed by a possible small increase at 0.02 s^{-1} . The final spectrum, with a broad shoulder at 450 nm, persisted for at least 10 min. A global fit employing rate constants from the single wavelength fits is shown in Figure A3.2C. Species 2 in this fit looks similar to the peroxy intermediate of MMO, although the extinction coefficient in the AMO case is approximately half of that species. No species comparable to the MMO Q intermediate ($\epsilon_{420\text{ nm}} > 8500\text{ M}^{-1}\text{s}^{-1}$) was observed.

In sum, this experiment yielded intriguing results with conditions far from optimized. The scarcity of protein is the single biggest impediment to further experiments, which should include a temperature dependence study to obtain activation parameters, a study of the effect of propylene on the single turnover experiment, and double mixing experiments with propylene if that work is promising. The effects of the other AMO component proteins might also be studied.

Reference

- (1) Small, F. J.; Ensign, S. A. *J. Biol. Chem.* **1997**, *272*, 24913-24920.

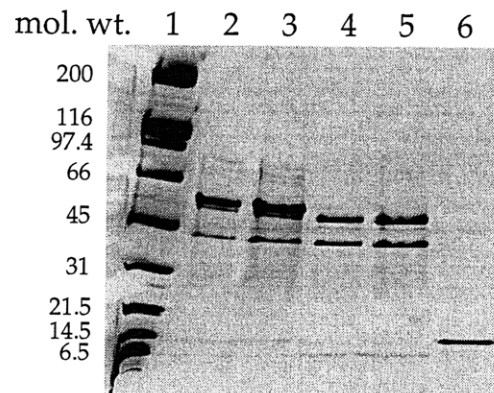


Figure A3.1. SDS-PAGE of AMO Proteins. Lane 1, broad range molecular weight markers, as indicated. Lanes 2 and 3, crude AMO-O before Superdex 200 column, Lanes 4 and 5, AMO-O after Superdex 200 column. Lane 6, purified AMO-SP.

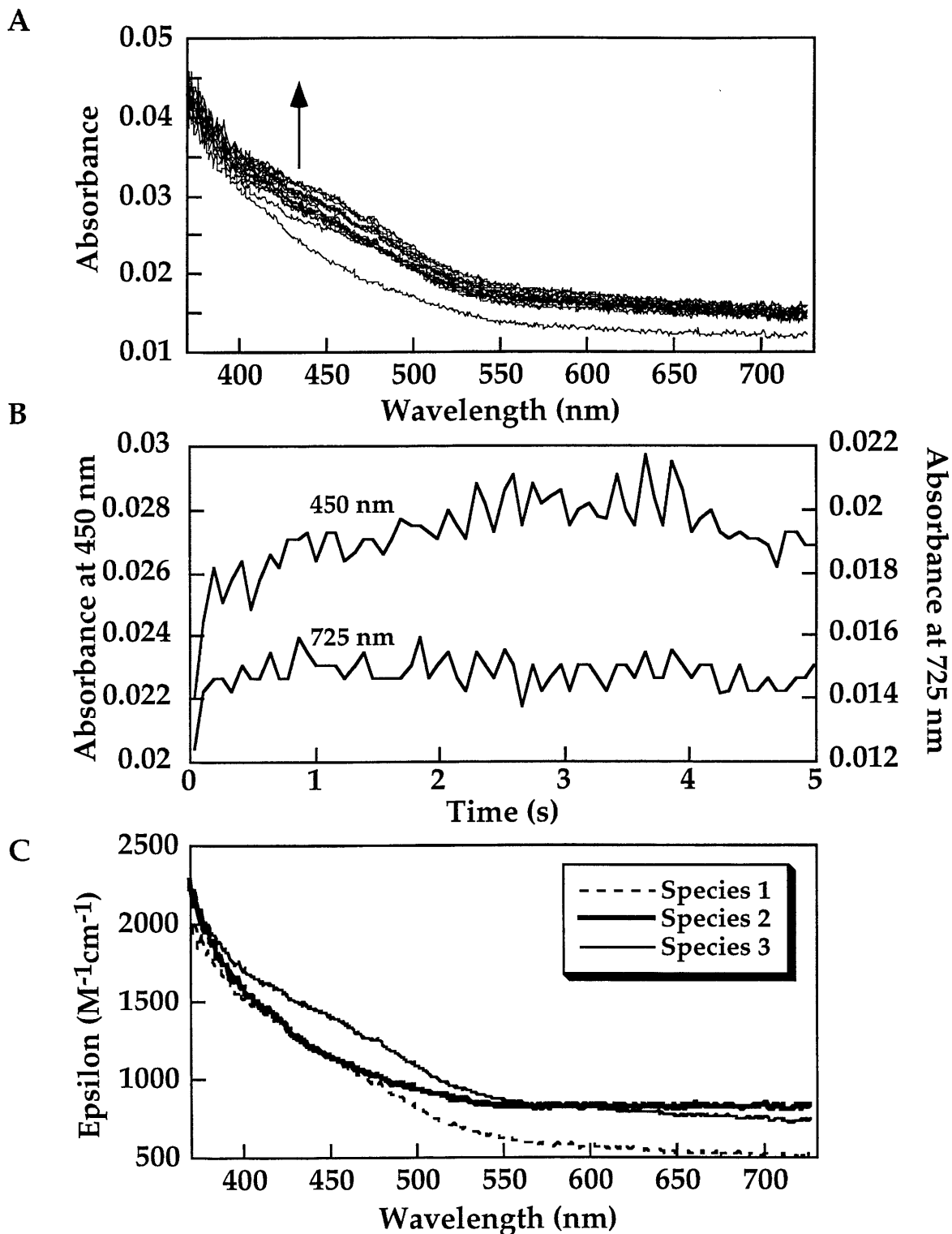


Figure A3.2. (A) Data from a stopped-flow experiment in which reduced AMO oxygenase ($40 \mu M$) in the presence of two equivalents of the small protein was mixed with dioxygen-saturated buffer at $4^\circ C$. 15 s of data are shown, one spectrum every 750 ms. (B) Spectral changes at 450 nm and 725 nm over the first 5 s of reaction. (C) Results of global fitting to the rate constants determined by single wavelength fits. Data were fit to Species 1 \rightarrow Species 2 \rightarrow Species 3 with $k_1 = 11 s^{-1}$ and $k_2 = 4 s^{-1}$.

Biographical Note

The author was born on November 24, 1971 in Pittsburgh, Pennsylvania to Janet and James Valentine and grew up there with younger siblings Amy, James, Elizabeth, and John. She graduated from Mount Lebanon High School in 1989 and attended the University of Virginia in Charlottesville, Virginia. She earned a B.S. in chemistry in 1993. Following her graduate studies at MIT, the author plans to do postdoctoral work with Professor Stephen J. Benkovic at the Pennsylvania State University.